



Dietary fibre manipulation as a potential endogenous mechanism of radiosensitisation in bladder cancer

DPhil Thesis

Supervisors:

Prof Anne E Kiltie and Prof Katherine A Vallis

Chee Kin Then

Balliol College

MRC Oxford Institute for Radiation Oncology

Department of Oncology

University of Oxford

Trinity Term 2022

Acknowledgements

I thank Professor Anne E Kiltie, Professor Katherine Vallis, and Dr. Salome Paillas for their fantastic supervision.

To Anne, I would like to say millions of thanks for all your very supportive and dedicated supervision. I extremely enjoyed all the discussion we had. These really inspired me and continue to motivate me to become a cancer scientist. It was great fun open-mindedly talking about all the possibilities behind some of the interesting phenomena we saw. It was a pleasure to meet such a great scientist of radiobiology. Thank you also for the delicious treats.

To Kate, I would like to say thanks for being my supervisor and it was really kind of you to always offer me help. To Salome, I am really grateful for your guidance in all the mouse experiments and I treasure those moments when we were working in the animal unit. Working together with you in the lab gave me great confidence. We went through a lot and those were amazing memories in my Oxford life.

I would like to thank all the lab members I had the pleasure of working with - Jia-Ling, Juri, Junetha, Edd, Rob and Susan. I learnt a lot from you. I miss the moments when we had scientific discussion and casual chats in the lab or during the lab away day. To Kristoffer and Ian, I would like to say millions of thanks for all the help during 2021-2022. Without that it would have been insurmountable challenge for me to continue my project.

To all my Taiwanese and Malaysian friends - Gu Lung, Mi Jun, Tzu Hao, Kuen Wei, Albert, Jeff, Cindy, Mu Huan, Zhi Yi and May. As a student from abroad, you created warmth and homeliness during all the gatherings. I will never forget all those sweet and happy moments while we were together with each other in Oxford.

To all my teachers from Tsun Jin High School and Taipei Medical University where I pursued my medical degree, especially Miss Chen Pei Ming, Mr Nio Wei How, Mr Tan Siew Kern, Miss Wong Cheng Yoke, and Professor Shing-Chuan Shen. Without your teaching and support, I would not be able to pursue my dream as a cancer scientist. Especially Professor Shen, I would like to say thanks for inspiring me and guiding me to the world of cancer research. Without the inspiration I obtained from her during my 7 years in medical school, I would never have had the chance to come to Oxford.

To my best friends – Yee Ling, Sook Yee, Poh Yee, Jia Jia, Yi Zhi, and Bosco. Many thanks for all your support and encouragement in my life. Although we do not see each other very often, I know you are always there.

To my family, especially my father and mother, I cannot thank you two enough for always being there through my life. I am really grateful for all your encouragement, care, and support. It is amazing to feel loved all the time no matter where I am in Malaysia, Taiwan, or the UK.

For everyone who helped me accomplish my DPhil project

I thank Dr. Ryoichi Saito and Professor William Kim (University of North Carolina, Chapel Hill) for giving us the UPPL1591 and BBN963 cell lines. I thank Professor Keith Syson Chan (Cedars Sinai Medical Centre) for giving us the G69 cell line. I thank Karla Watson and Magda Flieger (Biomedical Services Department, University of Oxford) for the animal housing and their expert care of the mice. I thank Dr. Mark Hill and Callum Beach (Department of Oncology, University of Oxford) for their assistance with the irradiation procedures, Dr. Jia-Yu Ke (Research Diets, Inc.) for formulation of the mouse diets, Daniel Sescu (University of Aberdeen, UK) for the immune cell quantification, Dr. Susan Kilgas (Department of Oncology, University of Oxford) for her assistance with the immunofluorescence experiment, Dr. Xuedan Wang and Professor Kevin Foster (Department of Zoology, University of Oxford) for their preparation of bacterial supernatants, Dr. Mariya Misheva and Professor James McCullagh (Department of Chemistry, University of Oxford) for the metabolomics analysis, Dr. Andrew Worth (The Jenner Institute, University of Oxford) for assistance with the flow cytometry analysis, Spyridoula Marinou (Centre for Clinical Vaccinology and Tropical Medicine (CCVTM), Churchill Hospital, Oxford) for the cytokine analysis, Dr. Joanna Hester (Nuffield Department of Surgical Sciences, John Radcliffe Hospital, Oxford) for the nanoString analysis, Dr Alejandro Suarez Bonnet and Professor Simon Priestnall (Royal Veterinary College, University of London) for the histopathology examination, and Oxford Genomics Centre (University of Oxford, UK) for the 16S rRNA gene sequencing on a MiSeq platform.

Abstract

New non-toxic radiosensitisers are needed in the treatment of muscle-invasive bladder cancer because elderly patients are very vulnerable to chemotherapy-related toxicity of currently available radiosensitisers. Our previous study showed that high fibre diets sensitised RT112 xenografts to irradiation by modifying the gut microbiota and this phenotype was positively correlated with *Bacteroides acidifaciens* (*BA*) abundance. As the gut microbiota can enhance anti-tumoural immune responses, I hypothesised that dietary fibre manipulation and its effects on the gut microbiota can radiosensitise tumours via microbiota secretion of metabolites and/or immunomodulation.

In preclinical mouse experiments, psyllium plus resistant starch (RS) or psyllium plus inulin significantly decreased tumour size (P=0.007 and <0.001, respectively) and they enhanced tumour control when combined with ionising radiation (IR; P<0.001 and 0.028, respectively) compared to 0.2% cellulose.

Psyllium plus inulin raised *Bifidobacterium* abundance (P<0.001), $CD8^+$ cell numbers (P=0.024), and caecal inosine levels (P<0.001), which have been shown to enhance immunotherapy efficacy. There was a significant correlation between immune response and tumour control versus Clostridiales order abundance. Systemic GM-CSF (granulocyte-macrophage colony-stimulating factor) and IL-2 cytokines levels were increased by IR. The caecal butyrate level was associated with the tumour control in the psyllium plus inulin group of both non-irradiated and irradiated mice (P=0.041). It is noted that threitol also negatively correlated with IR response. Psyllium plus RS increased several metabolite levels that have anti-tumourigenic properties, and significantly radiosensitised the tumours (P=0.004). Furthermore, the two diets mitigated the radiation injury caused by 14 Gy in intestinal crypt assays (P=0.08 and 0.011). All psyllium-containing diets increased caecal short-chain fatty acids (SCFAs, P<0.001), and prevented the delayed weight gain seen with 0.2% cellulose after IR.

We previously found that inulin enhanced the relative abundance of *BA*. Based on *cell* experiments, the supernatants of co-cultures of *BA* and *Faecalibactrium prausnitzii* (*FP*, butyrate-producer) conferred greater cytotoxicity than *BA* alone ($P<0.001$) or co-cultures of *Bifidobacterium* (acetate-producer) and *FP* ($P<0.001$), and also increased histone acetylation levels. Bacterial supernatants of *BA*+*FP* increased DNA damage and delayed DNA repair following 2 Gy IR ($P<0.05$) and increased radiosensitivity of bladder tumour cells ($P=0.008$ at 8 Gy). Overall, I demonstrated that dietary fibre supplements radiosensitised bladder tumours, with associated gut microbiota modification and enhancement of immune responses and metabolite levels. Since psyllium plus either RS or inulin achieved a more favourable therapeutic ratio with improved tumour control with decreased side effects, I propose that dietary fibre supplements may be useful adjuncts to radiotherapy in patients with pelvic malignancy.

Table of Contents

Acknowledgements ii

Abstract v

Table of Contents vii

Table of Figures xiii

Table of Tables xviii

List of abbreviations xx

Chapter 1: Introduction 1

1.1 Bladder cancer 1
1.1.1 Epidemiology and presenting symptoms 1
1.1.2 Tumour types and stages 1
1.1.3 Muscle-invasive molecular subtypes 2
1.1.4 Treatment options 5
1.2 Radiotherapy 6
1.2.1 Radiation-induced cell killing 6
1.2.2 Radiotherapy of bladder cancer 7
1.2.3 Acute and late side effects in the pelvis 8
1.2.4 Aim to increase therapeutic ratio of radiotherapy 8
1.2.5 Concept of radiosensitisation 9
1.3 Anatomy of the intestine 11
1.3.1 Macroscopic - small and large intestine, caecum 11
1.3.2 Microscopic - crypts and Peyer's patches 11
1.3.3 Sensitivity to IR and physiology/function 14
1.4 Gut barrier functions 15
1.5 Radiation effects on the intestine 17
1.6 Dietary fibre 18
1.6.1 Distinguishing soluble/insoluble from nondigestible/digestion-resistant fibres 18
1.6.2 Types of dietary fibre 18
1.6.3 Relevance to pelvic radiotherapy clinically 19
1.6.4 Psyllium 19
1.6.5 Resistant starch 20
1.6.6 Inulin 20
1.7 Short-chain fatty acids 22
1.7.1 Acetate, propionate, butyrate 22
1.7.2 SCFA-producing colonic bacterial species 23
1.7.3 Effects of butyrate 25
1.7.4 The Warburg effect 26

1.7.5 Radiosensitisation by histone deacetylase inhibitors 28
1.8 Gut microbiota 30
1.8.1 The basics and the main phyla in the intestine 30
1.8.2 Influence of dietary fibre 31
1.8.3 SCFA-producing colonic bacterial species and how they produce SCFAs and other metabolites 31
1.8.4 The gut microbiota changes with age 32
1.9 The urinary microbiota and bladder cancer 33
1.10 Prebiotics and probiotics 34
1.10.1 Prebiotics 34
1.10.2 Probiotics 34
1.11 Immunology 35
1.11.1 The basics 35
1.11.2 Immune responses to radiotherapy 38
1.11.3 Immune responses to dietary fibre 40
1.11.4 Gut microbiota and SCFAs – tumour responses, gut responses, and barrier function. 40
1.12 How dietary fibre manipulation, gut microbiota and SCFAs have been used to improve the RT therapeutic ratio to date 42
1.12.1 Effects on normal tissue responses 42
1.12.2 Effects on tumour growth 43
1.12.3 Non-IR studies 44
1.12.4 Association of the gut microbiota with high-fibre diet-mediated radiosensitisation 46
1.13 Methods to investigate the gut microbiota and SCFAs 49
1.13.1 16S rRNA gene sequencing 49
1.13.2 Taxonomy and phylogenetics 50
1.13.3 Alpha and beta diversity 51
1.13.4 Linear discriminant analysis effect size 52
1.14 Aims of this study 53

Chapter 2: Materials and methods 55

2.1 Mouse experiments 55
2.1.1 Cell lines used in animal experiments 55
2.1.2 Mouse strains 56
2.1.3 Mouse bladder tumour models 56
2.1.4 Diets in non-tumour-bearing mice 56
2.1.5 Diets with or without irradiation in tumour-bearing mice 57
2.1.6 Diets with or without irradiation in non-tumour-bearing mice 58
2.1.7 Irradiation 58
2.1.8 Tumour growth and survival analyses 59
2.1.9 Monitoring of mice and welfare end-points 60

2.1.10 Sacrifice, sample harvesting and processing 60
2.1.11 Histological and functional assays for normal tissue toxicity 61
2.1.12 Gut microbiota analysis 63
2.1.13 Untargeted metabolomics analysis 66
2.1.14 Immunological analyses 67
2.1.15 Statistical analysis 71
2.2 Cell experiments 72
2.2.1 Cell lines 72
2.2.2 Drugs 72
2.2.3 Irradiator 72
2.2.4 Bacterial strains and their supernatants 73
2.2.5 Colony formation assay 73
2.2.6 Cell survival analysis 74
2.2.7 Western blotting 74
2.2.8 Immunofluorescence microscopy and irradiation 75
2.2.9 Statistical analysis 75
Chapter 3: Bladder cancer mouse models and gut microbiota related to dietary fibre ... 77
3.1 Radiosensitivity of different cell lines 80
3.2 Establishment of mouse bladder tumour models 81
3.2.1 UPPL1591 and BBN963 mouse bladder cancer cell line allografts in C57BL/6 mice 81
3.2.2 G69 mouse bladder cancer cell line allograft in FVB mice 83
3.3 The gut microbiota related to dietary fibre and mouse strain 85
3.3.1 The gut microbiota of different strains of non-tumour-bearing mice fed with low and high dietary fibre 85
3.3.2 The gut microbiota of non-tumour-bearing mice fed with different types of dietary fibre diets 88
3.4 Discussion 91
Chapter 4: Effects of combining dietary fibre manipulation and ionising radiation on tumour growth 93
4.1 Tumour growth following ionising radiation 97
4.1.1 Overview 97
4.1.2 Effect of different IR doses on tumour growth 98
4.2 Tumour growth associated with fibre diets containing corn starch 99
4.2.1 Overview 99
4.2.2 Body weight change after modified diets 99
4.2.3 Tumour growth in low and high fibre groups 101
4.2.4 The caecal size and length of the large intestine after six weeks of modified diets 103
4.2.5 The gut microbiota of tumour-bearing mice fed with low and high dietary fibre 105

4.3 Tumour growth associated with fibre diets containing dextrose 109
4.3.1 Overview 109
4.3.2 Growth delay in bladder cancer cell xenografts in the high fibre groups 111
4.3.3 The gut microbiota of tumour bearing mice fed with low and high dietary fibre when the tumours reached 100 mm^3 113
4.3.4 Untargeted metabolomics profiling of caecal contents 116
4.4 Tumour growth following dietary fibre and ionising radiation 122
4.4.1 Overview 122
4.4.2 Body weight changes of tumour-bearing mice fed with modified diets 122
4.4.3 Psyllium plus RS or psyllium plus inulin increased growth delay in bladder tumours 124
4.4.4 Psyllium plus RS or psyllium plus inulin combined with IR increased growth delay in bladder tumours 124
4.4.5 Psyllium plus RS increased radiosensitivity of bladder tumour 128
4.4.6 Psyllium plus RS increased time to quadruple tumour volume 128
4.4.7 The gut microbiota of tumour-bearing mice fed with low and high dietary fibre when the tumours reached 700 mm^3 132
4.4.8 Correlation between gut microbiota versus tumour responses 135
4.4.9 Untargeted metabolomics analysis 141
4.5 Discussion 153

Chapter 5: Dietary fibre manipulation spares IR-induced normal tissue toxicities 156

5.1 Acute intestinal toxicity after IR 160
5.1.1 Overview 160
5.1.2 The remaining crypts in small intestine and the length of large intestine after IR 162
5.1.3 Body weight change after 2-week modified diets and after IR 164
5.1.4 The gut microbiota of non-tumour bearing mice fed with low and high dietary fibre with or without IR 166
5.1.5 Beta diversity of gut microbiota in non-tumour-bearing mice 3.75 days after SARRP IR 169
5.1.6 Untargeted metabolomics profiling and SCFA levels of caecal contents 171
5.2 Late intestinal toxicity after IR 175
5.2.1 Overview 175
5.2.2 Body weight change after IR 176
5.2.3 Stool analysis 178
5.2.4 Urine analysis 180
5.3 Discussion 182

Chapter 6: Immunology 185

6.1 Local tumour immune response following ionising radiation alone 189
6.2 Local tumour and systemic immune responses to dietary fibre alone 190
6.2.1 Overview 190

6.2.2 Local intratumoural $CD8^+$ cells 190
6.2.3 Systemic immunity 192
6.3 Local tumour and systemic immune responses following dietary fibre and ionising radiation 194
6.3.1 Overview 194
6.3.2 Systemic immune responses 196
6.3.3 Local tumour and systemic immunity in psyllium plus inulin group by IR response 198
6.3.4 Correlation between gut microbiota and immune responses 201
6.4 Local gut and systemic immune responses for dietary fibre and ionising radiation 203
6.5 Discussion 206

Chapter 7: Gut microbiota-derived metabolites increase tumour radiosensitivity 208

7.1 Short-chain fatty acids mediated radiosensitisation 210
7.1.1 SCFAs conferred radiosensitivity in bladder cancer cells 210
7.1.2 SCFAs increased histone acetylation levels of bladder cancer cells 211
7.2 Microbial metabolite-mediated radiosensitisation 213
7.2.1 Bacterial supernatants of co-cultures of *B. acidifaciens* and *F. prausnitzii* induced stronger cytotoxic response 213
7.2.2 Bacterial supernatants of co-cultures of *B. acidifaciens* and *F. prausnitzii* increased histone deacetylase inhibition and IR-induced DNA damage 215
7.2.3 Bacterial supernatants of co-culture of *B. acidifaciens* and *F. prausnitzii* delayed IR-induced DNA damage repair in RT112 and T24 cell lines 217
7.2.4 Untargeted metabolomics analysis of bacterial supernatants 219
7.2.5 Bacterial supernatants conferred increased radiosensitivity in bladder cancer cells 221
7.3 Discussion 222

Chapter 8: Discussion 225

8.1 Novelty of dietary fibre and gut microbiota study for bladder cancer 225
8.2 Psyllium-containing diets are safe to use mice 226
8.3 Psyllium-containing diets increased bacterial fermentations 227
8.4 Psyllium plus inulin increased tumour control with or without IR, with enhancement of SCFAs and immune responses 228
8.5 Psyllium plus RS increased tumour control combined with IR, with enhancement of SCFAs and other metabolites but not immune response 229
8.6 Psyllium plus RS and psyllium plus inulin rescued crypt survival at high IR dose and all psyllium-containing diets prevented the delayed weight gain post IR 230
8.7 The role of butyrate in cancers outside the intestine 231

8.8 Different gut microbiota profiles between tumour-bearing and non-tumour bearing mice 232
8.9 Limitations 233
8.10 Co-culture of *B. acidifaciens* and *F. prausnitzii* increased bacterial fermentation and conferred stronger phenotypes compared to other bacteria 234
8.11 Other evidence for and against the role of the gut microbiota in radiotherapy ...235
8.12 Importance of the work and how it could lead to patient benefits....235
Conclusions....236
Future work....237
List of publications....240
List of oral presentations....241
List of poster presentations....242
References....244
Appendix....270
Glossary....291

Table of Figures

Figure 1 Staging of bladder cancer: non-muscle-invasive bladder cancer (NMIBC) and muscle-invasive bladder cancer (MIBC). 2

Figure 2 Molecular subtypes of bladder cancer: luminal and basal MIBC. 3

Figure 3 Improving the therapeutic ratio of radiotherapy by increasing tumour control and sparing normal tissue toxicity. 9

Figure 4 Intestinal crypts. 12

Figure 5 Gut-associated lymphoid tissue. 13

Figure 6 Gut barrier. 16

Figure 7 Fermentation of dietary fibre by the gut microbiota in production of short-chain fatty acids. 23

Figure 8 Pathways of short-chain fatty acids production. 24

Figure 9 The Warburg effect causes butyrate accumulation and HDAC inhibition. 27

Figure 10 Histone deacetylase inhibition is a promising mechanism of radiosensitisation. 29

Figure 11 Acetate, propionate and butyrate production by gut bacterial fermentation of dietary fibre. 32

Figure 12 T helper cell differentiation. 37

Figure 13 The immune response to IR. 39

Figure 14 Soluble HF causes increased growth delay in irradiated bladder cancer cell xenografts. 48

Figure 15 16S rRNA gene sequencing. 49

Figure 16 Taxonomic classification. 50

Figure 17 Alpha and beta diversity. 51

Figure 18 Cladogram. 52

Figure 19 Flow chart of 16S rRNA gene analysis pipeline. 66

Figure 20 Radiosensitivity of four bladder cancer cell lines.. 80

Figure 21 Tumour growth curves and histological patterns of UPPL1591 and BBN963 mouse bladder cancer cell lines in C57BL/6 mice. 82

Figure 22 Tumour growth curve of G69 mouse bladder cancer cell lines in FVB mice.....84

Figure 23 A unique profile of gut microbiota presented in different strains of mice. 86

Figure 24 High fibre diet increased *B. acidifaciens* abundance in different strains of mice. ...87

Figure 25 Phylogenetic composition, alpha and beta diversity of faecal microbiota a at the species level. 89

Figure 26 Psyllium increased *B. acidifaciens* abundance in FVB mice. 90

Figure 27 Overview of UPPL1591 bladder tumours exposed to different doses of IR. 97

Figure 28 Six to 10 Gy ionising radiation delayed bladder tumour growth. 98

Figure 29 Overview of dietary fibre (corn starch) and UPPL1591 bladder tumour experiment. 100

Figure 30 Psyllium plus either RS or inulin increased growth delay in UPPL1591 bladder tumour allografts. 102

Figure 31 Larger caecal size and longer large intestine in mice fed with psyllium plus RS or inulin. 104

Figure 32 Phylogenetic composition, alpha and beta diversity of faecal microbiota a at the species level. 106

Figure 33 Inulin diet increased *B. animalis* abundance. 107

Figure 34 Overview of dietary fibre (dextrose) and UPPL1591 bladder tumours experiment. 110

Figure 35 Psyllium plus RS and psyllium plus inulin cause increased tumour growth delay in bladder cancer cell allografts. 112

Figure 36 Phylogenetic composition of the faecal microbiota a at the species level. 114

Figure 37 Alpha and beta diversity of the faecal microbiota. 115

Figure 38 Untargeted metabolomics analysis of caecal contents in all dietary groups. 117

Figure 39 Caecal metabolites enriched in different dietary groups. 118

Figure 40 Caecal metabolites enriched in psyllium plus RS. 119

Figure 41 KEGG pathways of pyrimidine, purine and ascorbate and aldarate metabolism enriched in psyllium plus inulin. 120

Figure 42 KEGG pathways of tryptophan, amino sugar and nucleotide sugar, and purine metabolism enriched in psyllium plus resistant starch. 121

Figure 43 Overview of dietary fibre, IR and tumour growth experiment. 123

Figure 44 Psyllium plus RS and psyllium plus inulin cause increased tumour growth delay in bladder cancer cell allografts. 125

Figure 45 Psyllium plus RS or psyllium plus inulin enhanced tumour control combined with IR in bladder cancer cell allografts. 127

Figure 46 Psyllium plus RS radiosensitised UPPL1591 bladder cancer cell allografts. 130

Figure 47 Survival analysis of tumour-bearing mice without and with IR in different dietary groups. 131

Figure 48 Phylogenetic composition of faecal microbiota at the species level. 133

Figure 49 Alpha and beta diversity of faecal microbiota at the species level. 134

Figure 50 Differences in bacterial components in responders and non-responders in the psyllium plus RS group. 136

Figure 51 Differences in bacterial components in responders and non-responders in the psyllium plus inulin group. 137

Figure 52 Unspecified *Bacteroides* species were associated with better tumour control in IR cohort of psyllium plus RS group. 138

Figure 53 S24-7 family was associated with worse tumour control in psyllium plus RS group. 139

Figure 54 Lachnospiraceae family and Clostridiales order were associated with better tumour control in IR cohort of psyllium plus inulin group. 140

Figure 55 Psyllium plus resistant starch or psyllium plus inulin increased caecal butyrate levels. 142

Figure 56 The caecal butyrate level was associated with better tumour control in non-IR and IR cohorts of psyllium plus inulin group. 143

Figure 57 KEGG pathways of metabolites associated with worse tumour control in psyllium plus inulin. 145

Figure 58 The caecal threitol level was associated with better tumour control in the IR cohort of psyllium plus inulin group. 146

Figure 59 KEGG pathways of metabolites associated with worse tumour control in psyllium plus RS. 149

Figure 60 The caecal N-acetyl-glucosamine-1-phosphate level was associated with better tumour control in the IR cohort of psyllium plus resistant starch group. 150

Figure 61 The caecal isoferulic acid level was associated with better tumour control in the IR cohort of psyllium plus resistant starch group. 151

Figure 62 Psyllium plus resistant starch increased caecal isoferulic acid levels. 152

Figure 63 Overview of acute normal tissue toxicity experiment. 161

Figure 64 Psyllium plus RS or psyllium plus inulin mitigated the radiation injury from 14 Gy in intestinal crypt assays. 163

Figure 65 Body weight change 3.75 days after SARRP IR. 165

Figure 66 Phylogenetic composition of faecal microbiota a at the species level. 167

Figure 67 Alpha diversity of gut microbiota in non-tumour-bearing mice 3.75 days after SARRP IR. 168

Figure 68 Beta diversity of gut microbiota in non-tumour-bearing mice 3.75 days after SARRP IR. 170

Figure 69 Untargeted metabolomics analysis of gut microbiota and caecal SCFAs in non-tumour-bearing mice after 3-week modified diet. 172

Figure 70 KEGG pathways enriched in psyllium plus inulin. 173

Figure 71 KEGG pathways enriched in psyllium plus resistant starch. 174

Figure 72 Overview of late normal tissue toxicity experiment. 175

Figure 73 Body weight change within 2 weeks after SARRP IR. 177

Figure 74 Stool frequency after SARRP IR. 179

Figure 75 Voiding volume and frequency after SARRP IR. 181

Figure 76 Ten Gy IR tended to increase intratumoural $CD8^+$ cell numbers. 189

Figure 77 Intratumoural $CD8^+$ cells increased by psyllium plus inulin, but decreased by psyllium plus RS.. 191

Figure 78 Systemic immune response. 193

Figure 79 Local immune responses. 195

Figure 80 Systemic immune responses.....197

Figure 81 Local tumour immunity in psyllium plus inulin stratified by tumour response and IR. 199

Figure 82 Systemic immunity in psyllium plus inulin stratified by tumour response and IR.. 200

Figure 83 Unspecified *Bacteroides* species and Clostridiales order were associated with better tumour control in IR cohorts of psyllium plus RS or inulin groups. 202

Figure 84 Local gut immunity in non-tumour-bearing mice after three-week modified diets. 204

Figure 85 Systemic immunity in non-tumour-bearing mice 3.75 days after SARRP IR. 205

Figure 86 SCFAs conferred radiosensitivity of bladder cancer cells. 210

Figure 87 SCFAs increased histone acetylation levels in bladder cancer cells in a dose-dependent manner. 212

Figure 88 Bacterial supernatants from *B. acidifaciens* enhanced the cytotoxic response in bladder cancer cells. 214

Figure 89 *BA+FP* increased histone acetylation levels and DNA damage in bladder cancer cells. 216

Figure 90 *BA+FP* increased histone acetylation levels and DNA damage in RT112 bladder cancer cells. 217

Figure 91 *BA+FP* increased histone acetylation levels and DNA damage in T24 bladder cancer cells. 218

Figure 92 Principal component analysis of metabolomes in all bacterial groups.....219

Figure 93 Metabolites enriched in the supernatant of *BA+FP*.....220

Figure 94 SCFAs conferred increased radiosensitivity in bladder cancer cells. 221

Table of Tables

Table 1 Function of genes or proteins in bladder cancers. 4

Table 2 Physiochemical characteristics of common dietary fibres. 21

Table 3 Functions of innate immune cells. 36

Table 4 Functions of adaptive immune cells. 36

Table 5 Definitions of immune cell populations based on expression of cell surface markers. 70

Table 6 Antibody titrations and catalogue numbers. 70

Table 7 Cytokine panels. 71

Table 8 Details of bladder cancer cell lines. 80

Table 9 Overview of the study and sample sizes. 93

Table 10 Metabolites that positively or negatively correlated to tumour growth in psyllium plus inulin. 144

Table 11 Metabolites that positively or negatively correlated to tumour growth in psyllium plus RS. 148

Table 12 Overview of the study and sample sizes. 157

Table 13 Immunology. 185

Table 14 Functions of immune cells. 186

Table 15 Physiochemical characteristics of common dietary fibres. 237

Table A1 Rodent diets used in the study with varying levels of cellulose, psyllium, resistant starch or inulin per 4000 kcal. 270

Table A2 Rodent diets used in the study with varying levels of psyllium plus resistant starch or inulin per 4000 kcal. 271

Table A3 Rodent diets without corn starch used in the study with varying levels of cellulose, psyllium, psyllium plus resistant starch, or inulin per 4000 kcal. 272

Table A4 Metabolites that positively or negatively correlated with tumour growth in psyllium plus inulin-treated mice. 273

Table A5 Metabolites that positively or negatively correlated with tumour growth in psyllium plus inulin-treated mice.....278

Table A6 Average and standard deviation of the relative abundance (%) for the top 30 taxa with the highest abundances for section 4.2.5.....283

Table A7 Average and standard deviation of the relative abundance (%) for the top 30 taxa with the highest abundances for section 4.3.3.....284

Table A8 Average of the relative abundance (%) for the top 30 taxa with the highest abundances for section 4.4.7.....285

Table A9 Standard deviation of the relative abundance (%) for the top 30 taxa with the highest abundances for section 4.4.7.....286

Table A10 Average of the relative abundance (%) for the top 30 taxa with the highest abundances for section 5.1.4 (0.2% cellulose and psyllium). 287

Table A11 Average of the relative abundance (%) for the top 30 taxa with the highest abundances for section 5.1.4 (psyllium plus RS and psyllium plus inulin).....288

Table A12 Standard deviation of the relative abundance (%) for the top 30 taxa with the highest abundances for section 5.1.4 (0.2% cellulose and psyllium).....289

Table A13 Standard deviation of the relative abundance (%) for the top 30 taxa with the highest abundances for section 5.1.4 (psyllium plus RS and psyllium plus inulin). 290

List of abbreviations

ANOVA	analysis of variance
APC	antigen-presenting cell
ASC	apoptosis-associated speck-like protein
ARRIVE	Animal Research: Reporting of In Vivo Experiments
B. acidifaciens	*Bacteroides acidifaciens*
B. animalis	*Bifidobacterium animalis*
BBN	N-butyl-N-(4-hydroxybutyl)-nitrosamine
Bif	*Bifidobacterium*
BSA	bovine serum albumin
CIS	carcinoma in situ
CTL	cytotoxic T lymphocyte
DAMP	damage-associated molecular pattern
DC	dendritic cell
DMEM	Dulbecco's modified eagle medium
DSB	double-strand break
DS-FDR	discrete false-discovery rate
DSS	dextran sulfate sodium
EMEM	Eagle's minimum essential medium
FACS	fluorescence activated cell sorting
FFPE	formalin-fixed paraffin embedded
FOS	fructo-oligosaccharide
F. prausnitzii	*Faecalibacterium prausnitzii*
GALT	gut-associated lymphoid tissue
GAM	Gifu anaerobic medium
GI	gastrointestinal
GM-CSF	granulocyte macrophage colony-stimulating factor
GPCR	G-protein-coupled receptor
GOS	galacto-oligosaccharide
Gy	gray
HAT	histone acetyltransferase
HBSS	Hank's balanced salt solution
HDAC	histone deacetylase
HDACi	histone deacetylase inhibitor
H&E	haematoxylin and eosin
HF	high fibre
IC-MS	ion chromatography mass spectrometry
Ig	immunoglobulin
IHC	immunohistochemistry
IL	interleukin
IR	ionising radiation
KEGG	Kyoto Encyclopedia of Genes and Genomes

KW	Kruskal Wallis
LDA	linear discriminant analysis
LEfSe	linear discriminant analysis effect size
LF	low fibre
LPS	lipopolysaccharide
MHC	major histocompatibility complex
MIBC	muscle-invasive bladder cancer
MTT	methylthiazolyldiphenyl-tetrazolium bromide
MW	Mann-Whitney
NHEJ	non-homologous end joining
NK cell	natural killer cell
nMIBC	non-muscle-invasive bladder cancer
OTU	operational taxonomic unit
PBS	phosphate-buffered saline
PCA	principle component analysis
PCoA	principal co-ordinates analysis
PD-1	programmed cell death 1
PERMANOVA	permutational multivariate analysis of variance
PGE	prostaglandin E
PLS-DA	partial least-squares discriminant analysis
QIIME2	Quantitative Insights Into Microbial Ecology 2
RS	resistant starch
RT	radiotherapy
RT	room temperature
SARRP	small animal radiation research platform
SCC	squamous cell carcinoma
SCFA	short chain fatty acid
SDS-PAGE	sodium dodecyl sulfate-polyacrylamide gel electrophoresis
SEM	standard error of the mean
SILT	solitary intestine lymphoid tissue
SPF	specific pathogen-free
STD	standard deviation
TAMs	tumour-associated macrophage
Th	T helper
TILs	tumour-infiltrating lymphocytes
TNF	tumour necrosis factor

Chapter 1: Introduction

1.1 Bladder cancer

1.1.1 Epidemiology and presenting symptoms

Bladder cancer is the tenth most prevalent cancer worldwide with 549,393 new cases (total number of male and female cases), causing 199,922 deaths in 2018 (Bray *et al.*, 2018). In the UK, 20,500 people are newly diagnosed with bladder cancer every year (*Action Bladder Cancer UK*, 2022) and the median age is approximately 73 years old (Erlich & Zlotta, 2016). The disease incidence increases with age, with 109, 293 and 546 cases per 100,000 person-years for the 60-69, 70-79 and 80-89 year-old populations, respectively (*Cancer Research UK Bladder cancer statistics*). Bladder cancer is more prevalent in men than in women (3.38:1 ratio) (Bray *et al.*, 2018), and diagnosis can often be late, especially in women, which leads to a worse survival. Cigarette smoking is the major risk factor for bladder cancer, accounting for 50%-65% and 20-30% of total cases in men and in women (Freedman *et al.*, 2011). There are 6% and 2% of total cases caused by occupational exposures to chemical and water contaminants, and ionising radiation, respectively (Kiriluk *et al.*, 2012). Microscopic or macroscopic (visible) blood in the urine (haematuria) is the most common symptom which is associated with an advanced pathological stage (Ramirez *et al.*, 2016). Some bladder cancer patients might also present with increased urinary frequency, urgency and dysuria (DeSouza *et al.*, 2014).

1.1.2 Tumour types and stages

Bladder cancer can be classified as non-muscle-invasive bladder cancer (NMIBC; 80%) and muscle-invasive bladder cancer (MIBC; 20%) (Figure 1) (Sanli *et al.*, 2017; Tran *et al.*, 2021). NMIBC includes carcinoma in situ (CIS), stage Ta and T1, whereas MIBC covers stage T2a, T2b, T3 and T4. CIS is an early, flat but poorly differentiated tumour confined to the mucosa. Ta and T1 refer to papillary tumours that are confined to mucosa or have invaded the lamina propria (submucosa), respectively. T2a or T2b tumours have invaded the superficial or deep muscle layer. T3 tumours have invaded beyond the muscularis propria into perivesical tissue. T4a tumours have invaded the prostate, uterus, vagina and/or bowel, whereas T4b tumours

have invaded the pelvic or abdominal walls. There is also a metastatic form of this disease which has spread to distant organs. The 5-year relapse-free survival rates were 43%, 33% and 23% for low-, intermediate- and high-risk NMIBC, and there was about 21% high-risk NMIBC would develop to MIBC (Lenis *et al.*, 2020). The 5-year overall survival rate was 36% to 48% for non-metastatic MIBC, and the 5-year relative survival was 36% and 5% for regional and distant metastatic MIBC.

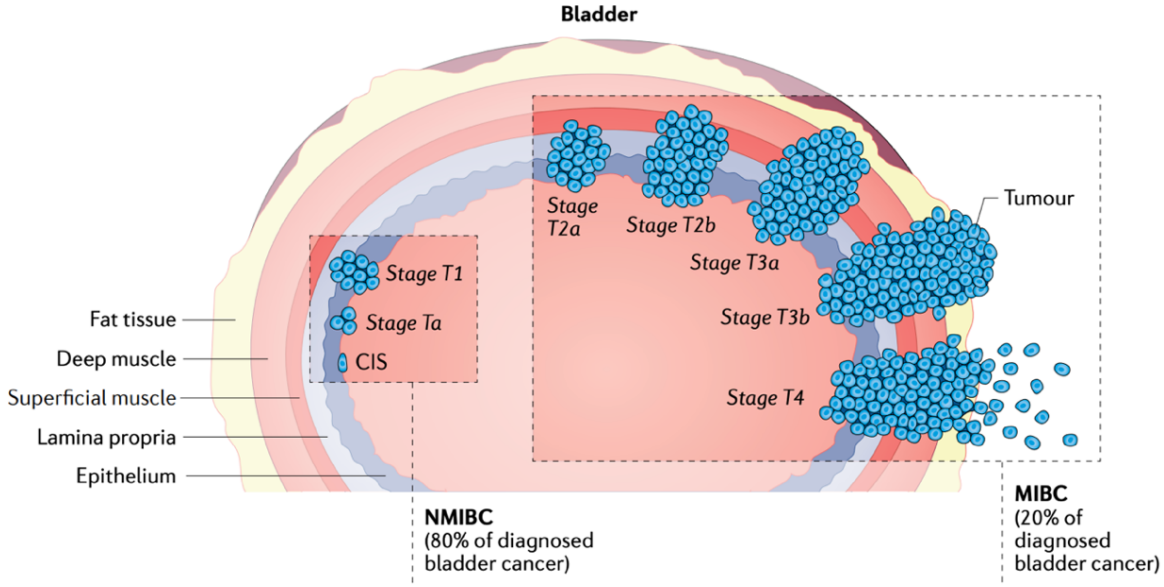


Figure 1 Staging of bladder cancer: non-muscle-invasive bladder cancer (NMIBC) and muscle-invasive bladder cancer (MIBC). It is generally classified as non-muscle-invasive (CIS, Ta, T1) and muscle invasive-bladder-cancer (T2a, T2b, T3, T4) with different clinical outcomes and treatment options. Highly specialised epithelium that lines the lower urinary tract is called urothelium. From Tran *et al.*, 2021.

1.1.3 Muscle-invasive molecular subtypes

Bladder cancer generally originates from the bladder urothelium, and is a consequence of chronic exposure of the urothelium to carcinogens (Choi, Czemiak*, et al.*, 2014). In MIBC, luminal- and basal-like subtypes are the two major intrinsic molecular subsets defined by the University of North Carolina (Figure 2) (Choi, Czemiak*, et al.*, 2014; Damrauer *et al.*, 2014), although a more recently further subclassification of six non-overlapping molecular subtypes that could stratify treatment responses have been described, namely luminal papillary (24%),

luminal nonspecified (8%), luminal unstable (15%), stroma-rich (15%), basal/squamous (35%), and neuroendocrine-like (3%) (Kamoun *et al.*, 2020).

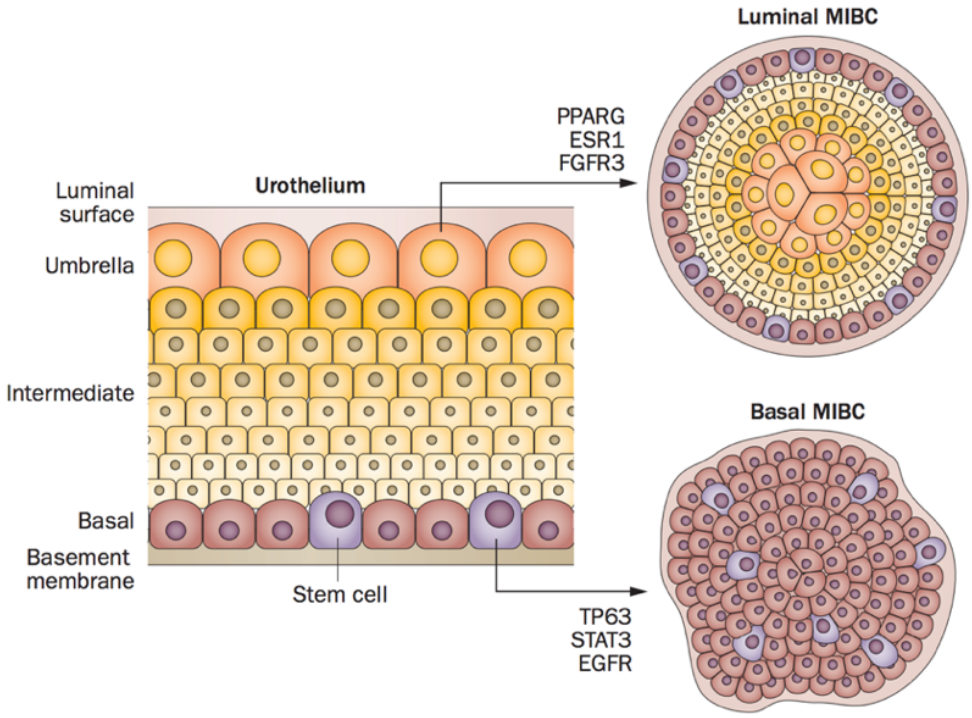


Figure 2 Molecular subtypes of bladder cancer: luminal and basal MIBC. The biomarkers are FOXA1, GATA3 and PPARG for luminal MIBC, and TP63, STAT3 and EGFR for basal MIBC. From Choi, Porten*, et al.*, 2014.

Luminal MIBCs arise from terminally differentiated umbrella cells that mediate the barrier function of the urothelium, and express uroplakins of UPK1–UKP3 that are urothelial lineage-specific proteins (Damrauer *et al.*, 2014). Luminal tumours display papillary histopathological features and so are considered as originating from NMIBCs. They are enriched with transcriptions factors, including FOXA1, GATA3 and PPARG, and are characterised by high frequencies of *GFR3*, *ERBB2* and *ERBB3* mutations. Basal MIBCs originate from basal and stem cells within the urothelium and exhibit squamous features (Cancer Genome Atlas Research, 2014). They are characterised by overexpression of EGFR and transcription factors, such as ΔNp63α, p63, STAT3 and HIF1. Function of genes or proteins in bladder cancers are listed in Table 1.

Table 1 Function of genes or proteins in bladder cancers.

Gene/protein	Functions
UPK	To form plaques on the apical surfaces of urothelium for the maintenance of permeability barrier (Carpenter *et al.*, 2016)
FOXA1	Its loss is associated with an increased tumour proliferation (DeGraff *et al.*, 2012)
GATA3	To suppress bladder cancer migration and invasion (Li *et al.*, 2014)
PPARG	To inhibit cell proliferation and promote apoptosis (Peng *et al.*, 2020)
GFR3	Its activation and overexpression are associated with cancer occurrence, development, and invasion (Mao *et al.*, 2019)
ERBB2	To promote proliferation and invasiveness of cancer cells (Chen *et al.*, 2021)
ERBB3	May inhibit cancer cell growth and migration (Chen *et al.*, 2021)
EGFR	To increase cell proliferation and angiogenesis, and inhibit apoptosis (Colquhoun & Mellon, 2002)
ΔNp63α	To promote survival, proliferation and tumourigenesis, and suppress epithelial-mesenchymal transition (Tran *et al.*, 2013)
p63	To inhibit tumourigenesis and metastasis (Tran *et al.*, 2013)
STAT3	To increase tumour cell viability and invasion (Gatta *et al.*, 2019)
HIF1	To promote epithelial-mesenchymal transition (Zhu *et al.*, 2018)

Basal MIBCs are more intrinsically aggressive and associated with advanced stage and metastatic disease at presentation. The basal subtype also has worse disease-specific and overall survival compared to the luminal subtype (Choi, Porten*, et al.*, 2014; Kamoun *et al.*, 2020). Between 40% to 60% patients respond to neoadjuvant chemotherapy for both luminal and basal subtypes (Choi, Porten*, et al.*, 2014) but they might respond differently to radiotherapy. Luminal unstable, one of the luminal subtypes, had elevated cell cycle activity and low hypoxia signals in comparison to basal subtypes, implying that the luminal unstable subtype might be more sensitive to radiotherapy (Kamoun *et al.*, 2020).

1.1.4 Treatment options

In general, NMIBCs are frequently managed with endoscopic resection - transurethral bladder tumour resection followed by intravesical bacille Calmette-Guérin or intravesical chemotherapy. MIBCs are managed by more aggressive treatments consisting of radical cystectomy (bladder removal) with or without neoadjuvant chemotherapy, or bladder-sparing approaches comprising chemotherapy and radiotherapy. Combining radiotherapy and immunotherapy is also being studied in several clinical trials (Daro-Faye *et al.*, 2021). For patients with metastatic disease or unresectable bladder cancer, systemic chemotherapy is currently the preferred treatment option. The mean of survival was less than 10 months in patients with metastatic bladder cancer (Shou *et al.*, 2021)

1.2 Radiotherapy

Radiotherapy (RT) is given to approximately 50% of cancer patients during their cancer management and attributes 40% of curative treatment (Harrington *et al.*, 2011). Compared to chemotherapy, RT is a localised treatment, specifically targeting defined volumes of tissue including tumours and normal tissues. It can be used in the following situations: definitive/curative (radical) treatment, adjuvant therapy following surgery or palliative treatment to ameliorate cancer-related symptoms.

1.2.1 Radiation-induced cell killing

In radiotherapy, ionising radiation (IR) consists of high-energy particles (alpha particles, beta particles, X-rays, gamma rays, and proton) that are capable of displacing electrons (ionisation) from molecules in cells (Reisz *et al.*, 2014). Ionised molecules are highly reactive that can initiate a cascade of chemical reactions, breaking chemical bonds and disrupting macromolecules. IR results in DNA damage either directly (approximately 33% of total damage) or indirectly (about 67% of total damage) (Olcina & Giaccia, 2016). Direct damage is caused by the interaction between ionising radiation and DNA molecules, whereas indirect damage results from interaction with water by ionisation, leading to production of highly reactive hydroxyl (HO•) and alkoxy (RO2•) radicals that damage DNA (Desouky *et al.*, 2015). Direct or indirect damage to DNA in the form of DNA breaks or replication stress elicits a DNA damage response, consisting of p53 activation and cell cycle arrest, senescence, or apoptosis.

IR damages DNA of cells and thus deprives them of their ability to proliferate (Jackson & Bartek, 2009). If unrepaired, the permanent damage to DNA ultimately results in killing of the cancer cells. The gray (Gy) is a derived unit of ionising radiation dose in the International System of Units, defined as the absorption of one joule of radiation energy per kilogram of matter. One Gy causes approximately 10^5 ionisations, 1,000 single-strand breaks (SSBs) and 20-40 double-strand DNA breaks (DSBs) per cell (Ward, 2000). Double strand DNA breaks are more responsible than single strand DNA breaks for most of the cell killing as they are the

most difficult lesions to repair and require homologous recombination (HR) and nonhomologous end-joining (NHEJ) processes. HR results in accurate repair and is restricted to the S and G2 phases of the cell cycle due to the need for a sister chromatid as a template, while NHEJ is intrinsically mutagenic and is active throughout the cell cycle and does not require a template (Mao *et al.*, 2008).

Effectively targeting the tumour while sparing normal surrounding tissue is the goal of radiotherapy. Normal cells can repair RT-induced DNA damage at a faster rate and retain their normal function status, while cancer cells have a less efficient ability in repairing the DNA damage, resulting in differential cancer cell killing (Begg *et al.*, 2011).

1.2.2 Radiotherapy of bladder cancer

Radiotherapy (RT) has an important role in the treatment of muscle-invasive bladder cancer because both radical radiotherapy (a complete treatment using potential curative, high dose radiation) and radical cystectomy can achieve 5-year cause-specific survival rates of 56.8% and 53.4%, respectively (Kotwal *et al.*, 2008). However, the survival rate is still not optimal as the five- and ten-year survival rates are only 57% and 39% (Efstathiou *et al.*, 2012). Although surgical removal of the bladder (cystectomy) is one of the current radical approaches in treating MIBC, urinary diversion after cystectomy can profoundly reduce the quality of life in elderly patients, and many are not sufficiently medical fit to undergo such radical surgery. Most MIBC patients respond to cisplatin-based neoadjuvant combination chemotherapy, but estimates of disease-specific survival suggest that chemotherapy has only a 5–10% benefit over conventional surgery (Grossman *et al.*, 2003; Sternberg *et al.*, 2013). Radical radiotherapy has been considered as an alternative to cystectomy, with similar cause-specific survival rates (Kotwal *et al.*, 2008). Chemoradiation is another promising treatment for MIBC for some years due to considerable interest in bladder preservation, particular in less fit patients (Boustani *et al.*, 2018; Hautmann *et al.*, 2012; James *et al.*, 2012). However, elderly patients are very vulnerable to chemotherapy-related toxicity as they typically have other medical comorbidities such as diabetes mellitus, chronic obstructive pulmonary disease, and congestive heart failure (Guancial *et al.*, 2015).

1.2.3 Acute and late side effects in the pelvis

The intestine is a dose limiting organ in abdominal and pelvic radiotherapy due to its high sensitivity to IR. Around 80% RT of patients develop acute gastrointestinal symptoms (Andreyev, 2005) as it is inevitable that some normal gut tissue is exposed to radiation during pelvic RT (Lawrie *et al.*, 2018). Radiation causes DNA damage, cell death and loss of epithelial integrity (Shadad *et al.*, 2013). These processes lead to acute symptoms, such as diarrhoea, vomiting, rectal bleeding, and tenesmus, usually occur during or immediately after RT. These symptoms are normally self-limited or resolve within three months after completion of RT (Do *et al.*, 2011). However, after 3 months and beyond, late symptoms may develop as a result of small vessel endothelial damage, fibrosis, ischemia and atrophy. These are gastrointestinal (GI) bleeding (7.5%), colostomy (0.7%), stricture (0.4%), and fistula (0.3%), which lead to malabsorption (S. Kim *et al.*, 2011; Turina *et al.*, 2008; Wang & Tepper, 2021). Delayed radiation enteropathy (intestinal radiation toxicity) might present 3 months to 6 years after RT and has been reported to occur in up to 40% of patients receiving abdominal or pelvic radiotherapy, less frequent than acute toxicity (Hauer-Jensen *et al.*, 2014).

1.2.4 Aim to increase therapeutic ratio of radiotherapy

The optimisation of the efficacy and safety of radiotherapy treatments is essential. The therapeutic ratio is an important parameter in efforts to achieve the balance between the effects on tumour tissue versus those on normal tissue. In RT, this ratio is considered as the ratio of the highest tumour exposure to IR that leads to acceptable toxicity of the normal tissue in the organs at risk (Zindler *et al.*, 2016). The therapeutic ratio presents as a sigmoidal relationship between the dose and effects on normal tissues and tumours; the therapeutic ratio is calculated as the difference between both curves (Figure 3).

There are biological and physical methods which can be used to increase the therapeutic ratio. Biologically, rather than giving one large dose of radiation, ‘fractionation’, the delivery of low doses usually daily, results in more tumour cells being killed compared to late-reacting cells such as endothelial cells and fibroblasts. Physically, modern radiotherapy techniques such as intensity modulated radiotherapy can deliver higher doses to the tumour while

minimising the dose delivered to the surrounding normal tissues (Intensity Modulated Radiation Therapy Collaborative Working, 2001).

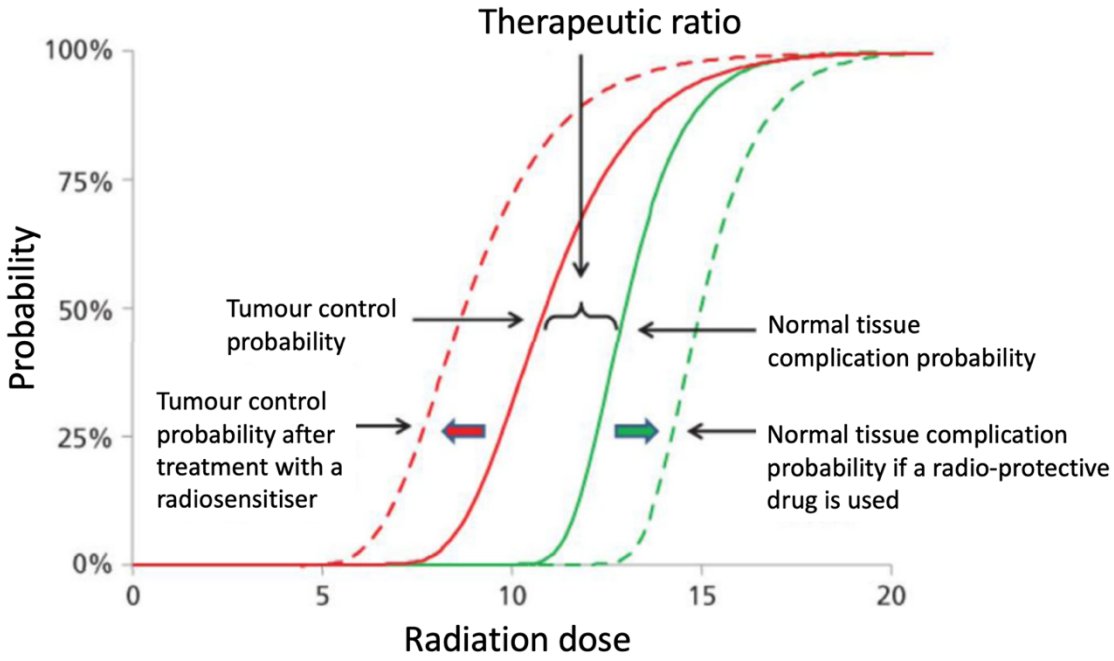


Figure 3 Improving the therapeutic ratio of radiotherapy by increasing tumour control and sparing normal tissue toxicity. The therapeutic ratio is a quantitative measurement of the relationship between the probability of tumour control and the likelihood of normal tissue damage. An improved therapeutic ratio represents a more favourable trade-off between tumour control and toxicity. Adapted from DuRoss *et al.*, 2019.

1.2.5 Concept of radiosensitisation

The therapeutic ratio can be increased by the use of radiosensitisers for tumours or the use of radioprotectors and mitigators for normal surrounding tissues. Radiosensitisation involves enhancing the radiosensitivity of tumour cells by introducing specific molecules (radiosensitisers) in combination with radiotherapy that increase damage to cancer cells. The earliest strategies of radiosensitisation applied the induction of free-radical damage by increasing oxygen delivery to the tumour using oxygen-mimicking compounds (Oronsky *et al.*, 2011). Oxygen is a well-known radiosensitiser because it has a high affinity for electrons and can be rapidly added to free radicals, thus generating a chain reaction of reactive radicals to damage the DNA, thus causing cell death. Nowadays, tumour radiosensitisation is

achieved by combining radiotherapy with chemotherapeutic agents, often platinum-based. In patients with bladder cancers, radiosensitisation with cisplatin is not ideal because many of these patients have impaired renal function or poor performance status. In the Bladder Cancer 2001 (BC2001) trial, synchronous chemoradiotherapy with fluorouracil and mitomycin C was shown to be more efficacious than radiotherapy alone (James *et al.*, 2012).

When investigating radiosensitisation, the clonogenic assay and tumour growth delay are the most well-accepted techniques to study the effects of radiation on cancer cells for cell and mouse experiments. The clonogenic assay is a cell survival assay used to determine the ability of a single cell to grow into a colony (defined as over 50 cells) as a measurement of cell reproductive death after treated with ionising radiation (Franken *et al.*, 2006). Tumour growth delay is an experimental animal tumour model to study the radiation effect. The non-irradiated tumour grows rapidly at a relatively uniform rate, while the irradiation causes a temporary shrinkage of the tumour, followed by regrowth exponentially after a period of time at the same growth rate as the non-irradiated tumours (Demidenko, 2010).

1.3 Anatomy of the intestine

1.3.1 Macroscopic - small and large intestine, caecum

The small and large intestines are a continuous tube starting from the stomach and ending at the anus with a columnar epithelium lining on the internal surface (Mowat & Agace, 2014). The small intestine is divided into three segments, namely, duodenum, jejunum, and ileum. The duodenum is connected to the pylorus of the stomach, followed by the jejunum and then the ileum that terminates at the ileocecal valve. The large intestine begins at the caecum, followed by the ascending (proximal) colon, the transverse colon, the descending (distal) colon and the rectum. The small intestine in humans arranges in multiple coils with a total length of six to seven metres; the colon has a wider diameter and is much shorter than the small intestine at 1.5 metres length. Descending the small and large intestines, there are increasing numbers of gut bacteria with higher amounts of short-chain fatty acids produced by them (Mowat & Agace, 2014).

1.3.2 Microscopic - crypts and Peyer's patches

Villi and crypts

In the small intestine, the epithelium is organised into fingered-like projections known as villi and crypts. One villus is surrounded by multiple crypts. In contrast, the caecum and the colon have no villi and the inner surface is flat. The intestinal crypt is the basic functional unit of the small and large intestines (Figure 4). Approximately 60% of the intestinal epithelial cell population proliferates through its cell cycle every 12 hours (Potten & Grant, 1998) which is one of the most rapidly renewing systems in the human body (Olcina & Giaccia, 2016). This intestinal surface epithelium is regularly renewed by ancestral stem cells that give rise to several types of mature epithelial cells. Most of these cells are absorptive enterocytes, and the others are Paneth cells, goblet cells and neuroendocrine cells. They migrate along the villi before being shed into the lumen and it takes about six to eight days for cells to move from the base of crypt to the tip of the villus.

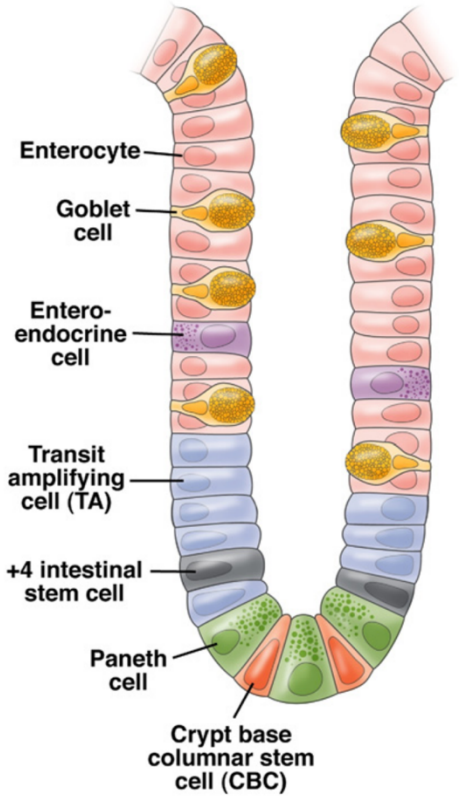


Figure 4 Intestinal crypts. Intestinal epithelial stem cells give rise to enterocytes and the secretory cell lineages, such as goblet cells, enteroendocrine cells, and Paneth cells. From Madison & Nakagawa, 2011.

Gut-associated lymphoid tissue (GALT)

Effector immune cells are diffusely distributed throughout the overlying epithelium and lamina propria. Beneath the intestinal epithelium, there are lymphoid aggregates that lie in the mucosa and submucosa, which are characterised by an overlying follicle-associated epithelium. They are known as gut-associated lymphoid tissue (GALT) and are the principal locations for priming adaptive immune responses, working together with the draining lymph nodes in the small and large intestine (Figure 5). Peyer's patches are the components of the GALT found along the mucosa and submucosa of the small intestine and mainly contain CD4, CD8 T cells and IgA-producing B cells. The size and density of Peyer's patches increase from the jejunum to the ileum and are particularly concentrated in the distal ileum (Mowat & Agace, 2014). Secretory IgA produced from activated B cells can either enter systemically into the mesenteric lymphatic system or protect the gut barrier by preventing pathogens

from adhering to the intestinal surface (Lycke & Bemark, 2017). The GALT also includes solitary isolated lymphoid tissues (SILTs) that are smaller lymphoid aggregates which can only be detected microscopically (Mowat & Agace, 2014). These are concentrated in the distal colon and are involved in initiating local gut IgA responses.

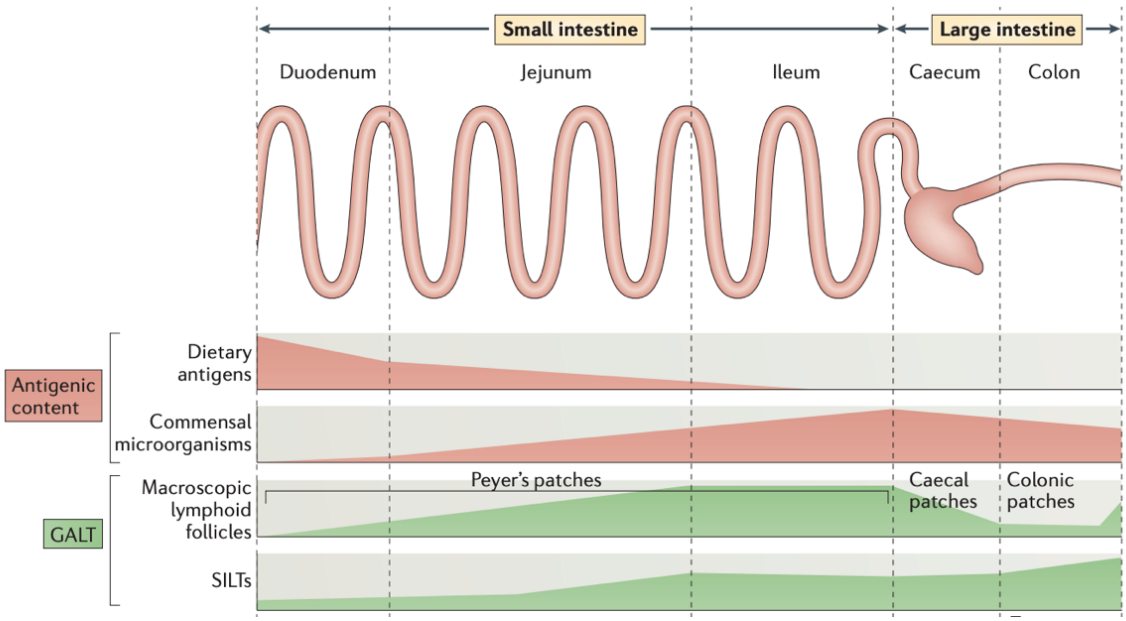


Figure 5 Gut-associated lymphoid tissue. The Peyer's patches increase along the small intestine and decrease in the caecum and colon. From Mowat & Agace, 2014.

1.3.3 Sensitivity to IR and physiology/function

Chromatin in mitotic cells is more susceptible to radiation-induced DNA damage than the dispersed chromatin of interphase cells (Stobbe *et al.*, 2002). Therefore, the gut mucosa is very sensitive to radiation due to its high turnover rate of 5 days (Potten, 1977). Apoptosis and mitotic cell death are the two major forms of cell death induced by irradiation (Hendry & West, 1997). The former is a form of programmed cell death in the absence of immune surveillance that includes blebbing, cell shrinkage and DNA fragmentation, while the latter one is the failure of cells to divide successfully due to chromosomal damage. Radiation doses higher than 10 Gy are sufficient to damage the intestinal mucosa which leads to gastrointestinal toxic effects in patients receiving abdominal and pelvic radiotherapy (Booth *et al.*, 2012). The more extensive apoptosis following high radiation doses leads to gastrointestinal failure due to the failure of repopulation of the intestinal epithelial cells. Within hours of exposure to ionising radiation, epithelial cells in the crypt undergo early p53-dependent apoptosis which results in shrinkage of the crypts, and inadequate replacement of the surface epithelium after apoptotic and mitotic death in the crypt results in damage to the intestinal epithelium. Once the epithelial barrier breaks down, intestinal mucositis symptoms, including abdominal pain, nausea, and diarrhoea, occur due to fluid loss and bacterial invasion (Erickson *et al.*, 1994).

After IR-induced intestinal epithelium damage, the regenerative responses occur in three phases: apoptotic phase, proliferative phase, and normalisation phase. The apoptotic phase occurs during the first 2 days after irradiation with the histology of continuous crypt loss, shrinkage of crypt size and shortening of the villi (Kim *et al.*, 2017). Between two to four days post irradiation, the subsequent regenerative phase is characterised by regeneration of entire crypts from the surviving crypt cells. The increase in proliferating cell numbers enlarges the size of regenerative crypts, despite the number of crypts decreasing in both small and large intestine. During the normalisation phase, the size of the crypts and the length of the villi are restored to the “homeostatic” conditions seen prior to irradiation.

1.4 Gut barrier functions

The three interacting components of gut mucosal barrier are the mucous layer, the intestinal epithelium, and the mucosal immune system (Figure 6). The intestinal mucous layer is composed of complex glycoproteins, called mucins, important as the first-line of defence and a transport vehicle between luminal contents and the intestinal epithelium. In the large intestine, there are two mucous layers, a loose outer layer where the gut microbiota resides and a dense inner layer that contains IgA and antimicrobial peptides. The intestinal epithelium forms a semipermeable barrier for the absorption of nutrients, electrolytes, and water, but also for protection of the host from the microbiota and toxic molecules entering the circulation (Camilleri *et al.*, 2019). Under the epithelium, various immune cells reside, including CD4, CD8 T cells and plasma cells (that can produce IgA), are all required for the regulation of immune responses.

Diet can shape the structure and function of the intestinal barrier. For instance, short-chain fatty acids (SCFAs) produced by the fermentation of high dietary fibre are utilised by the colonic enterocytes as their primary energy source. In addition, butyrate can activate regulatory T cells to induce immune tolerance. Gut microbiota-derived metabolites can also increase IL-22 produced by innate lymphoid cells. This can further enhance the production of mucin and antimicrobial peptides by the intestinal epithelium for the reinforcement of gut barrier function (Chelakkot *et al.*, 2018).

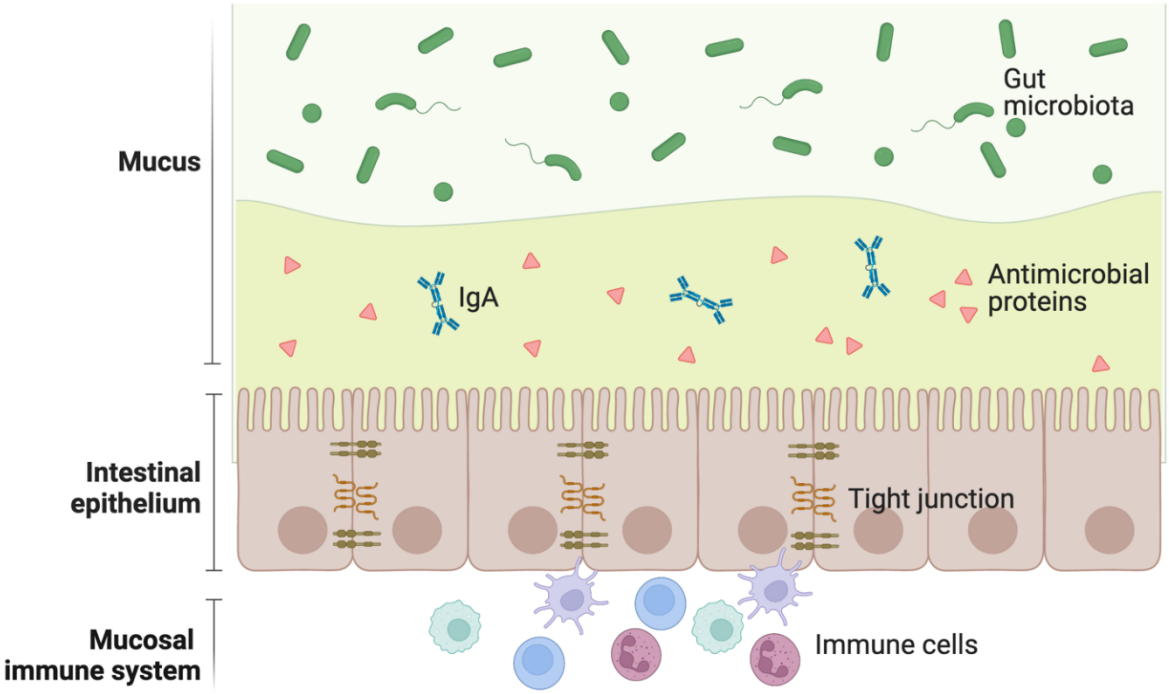


Figure 6 Gut barrier. Gut barrier is constituted of mucus, intestinal epithelium, and mucosal immune system. Figure created with Biorender.com.

1.5 Radiation effects on the intestine

The crypt is the basic functional unit of the intestine. Intestinal stem cells and progenitor cells reside at the crypt base and are responsible for the rapid renewal of the epithelium, brought about by those cells dividing, differentiating, and migrating up to the tip of the intestinal villi. These stem cells and progenitor cells are mitotic cells targeted by ionising radiation and their death is the primary cause of radiation-induced gastrointestinal symptoms.

Paris *et al.* showed that clinically-relevant total body irradiation doses, above 8 Gy, cause dose-dependent stem cell death resulting in impairment of crypt regeneration, insufficient to rescue the gastrointestinal mucosa in C57BL/6 mice (Paris *et al.*, 2001). In that decompensation situation, by 6 to 7 days post irradiation, progressive epithelial damage leads to gastrointestinal acute radiation syndrome (GI-ARS) and death of mice. The GI-ARS includes diarrhoea, dehydration, enterobacterial infection, and even septic shock and death. The survival rate at 14 Gy differed significantly from that after 15 Gy, which might be strain-dependent. When the mice received 12 to 14 Gy, most of them died 10 to 13 days post-irradiation with bone marrow aplasia but an intact intestinal mucosa. In contrast, following exposure to 15 Gy, most of the mice died within 6 to 8 days. At that time, the animals only had partially damaged bone marrow, but denudation of the intestinal crypt and villus system. Another study found that IR doses of higher than 8 Gy induced loss of crypts in the small intestine, with death within 10 days (Booth *et al.*, 2012). There were about 50% and 10% crypts remaining in the small intestine after exposure to 8 Gy and 11 Gy irradiation, respectively.

1.6 Dietary fibre

1.6.1 Distinguishing soluble/insoluble from nondigestible/digestion-resistant fibres

Dietary fibre is the edible part of plant material which is resistant to enzymatic digestion in small intestine and partially or completely fermented in the large intestine (Dhingra *et al.*, 2012). It can be divided into three broad categories: resistant oligosaccharides, non-starch polysaccharides, and resistant starch (RS) (Dhingra *et al.*, 2012). Oligosaccharides and polysaccharides are the main components of plant cell walls. Resistant starch is the plant's energy store in the human diet and some of them are formed after cooking. Dietary fibres are diverse in chemical structure and physico-chemical properties, and they can be generally classified based on their water solubility, viscosity and fermentability, that influence their functional effects in the gastrointestinal tract.

1.6.2 Types of dietary fibre

Fibre solubility refers to the extent to which dietary fibres can dissolve in water (Gill *et al.*, 2021). Soluble fibres have a high affinity for water and insoluble fibres remain as discrete particles. Most of the insoluble fibres, such as cellulose and hemi-cellulose, have a faecal bulking effect, as they reach the colon and are not, or poorly, digested by the gut bacteria. In contrast, most soluble fibres, including amylose, amylopectin, and inulin, do not contribute to faecal bulking, but are fermented by the gut bacteria and thus produce short-chain fatty acids and gas.

Viscosity is the degree of resistance to flow and generally relates to the ability of a fibre, when hydrated, to thicken in a concentration-dependent manner (Dikeman & Fahey, 2006). Most soluble non-starch polysaccharides, especially polymers with high molecular weight, such as guar gum, certain pectins, β-glucans, and psyllium, are viscous. They can form a gel structure in the intestinal tract that delays the absorption of glucose and lipids, and thus blunts the glycaemic responses, that is, the effect of food on blood glucose levels after consumption, and reduces plasma cholesterol levels (Chutkan *et al.*, 2012).

Fibre fermentability is the extent to which dietary fibres can be broken down by the gut microbiota to predominantly result in the production of SCFA such as acetic, propionic, and butyric acids. A range of other carboxylic acids can also be produced, including lactic acid (Tan *et al.*, 2014). Examples of fermentable fibres include inulin-type fructans, galacto-oligosaccharides and resistant starch. Greater intake of dietary fibre, particularly from foods high in the fermentable fibres, sometimes could be associated with higher stool SCFA concentrations in adults (Baxter *et al.*, 2019).

1.6.3 Relevance to pelvic radiotherapy clinically

As well as disease prevention, dietary fibre has the potential to be used as a therapeutic intervention, in particular for disorders of the gastrointestinal tract, such as alleviating constipation and reducing the risk of developing colorectal cancer. In cancer patients receiving radiotherapy, several dietary fibres can mitigate the side effects of radiotherapy. For example, psyllium has been shown to be effective in reducing the incidence and severity of radiation-induced diarrhoea (Murphy *et al.*, 2000). In addition, intake of hydrolysed rice bran was also associated with the alleviation of diarrhoeal symptoms after chemoradiotherapy in patients with cervical cancer (Itoh *et al.*, 2015). A combination of prebiotics, 50% inulin plus 50% fructo-oligosaccharide, improved stool consistency by lowering the number of days with watery stool in gynaecological cancer patients receiving radiotherapy (Garcia-Peris *et al.*, 2016).

1.6.4 Psyllium

Psyllium husk, derived from the seeds of Plantago ovata, is a non-fermentable fibre but its high solubility and viscosity results in unique therapeutic effects including improved glycaemic control and reduced blood cholesterol levels. Psyllium can absorb excess water in the small and large intestine, and thereby, it can relieve the symptoms of both constipation and mild diarrhoea. A recent clinical study of psyllium showed that higher amounts of faecal water increased the abundance of butyrate-producing bacteria, namely, *Faecalibacterium*, *Lachnospira and Roseburia*, that was also associated with increased faecal SCFAs levels (Jalanka *et al.*, 2019).

1.6.5 Resistant starch

Resistant starch is a starch that escapes digestion in the small intestine and reaches the large intestine in which it is fermented by the gut bacteria. RS can be found in peas, legumes, cereals, and non-mature fruits like green bananas (Birt *et al.*, 2013). Resistant starch can be classified into five categories: RS-1 (physically inaccessible such as whole-kernel grains), RS-2 (granules such as high amylose), RS-3 (retrograded such as cooked and cooled starchy foods), RS-4 (chemically modified such as octenyl succinate starch) and RS-5 (starch–lipid complexes such as stearic acid-complexed high-amylose starch) (Birt *et al.*, 2013). Fermentation of RS results in production of short-chain fatty acids and a reduction in pH in the proximal large intestine. Resistant starch is well-known as a source of butyrate production via bacterial fermentation in the colon (Schwiertz *et al.*, 2002), and butyrate is the main energy source of colonocytes and an anti-inflammatory agent.

1.6.6 Inulin

Inulin is a water-soluble polysaccharide and belongs to a group of non-digestible carbohydrates called fructans. Inulin is found extensively in about 3,000 vegetables; chicory roots are considered as the richest source of inulin (Shoaib *et al.*, 2016). Inulin is not digested by enzymes in the small intestine because of the repetitive fructosyl units linked by β(2,1) bonds, but it is a readily fermentable fibre by the gut bacteria to produce large amounts of short-chain fatty acids. Inulin stimulates the development and metabolic action of a limited number of bacteria in the colon, particularly *Bifidobacterium* and *Lactobacilli*, and thus promotes host health via suppression of intestinal inflammation (Furrie *et al.*, 2005) and reduction in the risk of developing colon cancer (Rafter *et al.*, 2007). A preclinical study also showed that inulin modulates the immune functions in mice by activating splenic natural killer cells when exposed to lymphoma cells or peritoneal macrophages when challenged with *Listeria monocytogenes*, respectively, compared to cellulose (Kelly-Quagliana *et al.*, 2003).

The common sources and physiochemical characteristics of cellulose, psyllium, resistant starch and inulin are listed in Table 2 (Gill *et al.*, 2021). Briefly, cellulose is insoluble, non-viscous and low in fermentability. Psyllium has medium viscosity, but is low in solubility and fermentability. Resistant starch and inulin are readily fermentable fibres.

Table 2 Physiochemical characteristics of common dietary fibres.

Fibre type	**Common sources**	**Physiochemical characteristics**		
		Solubility	Viscosity	Fermentability
Cellulose	All green plant cell walls	Insoluble	Non-viscous	Low
Psyllium	Seeds of Plantago	Low to medium	Medium	Low
Resistant starch (RS-2)	Cereals, raw legumes, raw fruits, vegetables	Low	Non-viscous	High
Inulin	Cereals, fruits, vegetables	Medium to high	Low to high	High

1.7 Short-chain fatty acids

1.7.1 Acetate, propionate, butyrate

Short chain fatty acids (SCFAs) are fatty acids with fewer than six carbon atoms, and acetate (CH3 -COO−), propionate (CH3 -CH2 -COO−) and butyrate (CH3 -CH2 -CH2 -COO−) are the three main ones. They account for approximately 90 to 95 percent of all SCFAs produced, in a constant molar ratio of 6:3:1, and the minor SCFAs are isobutyric, valeric, isovaleric and caproate acid. SCFAs are fermented from dietary fibres by the gut microbiota and generated mostly (≥95%) in the colon (humans) and caecum (rodents). (Figure 7). Given that the gut microbiota prefers to ferment carbohydrates over proteins, the concentrations of SCFAs are highest in the proximal colon (70-140 mM), where most substrates for fermentation are available (Wong *et al.*, 2006). It has been estimated that SCFAs contribute to approximately 60–70% of the energy requirements of colonic epithelial cells and 5–15% of the total caloric requirements of humans (Liu *et al.*, 2018). Butyrate is the major energy source for colonocytes. Propionate is largely taken up by the liver. Acetate enters the peripheral circulation to be metabolised by peripheral tissues. The ability of SCFAs to modulate biological responses of the host depends on two major mechanisms, namely, to regulate gene expression via histone deacetylase inhibition and to activate the G-protein-coupled receptors (GPCRs), such as GPR41, GPR43, and GPR109A.

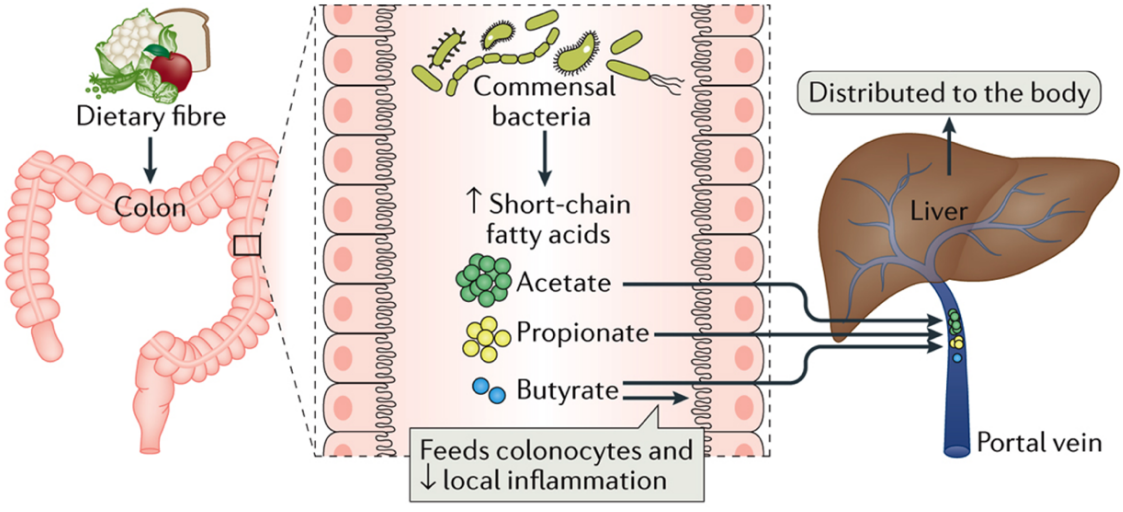


Figure 7 Fermentation of dietary fibre by the gut microbiota in production of short-chain fatty acids. Dietary fibre is fermented by commensal bacteria. Adapted from Marques *et al.*, 2018.

SCFAs play a mediatory role in communication between the gut microbiota and the mucosal immune system. For example, butyrate confers anti-inflammatory effects via reduction of NF-κB activity (Segain *et al.*, 2000) and suppresses the production of proinflammatory molecules TNFα, IL-1b, nitric oxide (Park *et al.*, 2007). Besides, Schulthess *et al.* showed that butyrate induces differentiation of monocytes to macrophages with potent antimicrobial functions via inhibition of histone deacetylase (HDAC) 3 (Schulthess *et al.*, 2019). Butyrate can also reduce oxidative stress in the colon, improve gut barrier function, and protect against colon cancer and ulcerative colitis, an inflammatory bowel disease (Bourassa *et al.*, 2016; Hallert *et al.*, 2003).

In terms of their effects on cancers, acetate, propionate, and butyrate have been shown to increase histone deacetylase inhibition and also radiosensitivity in bladder cancer cells (Then *et al.*, 2020). Furthermore, cell experiments showed that SCFAs have anti-cancer effects in several cancers outside the intestine. For example, propionate induced apoptosis in lung cancer cells (Kim *et al.*, 2019), and butyrate and propionate suppressed proliferation of breast cancer cells (Semaan *et al.*, 2020).

1.7.2 SCFA-producing colonic bacterial species

When the dietary fibres reach the large intestine, the gut microbiota hydrolyses the indigestible carbohydrates to hexoses, deoxy-hexoses and pentoses (Deleu *et al.*, 2021). These monosaccharides are further converted to pyruvate, the main precursor for SCFAs, through the glycolytic pathway and the pentose phosphate pathway (Figure 8). Two-thirds of the acetate is produced from acetyl-coA by the gut microbiota from a range of different classes. The remaining one-third originates from acetogenic bacteria, which synthesise acetate from hydrogen and carbon dioxide or formic acid through the Wood–Ljungdahl pathway. There are two pathways able to produce propionate which are the succinate pathway used by Bacteroidetes and Negativicutes, and the propanediol pathway used by

Lachnospiraceae. Butyrate is produced by the butyrate kinase pathway and the butyryl-CoA: acetate CoA-transferase pathway, converting butyryl-CoA into butyrate. Only a minority of butyrogenic taxa such as *Coprococcus comes* and *Coprococcus eutactus* using the butyrate kinase route whereas the majority, including *Faecalibacterium prausnitzii*, *Eubacterium rectale* and *Eubacterium hallii*, use the latter pathway.

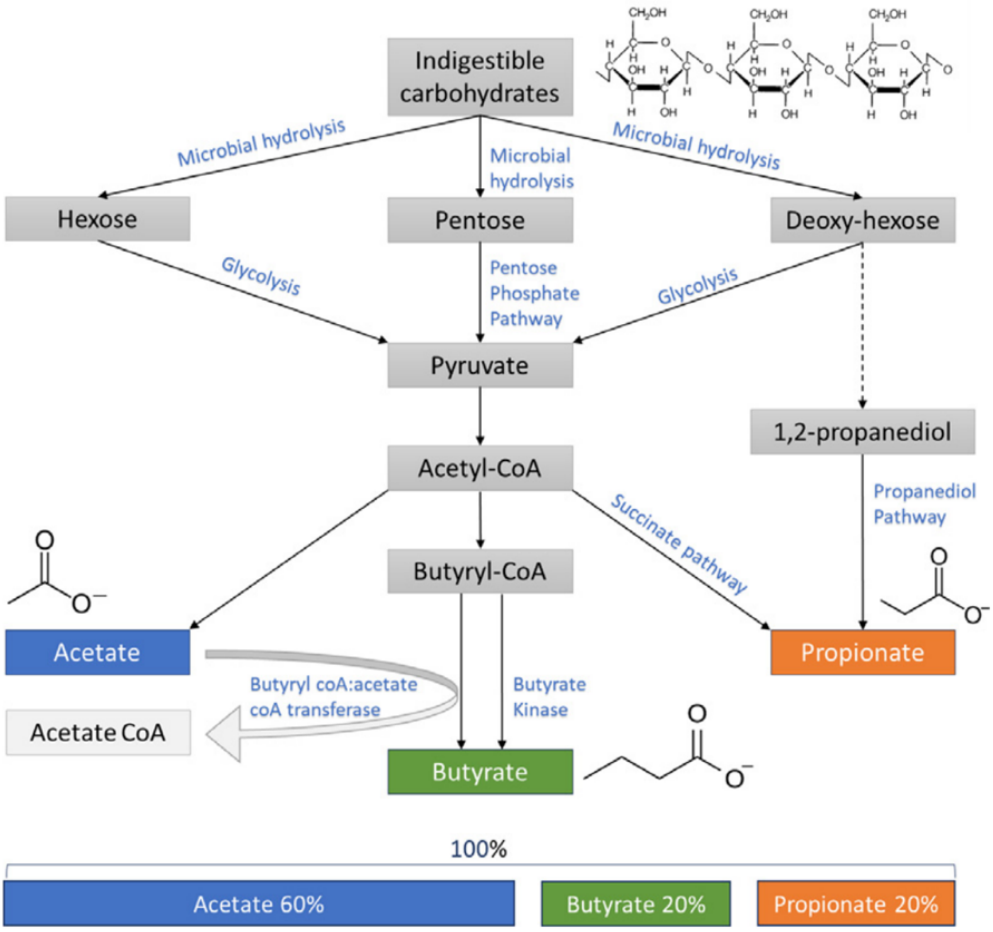


Figure 8 Pathways of short-chain fatty acids production. Indigestible carbohydrates are hydrolysed by the gut microbiota and converted to pyruvate via glycolysis or the pentose phosphate pathway. Most of the acetate is converted by various classes of the gut microbiota from acetyl-coA and a minority is derived from hydrogen and carbon dioxide or formic acid through the Wood–Ljungdahl pathway. Propionate is produced via the succinate pathway and the propanediol pathway, while butyrate is produced via butyrate kinase pathway and the butyryl-CoA: acetate CoA-transferase pathway. From Deleu *et al.*, 2021.

1.7.3 Effects of butyrate

Butyrate metabolism is gaining increased attention during the last decades due to the association between butyrate and various diseases involving inflammatory processes. Butyrate modulates biological responses in host gastrointestinal health by acting as a histone deacetylase (HDAC) inhibitor and by binding to several specific G protein–coupled receptors (GPCRs).

HDAC inhibition

Butyrate was one of the first discovered HDAC inhibitors, using erythroleukemic cells as a model (Candido *et al.*, 1978), and has the strongest HDAC inhibitory activity of the SCFAs (Sunkara *et al.*, 2012). Butyrate can elicit many anticancer activities which are mediated through HDAC inhibition, including inhibition of cell proliferation (Li *et al.*, 2018), induction of cell differentiation (Klepinina *et al.*, 2021) and apoptosis (Salimi *et al.*, 2017), and re-expression of the *apoptosis-associated speck-like protein* (*ASC*) gene (Zhang *et al.*, 2012). In addition, butyrate confers its anti-inflammatory effects partly through HDAC inhibition in macrophages (Chang *et al.*, 2014) and regulatory T cells (Arpaia *et al.*, 2013). Besides of butyrate, valeric acid is also another short-chain fatty acid which can be produced by human gut bacteria (Yuille *et al.*, 2018) and confer anti-tumour effects in liver (Han *et al.*, 2020), breast (Shi *et al.*, 2021), and prostate (Han *et al.*, 2022) cancer cells by acting as HDAC inhibitor.

Intestinal barrier function

In addition to acting as the primary energy source in the large intestine, butyrate is well known to elicit beneficial effects on the intestinal tract. Butyrate can repair and enhance barrier function of intestinal epithelial cells. For example, Peng *et al.* showed that butyrate enhanced the intestinal barrier by facilitating tight junction assembly in Caco-2 cell monolayers (Peng *et al.*, 2009). In addition, Liang *et al.* showed that butyrate is capable of repairing the gut mucous barrier by upregulating the mucin production and the proportion of mucin-secreting goblet cells in the colonic crypts (Liang *et al.*, 2022).

Intestinal mucosal immunity

In terms of mucosal immunity, Schauber *et al.* showed that butyrate stimulates the production of antimicrobial peptides, such as LL-37 that is an important effector in intestinal mucosal defence (Schauber *et al.*, 2003). In addition, butyrate can also modulate the chemotaxis and adhesion of immune cells by increasing neutrophil migration through raising L-selectin, an adhesion molecule, expression on neutrophils and the release of CINC-2αβ, a cytokine (small proteins controlling the growth and activity of immune cells) (Vinolo *et al.*, 2009).

1.7.4 The Warburg effect

The Warburg effect, the metabolic reprogramming of cancer cells to aerobic glycolysis, provides the primary energy source in urothelial cancer cells, promoting tumourigenesis (Massari *et al.*, 2016). High glycolytic flux increases glycine synthesis and purine synthesis, which sustains uncontrolled proliferation of tumour cells (Massari *et al.*, 2016). In normal colonocytes, butyrate can act as the primary energy source, which provides about 70% of ATP production, via mitochondrial β-oxidation (Roediger, 1980). However, in cancer cells, decreased use of the Kreb's cycle, along with upregulation of the pentose phosphate pathway and fatty-acid synthesis, results in more butyrate accumulating in the nucleus, to a level sufficient for histone deacetylase inhibition (Figure 9) (Donohoe *et al.*, 2012). Butyrate is fermented from dietary fibre. Its levels are increased by consumption of a high fibre diet, and it is involved in cellular activities which include mitochondrial activity, G-protein coupled receptors, microbiome homeostasis and HDAC inhibition (Bourassa *et al.*, 2016). Davie *et al.* proposed that butyrate inhibits HDAC1 and HDAC2 which are recruited by SP1 and SP3, and this leads to histone hyperacetylation (Davie, 2003). Butyrate can also be metabolised to the essential cofactor - acetyl-CoA, stimulate the activity of histone acetyltransferase (HAT) and further induce histone acetylation (Donohoe *et al.*, 2012).

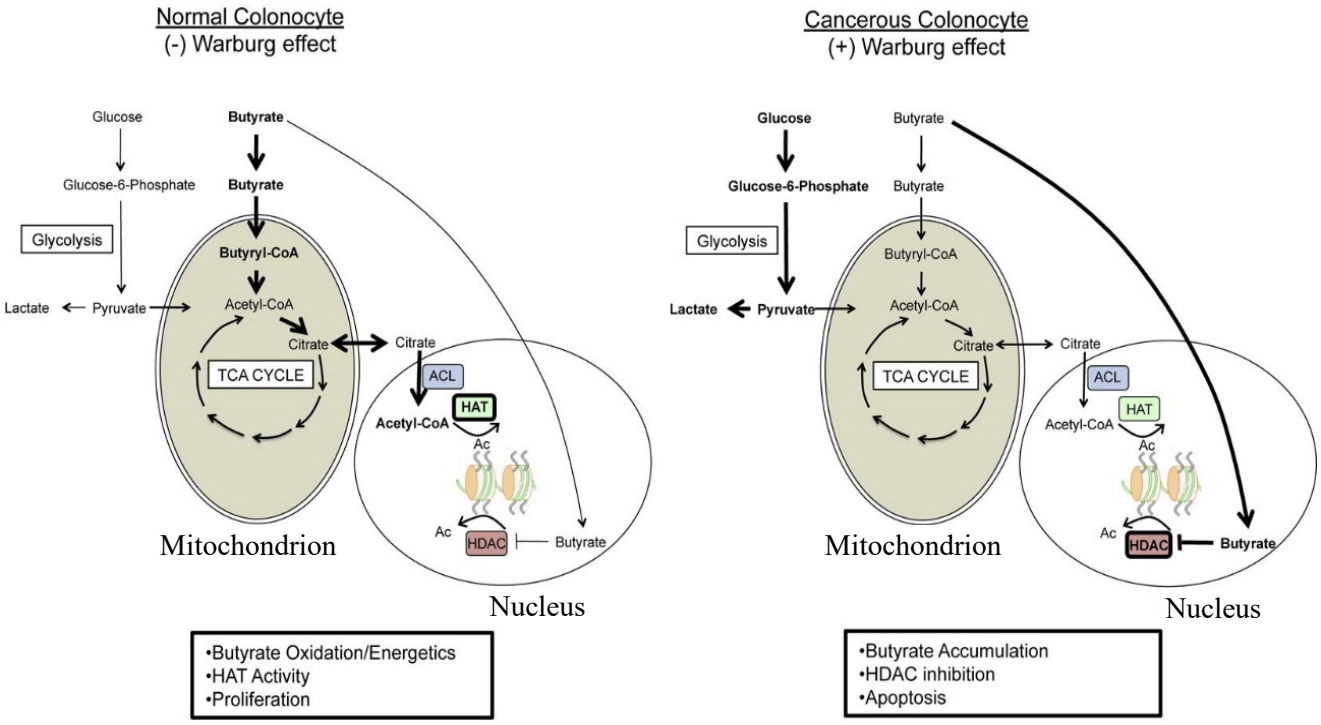


Figure 9 The Warburg effect causes butyrate accumulation and HDAC inhibition. Normal colonocytes consume butyrate as their primary energy source. Due to the Warburg effect, cancerous colonocytes consume glucose as their primary energy source so that butyrate accumulates to levels sufficient to cause HDAC inhibition. Adapted from Donohoe *et al.*, 2012.

1.7.5 Radiosensitisation by histone deacetylase inhibitors

Histone deacetylases (HDACs) are a class of enzymes that remove acetyl groups from lysine residues on histones and nonhistone proteins, resulting in the histones being able to wrap the DNA more tightly. HDAC expression is aberrant in multiple cancer types, including bladder cancer (Ozawa *et al.*, 2010) and histone deacetylase inhibitors have been used as anti-tumoural agents that induce tumour cell death, differentiation, or cell cycle arrest (Bolden *et al.*, 2006). Groselj *et al.* in our laboratory previously demonstrated that panobinostat, a histone deacetylase inhibitor, is a promising radiosensitiser, which delayed the growth of RT112 bladder cancer xenografts (Figure 10A) but did not exacerbate local acute (3.75 days) and late (12 weeks) toxicity to the intestinal tract (Groselj *et al.*, 2018). We found similar results in Paillas *et al.* where romidepsin, another HDAC inhibitor, also conferred a radiosensitising effect by inhibiting the DNA damage response (Figure 10B) (Paillas *et al.*, 2020). Therefore, histone deacetylase (HDAC) inhibition is a promising mechanism of radiosensitisation. Sodium butyrate was the first described HDAC inhibitor (Boffa *et al.*, 1978) and has the strongest HDAC activity of the SCFAs (Korsten *et al.*, 2022). It also has been shown to exert radiosensitising properties in colorectal cancer cells (Arundel *et al.*, 1985) and bladder cancer cells (Then *et al.*, 2020). However, its very short plasma half-life limits its clinical utility (Miller *et al.*, 1987).

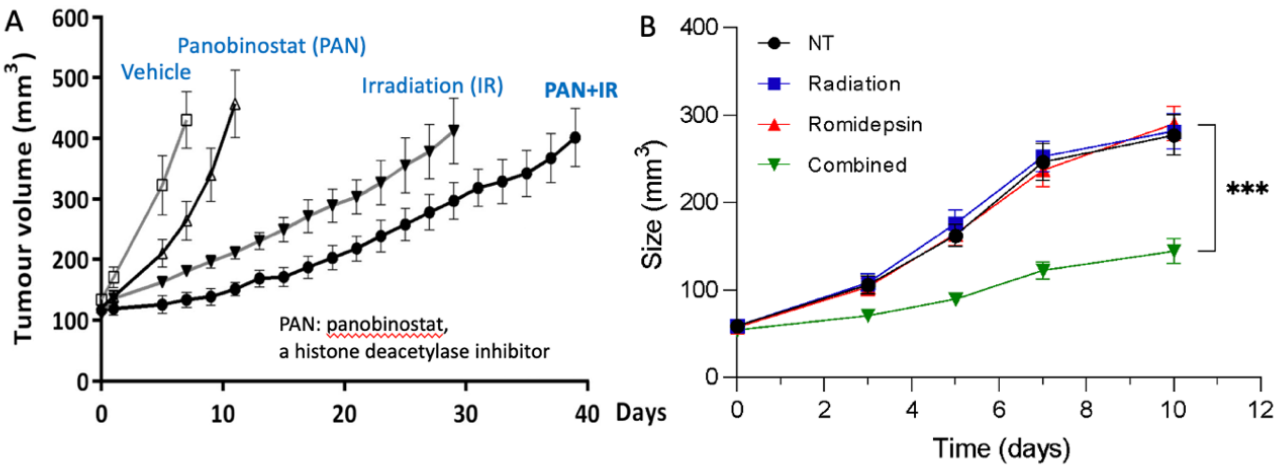


Figure 10 Histone deacetylase inhibition is a promising mechanism of radiosensitisation. (A) RT112 xenografts were treated with vehicle, panobinostat, IR (5x4 Gy) or panobinostat plus IR. Adapted from Groselj *et al.*, 2018. (B) RT112 xenografts received vehicle, romidepsin, IR (6 Gy) or romidepsin plus IR. Adapted from Paillas *et al.*, 2020.

1.8 Gut microbiota

Terminology relating to microbiota studies is listed in the glossary section.

1.8.1 The basics and the main phyla in the intestine

The gut microbiota is a collective of microorganisms, namely, protozoa, archaea, eukaryotes, viruses and predominantly bacteria that live symbiotically in the gastrointestinal tract, mainly in the large intestine. Compared to other body sites, such as nose, skin, and the urogenital system, the gut microbiota is diverse and a large variation in the constituents exists among health individuals (Huttenhower *et al.*, 2012). The gut microbiota contains 1.3 times more cells and 100 times more genes than the host (Savage, 1977). More than 90% of all bacterial phylogenetic types (phylotypes) belong to the Bacteroidetes, Firmicutes, Proteobacteria, and Actinobacteria phyla. The development of the microbiota is generally considered to begin from birth. After birth, the gastrointestinal tract is rapidly colonised, and this can be influenced by several factors such as host genotype, lifestyle or diet, environment and immune system (Turnbaugh *et al.*, 2007). Chaotic shifts of the gut microbiota can be caused by life events such as changes in dietary habit, use of antibiotics and illness (Thursby & Juge, 2017).

The gut microbiota has a huge beneficial impact on human physiological functions, such as maintaining mucous membrane integrity, conferring protection against enteropathogenic bacteria, including *Salmonella*, *Shigella*, and *Yersinia*, and preservation of normal immune function (Okumura & Takeda, 2018). Alterations in the oral or gut microbiota are associated with the development of cancers, such as gastric cancer (*Helicobacter pylori*) (Parsonnet *et al.*, 1991), colorectal cancer (*Fusobacterium nucleatum*) (Castellarin *et al.*, 2012) and pancreatic cancer (*Porphyromonas gingivalis*) (Fan *et al.*, 2018). The gut microbiota have also been shown to modulate the efficacy of anticancer treatments including immunotherapy (Gopalakrishnan *et al.*, 2018; Matson *et al.*, 2018; Routy *et al.*, 2018; Sivan *et al.*, 2015), chemotherapy (Daillere *et al.*, 2016; Geller *et al.*, 2017; Iida *et al.*, 2013; Viaud *et al.*, 2013), chemoradiation (Sims *et al.*, 2021), and radiotherapy (Shiao *et al.*, 2021; Uribe-Herranz *et al.*, 2020; Yang *et al.*, 2021) in both preclinical models and human studies.

1.8.2 Influence of dietary fibre

Diet has a major impact on gut microbiota composition, diversity, and richness. Pronounced alterations in bacterial diversity and faecal SCFAs production can occur very rapidly, in as little as 24 hours in humans switching to a plant-based diet (David *et al.*, 2014). Desai *et al.* emphasised the importance of dietary fibre on the gut health. They found that dietary fibre deprivation made the gut microbiota consume host-secreted mucous glycoproteins, resulting in the erosion of the colonic mucosal barrier and lethal colitis, caused by the invasion of *Citrobacter rodentium* in gnobiotic mice colonised with human gut microbiota (Desai *et al.*, 2016). In addition, the Western-style diet, low in microbiota-accessible carbohydrates, reduces microbial diversity and contributes to the development of chronic inflammatory diseases such as inflammatory bowel disease, colorectal cancer, and obesity and its associated pathologies (Sonnenburg *et al.*, 2016).

1.8.3 SCFA-producing colonic bacterial species and how they produce SCFAs and other metabolites

Complex carbohydrates are mainly broken-down by certain abundant species within the phylum Bacteroidetes, one of the largest groups in the intestine to produce SFCA (Figure 11) (Kim, 2021; van der Hee & Wells, 2021). Acetate production is common to many bacterial groups in this phylum Bacteroidetes. Propionate is produced by a few dominant genera, including *Akkermansia muciniphila*, *Bacteroides vulgatus*, *Bacteroides thetaiotaomicron* and *Coprococcus catus*. The Lachnospiraceae and Ruminococcaceae, comprising around 20% of the total bacteria, are the major butyrate-producing families. By mapping the bacterial genome to the genes which are involved in the butyrate synthesis pathways, the potential butyrate producers have been identified as belonging to the bacterial phyla Firmicutes, Actinobacteria, Bacteroidetes, Fusobacteria, Proteobacteria, Spirochaetes and Thermotogae. *Faecalibacterium prausnitzii*, belonging to clostridial clusters IV of Firmicutes, is the most abundant and important butyrate-producing group in humans. Faecal SCFA levels can be increased by high fibre diets, and this was associated the abundance of *Bifidobacterium*, Lachnospiraceae and Muribaculaceae (Bishehsari *et al.*, 2018).

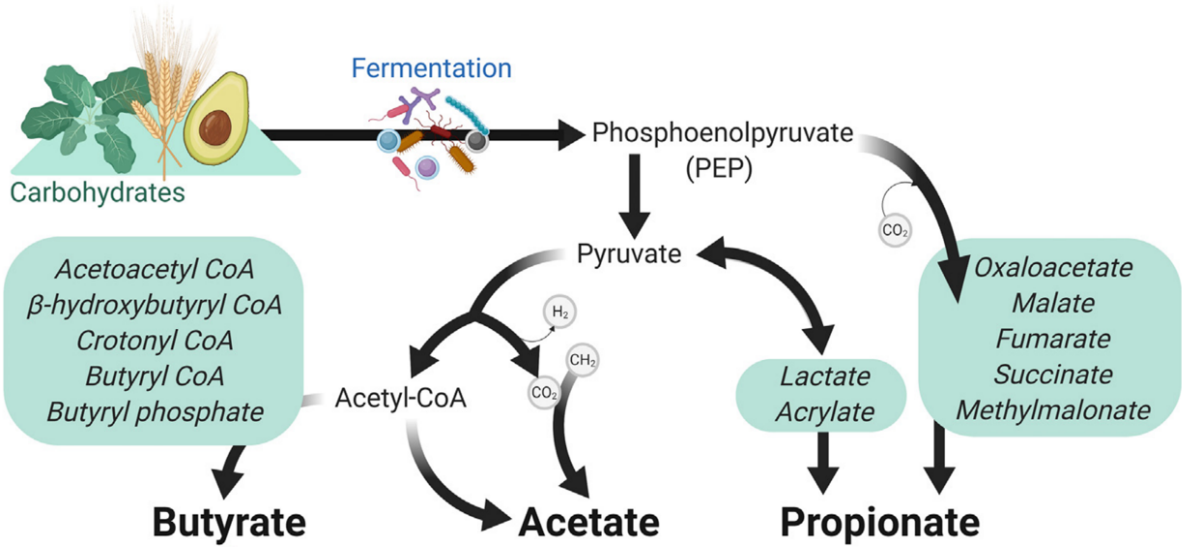


Figure 11 Acetate, propionate and butyrate production by gut bacterial fermentation of dietary fibre. SCFAs, such as acetate (C2), propionate (C3), and butyrate (C4), are produced from nondigestible fibre and digestion-resistant starches by the cooperative catabolic activity of commensal gut microbiota. Adapted from van der Hee & Wells, 2021.

1.8.4 The gut microbiota changes with age

Bladder cancer is prevalent in the elderly population, with a median age of 73 years old (Erlich & Zlotta, 2016). As age increases, the gut microbiota shifts to a decreased diversity (O'Toole & Jeffery, 2015), a reduction of SCFA-producing bacterial abundance (Biragyn & Ferrucci, 2018) and a bacterial composition that is less likely responding to anti-cancer treatments (Spakowicz *et al.*, 2021). Three gut microbes, namely, *Akkermansia muciniphila* (Routy *et al.*, 2018), *Bifidobacterium* (Sivan *et al.*, 2015) and *Faecalibacterium prausnitzii* (Gopalakrishnan *et al.*, 2018), which have been shown to enhance immunotherapy efficacy via immunomodulation, are depleted in older adults (Collado *et al.*, 2007; Wu *et al.*, 2019). Therefore, the gut microbiota could be a therapeutic target to be modulated by dietary fibre to overcome the ageing-induced perturbation of gut microbiota and hence promote radiotherapy responses, as immunomodulation may be needed to increase the radiotherapy response (Wang *et al.*, 2018).

1.9 The urinary microbiota and bladder cancer

Although urine was traditionally thought sterile (Zasloff, 2007), due to the advanced sequencing technologies, it has been found to have low biomass of microbiota ($<10^5$ colony-forming units per mL) which was considered low abundant compared to that of 10^{12} CFU/g in faeces (Pearce *et al.*, 2014). In both men and women, the major phyla are Firmicutes phylum (65% in males vs 73% in females), Actinobacteria (15% males vs 19% females), Bacteroidetes (10% males vs 3% females) and Proteobacteria (8% males vs 3% females) (Modena *et al.*, 2017). Chronic urinary tract infection is one of the risk factors of bladder cancer, so it is speculated that the perturbation of urinary microbiota might be involved in the development of bladder cancer (Pearce *et al.*, 2014). Several clinical studies have shown that the patients with transitional cell carcinoma, the most common type of bladder cancer, were enriched with *Acinetobacter*, *Anaerococcus*, *Sphingobacterium* (Wu *et al.*, 2018), *Fusobacterium* (Popovic *et al.*, 2018), and *Actinomyces* (Bi *et al.*, 2019) genus. Intravesical immunotherapy Bacillus Calmette-Guérin (BCG), a live and attenuated strain of *Mycobacterium bovis* is the gold-standard adjuvant treatment for non-muscle-invasive bladder cancer following tumour resection (Pettenati & Ingersoll, 2018). BCG immunotherapy can induce local innate, adaptive, and even systemic immune responses to improve tumour control, and increase the complete response rates of anti-cancer treatments (Ingersoll & Albert, 2013). Therefore, urinary microbiota is a potential target to modulate anti-tumour responses as it may affect the development of bladder cancer and directly interact with tumour microenvironment in bladder.

1.10 Prebiotics and probiotics

1.10.1 Prebiotics

A prebiotic is defined as a substrate that is selectively utilised by host microorganisms conferring a health benefit (Gibson *et al.*, 2017). Fructans (fructo-oligosaccharides (FOS) and inulin) and galacto-oligosaccharides (GOS) are the two major categories of prebiotics. More recently, other substances such as polyphenols and polyunsaturated fatty acids that convert to respective conjugated fatty acids have also been deemed to fit the latest prebiotic definition. Prebiotics mainly elicit their effects by acting through the enrichment of *Lactobacillus* and/or *Bifidobacterium* species, although other beneficial taxa including *Roseburia*, *Eubacterium* or *Faecalibacterium* species are now being recognised as having health benefits. Resistant starch has also been proposed as a prebiotic, as it can promote health by enhancing butyrate levels and it produced the highest level of butyrate compared to other types of fibre, including oat bran, guar gum and pectin (Fuentes-Zaragoza *et al.*, 2011).

1.10.2 Probiotics

Whereas prebiotics are non-viable substrates, probiotics are 'live microorganisms that, when administered in adequate amounts, confer a health benefit on the host' (Hill *et al.*, 2014). Probiotics have been widely used for inhibition of potential pathogens, production of short-chain fatty acids, regulation of intestinal transit and increased turnover of enterocytes. Several well-characterised strains that are available for human use included *Bifidobacterium* (*adolescentis*, *animalis*, *bifidum*, *breve* and *longum*) and *Lactobacillus* (*acidophilus*, *casei*, *fermentum*, *gasseri*, *johnsonii*, *paracasei*, *plantarum*, *rhamnosus* and *salivarius*). Five out of six clinical trials in our systematic review showed a consistent result that probiotics reduce the risk of radiation-induced diarrhoea in abdominal or pelvic cancer patients who received radiotherapy (Bartsch *et al.*, 2021).

1.11 Immunology

1.11.1 The basics

The immune system comprises innate and adaptive immunity (Chaplin, 2010). Innate immunity is the first line of defence against pathogens, foreign substances, damaged cells, and cancer cells. It is constituted of physical barriers (mucous layer, epithelial cilia, and epithelial cell layer), soluble mediators (cytokines, complement and acute phage proteins) and immune cells, including phagocytic leukocytes, dendritic cells, and natural killer cells. The adaptive immune system is a more versatile and accurate mechanism of defence, constituted of B lymphocytes, T lymphocytes and antibodies. The innate and adaptive immune systems usually interact with each other and act together in the defence against pathogens and cancer cells. The innate response is immediate in onset, and the adaptive response becomes prominent after clonal expansion, i.e. the rapid increase of T and B lymphocytes, which takes several days.

Innate immunity

The cellular components of the innate immune system include the neutrophils, eosinophils, basophils, monocytes, macrophages, dendritic cells, and natural killer cells. Their functions are listed in Table 3 below (Marshall *et al.*, 2018). They are needed for elimination of microbial agents, damaged cells, and cancer cells, and for activation of the more efficient, antigen-specific adaptive immune response.

Table 3 Functions of innate immune cells.

Cell	% in adults	Functions
Neutrophils	40-75%	Phagocytosis and degranulation (discharge of cell contents)
Eosinophils	1-6%	Degranulation and release of enzymes, growth factors and cytokines
Basophils	<1%	Degranulation and release of histamine, enzymes, and cytokines
Monocytes	2-6%	Differentiation into macrophages and dendritic cells to elicit an immune response
Macrophages	Varies	Phagocytosis and antigen presentation to T cells
Dendritic cells	<1%	Antigen presentation to trigger adaptive immune response
Natural killer cells	15%	Tumour rejection, destruction of infected cells, and release of perforin and granzymes which induce apoptosis

Adaptive immunity

The adaptive immunity is mediated by the T lymphocytes (T cells) and B lymphocytes (B cells) to elicit a more specific immune response to antigenic stimuli (Table 4). The adaptive immune response can be classified as humoral- and cell-mediated (Marshall *et al.*, 2018). T lymphocytes mediate the cell-mediated immune response against infected or cancer cells that present small antigenic determinants on MHC molecules. B lymphocytes mediate the humoral immune response against antigens present outside the cells, in the blood and body fluids.

Table 4 Functions of adaptive immune cells.

Cell	Function
Helper T cells	Secretion of cytokines and activation of B cells to secrete antibodies. Activation of macrophages to destroy ingested microbes and cytotoxic T cells to kill target cells
Cytotoxic T cells	Induction of apoptosis of cells displaying foreign antigens or derived peptides on their surface, such as virus-infected cells and cancer cells
B cells	Production of antibodies against foreign antigens

Helper T cells are arguably the most important regulators in adaptive immunity. After activated by antigen presenting cells (APC), a heterogeneous group of immune cells that process and present antigens for T cells recognition, helper T cells release cytokines to activate many cell types. Those cytokines can be classified into the major subsets Th1, Th2, Th17 and Treg (Figure 12) (Majchrzak *et al.*, 2016). Naive $CD4^+$ T cells differentiate based on the presence of various cytokines. For example, IL-12 influences Th1 cell development and promotes immunity in the presence of IFN-γ, TNF-α and IL-2 (Knochelmann *et al.*, 2018). Th1 and Th2 cytokine panels are generally considered as tumour-suppressing (immunostimulatory) and tumour-promoting (immunosuppressive), respectively (Burkholder *et al.*, 2014). The cytokines, IL-2, IL-6 and TNFα, can be elevated after irradiation of tumours (Marconi *et al.*, 2019) or be administered, mostly subcutaneously (Vacchelli *et al.*, 2016), to enhance the efficacy of radiotherapy (Palata *et al.*, 2019).

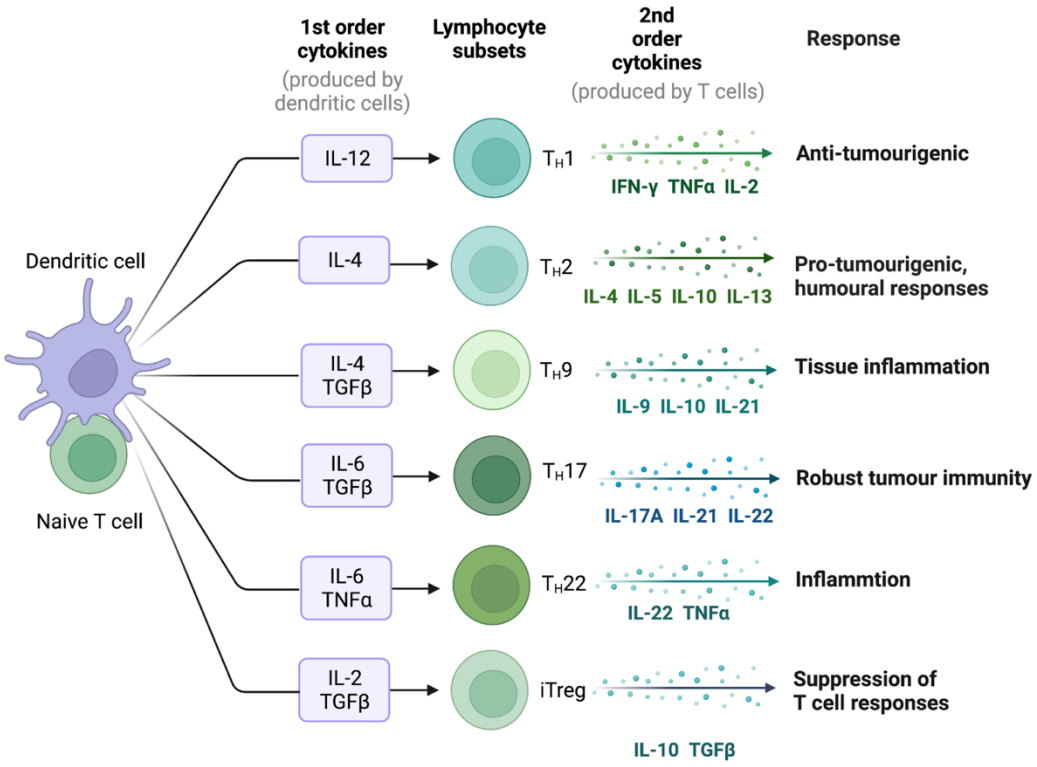


Figure 12 T helper cell differentiation. Cytokines play critical roles in differentiation and effector functions of Th1, Th2, Th9, Th17, Th22 and iTreg cells. Upon T-cell receptor activation triggered by dendritic cells, one of the antigen-presenting cells, naive CD4 T cells differentiate into distinct Th lineages in the context of combinations of cytokines. Figure created with Biorender.com.

1.11.2 Immune responses to radiotherapy

Ionising radiation (IR) causes DNA damage in cancer cells that may undergo senescence cell death (Adjemian *et al.*, 2020). There are several types of IR-induced cell death, including apoptosis, necrosis, and necroptosis, a RIPK3/MLKL regulated type of necrosis that was identified recently. These cell death modalities can lead to different immune responses. Apoptosis is considered as less immunogenic, while necrosis and necroptosis are more inflammatory. Studies suggested that low doses of IR would induce apoptosis, and a higher dose would trigger necrosis.

Immunogenic cell death is the cell death caused by ionising radiation which elicits a series of immune responses (Brandmaier & Formenti, 2020). It is a form of regulated cell death that releases damage-associated molecular patterns (DAMPs), molecules released from damaged or dying cells, in the tumour microenvironment and increases tumour immunogenicity, the ability of a tumour to induce an immune response (Figure 13). IR can also increase cytokine release in the tumour microenvironment by immune cells, and MHC class I (major histocompatibility complex class I; the molecules that bind peptides derived from a cell's expressed genes) expression on tumour cells or adhesion molecules on vascular endothelial cells. These molecules engage with leukocyte counter-receptors to mediate firm adhesion and/or transendothelial migration (Carvalho & Villar, 2018; Shiao & Coussens, 2010). Through these, leukocytes including macrophage and dendritic cells, migrate to the tumour and these functional antigen-presenting cells (APC) capture, process, and present antigens to stimulate the downstream anti-tumour T cells responses in the draining lymph node. Helper T cells expressing cell-surface CD4 and cytotoxic T cells expressing CD8, the most powerful effectors in the anticancer immune response, then infiltrate tumours and induce apoptosis of cancer cells (Raskov *et al.*, 2021).

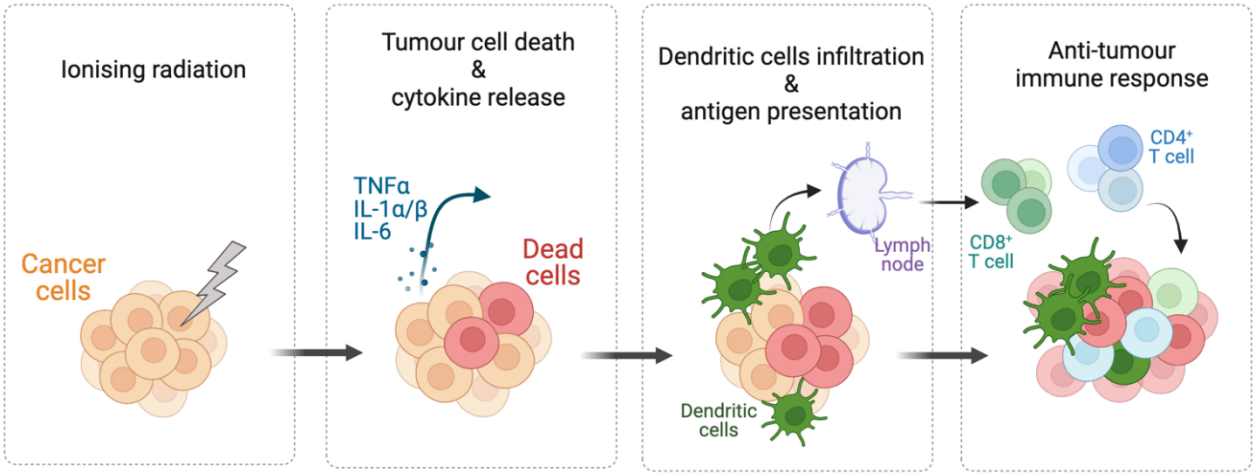


Figure 13 The immune response to IR. Tumour cells respond to IR by increasing cytokine release, MHC class I and adhesion molecule expression. This response recruits dendritic cells into tumours and which circulate to the draining lymph nodes for antigen presentation. Tumour-specific T cells are activated and infiltrate the tumours. Adapted from (Shiao & Coussens, 2010). Figure created with Biorender.com.

IR and local tumour immune response

There is mounting evidence of IR-mediated immunomodulation in tumours. Aguilera *et al.* showed that ionising radiation alone increased tumour-infiltrating leukocytes and cytotoxic T cells in mouse mammary tumours and it led to shrinkage of tumours when combined with immunotherapy using CTLA-4 and PD-1 antibodies (Aguilera *et al.*, 2016). Philippou *et al.* also found that 3 x 5 Gy of IR significantly boosted the numbers of macrophages, dendritic cells, and helper T cells 7 days post irradiation (Philippou *et al.*, 2020). Jones *et al.* showed a similar result with increased macrophages, neutrophils, MDSCs and helper T cells, and expression of major histocompatibility complex (MHC) class I after 10 Gy IR in mouse colorectal and pancreatic tumours (Jones *et al.*, 2018).

1.11.3 Immune responses to dietary fibre

The fermentable dietary fibres can also modulate the immune system, including the gut-associated lymphoid tissues (GALT), spleen, peripheral circulation and intestinal mucosal secretion of antibodies (Schley & Field, 2002). These immunomodulations can be achieved via the direct contact of gut microbiota or fermentation products with intestinal immune cells, direct simulation of dietary fibre on the immune system, enhancing intestinal barrier function or improving nutrient absorption (Schley & Field, 2002; Shokryazdan *et al.*, 2017). Trompette *et al.* showed that 30% inulin protects against flu infection by increasing the patrolling monocytes from bone marrow haematopoiesis in comparison to 30% cellulose (Trompette *et al.*, 2018). Pierre *et al.* also showed that 5.8% small chain fructo-oligosaccharide of total diet (gram / 100 gram dry matter) increases the number of lymphoid nodules in the small intestine compared to 2% cellulose (Pierre *et al.*, 1997). Pectin can raise serum IgA and IgG levels and the splenic $CD4^+/CD8^+$ ratio relative to cellulose (Lim *et al.*, 1997). In addition, inulin-type fructan increased caecal IgA production and the cytokines production, IFN-γ and IL-10, of $CD4^+$ T cells in the lamina propria of caecum (Ito *et al.*, 2011). In a clinical trial, oligofructose-enriched inulin decreased the inflammatory marker of interleukin-6 and tumour necrosis factor-α in women with type 2 diabetes (Dehghan *et al.*, 2014). In addition, consumption of xylo-oligosaccharide in combination with inulin increased faecal SCFA concentrations and decreased lipopolysaccharide (LPS) concentrations and LPS-induced IL-1β gene expression in blood (Lecerf *et al.*, 2012).

1.11.4 Gut microbiota and SCFAs – tumour responses, gut responses, and barrier function.

The gut lamina propria is the richest source of lymphocytes in the whole body where the effector T cells, namely, Tregs, Th1, Th2 and Th17 reside in a delicate balance (Jain *et al.*, 2021). This local gut immunity can be altered by the gut microbiota to enhance the systemic immune system in terms of induction of cytotoxic T cells (Tanoue *et al.*, 2019) and function of Th17 cells (Viaud *et al.*, 2013). For example, *Bacteroides fragilis* raised the splenic $CD4^+$ T cell numbers with appropriate cytokine production in germ-free mice to the level seen in

specific pathogen-free mice, demonstrating that the gut microbiota is necessary for the development of the host immune system, including helper T cells (Mazmanian *et al.*, 2005). A consortium of 11 human commensal bacterial strains from healthy human donor faeces successfully induced both local and systemic IFNγ^{+} CD8 T cells in germ-free mice which was dependent on dendritic cells and MHC class Ia molecules (Tanoue *et al.*, 2019). Moreover, *L. johnsonii* and *E. hirae* facilitated the reconstitution of the splenic pathogenic T helper 17 cells that were needed for overcoming cyclophosphamide resistance in mouse fibrosarcoma (Viaud *et al.*, 2013).

In the tumour microenvironment, the gut microbiota can also activate both innate and adaptive immunity including dendritic cells (Uribe-Herranz *et al.*, 2020), natural killer T cells (Ma *et al.*, 2018), macrophages (Pushalkar *et al.*, 2018), and CD8^{+} T cells (Sethi *et al.*, 2018) for tumour control. The prebiotic inulin boosted splenic cytotoxic T lymphocyte functions and overcame melanoma resistance to MEK inhibitors which was associated with an increase of the intestinal *Bifidobacterium* species (Li, Elmen*, et al.*, 2020). Microbial SCFAs and butyrate have also been shown to improve adoptive immunotherapy, that is giving gene-modified T cells expressing novel T cell receptors or chimeric antigen receptors to patients to elicit an anti-tumour effector function, and chemotherapy, by enhancing antitumour cytotoxic CD8^{+} T cell immunity (He *et al.*, 2021; Luu *et al.*, 2021). In addition, butyrate treatment directly boosted the antitumour cytotoxic CD8^{+} T cell responses in mouse subcutaneous colorectal tumours receiving oxaliplatin by promoting the IL-12 signalling pathway (He *et al.*, 2021). In cancer patients receiving oxaliplatin, the responders exhibited higher levels of serum butyrate and activated CD8^{+} T cells than non-responders.

1.12 How dietary fibre manipulation, gut microbiota and SCFAs have been used to improve the RT therapeutic ratio to date

1.12.1 Effects on normal tissue responses

Preclinical studies

A preclinical study showed that 15% oat bran decreased the systemic proinflammatory cytokines raised by radiotherapy in the mouse colorectal region (Patel *et al.*, 2020). *Lactobacillus*, a probiotic species, improved the intestinal mucosal ulceration in rats given 11 Gy of γ-radiation to the abdominopelvic area (Demirer *et al.*, 2006). Guo *et al.* also found that Lachnospiraceae and Enterococcaceae, together with the downstream metabolites, propionate and tryptophan, can protect the hematopoietic and gastrointestinal systems against radiation (Guo *et al.*, 2020). In addition, Xiao *et al.* demonstrated that gut microbiota-derived indole 3-propionic acid reduced hematopoietic and gastrointestinal injury after radiation exposure. It attenuated local and systemic inflammatory levels, such as IL-6 and TNFα in the small intestine and peripheral blood, and reversed radiation-induced shortening of the colon, achieved by retaining the acyl-CoA-binding protein (Xiao *et al.*, 2020).

Clinical studies

In a large clinical study of patients receiving radiotherapy to their prostate and pelvic lymph nodes, RT changed the gut microbiota and this was associated with early and late enteropathy in patients (Reis Ferreira *et al.*, 2019). In a recent systematic review including twenty-three randomised controlled trials (1919 patients), we showed that biotic supplements, especially probiotics and synbiotics, reduce acute symptoms of diarrhoea in patients undergoing pelvic radiotherapy (Bartsch *et al.*, 2021). Compared with placebo, probiotics, synbiotics and polyphenols were significantly associated with a lower risk of diarrhoea. In addition, biotic supplements also reduced the risk of moderate to severe diarrhoea and the need for anti-diarrhoeal medication. Prebiotics, including psyllium, hydrolysed rice bran and inulin plus 50% fructo-oligosaccharide, were also found to bring benefits for diarrhoea control in cancer patients receiving pelvic or abdomen radiotherapy (Garcia-Peris *et al.*, 2016; Itoh *et al.*, 2015; Murphy *et al.*, 2000). In a clinical study, SCFAs

have been used to improve therapeutic efficacy in acute radiation proctitis which supported the anti-inflammation effects of butyrate at inflamed sites (Vernia *et al.*, 2000)

1.12.2 Effects on tumour growth

Preclinical studies

In terms of tumour control, Taper *et al.* showed that inulin and pectin can slow breast and liver tumour growth (Taper & Roberfroid, 1999). In addition, in a mouse experiment, Wei *et al.* showed that an unspecified high fibre diet (8%) decreased the growth rates of subcutaneous lymphoma xenografts compared to a low-fibre diet, with similar findings in both immune-deficient and immune-competent models (Wei *et al.*, 2016). This enhanced tumour control was associated with increased plasma and tumour butyrate levels. In terms of anti-cancer treatment efficacy, Iida *et al.* first found that antibiotics impaired the efficacy of immunotherapy in preclinical mouse melanoma models with down-regulation of the tumour necrosis factor (TNF) response (Iida *et al.*, 2013). They also showed that antibiotics reduced the tumour cytotoxicity and regression of lymphoma induced by oxaliplatin.

Clinical studies

Gopalakrishnan *et al.* showed that melanoma patients responding to anti-programmed cell death 1 protein (PD-1) immunotherapy had significantly higher alpha diversity, a measure of similarity within communities, of the gut microbiota and Ruminococcaceae family abundance (Gopalakrishnan *et al.*, 2018). There was a positive correlation between a favourable gut microbiota and enhanced systemic and local anti-tumour immunity in responding patients. The causal effect of gut microbiota on the efficacy of this immune checkpoint inhibitors has been proven using faecal transplantations of immunotherapy-responding patients in germ-free recipient mice. Faecal transplantation is the transfer of the gut microbiota from the stool of healthy or responding individuals to reconstruct the gut microbiota in recipients. This intervention successfully decreased the tumour size and increased $CD8^+$ cell numbers in both the gut and tumour of mice colonised with the gut microbiota from responders compared to non-responders. In addition, recent studies identified several bacterial taxa, namely,

Akkermansia muciniphila and some *Bifidobacterium* strains, which can improve anti-tumour immune responses and the efficacy of immunotherapy (Matson *et al.*, 2018; Routy *et al.*, 2018; Sivan *et al.*, 2015). Sim *et al.* has also demonstrated that a higher gut microbiota diversity was associated with increased immune responses and favourable chemoradiation efficacy in cervical cancer patients (Sims *et al.*, 2021).

There are relatively limited studies of gut microbiota and the efficacy of radiotherapy. Vancomycin, an antibiotic that kills Gram-positive bacteria in the gut, has been shown to enhance radiotherapy efficacy via increasing dendritic cell antigen presentation (Uribe-Herranz *et al.*, 2020; Yang *et al.*, 2021). In contrast, an antibiotic cocktail of ampicillin, imipenem, cilastatin, and vancomycin reduced efficacy of radiotherapy with depletion of the commensal bacteria (Shiao *et al.*, 2021). These three studies all used an antibiotics-based approach to deplete specific groups of gut microbiota to change the RT efficacy and two studied cancers outside the gastrointestinal tract.

1.12.3 Non-IR studies

The gastrointestinal side effects of radiotherapy, such as diarrhoea, nausea and vomiting are caused by radiation-induced intestinal inflammation (radiation enteritis). SCFAs and other metabolites produced by the gut microbiota are not only the primary energy sources for gut epithelial cells, but they can also confer anti-inflammatory effects which could alleviate the radiation side effects.

In terms of prebiotics, Ogata *et al.* showed, in colitic mice, that 5% and 10% psyllium improved the colonic damage and inflammation characterised by colonic shortening, increased pro-inflammatory cytokines and decreased tight junction protein expression (Ogata *et al.*, 2017). Colon length is often used as a morphological parameter to reflect the degree of inflammation, and colon shortening is associated with histological changes in colitic mice (Yan *et al.*, 2009).

Kang *et al.* showed that the enteric-coated superoxide dismutase of *B. amyloliquefaciens* can reduce oxidative stress in both γ-radiation- and dextran sulphate sodium (DSS)-induced

mouse models (Kang *et al.*, 2018). More recently, two different prolyl hydroxylase domain–containing enzyme (PHD) inhibitors, FG-4497 and dimethyloxallyl glycine, have been shown to result in mucosal protection in murine models of gastrointestinal damage, caused by chemically-induced colitis (Robinson *et al.*, 2008) and radiation-induced toxicity (Taniguchi *et al.*, 2014), respectively. The similar result of two mouse models implies that the benefits of psyllium observed in the DSS model might be applied to an ionising radiation model.

1.12.4 Association of the gut microbiota with high-fibre diet-mediated radiosensitisation

Wei *et al.* have shown a slower growth of transplanted tumours in mice fed high-fibre diets (Wei *et al.*, 2016) and prebiotics can enhance immunotherapy efficacy (Spencer *et al.*, 2021). Histone deacetylase inhibition is a promising mechanism of radiosensitisation, and tumour cells can accumulate the short chain fatty acid butyrate to sufficient levels to cause histone deacetylation inhibition, due to the Warburg effect. We hypothesised that mice fed a high-fibre diet would have improved tumour control following ionising radiation (IR) and that this would be mediated through the gut microbiota. In a previous animal experiment done in our laboratory, RT112 human bladder cancer cell line flank xenografts were implanted into CD1 nude mice at the same time as starting low fibre (0.2% cellulose) and high mixed fibre (5% cellulose plus 5% inulin), high insoluble fibre (10% cellulose), and high soluble (10% inulin) fibre diets for their lifetime (Then *et al.*, 2020). Significantly higher relative abundance of *B. acidifaciens* was seen in the gut microbiota of the high soluble fibre group after 2 weeks of the diet. In Kaplan Meier analysis, high soluble fibre resulted in delayed time to treble tumour volume after IR compared to the other groups (Figure 14A). Within this group, the mice were categorised into responders and non-responders based on their tumour growth curves reflecting their response to treatment (Figure 14B). Responders to IR had significantly higher abundance of *B. acidifaciens* than non-responders (Figure 14C). When all mice fed with different diets were pooled, an association was found between the survival time of mice and relative abundance of *B. acidifaciens* (Figure 14D). Therefore, we showed that a high soluble fibre diet containing inulin sensitised RT112 xenografts to irradiation and this was associated with modification of the gut microbiota. We also proposed that the gut microbiota could act as a potential radiosensitiser because *B. acidifaciens* abundance, which was enhanced by dietary fibre, positively correlated with tumour response to radiation. However, the causal relationship between the gut microbiota and radiosensitisation and its underlying mechanism remained unclear.

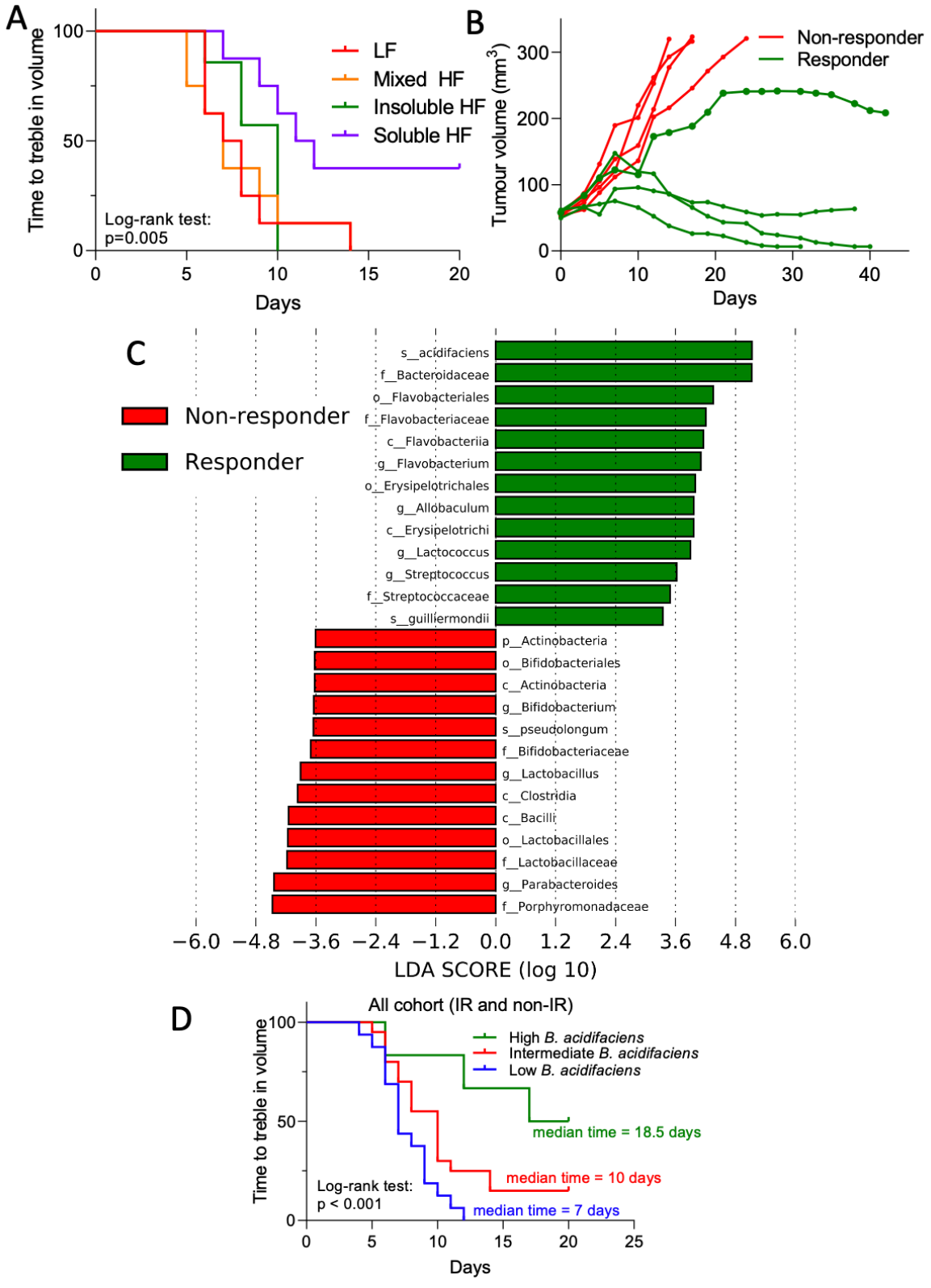

A
Time to treble in volume
100
50
0
0
5
10
15
20
Days
LF
Mixed HF
Insoluble HF
Soluble HF
Log-rank test:
p=0.005
B
Tumour volume (mm3)
300
200
100
0
0
10
20
30
40
Days
Non-responder
Responder
C
Non-responder
Responder
s__acidifaciens
f__Bacteroidaceae
o__Flavobacteriales
f__Flavobacteriaceae
c__Flavobacteriia
g__Flavobacterium
o__Erysipelotrichales
g__Allobaculum
c__Erysipelotrichi
g__Lactococcus
g__Streptococcus
f__Streptococcaceae
s__guilliermondii
p__Actinobacteria
o__Bifidobacteriales
c__Actinobacteria
g__Bifidobacterium
s__pseudolongum
f__Bifidobacteriaceae
g__Lactobacillus
c__Clostridia
c__Bacilli
o__Lactobacillales
f__Lactobacillaceae
g__Parabacteroides
f__Porphyromonadaceae
−6.0 −4.8 −3.6 −2.4 −1.2 0.0 1.2 2.4 3.6 4.8 6.0
LDA SCORE (log 10)
D
All cohort (IR and non-IR)
Time to treble in volume
100
50
0
0
5
10
15
20
25
Days
High B. acidifaciens
Intermediate B. acidifaciens
Low B. acidifaciens
median time = 18.5 days
median time = 10 days
median time = 7 days
Log-rank test:
p < 0.001

Figure 14 Soluble HF causes increased growth delay in irradiated bladder cancer cell xenografts. (A) Treatment of irradiated (6 Gy) RT112 xenografts with low fibre (0.2% cellulose), high mixed fibre (5% cellulose plus 5% inulin), high insoluble fibre (10% cellulose), and high soluble (10% inulin) fibre diets (n=8 for each group). Kaplan–Meier survival curves of mice with RT112 xenografts showing plots of time to treble tumour volume. (B) Slopes of tumour curves in the high soluble fibre group were calculated by linear regression to classify them into responders and non-responders to IR. (C) Linear discriminant analysis (LDA) scores computed for differentially abundant taxa in the microbiotas of responders (green) and non-responders (red). (D) Kaplan-Meier plots of time for tumours to treble in volume based on *B. acidifaciens* abundance in whole cohorts from different diet groups combining IR and non-IR-treated mice. Adapted from Then *et al.*, 2020.

1.13 Methods to investigate the gut microbiota and SCFAs

1.13.1 16S rRNA gene sequencing

16S ribosomal RNA (rRNA) is a component of the 30S small subunit of the prokaryotic ribosome and is coded by the 16S rRNA gene (Figure 15). Bacterial 16S rRNA gene sequencing is the general approach used to survey microbial communities by reconstructing phylogenies (Yarza *et al.*, 2014), using the species-specific sequences within given hypervariable regions. It is noted that the V1 to V4 region is more divergent than V4 to V7 (M. Kim *et al.*, 2011; Ward *et al.*, 2012). In addition, hypervariable V3/V4 regions have the maximum nucleotide heterogeneity and display the maximum discriminatory power (Chen *et al.*, 2019; Sirichoat *et al.*, 2021), so these regions provide a higher resolution in bacterial clustering for stool samples.

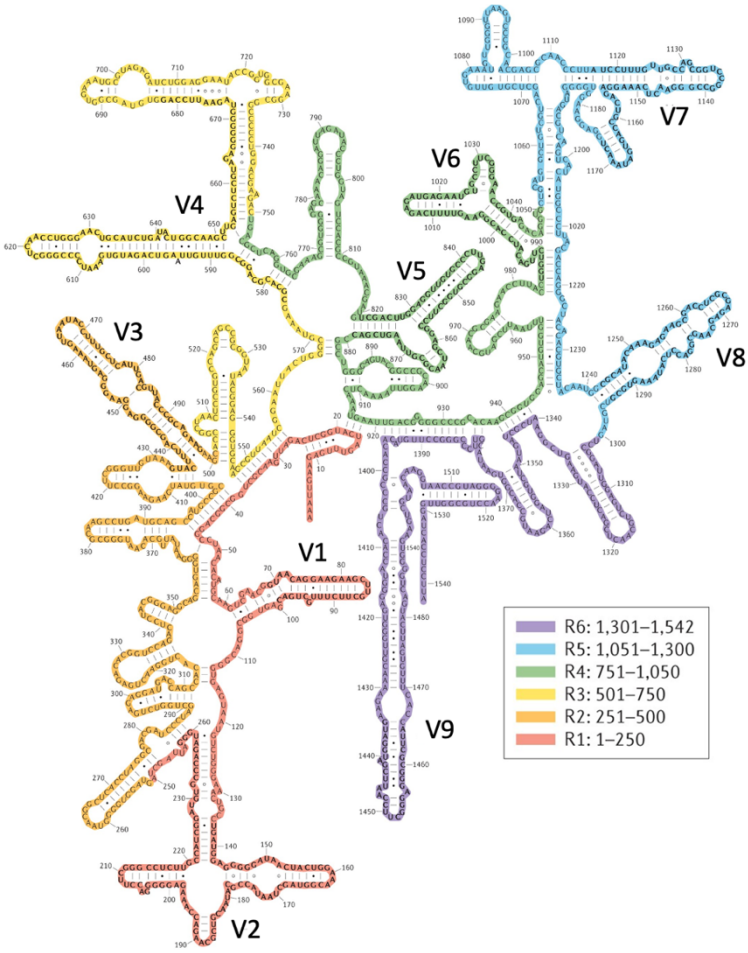


Figure 15 16S rRNA gene sequencing. Secondary structure of 16S rRNA of *E. coli* which contains nine hypervariable regions in the six R fragments. Adapted from Yarza *et al.*, 2014.

1.13.2 Taxonomy and phylogenetics

Taxonomy is the identification system used to classify biological organisms on the basis of shared characteristics. In this classification, organisms are grouped together into taxa (singular: taxon) and these groups are given a taxonomic rank. Taxonomic ranks include kingdom, phylum, class, order, family, genus, species, and strain (Figure 16). Phylogenetics is the study of the evolutionary history and relationships among species. These relationships are discovered through DNA sequences under a model of evolution. The result of these analyses is a phylogeny (or phylogenetic tree) – a diagrammatic depiction of the evolutionary relationships of different species.

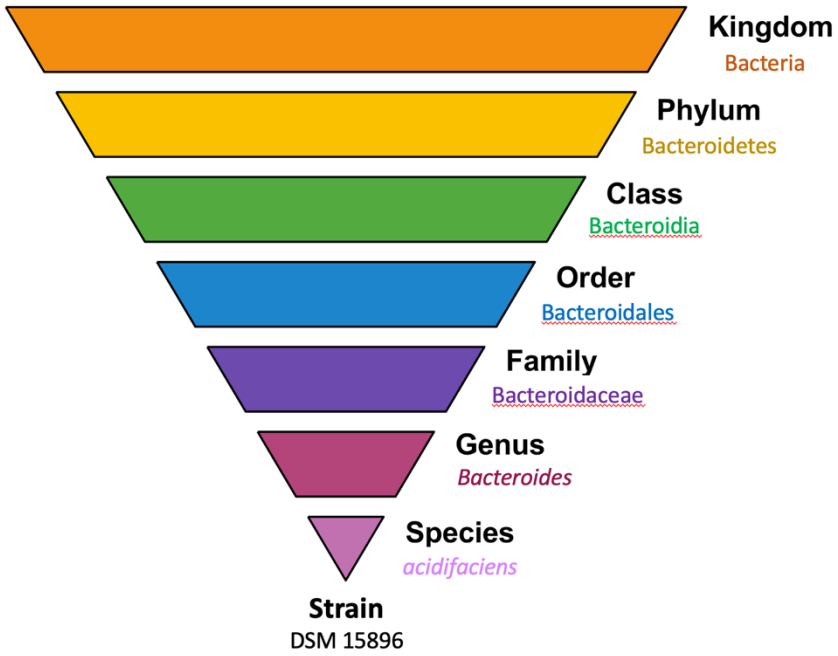


Figure 16 Taxonomic classification. The major taxonomic ranks as applied to *B. acidifaciens*.

1.13.3 Alpha and beta diversity

To quantify how the overall gut microbiota is changed by dietary fibre or ionising radiation, evaluation of diversity is applied to assess the changes in community. Diversity implies a measure of both species' richness and evenness. Species richness is a measure of the total number of species in a community; evenness expresses how evenly the species in a community are distributed among each other. Alpha diversity (also called 'local diversity') refers to diversity within a particular community (Figure 17). Beta diversity is species diversity between different communities that highlights taxonomical differences between pairs of samples (Anderson *et al.*, 2006; Finotello *et al.*, 2018).

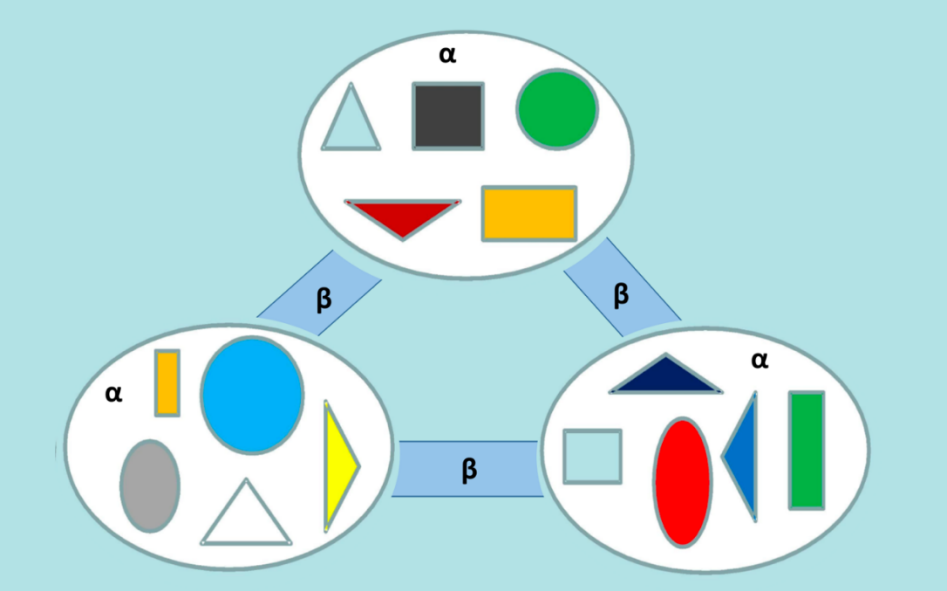


Figure 17 Alpha and beta diversity. Alpha diversity refers to a measure of similarity within communities. Beta diversity refers to a measure of similarity between communities.

1.13.4 Linear discriminant analysis effect size

Linear discriminant analysis effect size (LEfSe) is an algorithm which is used to discover the differentially abundant taxa between two or more biological conditions (Figure 18) (Segata *et al.*, 2011). It validates statistical significance, biological consistency and effect relevance using the non-parametric factorial Kruskal Wallis (KW) sum-rank test. Cladograms, diagrams that show hypothetical relationships between groups of organisms, are used to show the taxa characterising differences between different study groups (Figure 18) and linear discriminant analysis (LDA) is used to estimate the effect size of each differentially abundant feature.

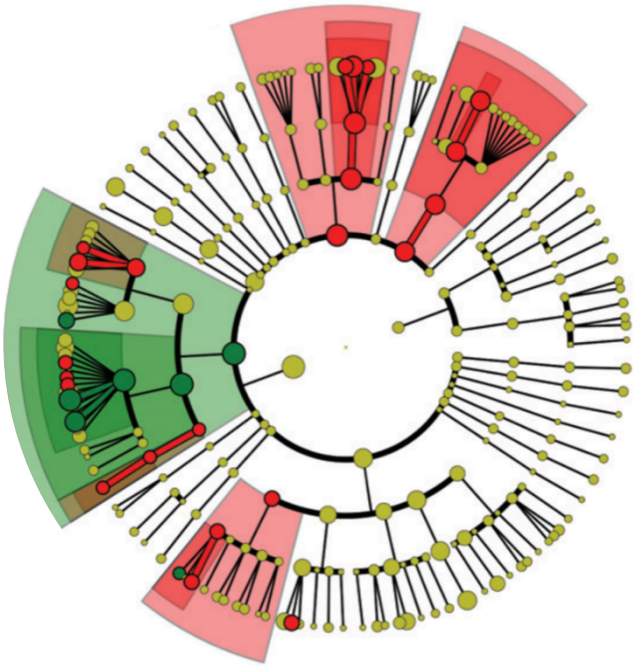


Figure 18 Cladogram. The cladograms depict the taxa (highlighted by small circles) characterising different abundance between different biological conditions. Differences are represented in the colour of the most abundant class (red and green indicating two different groups, yellow indicating non-significant).

1.14 Aims of this study

Emerging evidence showed that dietary fibre and the gut microbiota can improve the efficacy of immunotherapy and chemotherapy, mainly in melanoma. There are very limited studies regarding the role of gut microbiota in changing radiotherapy efficacy for cancers outside the intestine. There are only three studies to date: one using antibiotics as an approach to modify gut microbiota to increase RT effectiveness in melanoma, lung and cervical cancer models (Uribe-Herranz *et al.*, 2020), one also using antibiotics but to diminish RT's effect in breast cancer model (Shiao *et al.*, 2021) and the other was our previous study using dietary fibre to enhance radiosensitivity in an immunocompromised bladder tumour model (Then *et al.*, 2020).

Given that RT (Shiao & Coussens, 2010), dietary fibre (Spencer *et al.*, 2021) and the gut microbiota (Gopalakrishnan *et al.*, 2018) can modulate anti-tumour immune responses, it is highly likely that immunomodulation could be involved in the radiosensitising effect of dietary fibre seen in our previous study, although these mice were deficient in T cells (Then *et al.*, 2020). Therefore, it is necessary to conduct studies in fully immunocompetent mice. The approach of using dietary fibre is especially important because elderly patients are vulnerable to the current chemotherapy-based radiosensitisation approaches (details in section 1.2.2). Our previous systematic review has shown that dietary supplements, including probiotics, synbiotics and polyphenols, may reduce the risk of diarrhoea, one of the most common gastrointestinal side effects, in patients undergoing pelvic radiotherapy. This potential radioprotection by dietary supplements fulfils the idea that dietary fibre could achieve a favourable radiotherapy therapeutic ratio by increasing tumour response and decreasing side effects.

In this DPhil project, I used several cohorts of C57BL/6 mice to study the effects of dietary fibre alone and in combination with IR on tumour response, and on radiation normal tissue toxicity, including acute and late effects. The dietary fibres used were psyllium (has been used to mitigate side effects after RT, section 1.4.4), resistant starch (well-known butyrate producing fibre, section 1.4.5) and inulin (readily fermentable fibre and potential

radiosensitiser, section 1.4.6). I hypothesised that the systemic effects of the gut microbiota in terms of secreted metabolites and immune responses, due to dietary fibre modification, could be exploited in conjunction with ionising radiation to achieve tumour radiosensitisation and amelioration of normal tissue effects. Consistent with this hypothesis, I also wished to investigate the potential radiosensitising effects of *Bacteroides acidifaciens,* as its abundance was enhanced by dietary fibre and positively correlated with tumour response to radiation (Then *et al.*, 2020), and there are no studies to date regarding its role in cancer cell survival and radiosensitisation.

The aims of this study were:

1) to examine the impact of the diet on the gut microbiota, metabolites, tumour growth and anti-tumour immune responses before and after irradiation,
2) to examine the impact of diets on the normal tissues without and after irradiation, and
3) to investigate the effects of bacterial metabolites on bladder cancer cell lines.

Chapter 2: Materials and methods

2.1 Mouse experiments

All animal experiments complied with UK Home Office Guidelines, following the ARRIVE (Animal Research: Reporting of In Vivo Experiments) guidelines. We obtained approval from the University of Oxford Animal Welfare and Ethical Review Body (AWERB), under University of Oxford project licences (PPLs) P8484EDAE and PP8415318. All mice were purchased from Charles Rivers Laboratories (UK). They were housed in a temperature-controlled environment with a 12-h reversed-phase light/dark cycle (lights on 07:00 h) and provided with food and water *ad libitum*. Mice were observed daily for general welfare.

2.1.1 Cell lines used in animal experiments

The murine bladder cancer cell lines UPPL591 and BBN963 were obtained from Professor William Kim at the University of North Carolina, Chapel Hill. They were maintained in DMEM, high glucose, GlutaMAX supplement, pyruvate (Gibco) medium supplemented with 10% fetal bovine serum (Gibco). Murine bladder cancer cell line G69, from Professor Keith Syson Chan's laboratory, was maintained in DMEM:F12 (1:1, Lonza) supplemented with 10% fetal bovine serum, recombinant EGF (BioLegend Inc), insulin-transferrin-selenium (0.1x, Life Technologies), D-glucose anhydrous (VWR), sodium pyruvate (Gibco) and non-essential amino acids (Invitrogen). All cell lines were cultured in a humidified atmosphere of 5% CO_2 at 37°C and sub-cultured by washing the cells with phosphate buffered saline pH 7.4 (PBS; Gibco) and trypsinising them with 0.25% Trypsin-EDTA solution (Gibco) to make new passages. At around 90% confluency, cells were passaged using 0.25% Trypsin-EDTA. Once passaged 10 times, a new batch of cells was thawed and cultured. A stock of cells was kept in a -80°C freezer in fetal bovine serum supplemented with 10% dimethyl sulfoxide. The cell lines UPPL1591 and BBN963 used in experiments tested mycoplasma negative in polymerase chain reaction (PCR) conducted by Professor Billy Kim's lab. The G69 cell was treated with plasmocin to avoid mycoplasma contamination by Professor Keith Chan's lab.

2.1.2 Mouse strains

Three mouse strains were used in this project: C57BL/6J (immunocompetent), FVB (immunocompetent) and CD1 nude (immunocompromised). They were all purchased from Charles Rivers except the mice in section 3.3.1 and 3.3.2 which were from the Biomedical Services Department, University of Oxford. All experiments were performed with female mice at 4-7 days post-delivery and when mice were 5-8 weeks old, except in section 3.3.1 and 3.3.2, where some male mice were used.

2.1.3 Mouse bladder tumour models

UPPL1591 and BBN963 models

At 7 to 8 weeks of age, C57BL/6 female mice were injected subcutaneously with 1.5 x 10^6 or 3 x10^6 UPPL1591 or BBN963 mouse bladder cancer cells in 200 µL of Hanks' Balanced Salt Solution (HBSS; Lonza) and phenol red-free Matrigel (BD Biosciences) mixture with a ratio of 1:1. The mice were culled 5-6 weeks after tumour injection. All tumour samples were stained with H&E stain and investigated for their microscopic diagnosis by the veterinary histopathologists Dr Alejandro Suarez Bonnet and Professor Simon Priestnall (Royal Veterinary College, University of London).

G69 model

At 5 to 6 weeks of age, FVB female mice were injected subcutaneously with G69 mouse bladder cancer cell. There were three groups, comprising 1x10^6 cells in 200 µL of PBS and Matrigel (1:1) mixture, 3x10^6 cells in in 200 µL of PBS and Matrigel (1:1) mixture and 3x10^6 cells in 200 µL PBS only. Tumour growth was monitored for up to 9 weeks.

2.1.4 Diets in non-tumour-bearing mice

Diets and three strains of mice

At seven to eight weeks of age, C57BL/6 female, CD-1 nude female, FVB female and male mice were fed with either low fibre diets (0.2% cellulose) or high soluble fibre diets (10%

inulin) for three weeks (Research Diets Inc, USA). Details of the diet formulae are listed in Appendix Table A1.

Different diets in FVB mice

At seven to eight weeks of age, FVB female mice were fed either 0.2% cellulose, 10% resistant starch, 10% inulin, 5% psyllium, 5% psyllium plus 5% resistant starch or 5% psyllium plus 10% resistant starch for three weeks. Details of the diet formulae are listed in Appendix Table A1 and A2.

2.1.5 Diets with or without irradiation in tumour-bearing mice

Diets (with corn starch) and UPPL1591 mouse bladder tumours

At five to six weeks of age, C57BL/6 female mice were injected subcutaneously under anaesthesia with $1.5x10^6$ UPPL1591 mouse bladder cancer cells with HBSS and Matrigel (2:1) at a total volume of 200 µL in the right flank. They started receiving either low fibre (0.2% cellulose) or high fibre diets including 5% psyllium, 10% RS, 10% inulin, 5% psyllium plus 10% RS or 5% psyllium plus 10% inulin until they were culled when their tumours reached 100 mm^3. Total consumption of modified diets by each group of the mice was not recorded. Details of the diet formulae are listed in appendix Table A1 and A2 (Research Diets Inc, USA).

Diets (with dextrose) and UPPL1591 mouse bladder tumours with or without IR

At five to six weeks of age, C57BL/6 female mice were injected subcutaneously under anaesthesia with $1.5x10^6$ UPPL1591 mouse bladder cancer cells with HBSS and Matrigel (1:1) at a total volume of 200 µL in the right flank. They started receiving either normal chow, low fibre diet (0.2% cellulose) or high fibre diets including 5% psyllium, 5% psyllium plus 10% RS or 5% psyllium plus 10% inulin. Total consumption of modified diets by each group of the mice was not recorded. Details of the diet formulae are listed in appendix Table A3 (Research Diets Inc, USA).

2.1.6 Diets with or without irradiation in non-tumour-bearing mice

Acute toxicity radiation experiment

At six to seven weeks of age, C57BL/6 female mice commenced low fibre (0.2% cellulose) or high fibre diets, including 5% psyllium, 5% psyllium plus 10% RS or 5% psyllium plus 10% inulin. Total consumption of modified diets by each group of the mice was not recorded. Details of the diet formulae are listed in appendix Table A3 (Research Diets Inc, USA).

Late toxicity radiation experiment

At six to seven weeks of age, C57BL/6 female mice started receiving either a low fibre (0.2% cellulose) or high fibre diets including 5% psyllium, 5% psyllium plus 10% RS or 5% psyllium plus 10% inulin for 9 weeks followed by normal chow for another 12 weeks. Total consumption of modified diets by each group of the mice was not recorded. Details of the diet formulae are listed in appendix Table A3 (Research Diets Inc, USA).

2.1.7 Irradiation

Gulmay ionising radiation for tumour growth delay

When the tumours reached 100 mm^3, flank allografts were treated prone with 6, 8 or 10 Gy of x-rays using a Gulmay-320 cabinet irradiator (Xstrahl Inc, UK). Throughout this procedure, mice were anaesthetised (1-3% isoflurane in 30% O_2-enriched air) with respiration monitoring and skin temperature maintenance at 35-37°C on a heat pad. Within 5-10 minutes, mice were fully anaesthetised and were placed inside the irradiator. Lead shields were used to cover the animals leaving only the tumour exposed. X-rays were delivered at a rate of 2.1 Gy/min. Radiation was given at 300 kV and 10 mA, for 2 min and 49 sec (6 Gy), 3 min and 46 sec (8 Gy) or 4 min and 43 sec (10 Gy). Mice were kept in an acclimatised rack at 37°C until they were fully recovered from anaesthesia.

Small Animal Radiation Research Platform (SARRP) ionising radiation for acute toxicity

Two and a half weeks after commencing the modified diets, mice were treated supine with 10, 12 or 14 Gy of x-rays (220 kVp, 13.0 mA copper filtered beam with a measured half-value layer (HVL) of 0.84 mmCu) to the lower abdomen, including the lower small intestine using a SARRP irradiator (Xstrahl Ltd, Camberley, UK). Irradiation was delivered using a 356-degree arc treatment with a 13.7-mm circular collimator (at isocentre) at a dose rate of approximately 2 Gy per minute. Dosimetry commissioning for the treatment planning software was performed using Gafchromic EBT3 Film (Ashland Advanced Materials, Bridgewater NJ). Throughout this procedure, mice were anaesthetised (1-3% isoflurane in 30% O_2-enriched air) using a custom-made 3D printed cradle that featured skull immobilisation, gas anaesthetic delivery, respiration monitoring and skin temperature maintenance at 35-37°C.

SARRP ionising radiation for late toxicity

Two weeks after commencing the modified diets, mice were treated supine using a SARRP with 5 Gy for 5 consecutive days, using a 356-degree arc treatment and 8.5-mm collimator, with the isocentre positioned at the posterior caudal bladder wall covering the lower large intestine, to avoid the small intestine. Throughout this procedure, mice were anaesthetised (1-3% isoflurane in 30% O_2-enriched air), and treated vertically, head down in a custom-made 3D printed cradle that featured skull immobilisation, anaesthetic delivery, respiration monitoring and skin temperature maintenance at 35-37°C.

2.1.8 Tumour growth and survival analyses

For mouse tumour growth delay experiments, tumour growth was measured three times a week using callipers and calculated using the following ellipsoid volume formula: length x width x height x π / 6 (Tomayko & Reynolds, 1989). Tumour growth curves were analysed for each group, and their slopes were compared using one-way ANOVA. Time to quadruple in volume was defined as the interval (in days) from the date of irradiation (growth to 100 mm^3) to the date for the tumour to quadruple in volume.

2.1.9 Monitoring of mice and welfare end-points

In tumour growth delay experiments, animals were weighed three times per week. For acute toxicity experiments, mice had their behaviour checked and were weighed daily until being culled at 3.75 days post irradiation. For late toxicity experiments, mice had their behaviour checked and were weighed daily for the first 5 days, then 3 times a week the following week and then twice a week during the rest of the experimental period. The mice were followed up to 24 weeks. The stool and urine analyses were performed 7, 12 and 17 weeks after IR. For all experiments, mice were closely monitored if a 10% loss in body weight was detected. In that case, mash of non-fibre food would be given, and the mice were weighted every day. Humane endpoints were applied if they showed any of the following conditions: weight loss of 15%, change from normal behaviour, compromised ambulation or food/water intake, anaemia, huddled posture or immobility, and diarrhoea.

2.1.10 Sacrifice, sample harvesting and processing

In the tumour growth experiments, mice were sacrificed with an intraperitoneal injection of 200 µL of 200 mg/kg sodium pentobarbitone, so that blood could be collected for plasma cytokine analysis by cardiac puncture. In acute and late toxicity experiments, mice were sacrificed by neck dislocation. In the experiments described in sections 5.1 and 5.2, small and large intestines were collected using the 'Swiss roll technique' described in section 2.2.11 (Moolenbeek & Ruitenberg, 1981). Tumours and Swiss rolls were collected and fixed in 10% neutral buffered formalin for 24 hours at 4°C and then transferred to 70% ethanol. Within 14 days of harvesting, these tissues were processed by an automated Tissue Processor (Leica, TP1020) through 100% ethanol (6 baths), followed by xylene (4 baths) and paraffin (2 baths). Samples were embedded in paraffin blocks. Cardiac puncture was performed and 1 mL of blood was incubated in prepared tubes containing 100 µL of 2.5 U/µL heparin sodium (Sigma) for 10 minutes on a rotator at room temperature. Tubes were kept on ice until centrifugation for 10 minutes at 1500 g at room temperature. Plasma was collected and stored at -80°C. Spleens were harvested and kept in PBS on ice for single cell suspension as described in section 2.2.14.

2.1.11 Histological and functional assays for normal tissue toxicity

Caecal size and colonic length

The caeca and colons were dissected and photographed. The caecal size (measured in area) and the length of colon was measured using the Fiji version of ImageJ software.

Crypt assay

Swiss rolls were made from small (three consecutive lengths) and large (one length) intestines. The samples were formalin-fixed overnight in 10% neutral buffered formalin and stored in 70% ethanol prior to paraffin-embedding. Five micrometre sections were cut and stained for haematoxylin and eosin (H&E) and the slides were scanned using an Aperio ScanScope (Leica Biosystems). The H&E-stained Swiss roll slides of small intestine were analysed using a crypt assay as previously described (Paillas *et al.*, 2020; Ruan *et al.*, 2021). As only part of the abdomen had been irradiated, the most affected areas in each Swiss roll were selected. Irradiated mouse samples were excluded if there was less than 3 mm of intestinal damage. Regenerating crypts (presence of >10 cells arranged in a distinct shape with no sign of apoptosis) were blind counted. The control number of crypts per length of small intestine was determined from the mean of three mock-treated mice. The percentage of surviving crypts in each group was calculated as:

$$\frac{\text{Number of regenerating crypts per mm}}{\text{Number of control crypts per mm}} \times 100\ \%$$

Stool analysis

Mice were singly housed for 24 hours and faeces were collected from each mouse, counted, and weighed. The numbers and weight of faeces were expressed in terms of the total number and dry weight per mouse. Pellets were photographed. After that, the length, shape, and number of pellets were analysed using the Fiji version of ImageJ software. Briefly, I set the scale by measuring 1 cm on image as known distance using line tool and set to show the measurements of area, bounding rectangle, fit ellipse, shape description, feret's diameter and display label. After that, I cropped the area of interest with stool pellets and adjusted the

images to 8-bit, binary, and filled hole. By the function of measure, I obtained the summary of all measurements and performed a particle analysis with a size range of 0.02 to infinite to obtain individual measurement values.

Urine analysis

After 24 hours isolation in individual cages for stool collection, mice were kept on bench surface protector (VWR International Ltd) in a transfer cage for 4 hours as previously described (Yu *et al.*, 2014). Briefly, the mice were handled calmly to avoid stressing the mice and causing reflex urination. At the end of the study period, the mice were returned to their normal housing. The urine spots on the bench protector paper were imaged using ultraviolet light on a transilluminator. Filters were photographed and the area of voiding spots was measured using the Fiji version of ImageJ software. Briefly, I set the scale by measuring 1 cm on image as known distance using line tool and measured the numbers and areas of urine spots to estimate the urine volume.

2.1.12 Gut microbiota analysis

Microbiota sample collection and DNA extraction

Faeces were snap-frozen in dry ice once they were collected from mouse intestines under aseptic conditions. All samples were kept at -80°C before DNA extraction. In the experiment of section 3.3.1, before DNA extraction, faeces were weighted and 19 μL spike-in control I (ZymoBIOMICS, Cat. No. D6320) was added to the faeces for absolute quantification of the gut microbiota. Bacterial genomic DNA was extracted using a DNeasy PowerSoil Pro DNA Isolation Kit (QIAGEN Ltd, Manchester, UK), as per the Human Microbiota Project (Human Microbiome Project, 2012a). Briefly, by adding sodium dodecyl sulfate (SDS), microbial cells were lysed by mechanical disruption in a mix of 0.1 mm and 0.5 mm zirconium bead tube (QIAGEN Ltd, Cat.) at 2,800 rpm for 10 minutes on digital Vortex-Genie 2 shaker (Scientific Industries), followed by binding of DNA tightly to a silica membrane in a Spin Filter device at high salt concentrations. Eventually, DNA was collected into sterile elution buffer and quantified using a NanoDrop spectrophotometer (Thermo Scientific, San Jose, CA, USA) and Qubit dsDNA BR assay kit (Life Technologies Ltd) on Qubit fluorometer (Invitrogen). All DNA samples were kept at -80°C before being sent for library preparation and sequencing at the Oxford Genomics Centre (Wellcome Centre for Human Genetics, University of Oxford, UK).

Bacterial 16S rRNA gene sequencing

16S rRNA gene sequencing methods were adapted from the methods developed for the NIH-Human Microbiota Project (Human Microbiome Project, 2012a, 2012b). The amplification and sequencing of 16S rRNA gene V3V4 regions were done by the Oxford Genomics Centre on a MiSeq platform (Illumina, Inc, San Diego, CA) using their 2x300 bp paired-end protocol, yielding paired-end reads with near-complete overlap. The primers containing adapters for Miseq sequencing were used for amplification and single-end barcodes, allowing pooling and direct sequencing of PCR products (Caporaso *et al.*, 2012).

MiSeq primers targeting V3V4 region of gut bacteria are shown below

341F CCTACGGGNGGCWGCAG

805R GACTACHVGGGTATCTAATCC

After receiving the raw sequence data, I analysed them using the QIIME2 platform, LEfSe and R packages. All 16S rRNA gene-based metagenomic analysis was conducted by myself using a QIIME2 platform (Hall & Beiko, 2018). I clustered quality filtered sequences with >97% identity into bins known as Operational Taxonomic Units (OTUs), using open-reference OTU picking. I obtained the relative abundance of each OTU from all samples. In the taxonomic analysis, I classified the microbiota at the phylum, class, order, family, genus and species levels by referring to the Greengenes database (Balvociute & Huson, 2017). Relative abundance of each taxon was calculated as the percent composition of a specific organism relative to the total number of organisms. In some cases, ';(prefix)_' means that the taxon did not have an assignment at the specific level and ';_' means that there were multiple matches at this level and taxonomy is uncertain.

The analysis pipeline is illustrated below (Figure 19):

i. All sequences were trimmed to a length of 300, since the quality dropped at this length based on the sequence quality plots.
ii. I de-noised sequencing errors by using the "Deblur" plugin in QIIME2 (Nearing *et al.*, 2018).
iii. Taxonomic assignment was performed with Greengenes (DeSantis *et al.*, 2006) by the "feature-classifier" command.
iv. To visualise the differences in microbial composition between gut contents and tissue, a taxonomic profile was generated by conducting differential abundance analysis using balances (balances are useful tools to investigate the relationship between proportions) in gneiss (a toolkit to study phylogenetic data) (Mandal *et al.*, 2015).
v. To identify the features characterising the differences between different groups, the LEfSe method of analysis was performed to compare abundances of all bacterial clades (Segata *et al.*, 2011). By validation using the Kruskal-Wallis test at the α setting of 0.05, effect size was obtained by LDA, a method to estimate the

effect size of each differentially abundant feature, based on the significantly different vectors resulting from the comparison of abundances between groups.

vi. To validate the significance of enrichment of bacterial taxa among different groups, discrete false-discovery rates (DS-FDR) were calculated (Jiang *et al.*, 2017).

vii. I generated a phylogenetic tree by using the "phylogeny" plugin in QIIME2.

viii. To investigate alpha and beta diversity, the diversity commands of "alpha-group-significance" and "beta-group-significance" were used to obtain Peilous's evenness, Faith's phylogenetic diversity, Shannon's index, and Bray-Curtis dissimilarity. By using the 'beta-group-significance' command, permutational multivariate analysis of variance (PERMANOVA) was performed to test whether distances between samples within a group were more similar to each other than they were to samples from the other groups (Anderson, 2001). A principal coordinates (PCoA) plot was obtained by using the Emperor Tool based on the results of Bray-Curtis dissimilarities.

ix. The OTU table was rarefied using the "alpha-rarefraction" command in QIIME2. The alpha rarefraction plot showed the richness of the samples with increasing sequence count.

x. To predict the metagenome functional profiles, PICRUSt, a bioinformatics software package, was used to collapse predicted functions (KEGG Orthology; KO) based on 16S rRNA surveys into higher categories (KEGG pathway) after picking OTUs and normalisation (Langille *et al.*, 2013).

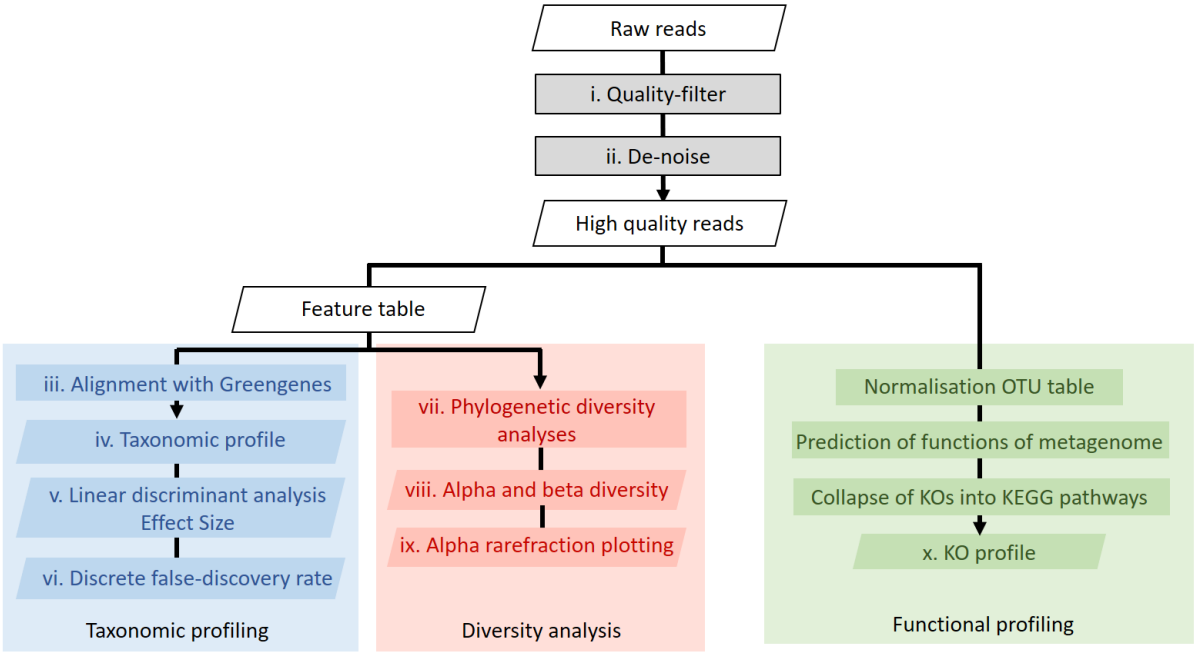


Figure 19 Flow chart of 16S rRNA gene analysis pipeline. Raw reads were first proceeded through a quality-filter and further de-noised to generate high quality reads and they were analysed further to investigate taxonomic profiles, diversity, and functional profiles. Roman numbers are used to match the analysis pipeline text and Figure 19.

2.1.13 Untargeted metabolomics analysis

Sample processing

Caecal (N=36 for section 4.3, N=43 for section 4.4, N=84 for section 5.1) contents were added to four-fold Millipore Synergy purified water at a ratio of 1:4 (caecal content:water) for homogenisation and were sent to the Department of Chemistry on dry ice for untargeted metabolomics analysis using ion chromatography-mass spectrometry (IC-MS). Dr Mariya Misheva from Professor James McCullagh's laboratory performed the following procedures. Supernatant was filtered using an Amicon ultra-0.5 centrifugal filter Unit (3 KDa Nominal Molecular Weight Limit; Merck, Cat. No. UFC500396) at 14,000 g for 25 min at 4°C and collected in total recovery vials (Waters Corporation). Samples were analysed as described previously (Walsby-Tickle *et al.*, 2020). Briefly, chromatographic separation was achieved using a partial loop injection (5 µL) of the supernatant to a Dionex ICS-5000+ Capillary HPIC system (Dionex, Sunnyvale, CA, USA) coupled to a Q-Exactive HF hybrid quadrupole-Orbitrap

mass spectrometer (Thermo Scientific, San Jose, CA, USA). The mass spectrometer was equipped with a HESI II probe in negative ion mode, and compounds were detected using a Dionex IonPac AS11-HC column (2 × 250 mm^2, 4 µm; Dionex, Sunnyvale, CA, USA) column. Analytes were separated with the following aqueous hydroxide ion gradient at a flow rate of 0.25 mL/min to elute the analytes from the column: 0 min, 0 mM; 1 min, 0 mM; 15 min, 60 mM; 25 min, 100 mM; 30 min, 100 mM; 30.1 min, 0 mM; 37 min, 0 mM. The presence of butyric acid was confirmed by retention time and accurate mass comparison with an authentic standard (Merck, Cat. No. CRM46975).

Metaboanalyst

Data analysis was performed on Metaboanalyst5.0 (Pang *et al.*, 2021). In brief, the peak intensities table was uploaded in .csv format, and data filtering was done by interquantile range to remove variables of very small values, near-constant values and those with low repeatability. Data was normalised by median or quantile with log transformation and auto scaling. One-way Analysis of Variance (ANOVA) and Partial Least Squares - Discriminant Analysis (PLS-DA) were used to study the metabolites significantly enhanced in specific groups and the distance (from one dietary group to another) of metabolite profiles among all dietary groups.

2.1.14 Immunological analyses

Immunohistochemistry

Mouse tumours were fixed in buffered 10% formalin solution overnight and transferred to 70% ethanol and stored at 4°C. The tumours were embedded in paraffin, and 5 µm sections were mounted on positively charged slides. Sections were deparaffinised and hydrated after incubating at 50°C for 20 minutes. After antigen retrieval in pH 9.0 Tris/EDTA buffer using a microwave, the sections were incubated with 3% H_2O_2, avidin/biotin blocking kit (SP-2001), and 2.5% normal horse serum blocking solution (MP-7401; Vector laboratories). Subsequently, I incubated the sections with CD3 (Abcam ab16669; 1:500 dilution) and CD8 (CST 98941; 1:400 dilution) primary antibodies overnight at 4°C. ImmPRESS (Peroxidase)

Polymer Anti-Rabbit IgG Reagent (MP-7401; Vector laboratories) was used as secondary antibody. The sections were visualised by DAB staining and counterstained with haematoxylin. The slides were mounted by DPX mounting medium after dehydration. Slides were digitally scanned using the Aperio ScanScope (Leica Biosystems). Cell number quantification of three parts of the tumour core for each tissue was performed by Chee Kin Then and Daniel Sescu on QuPath.

To quantify CD8 staining, I randomised the slide order to minimise bias. After that, Then and Sescu manually counted the $CD3^+$ and $CD8^+$ nucleated cells. Three regions of interest of the tumour core, each of approximately 115,000 μm^2 area, were delineated at low magnification across each tumour tissue. Then, at approximately 40x magnification, nucleated cells with nuclei at least 50% within the region of interest were marked as positively stained for CD3 and CD8. The density of $CD3^+$ and $CD8^+$ cells within each region of interest could thus be calculated by dividing the positive-stained cell numbers by the analysed area.

Nanostring

Total RNA was extracted from three 5 µm sections of formalin-fixed paraffin-embedded (FFPE) tissue samples using a RNeasy FFPE kit (Qiagen, 160012457). Briefly, paraffin was removed from the FFPE tissue sections by citroclear (TCS Biosciences, UK) and lysed with proteinase K digestion followed by heat treatment. The supernatant was treated with DNase, Buffer RBC, and ethanol. After binding total RNA to a RNeasy MinElute column, it was washed using buffer RPE. Eventually, RNA was collected into RNase-free water and quantified using a NanoDrop spectrophotometer (Thermo Scientific, San Jose, CA, USA). Nucleic acid fragmentation was measured by an Agilent RNA 6000 Nano Kit on an Agilent 2100 Bioanalyzer System. After the hybridisation of targets, capture probes and reporter probes was completed, the cartridge was analysed by Dr. Joanna Hester at the Nuffield Department of Surgical Sciences, John Radcliffe Hospital, Oxford. Data were analysed using the nCounter mouse PanCancer Immune Profiling Panel, and data acquired with the nCounter SPRINT profiler (NanoString). Data were imported into nSolverTM analysis software v2.5 for quality control and normalisation of gene transcripts using NanoString

analysis guidelines and housekeeping genes. Genes were tested for differential expression and volcano plot was created to show the $\log_2$ fold change and $-\log_{10}$(p-value) of each gene with the covariate of tumour response. A single linear regression was fit for each gene using all selected covariates to estimate its expression.

Flow cytometry

Mouse spleens were kept in PBS on ice and processed to obtain single cell suspensions within two hours of harvest. The spleens were transferred into 70 µL cell strainers (Corning) sitting in a 6 well dish, homogenised gently using the top of a plunger of a 5 mL syringe and rinsed with PBS buffer with 1% bovine serum albumin (BSA). After centrifugation of the cells at 130 x g for 3 minutes, red blood cells were lysed by using ACK lysis buffer (BioLegend Inc). The splenocytes were frozen in BSA with 10% DMSO until further flow cytometry analysis, as previously described (Bayne & Vonderheide, 2013).

On the day of flow cytometry analysis, the cells were centrifuged at 130 x g for 3 minutes and resuspended in 50 µL PBS buffer with 1% BSA followed by treatment with two panels of antibody mixtures. The myeloid panel included CD45, CD11b, CD11c, Ly6G, F4/8b and Gr-1. The lymphoid panel included CD45, CD3, CD8, CD49b, CD19 and CD4. Cell surface markers of immune cells are listed in Table 5 and details of antibodies used are listed in Table 6. After incubations of the cells on ice for 30 minutes, the samples were run on a LSR II Flow Cytometer (Becton Dickinson) at the Jenner Institute, University of Oxford and analysed on Flow-Jo (Becton Dickinson).

Table 5 Definitions of immune cell populations based on expression of cell surface markers.

Immune cell population	Cell surface markers
Total leukocytes	$CD45^+$
T lymphocytes	$CD45^+$ $CD3^+$
CD8 T cells	$CD45^+$ $CD3^+$ $CD8^+$
CD4 T cells	$CD45^+$ $CD3^+$ $CD4^+$
B lymphocytes	$CD45^+$ $CD19^+$
Natural killer (NK) cells	$CD45^+$ $CD49b^+$
Macrophages	$CD45^+$ $F4/80^+$
Dendritic cells (DC)	$CD45^+$ $CD11c^+$
Immature myeloid cells	$CD45^+$ $Gr\text{-}1^+$ $CD11b^+$

Table 6 Antibody titrations and catalogue numbers.

Fluorophore	Myeloid panel	Lymphoid panel
416/451	Fixable Violet Dead Cell Stain Kit (1:650; L34963)	
AF700	CD45 (1:40; eBioscience 56-0451-82)	
APC	Ly6G (1:650; eBioscience 17-5931-82)	CD49b (1:80; Cat #17-5971-82)
PE-Cy7	CD11b (1:10000; Cat #25-0112-82)	CD3 (1:40; eBioscience 25-0031-81)
FITC	CD11c (1:800; Cat #11-0114-82)	CD8 (1:160; eBioscience 11-0081-82)
PE	F4/8b (1:650; eBioscience 12-4801-82)	CD19 (1:650; Cat #12-0193-82)
PerCP-Cy5.5	Gr-1 (1:650; Cat #45-5931-80)	CD4 (1:400; Cat #45-0042-82)

Plasma $CD4^+$ T-helper cell cytokine assay

Blood was withdrawn from mice under terminal anaesthesia by cardiac puncture using a needle rinsed with heparin and transported on ice for centrifugation for 10 minutes at 1,000 x g. Plasma samples were then stored at -80°C before downstream analysis. Cytokine and chemokine concentrations in the supernatant (pg/mL) were measured using MILLIPLEX mouse 16-plex (IL-1β, IL-2, IL-4, IL-5, IL-6, IL-10, IL-12p70, IL-13, IL-17A, IL-21, IL-22, IL-23, IL-27, GM-CSF, IFNγ, TNFα), IL-18 single plex and TGFβ1 single plex magnetic bead kits (Millipore, MA). Details of cytokine panels used are listed in Table 7. Briefly, the plate was cleaned by wash buffer on a plate shaker. After that, standards, controls, assay buffer, serum matrix and plasma samples were loaded on the plate. After adding the Luminex beads with cytokine-specific capture antibodies, the samples were incubated overnight at 4°C with shaking. The samples were washed using a handheld magnetic separation block (Millipore)

for 30 seconds on a shaker twice, followed by addition of biotinylated detection antibodies specific to the cytokines of interest, to form an antibody-antigen sandwich. Streptavidin-Phycoerythrin was then added to bind with the detection antibodies. After washing the plate for 30 seconds twice again, the samples were resuspended on Luminex drive fluid (Millipore) and the plate was sent to Spyridoula Marinou at Centre for Clinical Vaccinology and Tropical Medicine (CCVTM), Churchill Hospital, Oxford to be read on a Luminex 200 instrument (Thermo Fisher).

Table 7 Cytokine panels.

Cytokine panels	Analytes
Th1/Th2	IL-1β, IL-2, IL-4, IL-5, IL-6, IL-12p70, IL-13, IL-18, GM-CSF, IFNγ, TNFα
Th9/Th17/Th22/Treg	IL-10, IL-17A, IL-21, IL-22, IL-23, IL-27

2.1.15 Statistical analysis

All results are mean ± standard error and $P < 0.05$ is considered statistically significant. All statistical analyses were performed on GraphPad Prism version 9.0 (La Jolla, CA). A one-way ANOVA with Dunnett's multiple comparison test was used to compare more than two groups.

In the gut microbiota analysis, alpha diversity was compared using the Mann-Whitney test. The LEfSe method of analysis was applied to determine the difference in faecal taxa, using the Kruskal-Wallis test. Significantly different taxa presented from the previous comparison were used as input for LDA, which produced an LDA score.

2.2 Cell experiments

2.2.1 Cell lines

The RT112 human bladder carcinoma cell line was obtained from DSMZ (Germany) and cultured in RPMI-1640 medium (Sigma) supplemented with 10% fetal bovine serum (Invitrogen). The T24 human bladder cancer cell line (ATCC, USA) was cultured in McCoy's 5A medium (Sigma) supplemented with 10% fetal bovine serum (Invitrogen). The human colon carcinoma cell line Caco-2 was obtained from DSMZ (German) and maintained in Eagle's Minimum Essential Medium (EMEM, Gibco) supplemented with 10% fetal bovine serum and 1% nonessential amino acids solution (Life Technologies Ltd). All cell lines were cultured in a humidified atmosphere of 5% CO_2 at 37°C and sub-cultured by washing the cells with phosphate buffered saline pH 7.4 (PBS; Gibco) and trypsinising them with 0.25% Trypsin-EDTA solution (Gibco) to make new passages. At around 90% confluency, cells were passaged using 0.25% Trypsin-EDTA. Once passaged 10 times, a new batch of cells was thawed and cultured. A stock of cells was kept in -80°C freezer in fetal bovine serum supplemented with 10% dimethyl sulfoxide. All cells used in experiments tested mycoplasma negative by using mycoplasma detection kit (Jena Bioscience).

2.2.2 Drugs

Sodium acetate (CALBIOCHEM), sodium propionate (≥ 99%, Sigma Aldrich) and sodium butyrate (98%, Sigma Aldrich) were dissolved in dH_2O.

2.2.3 Irradiator

For ionising radiation, cells were irradiated in complete medium at a dose rate of 1.5 Gy/min using a Gamma-Service Medical GmbH GSR D1 irradiator.

2.2.4 Bacterial strains and their supernatants

Dr Xuedan Wang from Professor Kevin Foster's laboratory prepared the bacterial supernatants according to the following procedures. All bacterial strains were obtained from DSMZ-German collection of microorganisms. Three strains of bacteria, namely *B. acidifaciens* (*BA*; DSM 15896), *Bifidobacterium animalis* (*Bif*; DSM10140), and *F. prausnitzii* (*FP*; DSM17677), and two cross-feeding combinations (*BA*+*FP* and *Bif*+*FP*) were cultured in Gifu Anaerobic Broth, Modified (GAM; Nissui Pharmaceutical, Japan). Medium broth was prepared anaerobically in a Coy anaerobic chamber (Coylabs, US, N_2 95%, H_2 5%). Bacteria (10^6 CFU/mL starting population for each strain) were inoculated into sealed Hungate tubes aseptically by injecting through a needle. They were then placed in a 37°C incubator for 24 hours with constant shaking. After collecting the supernatants from Dr Wang, I neutralised them to the same pH as GAM broth (pH 7.2) by adding a minimal volume of 3M NaOH or 3M HCl and by using a pH meter to measure the pH value. Finally, I centrifuged them at 2,200 x g for 10 minutes before filtering through a 0.22 µm polyethersulfone syringe filter (Millipore) and stored the bacterial supernatants in -80°C freezer.

2.2.5 Colony formation assay

Cells were seeded in 6-well plates at appropriate densities in triplicate, treated with short-chain fatty acids dissolved in ddH_2O or bacterial supernatants for 24 hours, and irradiated with 0, 2, 4, 6, and 8 Gy. For RT112, the cell densities in each well were 200 for 0 and 2 Gy, 400 for 4 Gy, 600 for 6 Gy and 800 for 8 Gy. After culturing for 10 days, colonies were fixed and stained with 0.5% crystal violet (Sigma; #548-62-9) in dH_2O and 20% methanol (Thermo Fisher Scientific; #67-56-1) for 1 minutes. Colony numbers were checked under a light microscope and colonies below 50 cells were excluded. Finally, they were quantified using a GelCount colony counter (Oxford Optronix). Plating efficiency at 0 Gy was determined by dividing the number of colonies counted per dish by the number of cells seeded without irradiation. The surviving fraction of cells was determined by normalising the number of colonies in each condition to the non-irradiated control.

2.2.6 Cell survival analysis

The MTT 3-(4,5-dimethylthiazol-2-yl)-2,5-diphenyltetrazolium bromide assay was used to assess cell viability. A total number of 5 x 10^4 RT112 cells or 2.5 x 10^4 T24 cells per well was seeded in triplicate in 24-well plates containing a final volume of in 500 µL per well for an overnight. The cells were then treated with SCFAs dissolved in ddH_2O or bacterial supernatants for one to three days. At the end of the experiment, they were incubated in 0.45 mg/mL MTT (Life Technologies) at 37°C for 30 minutes. After the removal of the culture medium, the formazan crystals were dissolved in 150 µL per well isopropanol and 100 µL of them from each well was moved to a 96-well plate. The absorbance at 595 nm of MTT-formazan was detected spectrophotometrically using an POLARstar Omega Microplate Readers (BMG Labtech). The percentage of cell viability was determined by normalising the absorbance value in each condition to the mock control. IC10 and IC50 were defined as the drug concentrations at which 90% and 50% of cells survived.

2.2.7 Western blotting

A total number of 1 x 10^6 RT112 cells per well were seeded in 6-well plate across three biological replicates. Cells were lysed using RIPA lysis buffer (Thermo Fisher, #89901) supplemented with freshly added protease (Thermo Fisher, A32955) and phosphatase (Thermo Fisher, #12821650) inhibitors. Cells were vortexed for 10-15 cycles for in 30 minutes on ice. Lysed cells were centrifuged at 20,000 x g for 10 minutes at 4°C. Protein in the supernatant was quantified using the bicinchoninic acid (BCA) assay (Thermo Fisher) and Omega software (BMG Labtech). Protein samples were prepared in Laemmli buffer and boiled at 95°C for 5 minutes. In general, around 30 µg of protein was loaded onto gels per sample. Samples were run on 4-20% SDS-PAGE precast gels (Bio-Rad) in 1X Running Buffer (Bio-Rad) at 100 V for approximately 1.5 hours. Protein samples were transferred onto a nitrocellulose membrane (Thermo Fisher Scientific) using a Bio-Rad turbo transfer kit with 1X Transfer Buffer (BioRad) for 10 minutes at 20 V. Nitrocellulose membranes were blocked in LI-COR blocking buffer for 1 hour at room temperature on a rocker (Stuart). Membranes were incubated in primary antibodies (H3K18Ac (Cell Signaling Technology, #9675), H3K23Ac

(Cell Signaling Technology, #14932), H3 (Cell Signaling Technologies, #4499S), phospho-histone H2A.X (Cell Signaling Technologies, #2577) and β-actin (Abcam, #A1978)) in LICOR antibody diluent overnight at 4°C on a rocker, washed 3 times for 10 minutes each with PBS-T (PBS and 0.005% w/v Tween-20). Membranes were incubated in a suitable secondary antibody (anti-mouse (LICOR, #925-32210), anti-rabbit (LICOR, # 925-68021)) in LICOR antibody diluent for 1 hour at room temperature on a rocker, washed again 3 times for 10 minutes each, and imaged using a LI-COR imaging system (Odyssey).

2.2.8 Immunofluorescence microscopy and irradiation

A total number of 3 x 10^5 RT112 cells per well were seeded in 6-well plate across three biological replicates. Cells were cultured on 10 mm No. 1 cover glasses (VWR) that had been sterilised with 70% ethanol and rinsed with PBS prior to ionising radiation. After incubated with bacterial supernatants for 24 hours, cells were irradiated at a dose rate of 1.5 Gy/min using a Gamma-Service Medical GmbH GSR D1 irradiator. Cells were allowed to recover for indicated times prior to permeabilisation with 0.3% Triton X-100 for 10 minutes at room temperature. Cells were fixed with ice cold 4% paraformaldehyde in PBS for 15 minutes at room temperature, and samples were blocked by incubation in 5% BSA in PBS for 1 hour at room temperature or overnight at 4°C. Incubation with primary γH2AX (mouse anti-phospho-Histone H2A.X (Ser139) IgG; clone JBW301, Millipore) and secondary antibodies (goat anti-mouse IgG, Alexa Fluor 488, ThermoFisher) was done in 2.5% BSA in PBS for 1 hour at room temperature, and coverslips were mounted on microscopy slides using mounting reagent, Flouromount G, with DAPI (Invitrogen). Fluorescent foci were imaged using a Zeiss 710 confocal microscopy using either a 40X or 63X objective. All microscopy images were analysed with FIJI (ImageJ) software.

2.2.9 Statistical analysis

All data in cell experiments are representative of 3 independent biological replicates unless otherwise stated, with results shown as mean and standard deviations. One-way ANOVA with Dunnett's multiple comparison test was performed to analyse the data of western blots and MTT assays. Two-way ANOVA with Dunnett's multiple comparison test was used to

analyse the linear quadratic survival curves in the colony formation assay. All analyses were conducted in QIIME2 and GraphPad Prism version 9.0 (La Jolla, CA).

Chapter 3: Bladder cancer mouse models and gut microbiota related to dietary fibre

Our previous study showed that inulin enhanced the radiotherapy efficacy in CD-1 nude mice (Then *et al.*, 2020). Given that this mouse strain lacks a thymus, making it unable to produce T-cells, thus rendering it immunodeficient, I was unable to study the role of immunomodulation in the tumour control achieved by dietary fibre. Given that IR modulates anti-tumour immune responses, and dietary fibre and the gut microbiota also enhance the efficacy of immunotherapy via activation of cytotoxic T cells, I needed to conduct experiments in immunocompetent mouse models to study the role of immunomodulation by dietary fibre in the mechanism of radiosensitisation.

To avoid transplant rejection, mouse bladder cancer cell lines are used for the inoculation into immunocompetent mice, including C57BL/6, C3H and FVB mice. There are two common murine bladder cancer models, namely, MBT-2 cell lines in C3H mice and MB49 cell lines in C57BL/6 mice. The former model was developed as an orthotopic model which involves more complex tumour inoculation and monitoring procedures (Jiang & Zhou, 1997). MB49 is a widely used model which originates from a carcinogen-induced tumour of bladder epithelial origin in C57BL/6 male mice (Summerhayes & Franks, 1979). It shares several similarities, including cell surface markers, sensitivity to apoptosis and immunological profile, with human bladder cancer (Loskog *et al.*, 2004; O'Donnell *et al.*, 2004). However, it is noted that MB49 bladder tumour cells grow so rapidly that tumours only take one week to quadruple in volume from 100 mm^3 to 400 mm^3 (Cekic *et al.*, 2012).

More recently, BBN963 and UPPL1591 cell lines were established by Professor William Kim's laboratory, and they have been shown to be more representative models of human bladder cancer than MB49 cells (Saito *et al.*, 2018). The primary basal-like BBN tumour was generated by administering N-butyl-N-(4-hydroxybutyl) nitrosamine (BBN) in the drinking water to C57BL/6 mice. The luminal-like UPPL tumour was generated by introducing a tamoxifen-inducible Cre recombinase under the promoter for uroplakin 3A, allowing

selective induction of inactivating mutations in both *PTEN* and *TRP53* genes in the urothelial cells of Upk3a-CreERT2; Trp53L/L; Pte/L/L; Rosa26LSL-Luc (UPPL) C57BL/6 mice. Cells from these tumours were cultured into cell lines, including BBN963 and UPPL1591, which can be injected subcutaneously or orthotopically into syngeneic mice. These were the first subtype-specific (basal subtype for BBN963 and luminal subtype for UPPL1591) murine models of bladder cancer, that can better mimic human bladder cancer compared to MB49 cells based on whole-transcriptome profiling and have the advantage over human tumour cell lines of being used as allografts in immunocompetent mice.

In addition, another murine bladder cancer cell line, G69, generated by Professor Keith Syson Chan's laboratory, produced results consistent with the human T24 bladder cancer cell line following gemcitabine treatment (Hayashi *et al.*, 2020). Briefly, K5.Stat3C (from FVB parental strain) transgenic mice were exposed to BBN water for ≥15 weeks. Orthotopic tumours were harvested from the bladder and dissociated to single-cell suspensions and cultured to form a cell line.

Therefore, I chose to use three mouse bladder cancer cell lines, namely, UPPL1591, BBN963 and G69, from our collaborators and injected them into a mouse subcutaneous allograft flank model. I assessed the radiosensitivity of these cell lines and compared them with RT112 human bladder carcinoma cells lines and investigated the tumour take rates (percent of mice with the formation of transplantable tumour) and growth curves in immunocompetent C57BL/6 and FVB (named after its susceptibility to Friend leukemia virus B) mice.

The gut microbiota profiles of different strains of mice, including C3H, C57, GFEC, CD1, CBA nu/nu and SCID, were found to be different (Friswell *et al.*, 2010). So, after establishment of the three murine bladder cancer immunocompetent models, I further explored how the gut microbiota was modified by inulin in these two mouse strains (C57BL6 and FVB mice) compared with our previous work in CD-1 nude mice. Besides inulin, resistant starch is another highly fermentable dietary fibre which is well-known for its high production of butyrate. In addition, I was also interested in psyllium as it is highly viscous due to its high water-holding capacity and might help bacterial fermentation. I therefore also conducted

two mouse experiments to compare the impact of low and high dietary fibres, including psyllium and resistant starch, on the gut microbiota in different strains of mice.

3.1 Radiosensitivity of different cell lines

I used four bladder cancer cell lines in my experiments, including RT112 (human; luminal) for cell experiments, and UPPL1591 (mouse; luminal), BBN963 (mouse; basal) and G69 (mouse; not identified) for mouse experiments. Seeding cell numbers in each well of 6-well plates and plating efficiencies are listed in Table 8. Figure 20 showed that the human RT112 cell line was more radiosensitive compared to the three mouse cell lines ($P<0.001$ for G69, $=0.004$ for UPPL1591 and $= 0.027$ for BBN963 at 4 Gy) in clonogenic assay. Plating efficiency was calculated by dividing the number of colonies counted per dish by the number of cells seeded for non-irradiated controls.

Table 8 Details of bladder cancer cell lines

Cell line	Species / subtypes	Seeding cell numbers	Plating efficacy
G69	Mouse / not identified	400	0.1-0.2
UPPL1591	Mouse / luminal	200	0.2-0.3
BBN963	Mouse / basal	200	0.2-0.5
RT112	Human / luminal	200	0.3-0.5

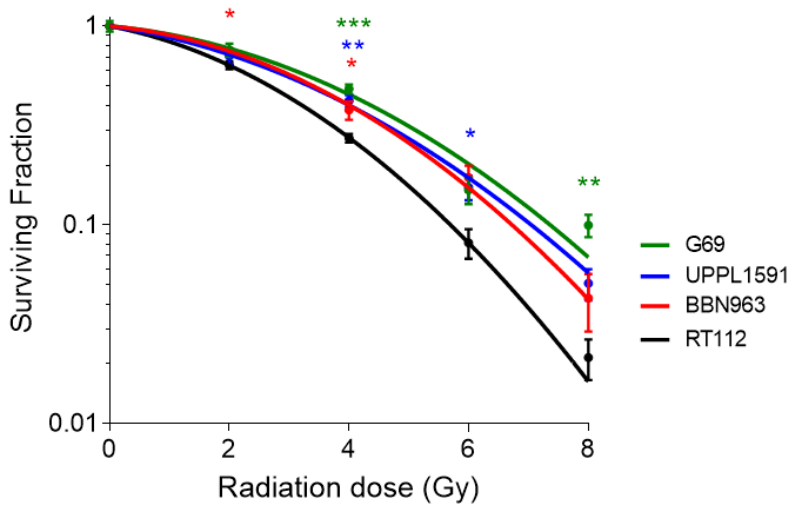


Figure 20 Radiosensitivity of four bladder cancer cell lines. Surviving fraction of G69, UPPL1591, BBN963 and RT112 cells upon indicated doses of IR. After seeding, cells were incubated for an overnight, received irradiation the next day and cultured for 8-14 days to allow colonies to form. Results are representative of three individual biological experiments in triplicate. Data was shown as mean and STD. All p-values were calculated with RT112 as a control in two-way ANOVA with Dunnett's multiple comparison test.

3.2 Establishment of mouse bladder tumour models

3.2.1 UPPL1591 and BBN963 mouse bladder cancer cell line allografts in C57BL/6 mice

I first studied whether UPPL1591 and BBN963 mouse bladder cancer cell line allografts in C57BL/6 mice were appropriate models for the future animal studies. To identify the optimal cell numbers for tumour inoculation, either $1.5x10^6$ or $3x10^6$ cells were injected with in HBSS and Matrigel (1:1) for each of the cell lines (n=3/group). After monitoring for up to 6 weeks, $1.5x10^6$ UPPL1591 cells and $3x10^6$ BBN963 cells yielded better tumour take rates and faster growth rates than $3x10^6$ UPPL1591 cells and $1.5x10^6$ BBN963 cells, respectively, so these cell numbers were chosen for future experiments (Figure 21). Veterinary pathologists, Dr Alejandro Suarez Bonnet and Professor Simon Priestnall, have identified that the histologic subtypes were moderately to poorly differentiated squamous cell carcinoma (SCC) for the UPPL1591 allograft, which was consistent with the Kim laboratory's finding of the squamous histology of UPPL tumours (Saito *et al.*, 2018), and moderately differentiated pseudoglandular SCC for BBN963 allografts.

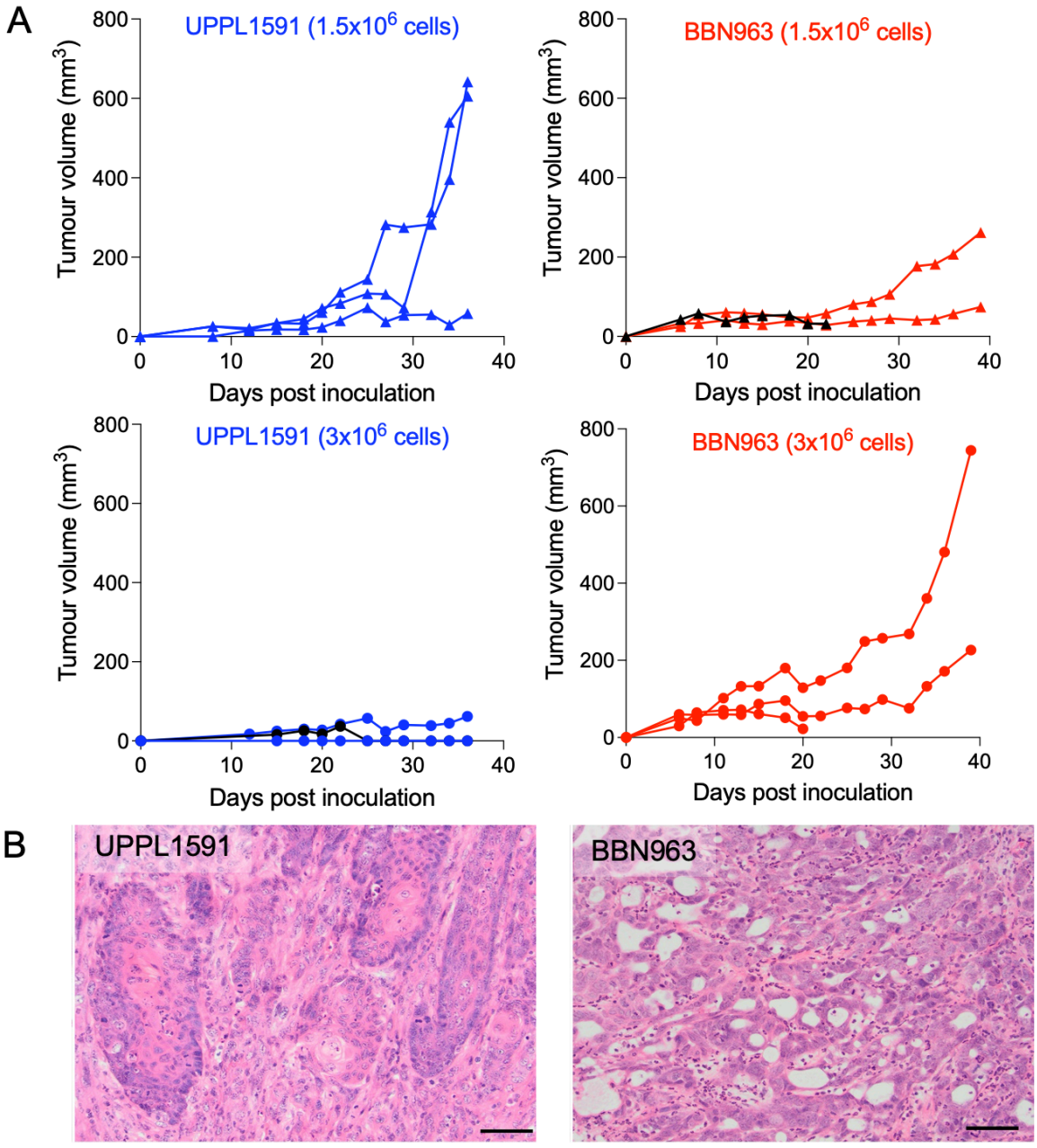


Figure 21 Tumour growth curves and histological patterns of UPPL1591 and BBN963 mouse bladder cancer cell lines in C57BL/6 mice. C57BL/6 mice (n=3 per group) were injected subcutaneously into the flank with 1.5 x10^6 or 3x10^6 UPPL1591 or BBN963 cells and the tumour growth was measured three times a week. (B) H&E staining shows the histologic subtypes of UPPL1591 and BBN963 were SCC and pseudoglandular SCC, respectively.

3.2.2 G69 mouse bladder cancer cell line allograft in FVB mice

The other immunocompetent subcutaneous model was the G69 mouse bladder cancer flank allograft in FVB mice. I investigated the tumour growth of G69 allografts inoculated in one of the following three conditions: $1x10^6$ or $3x10^6$ cells in 200 µL PBS and Matrigel (1:1) mixture and $3x10^6$ cells in 200 µL HBSS only. The tumours were monitored for up to 9 weeks. Compared to $3x10^6$ cells inoculated without Matrigel, tumours from inoculations of $1x10^6$ and $3x10^6$ cells with Matrigel grew at a significantly higher rate and both the p-values were <0.001 (Figure 22).

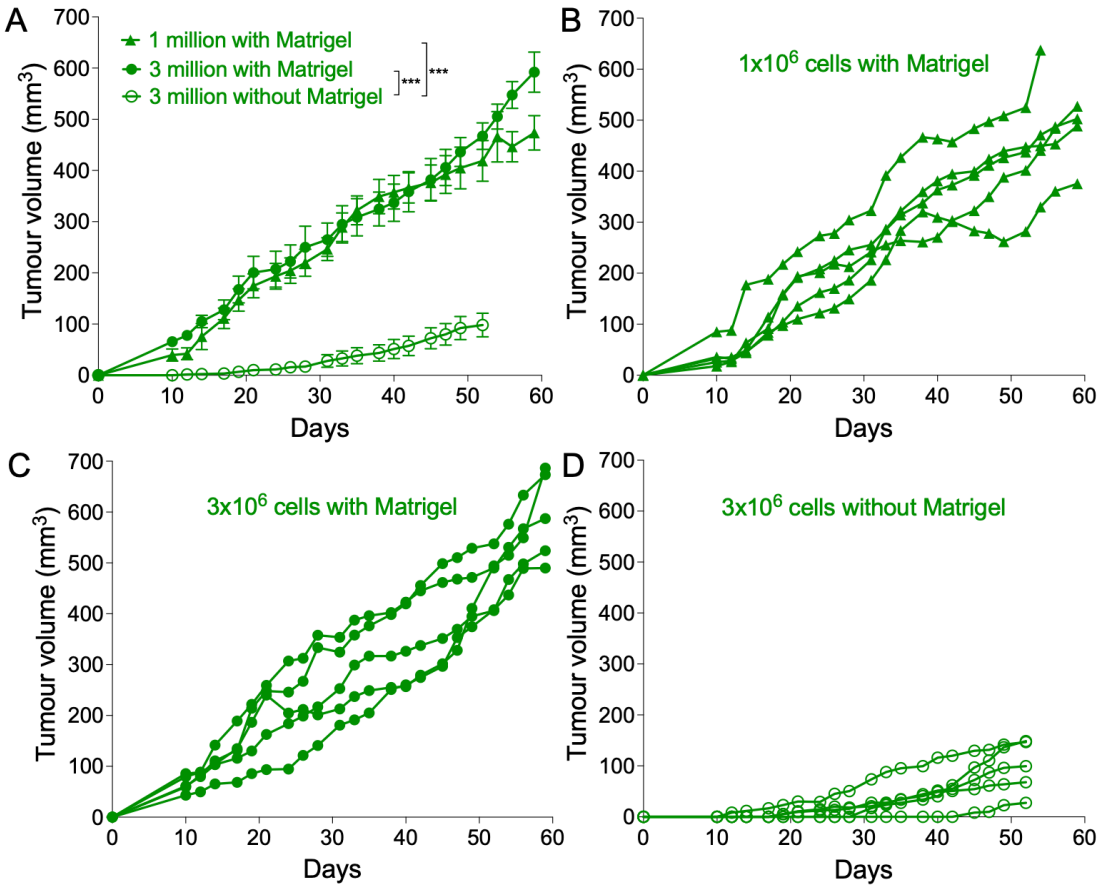


Figure 22 Tumour growth curve of G69 mouse bladder cancer cell lines in FVB mice. FVB mice (n=5 per group) were injected subcutaneously into the flank with $1x10^6$ or $3x10^6$ G69 cells with or without Matrigel and tumour growth was measured three times a week. (A) Overall and (B-D) individual tumour growth in flank xenograft was presented. Error bars represent the standard error. Tumour curve slopes were calculated by linear regression to represent tumour growth rates and compared by ANOVA.

3.3 The gut microbiota related to dietary fibre and mouse strain

3.3.1 The gut microbiota of different strains of non-tumour-bearing mice fed with low and high dietary fibre

To study how the high and low dietary fibre modified the gut microbiota, three strains of mice, namely, C57BL/6, CD-1 nude, FVB male and female, were fed with low fibre (0.2% cellulose) and high fibre (10% inulin) diets for three weeks. Cellulose is a dietary fibre that has low solubility, viscosity and fermentability, whereas inulin is a potential radiosensitiser that is highly soluble and fermentable. Three weeks after modified diets, faeces were collected for 16S rRNA gene sequencing.

The gut microbiota composition in taxonomical terms is shown in Figure 23A and the bacteria with the three highest abundances were S24-7, *Bacteroides* and *Parabacteroides*. Different strains of mice had their own unique gut microbiota, and it is noted that more *B. acidifaciens* (pink bar) and *A. muciniphila* (light green bar) were found in C57BL/6 mice, more unspecified *Parabacteroides* species (green bar) in CD-1 nude mice and unspecified *Bacteroides* species (red) in FVB mice.

In terms of alpha diversity, mice treated with high fibre diets had a decrease in observed OTUs (Figure 23B). This might be due to the overpopulation by particular bacteria increased by high fibre, which caused the reduction in overall diversity. In the PCoA plot (a method of showing distances between samples in a low-dimensional, e.g. as a 3D graphics), the gut microbiota profiles clustered within their strains, and these were rather different compared to the other strains (Figure 23C). In addition, the clustering effect of the gut microbiota was still seen in mice fed with the same diet within each mouse strain. In terms of *B. acidifaciens*, a bacterium of interest in our previous study, the high fibre diets increased its absolute and relative abundance in C57BL/6 and FVB male and female mice (Figure 24A and B). The difference was not seen in CD-1 nude mice, but a similar result was also found in our previous study, in that some mice did not harbour this bacterium in the high fibre diet group. In C57BL/6 mice, *B. animalis* (Figure 24C) and *A. muciniphila* (Figure 24D) were also enhanced by high fibre.

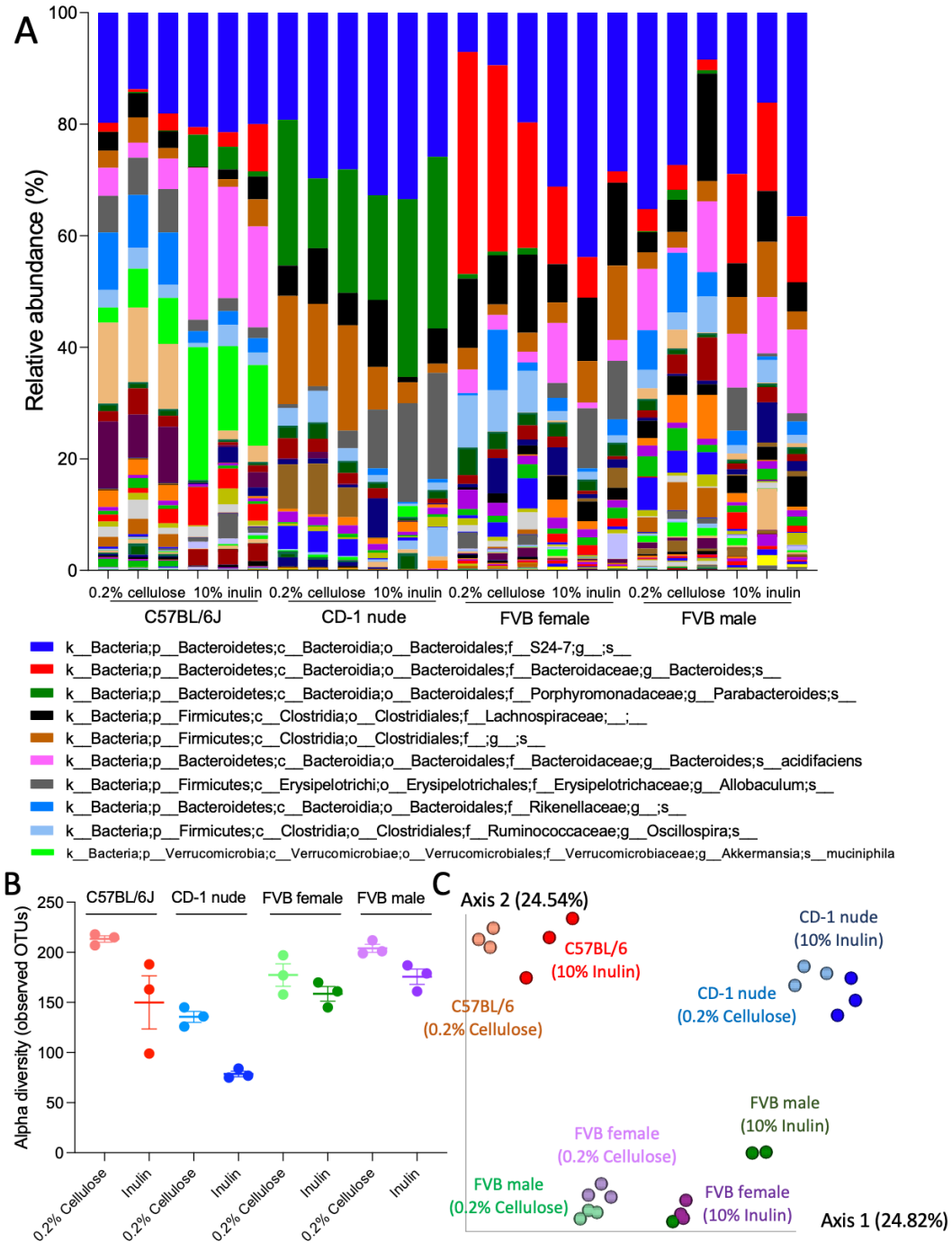


Figure 23 A unique profile of gut microbiota presented in different strains of mice. C57BL/6, CD-1 nude, FVB male and female mice received low fibre (0.2% cellulose) and high fibre (10% inulin) for 3 weeks. (A) Stacked bar plot of the phylogenetic composition of common bacterial taxa at the species level. (B) Alpha diversity and (C) beta diversity using Bray-Curtis Dissimilarity of gut microbiota.

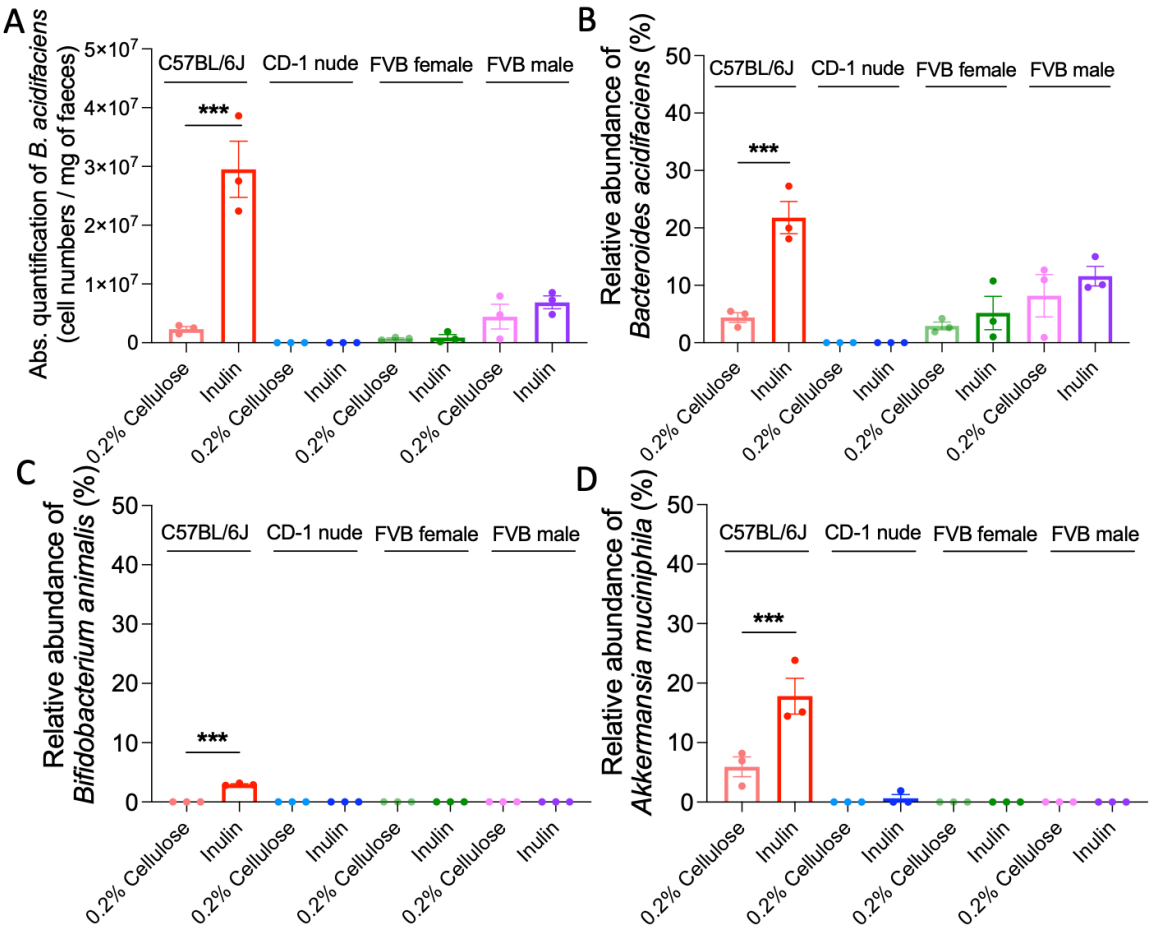


Figure 24 High fibre diet increased *B. acidifaciens* abundance in different strains of mice. Similar trend between (A) absolute and (B) relative abundance of *B. acidifaciens.* Relative abundance of (C) *B. animalis* and (D) *A. muciniphila* and increased relative abundance of these bacteria for inulin in comparison to 0.2% cellulose in C57BL/6.

3.3.2 The gut microbiota of non-tumour-bearing mice fed with different types of dietary fibre diets

Psyllium is given for diarrhoea control in patients receiving pelvic radiotherapy and resistant starch is a well-known butyrate producer. I further explored how these dietary fibres affected the gut microbiota. I used FVB mice and fed them with 0.2% cellulose, 10% inulin, 5% psyllium, 5% psyllium plus 5% RS and 5% psyllium plus 10% RS for 3 weeks. The gut microbiota composition in taxonomical terms is shown in Figure 25A and the bacteria with the top 3 highest abundances were the S24-7 family, *B. acidifaciens* species and a *Bacteroides* species. In terms of alpha diversity, mice treated with high fibre diets, including 10% inulin and three psyllium diets, had decreased observed OTUs compared with normal chow and 0.2% cellulose groups (Figure 25B). In the PCoA analysis, the gut microbiota profiles clustered within their dietary groups, especially all psyllium diets and inulin, and these were rather different compared to the other dietary groups (Figure 25C). The three psyllium diets had higher relative abundances of *B. acidifaciens* (Figure 26A), but not *B. animalis* (Figure 26B) and *A. muciniphila* (Figure 26C).

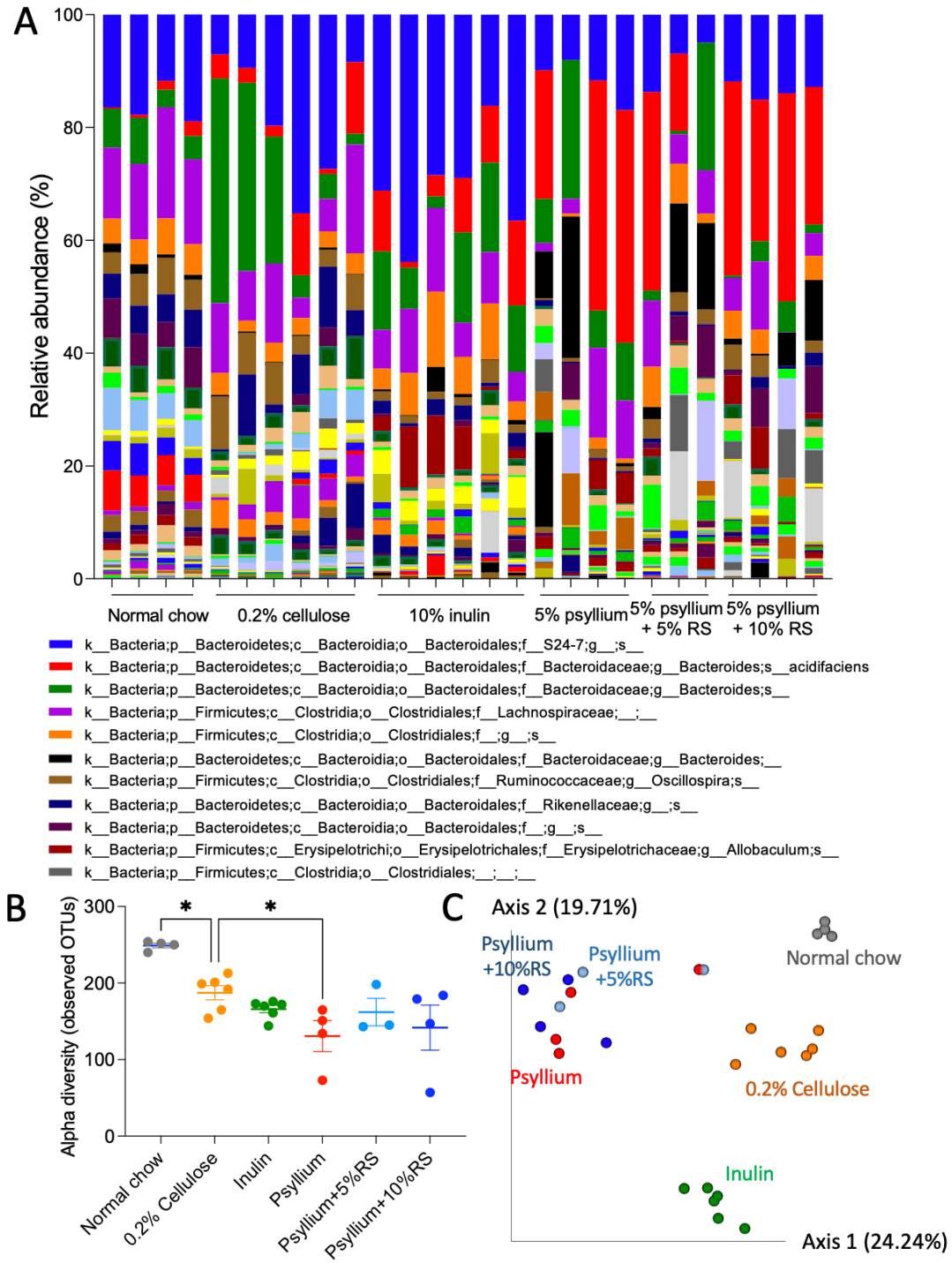


Figure 25 Phylogenetic composition, alpha and beta diversity of faecal microbiota a at the species level. FVB male and female mice fed with normal chow, low fibre (0.2% cellulose) and high fibre (10% inulin, 5% psyllium, 5% psyllium plus 5% RS and 5% psyllium plus 10% RS) for 3 weeks. (A) Stacked bar plot of the phylogenetic composition of common bacterial taxa at the species level. (B) Alpha diversity and (C) beta diversity of gut microbiota.

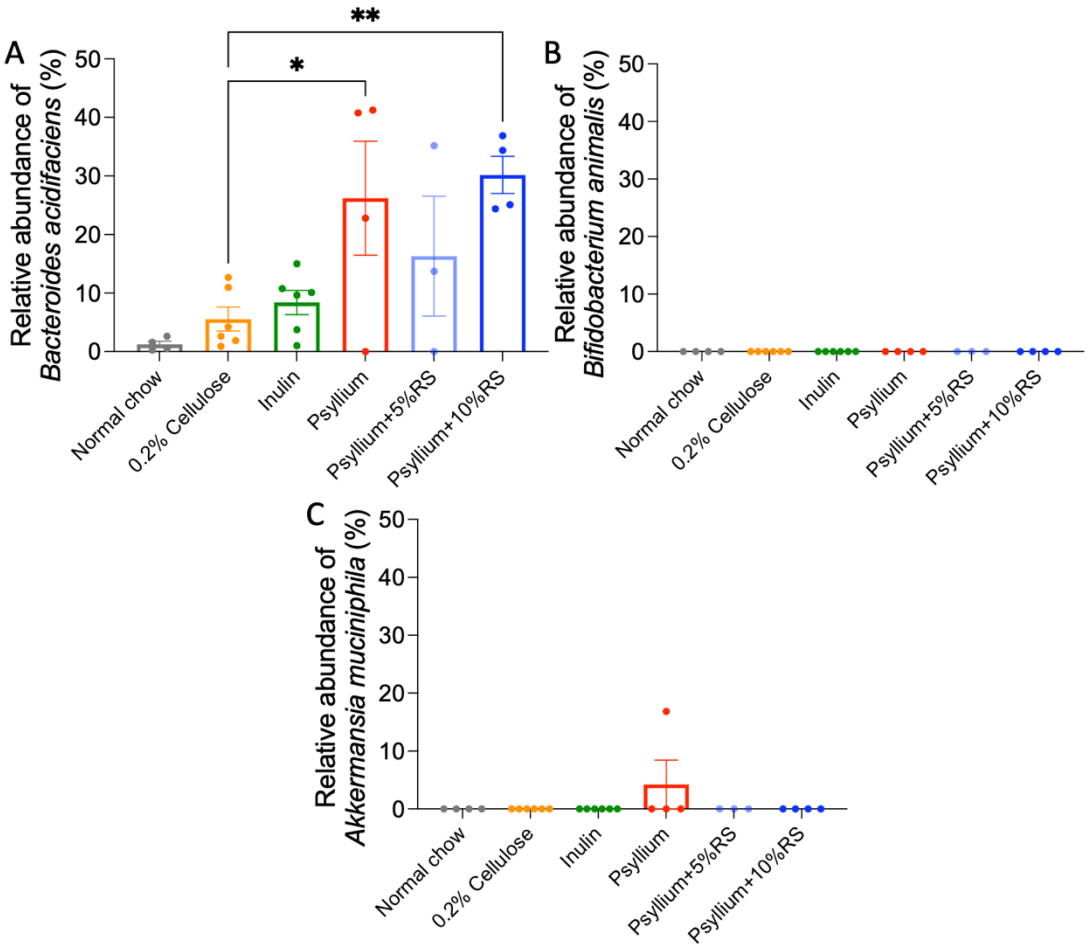


Figure 26 Psyllium increased *B. acidifaciens* abundance in FVB mice. Relative abundance of (A) *B. acidifaciens,* (B) *B. animalis* and (C) *A. muciniphila* and increased *B. acidifaciens* abundance in for psyllium-containing diets in comparison to normal chow, 0.2% cellulose and inulin. Psyllium (n=4 for male), psyllium+5% RS (n=3 for female), psyllium+5%RS (n=2 for female and n=2 for male).

3.4 Discussion

Clonogenic assay showed that the survival fractions of RT112 were 0.08 at 6 Gy which was more radiosensitive than in previous studies at 0.1 (El-Awady *et al.*, 2003) and 0.2 (Paillas *et al.*, 2020). However, a similar result of higher radiosensitivity of this cell line has been shown in that the survival fraction was 0.1 at 5 Gy (Lambin *et al.*, 1994). At the lower dose of 4 Gy, all studies had a similar survival fraction of 0.2-0.3 to my result of 0.27. This variation existed mainly at higher doses where the cells had lower survivals. The low colony number might be the reason that caused this difference of survival fractions between my results and the others.

Consistent with Saito *et al.* who used 1×10^6 cells for UPPL1541 and 1×10^7 for BBN963 cell lines (Saito *et al.*, 2018), I did find that higher cell numbers were needed for BBN963 (3×10^6 cells) compared to UPPL1591 (1.5×10^6 cells) to generate higher take rates. In addition, we both showed that UPPL tumours had a faster tumour growth rate, which took approximately a week to grow from 200 mm^3 to 400 mm^3, compared to BBN tumours that needed around 20 days. Professor Kim's laboratory found that the take rate was 50-100% for BBN963 (uncertain for UPPL1591) whereas I had the take rate of 60% for both $1.5x10^6$ and $3x10^6$ BBN963 cells.

My results also showed that higher cell numbers increased the tumour take rates in BBN963. However, this was the opposite for UPPL1591, probably due to its larger cell size which was seen under microscope and the resultant 'crowding' effect of cells. In addition, a lower cell number enabled each cell to gain more nutrients and oxygen, critical for the tumour cells' survival. For G69 cell lines, I obtained consistent results of tumour growth to Professor Chan's laboratory, in that it took a week for tumours to double their volume (Nikolos *et al.*, 2022). In my case, I further investigated the tumour growth of G69 allografts in different inoculation conditions and found that the growth rate and take rate were similar between $1x10^6$ and $3x10^6$ cells with Matrigel but were significant lower while inoculated without Matrigel. This suggested that Matrigel is a critical component to increase the tumour take rate which is consistent with the previous studies that Matrigel increased the tumour take

rates in small cell lung cancer, melanoma and renal cell carcinoma mouse models (Fridman *et al.*, 1990; Fridman *et al.*, 1991).

In terms of the gut microbiota profiles seen in different mouse strains, the high fibre diet, inulin, significantly increased the relative abundance of *B. acidifaciens* (potential radiosensitiser), *B. animalis* (acetate-producer) and *A. muciniphila* (associated with an increased immunotherapy and chemotherapy efficacy; able to restore colonic mucosa) in C57BL/6 mice (Ruan *et al.*, 2021). It is noted that *B. animalis* and *A. muciniphila* were not found in FVB mice. Therefore, I chose C57BL/6 for subsequent experiments and this also allowed us to more easily compare the gut microbiota results with other studies, as C57BL/6 mice are much more widely used than FVB mice (*Laboratory Mice and Rats*, 2012). Furthermore, all psyllium diets increased the *B. acidifaciens* abundance that was positively associated with post-IR tumour control in our previous experiment (Then *et al.*, 2020), so I adopted the combinations of psyllium plus inulin and psyllium plus RS for subsequent experiments.

Chapter 4: Effects of combining dietary fibre manipulation and ionising radiation on tumour growth

After confirming the optimal conditions for the UPPL1591 allografts (an immunocompetent model) and determining that C57BL/6 had a gut microbiota containing *B. acidifaciens*, the abundance of which could be enhanced by high dietary fibre, I explored how the IR and dietary fibre changed the caecal metabolome and influenced tumour growth in four sets of mouse experiments (Table 9). They were all subcutaneous allograft flank model. A tumour growth delay model was applied in all of these experiments to measure the radiation effect (see details in section 1.2.5).

Table 9 Overview of the study and sample sizes.

	Sample collected when tumour growth reached:	**Diets**		**Radiation**	**Sample size /group**
1. (N=20)	100 mm^3 (HBSS:Matrigel=1:1)	Normal chow		- + (6 Gy) + (8 Gy) + (10 Gy)	5
2. (N=42)	Day 40 (HBSS:Matrigel=2:1)	Corn starch	0.2% Cellulose	-	7
			RS		
			Inulin		
			Psyllium		
			Psyllium+RS		
			Psyllium+inulin		
3. (N=30)	100 mm^3 (HBSS:Matrigel=1:1)	Normal chow Dextrose	0.2% Cellulose Psyllium Psyllium+RS Psyllium+inulin	-	6
4. (N=60)	700 mm^3 (HBSS:Matrigel=1:1)	Dextrose	0.2% Cellulose	-	5
			Psyllium		
			Psyllium+RS		
			Psyllium+inulin		
			0.2% Cellulose	+ (6Gy)	10
			Psyllium		
			Psyllium+RS		
			Psyllium+inulin		

From the result of clonogenic assays of the various cell lines, I saw that mouse bladder cancer cell lines were less sensitive to radiation than RT112 cells which had been used as xenografts in our previous diet experiments in CD1 nude mice, so I assessed whether the 6 Gy IR used in our previous radiosensitisation experiment in the immunocompromised model (Then *et al.*, 2020) was sufficient in C57BL6 mice, or whether higher doses of eight Gy or ten Gy were necessary to achieve tumour control in this model.

In the second set of experiments, I studied the effects of diet alone on tumour growth, but the tumour take rate and growth rate were low. Therefore, I increased the percentage of Matrigel for tumour inoculation in the next set of experiments. I also replaced the corn starch in the modified diets with dextrose to avoid the possible confounding factor of corn starch acting as a possible fermentable dietary fibre in the 0.2% cellulose group, despite the assumption that it would be digested in the small intestine, in subsequent experiments. In the third experiment, with these modifications, the tumour take rate was 100% and the baseline gut microbiota, caecal metabolome and immune response were investigated in mice received different dietary fibres.

After identifying the minimum radiation dose which managed to achieve increased tumour control and establishing the effects on tumour growth of the dietary fibres alone, the fourth experiment was performed to determine the radiosensitising effects of the dietary fibres and I correlated the tumour responses with the composition of the gut microbiota, caecal metabolome, local tumour, and systemic peripheral immune responses. Radiosensitisation is an important approach to enhance the radiosensitivity of tumours by introducing specific molecules (radiosensitisers) in combination with radiotherapy that enhance damage to tumour tissue while minimizing additional toxicity to the surrounding normal tissue. In this study, I aimed to investigate whether the radiosensitivity of bladder tumours could be increased by dietary fibre with its associated enhancement of the gut microbiota, metabolites, and immunomodulation.

In this chapter, three kinds of dietary fibres, namely, psyllium, resistant starch, and inulin, were studied. They have their own characteristics as shown in Table 2. Psyllium is a non-

fermentable fibre but its high solubility and viscosity leads to several therapeutic effects such as relieving constipation (Soltanian *et al.*, 2018), improving glycaemic control (Ziai *et al.*, 2005) and reducing blood cholesterol levels (Wei *et al.*, 2009). In addition, psyllium husk had both the properties of laxative and antidiarrhoeal, and it had been shown to be effective for radiation-induced diarrhoea (Murphy *et al.*, 2000). It is now prescribed for bladder and prostate cancer patients during radiotherapy for their acute diarrhoeal reaction.

Resistant starch is a prebiotic that resists digestion in the small intestine and reaches the large intestine in which it is fermented by the gut microbiota. RS promotes butyrate-producing bacteria and increases fermentation to produce short-chain fatty acids, mainly acetate, propionate, and butyrate. Butyrate is the main energy source of colonocytes and induces proliferation of normal cells at the crypt base. Conversely, butyrate inhibits tumour growth of colorectal cancers and enhances the efficacy of chemotherapy (Geng *et al.*, 2021).

Inulin is another readily fermentable fibre by gut microbiota that generates large amounts of short-chain fatty acids (Ahmed & Rashid, 2019). Inulin stimulates the development of beneficial bacteria in colon (Le Bastard *et al.*, 2020), mainly *Bifidobacterium* that can degrade inulin (Rossi *et al.*, 2005). Inulin has been previously shown in our laboratory to modify gut microbiota, which was associated with radiosensitisation in RT112 bladder tumour flank xenografts (Then *et al.*, 2020). In addition, it also suppresses the tumour growth of colorectal cancer and melanoma and increases the efficacy MEK inhibitors against melanoma (Li, Elmen*, et al.*, 2020).

Psyllium, resistant starch, and inulin have their own unique characteristics, namely that psyllium is high in viscosity, and resistant starch and inulin are high in fermentability and solubility. A recent study has shown that combination of psyllium and inulin is well-tolerated in humans with lesser gas production, but the bacterial fermentation remained the same (Gunn *et al.*, 2021). More importantly, psyllium can shift the fermentation of high amylose corn starch from the caecum along the colon and increased butyrate production in rats (Morita *et al.*, 1999). Therefore, I speculated that adding psyllium (highly viscous) to resistant

starch or inulin (highly fermentable) can increase the bacterial fermentation to a sufficient level for enhancing tumour control and radiosensitisation.

Dietary fibre and the resulting modified gut microbiota can increase production of short-chain fatty acids and other metabolites, such as inosine, tryptophan, and indole derivatives (Krautkramer *et al.*, 2021). Previous studies showed that these gut microbiota-produced metabolites modulated the efficacy of chemotherapy and immunotherapy (He *et al.*, 2021; Luu *et al.*, 2021). These metabolites are the functional output of host-microbial interactions. Therefore, the untargeted metabolomics analysis of caecal contents was performed to explore the metabolites enhanced by dietary fibre and the gut microbiota that are needed to enhance tumour control. We worked together with the Department of Chemistry, University of Oxford, to apply an untargeted method using anion-exchange tandem mass spectrometry (IC-MS) that provides comprehensive coverage of hundreds of metabolites and central metabolic pathways (Walsby-Tickle *et al.*, 2020).

4.1 Tumour growth following ionising radiation

4.1.1 Overview

In these experiments, I aimed to find the minimum dose of radiation which could achieve tumour control for use in future radiosensitisation experiments (Figure27). At seven to eight weeks of age, the UPPL1591 mouse bladder cancer cell line was injected subcutaneously into the mouse right flank. When the tumours had grown to 100 mm^3, which took about 2 weeks, I irradiated the mouse tumours with irradiation doses of 6, 8 and 10 Gy from a Gulmay-320 cabinet irradiator (Xstrahl Inc, UK) and monitored them until they reached 700 mm^3. Tumours were collected for immune analysis of CD3 and CD8, markers of general lymphocyte and cytotoxic T cells (section 6.1).

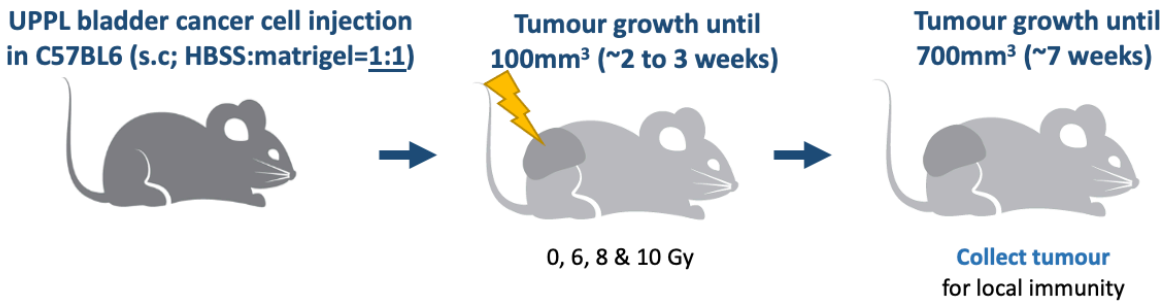


Figure 27 Overview of UPPL1591 bladder tumours exposed to different doses of IR. Tumours were irradiated at 100 mm^3 and harvested for immune analysis when they reached 700 mm^3.

4.1.2 Effect of different IR doses on tumour growth

Ionising radiation significantly delayed UPPL1591 bladder tumour growth and the p-values were 0.029, 0.002 and <0.001 for 6, 8 and 10 Gy, respectively compared to the non-IR group (Figure 28). There was no significant difference in tumour growth between 6 Gy and 8 Gy, but 10 Gy exceeded the effect of these two doses (p value <0.001 for 6 Gy and 0.006 for 8 Gy). Six Gy was chosen as the radiation dose for subsequent experiments as it was the minimum dose which decreased the tumour size of UPPL1591 allografts and a high IR dose like 10 Gy might mask the radiosensitising effect by dietary fibre.

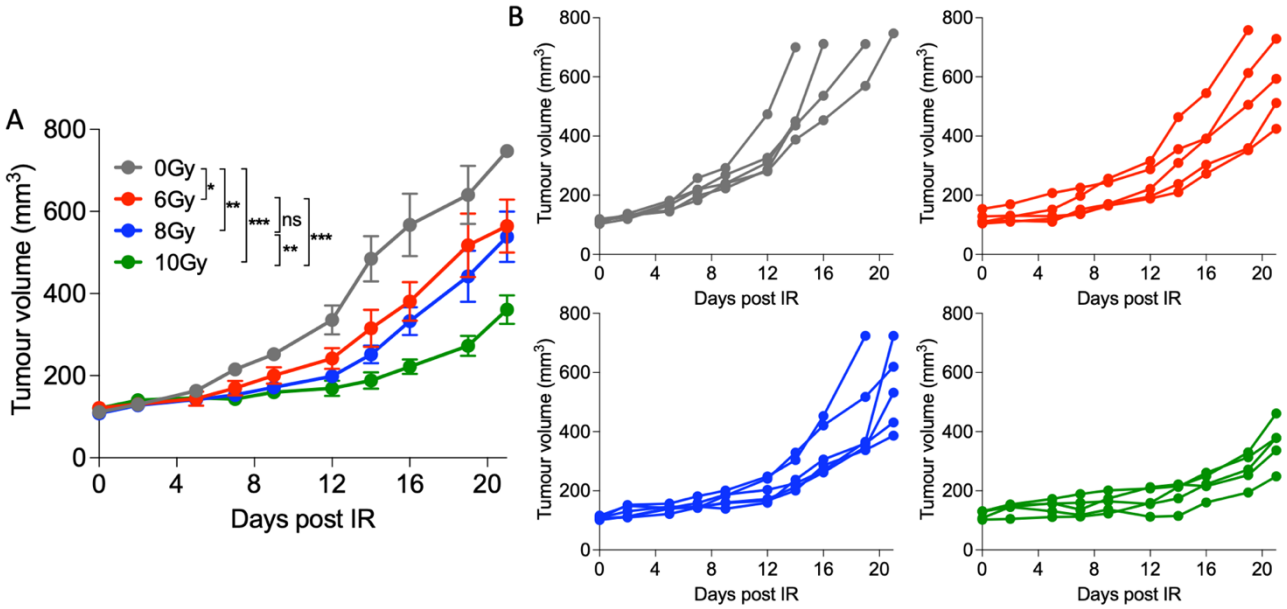


Figure 28 Six to 10 Gy ionising radiation delayed bladder tumour growth. C57BL/6 mice (n=5 per group) were injected subcutaneously into the flank and tumour growth was measured three times a week. (A) Pooled and (B) individual growth curves of UPPL1591 bladder tumours which received 6 to 10 Gy ionising radiation when they reached 100 mm^3. Error bars represent the standard error. Tumour curve slopes were calculated by linear regression to represent tumour growth rates and compared by ANOVA.

4.2 Tumour growth associated with fibre diets containing corn starch

4.2.1 Overview

After defining the optimal radiation dose, I further studied the effects of dietary fibre alone on tumour growth, gut microbiota, caecal size, and large intestinal length. In this experiment, I injected the UPPL1591 mouse bladder cancer cells in the HBSS/Matrigel (2:1) mixture and started low and high fibre diets on the same day (Figure 29A). The low fibre diet was 0.2% cellulose and the high fibre diets were 10% RS, 10% inulin, 5% psyllium, 5% psyllium plus 10% RS or 5% psyllium plus 10% inulin. Subcutaneous flank tumour growth was monitored for up to 6 weeks and faeces were collected at the end of this experiment.

For this second set of experiment (N=42), mice were culled when the tumours reached 100 mm^3. Faeces, caecum, and large intestines were taken to investigate the gut microbiota and intestinal structure at baseline. The caecal size and colonic length were measured by ImageJ.

4.2.2 Body weight change after modified diets

To assess whether high fibre diets, especially psyllium plus RS or inulin, were tolerated by the mice, I recorded body weight and calculated the changes three times per week. Body weight changes in Figure 29B showed that all mice stably gained weight across the experiment. It is noted that the three psyllium diets tended to have higher rates of weight gain compared to 0.2% cellulose, 10% RS and 10% inulin.

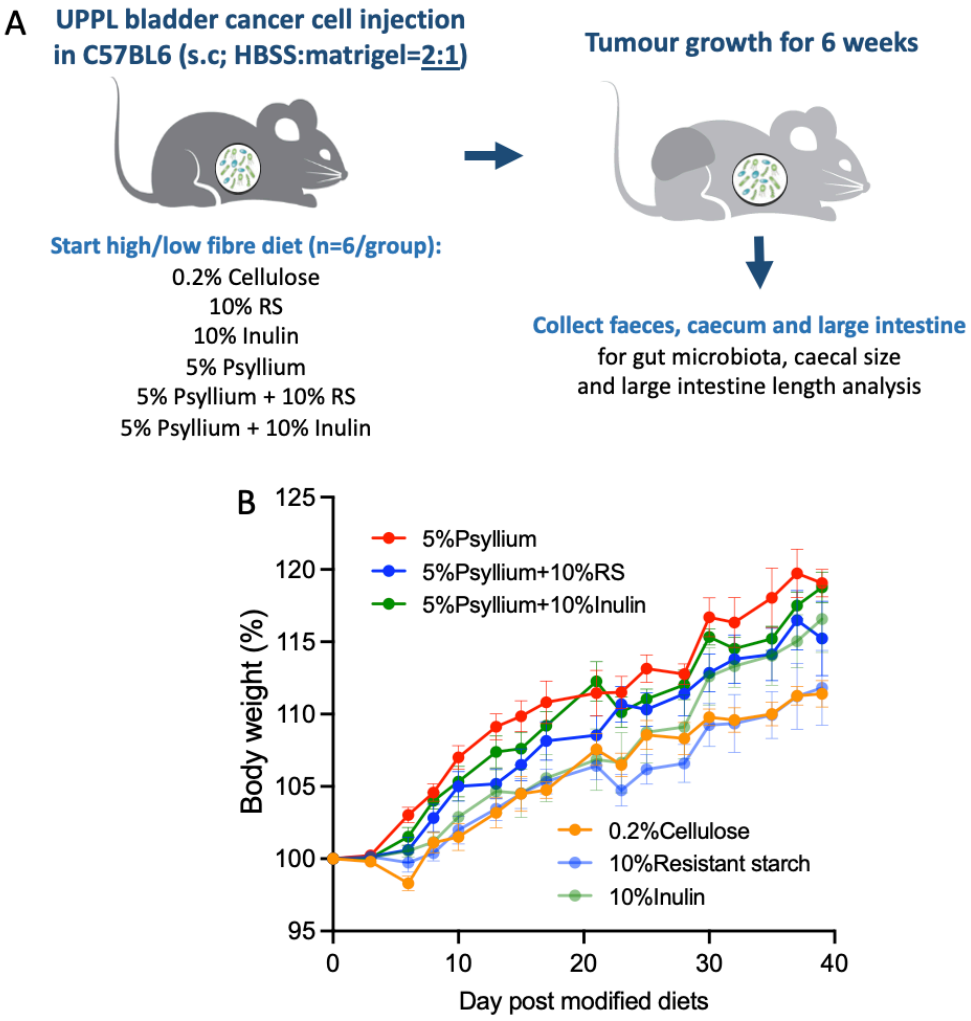


Figure 29 Overview of dietary fibre (corn starch) and UPPL1591 bladder tumour experiment. (A) UPPL1591 bladder cancer cells were injected subcutaneously in the flank of C57BL/6 mice on the same day that they started on the low or high fibre diets (n=7/group). Tumours were monitored until they reached 100 mm^3 or for up to 40 days. At the end of experiment, faeces, caeca, and large intestines were collected to study the gut microbiota and intestinal structure after modified diets. (B) Body weight changes of mice fed with modified diets for six weeks. Error bars represent the standard error.

4.2.3 Tumour growth in low and high fibre groups

After monitoring for up to 6 weeks, psyllium plus RS (P=0.104) and psyllium plus inulin (P=0.027) delayed the tumour growth compared to 0.2% cellulose (Figure 30A). Examining the tumours that reached 100 mm^3 or were still visible on day 39, there were 75% (n=6) in the 0.2% cellulose group, 62.5% (n=5) in the RS group, 25% (n=2) in the inulin group, 37.5% (n=3) in the psyllium group, 12.5% (n=1) in the psyllium plus RS group and 0% (n=0) in the psyllium plus inulin group. Figure 30B showed that individual tumour growth was heterogenous in each dietary group.

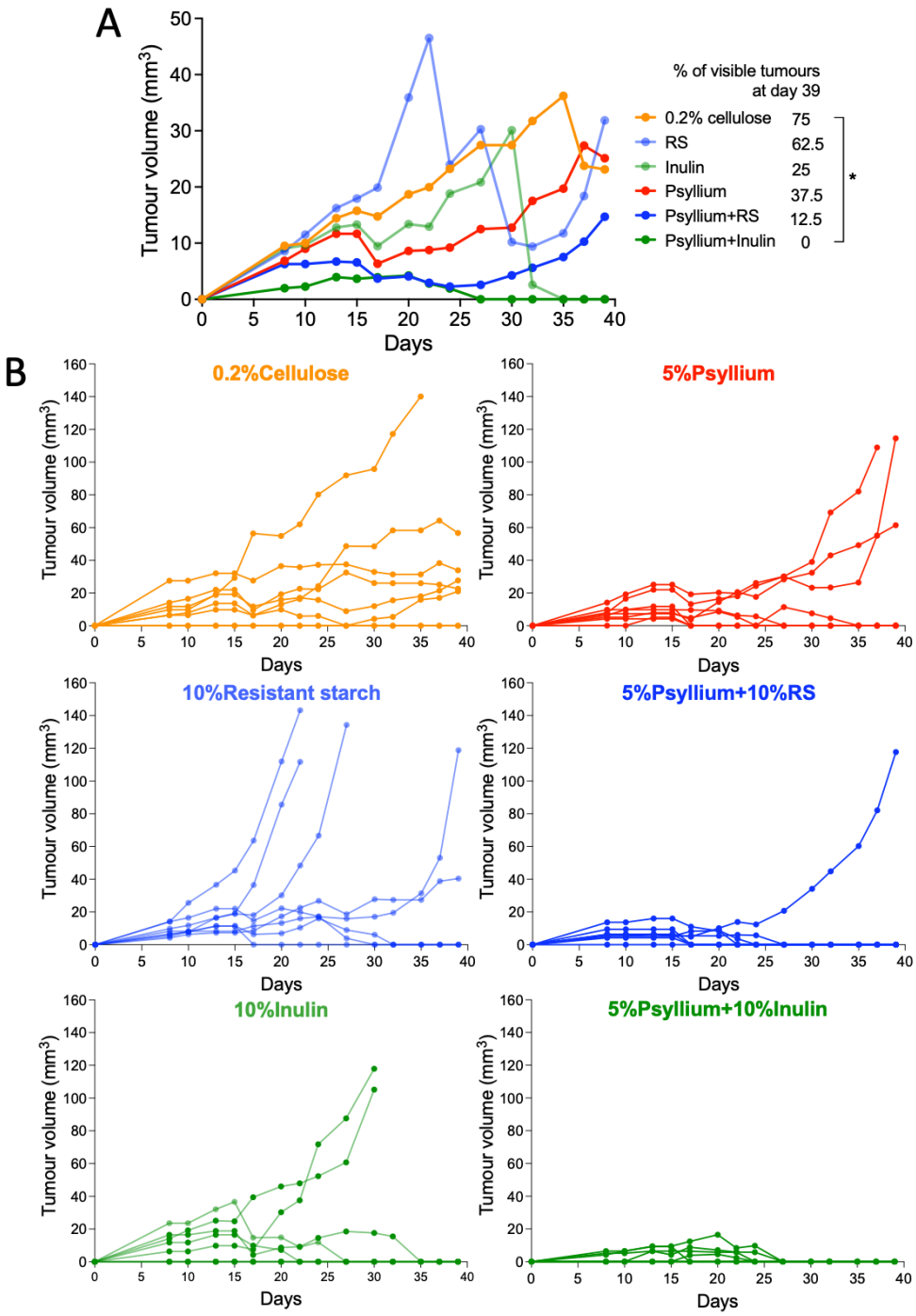


Figure 30 Psyllium plus either RS or inulin increased growth delay in UPPL1591 bladder tumour allografts. (A) Pooled and (B) individual growth curves of UPPL1591 bladder tumours in mice fed with low and high fibre diets (n=8/group). Error bars represent the standard error. Tumour curve slopes were calculated by linear regression to represent tumour growth rates and compared by ANOVA.

4.2.4 The caecal size and length of the large intestine after six weeks of modified diets

The caecum is the major site for bacterial fermentation and dietary fibre has been previously shown to prevent the shortening of the large intestine seen in colitic mice (Ogata *et al.*, 2017). Therefore, I investigated the caecal size and length of the large intestine in mice fed with these modified diets. All dietary fibre types significantly increased caecal sizes compared to 0.2% cellulose, and it is noted that the psyllium plus inulin group were the largest ($P<0.001$), implying higher levels of bacterial fermentation (Figure 31A). All high fibre groups also had significantly longer large intestines compared to 0.2% cellulose, especially psyllium plus RS ($P<0.001$) or psyllium plus inulin ($P<0.01$; Figure 31B). Representative figures of caeca and large intestines of different dietary groups are shown in Figure 31C.

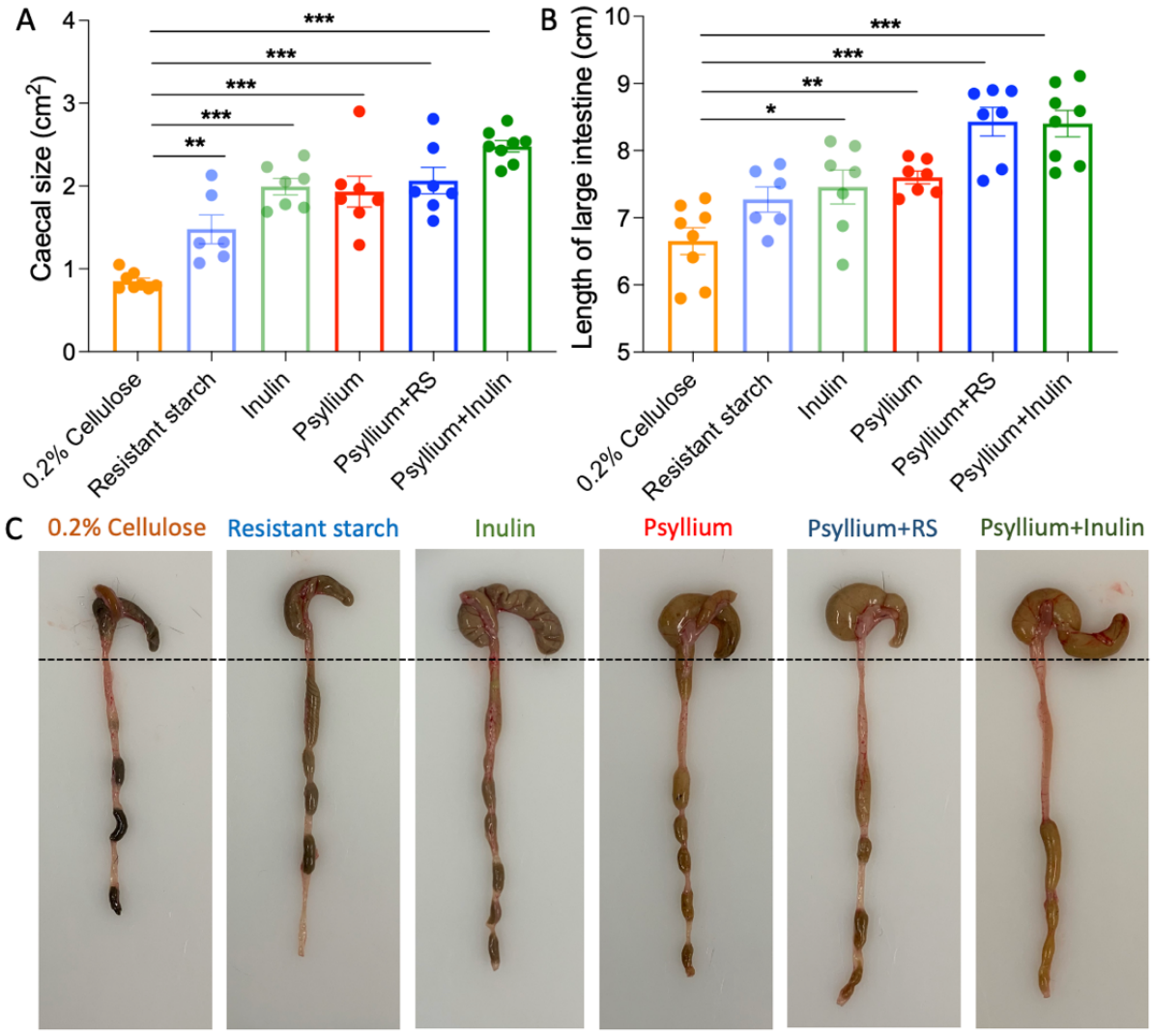


Figure 31 Larger caecal size and longer large intestine in mice fed with psyllium plus RS or inulin. At the end of experiment, caeca and large intestines were collected, and the size or length were measured by ImageJ. (A) Caecal size (length x width) and (B) length of large intestine were compared among low and high fibre diet groups by ANOVA. Error bars represent the standard error. (C) Representative images are shown.

4.2.5 The gut microbiota of tumour-bearing mice fed with low and high dietary fibre

Figure 32A shows the gut microbiota profiles from mice fed with low and high fibre diets. The legends for the top 20 taxa with the highest abundances were shown in Table A6. The top 10 largest relative abundances of bacteria were *Lactobacillus*, S24-7, unspecified order Clostridales, *B. animalis*, unspecified Bacteroidales order, *B. pseudolongum*, *B. acidifaciens*, unspecified *Bacteroidetes* genus, unspecified Rikenellaceae family and unspecified Clostridales order. Inulin ($P<0.001$) and all psyllium diets significantly increased the relative abundance of *B. acidifaciens* compared to 0.2% cellulose (Figure 33A). There were approximately 6-10% increases and the p-values were <0.001 for psyllium, 0.001 for psyllium plus RS and 0.020 for psyllium plus inulin. The relative abundance of *B. animalis* was significantly enriched in the inulin group (12.3%; $P=0.001$) and it was over two-fold higher, up to 30.4%, in the psyllium plus inulin group ($P<0.001$) (Figure 33B).

In terms of alpha diversity, mice treated with high fibre diets, including 10% inulin and psyllium plus inulin, had decreased observed OTUs due to the overriding abundance of *B. animalis* (Figure 32B). Principal coordinate analysis in Figure 32C showed that the gut microbiota of psyllium versus psyllium plus RS and inulin versus psyllium plus inulin were more similar to each other than those of 0.2% cellulose and RS. This implies that psyllium and inulin were able to shape the gut microbiota into a defined profile.

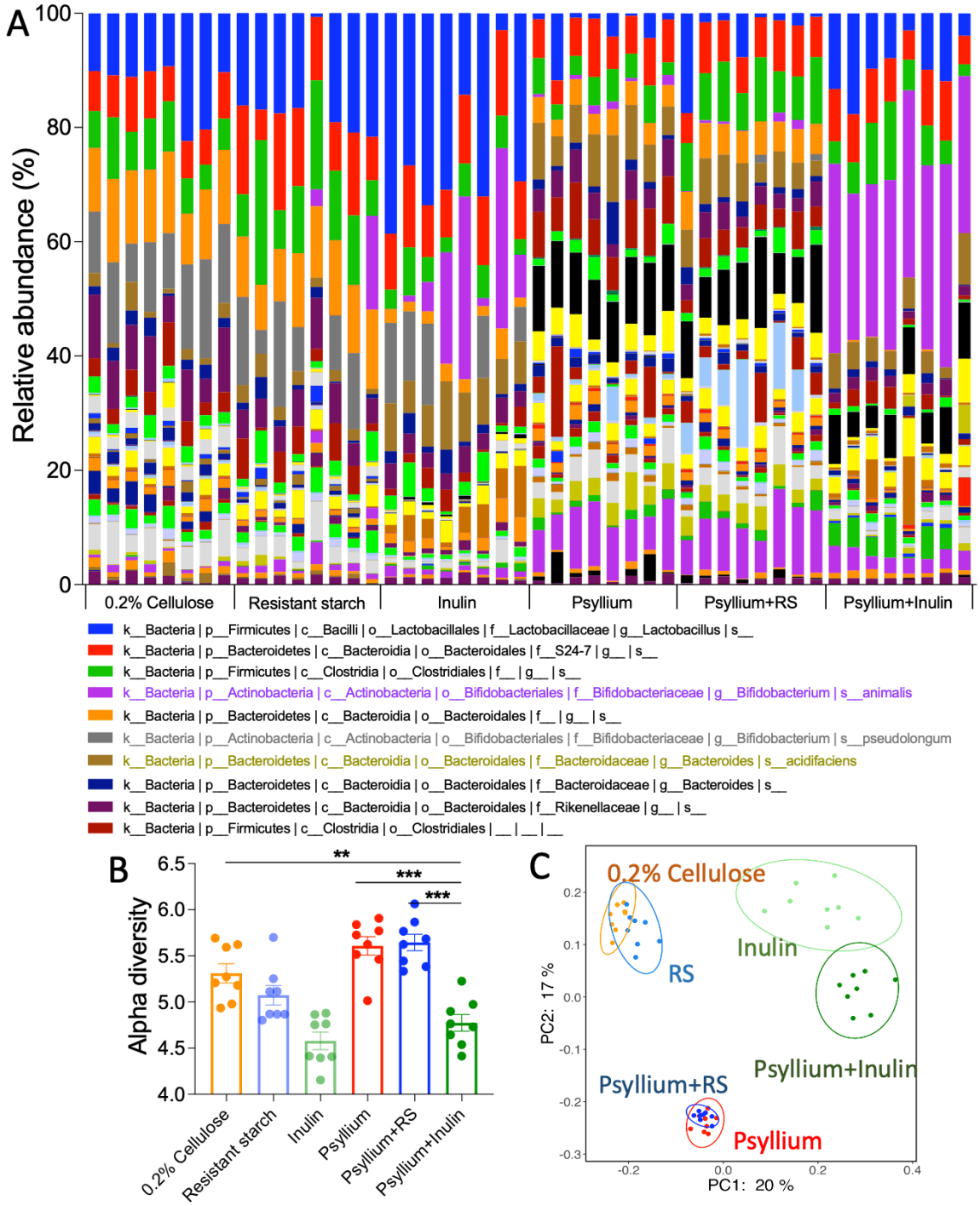


Figure 32 Phylogenetic composition, alpha and beta diversity of faecal microbiota a at the species level. (A) Faecal samples were collected when tumours reached 100 mm^3 or on day 39 after tumour inoculation (n=8/group). (B) Alpha diversity using Shannon index and (C) principal coordinate analysis of faecal microbiotas using Bray-Curtis dissimilarity. A notable clustering effect by diets was seen in the gut microbiota.

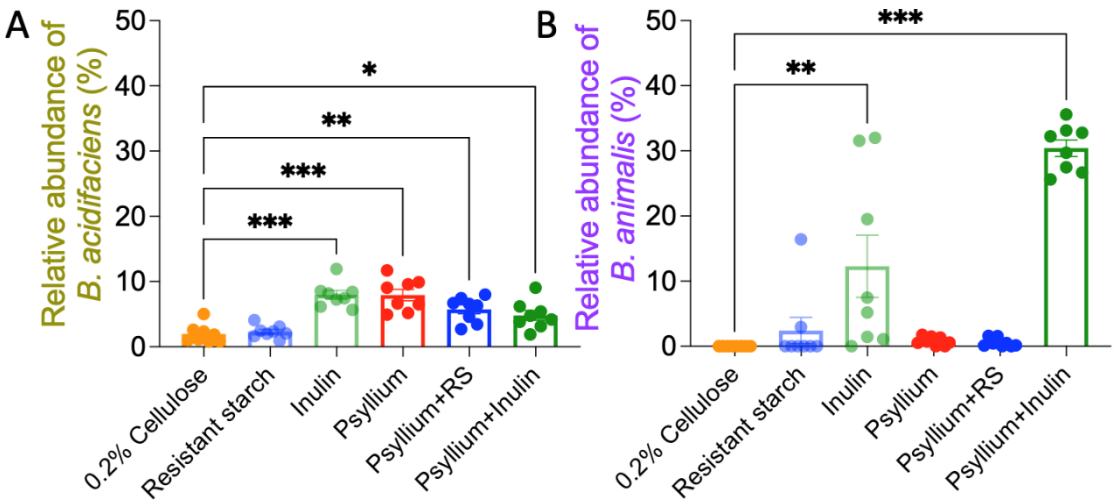


Figure 33 Inulin diet increased *B. animalis* abundance. Relative abundance of (A) *B. acidifaciens* and (B) *B. animalis* in high fibre groups compared with 0.2% cellulose by ANOVA. Error bars represent the standard error.

From this experiment, all high fibre diets were well tolerated by mice since they had been stably gaining weight across the whole experiment. Psyllium plus resistant starch or psyllium plus inulin also significantly increased the caecal size and the colonic length, probably due to water retention, compared to RS, inulin and psyllium alone which is consistent with previous studies (Morita *et al.*, 1999; Pontifex *et al.*, 2021). This supports previous evidence that psyllium may increase metabolites production as the caecum is the major site for bacterial fermentation and also prevented the shortening of large intestine caused by low fibre diets. Therefore, combinations of psyllium plus either RS or inulin were taken forward to subsequent experiments. In addition, I observed the potential beneficial effects of high fibre diets, in that psyllium plus RS or inulin slowed down the tumour growth and decreased the percentage of tumours reaching 100 mm^3 or that were visible on day 39. However, the tumour take rate was relatively low, thus an experiment with higher tumour take rates was needed to confirm the effects of these dietary fibres on tumour control.

4.3 Tumour growth associated with fibre diets containing dextrose

4.3.1 Overview

The tumour take rate was low in the previous experiment which made investigating the addition of IR unfeasible. To improve this issue and to increase the robustness of the experimental set up, I modified the conditions of tumour inoculation by changing the ratio of HBSS and Matrigel from 2:1 to 1:1. In this experiment, the corn starch in all diets was replaced by dextrose to avoid its possible effect on enhancement of butyrate production as corn starch may increase the faecal butyrate level (Weaver *et al.*, 1992).

I subcutaneously injected UPPL1591 mouse bladder cancer cells into the flank of C57BL/6 mice and started feeding them with normal chow and modified diets, namely, 0.2% cellulose, psyllium, psyllium plus RS or psyllium plus inulin, on the same day (Figure 34A). Body weight stably increased within 2 weeks in all dietary groups (Figure 34B). When tumours reached 100 mm^3, around two to three weeks post inoculation, I collected faeces, caecal contents, spleens, and tumours to investigate the baseline gut microbiota, caecal metabolites, and systemic and local tumoural immunity.

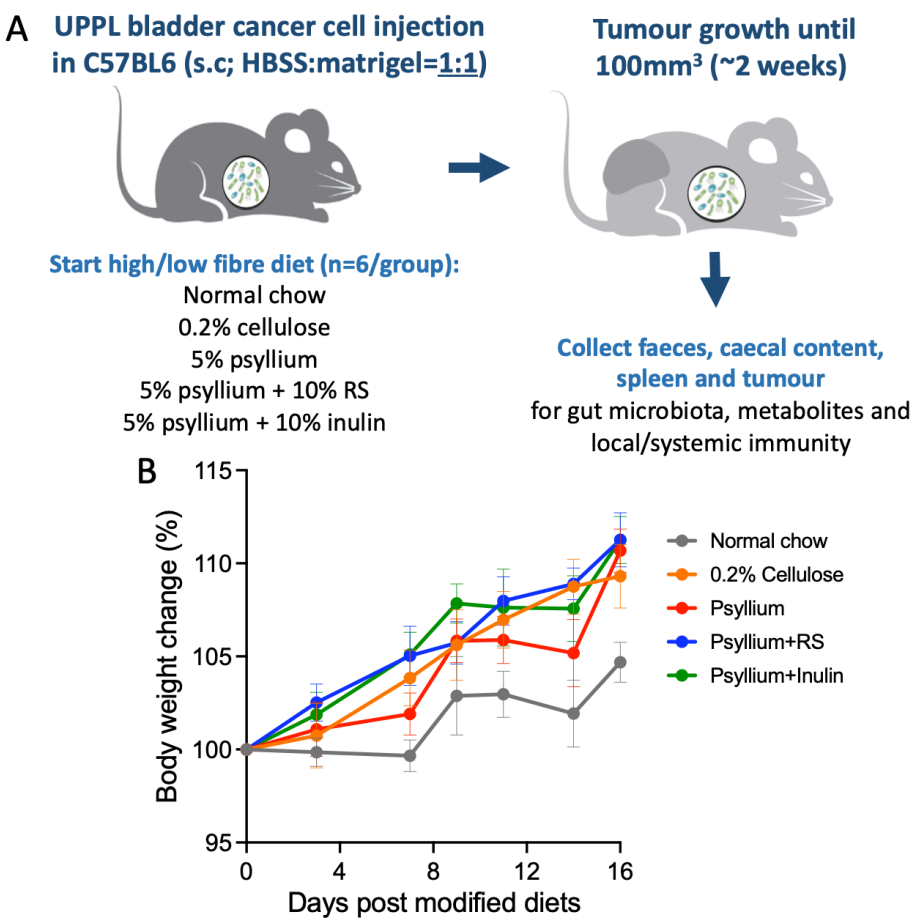


Figure 34 Overview of dietary fibre (dextrose) and UPPL1591 bladder tumours experiment. (A) UPPL1591 bladder cancer cells were injected subcutaneously in the flank of C57BL/6 mice on the same day that they received low or high fibre diets (n=6/group). Tumours were monitored until they reached 100 mm^3. At the end of experiment, faeces, caecal contents, spleens, and tumours were collected to study the baseline gut microbiota, caecal metabolites, and local and systemic immunity. (B) Body weight changes of mice fed with modified diets for two weeks. Error bars represent the standard error.

4.3.2 Growth delay in bladder cancer cell xenografts in the high fibre groups

In this diet (with dextrose) alone and tumour experiment, tumour inoculation was done using the cell mixture in a HBSS:Matrigel ratio of 1:1. In addition, thirty five percent corn starch of the whole diet was replaced by dextrose, but the other ingredients remained unchanged. The tumour take rate was 100% in this experiment, suggesting that the modifications had been successful. Psyllium plus either RS ($P=0.007$) or inulin ($P<0.001$) significantly delayed tumour growth compared to the 0.2% cellulose group (Figure 35A). The mean tumour size was 80 and 60 mm^3 in psyllium plus RS or psyllium plus inulin, respectively, at the time that 100 mm^3 was reached in the 0.2% cellulose and psyllium groups. Taking the time for the tumour to reach 100 mm^3 as the endpoint of the survival analysis, log-rank testing showed that the median times were significantly different ($P=0.037$) among dietary groups, at 15, 13, 13, 16 and 21 days for normal chow, 0.2% cellulose, psyllium, psyllium plus RS or psyllium plus inulin, respectively (Figure 35B).

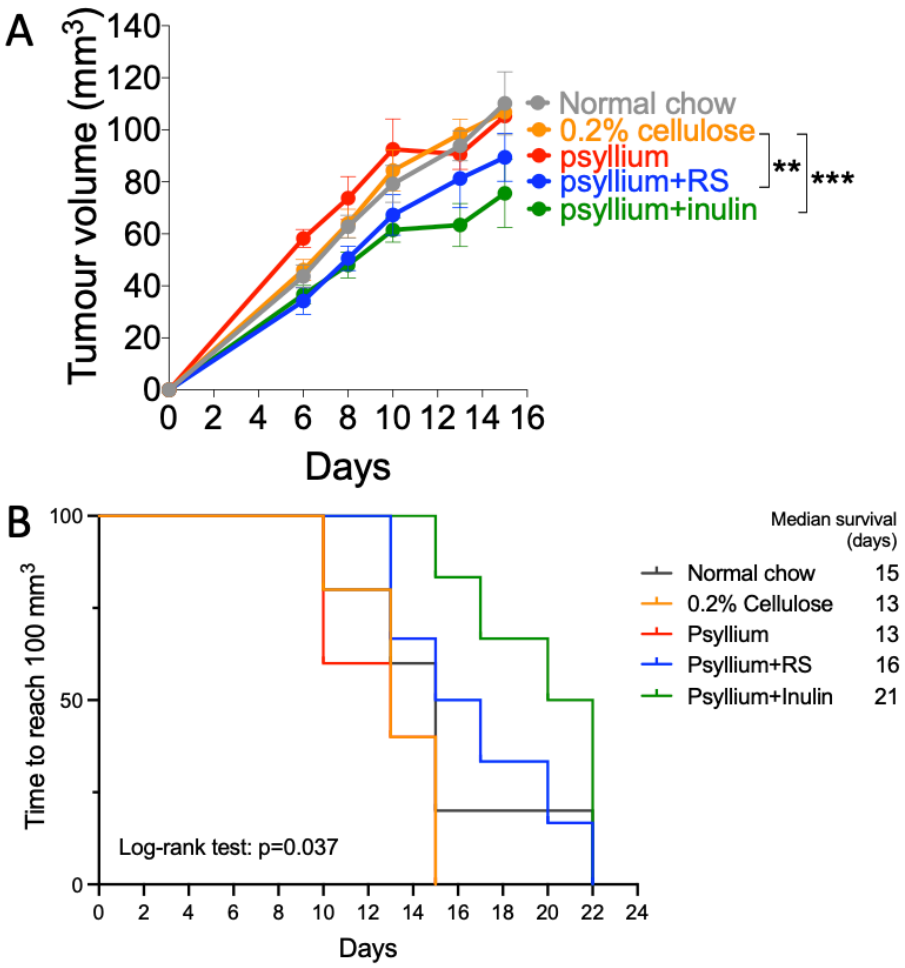


Figure 35 Psyllium plus RS and psyllium plus inulin cause increased tumour growth delay in bladder cancer cell allografts. (A) Treatment of UPPL1591 allografts with normal chow, low fibre (0.2% cellulose) and high fibre diets including psyllium, psyllium plus RS or inulin (n=6 for each group). Slopes of tumour curves were calculated by linear regression to represent tumour growth rates and compared by ANOVA test. Error bars represent the standard error. (B) Kaplan–Meier survival curve of mice with UPPL1591 allografts showing plots of time to tumour volume of 100 mm^3.

4.3.3 The gut microbiota of tumour bearing mice fed with low and high dietary fibre when the tumours reached 100 mm^3

Figure 36A shows the gut microbiota profiles from mice fed with low and high fibre diets. The legends for the top 20 taxa with the highest abundances were shown in Table A7. S24-7 family, *B. animalis* and *B. acidifaciens* were still within the top 10 bacteria of largest abundance. The relative abundance of *B. acidifaciens* was approximately 5-10% in all psyllium diets groups (Figure 36B). Psyllium plus inulin increased the *B. animalis* abundance up to 35% which was significantly higher than in all the other dietary groups (Figure 36C).

The psyllium plus inulin group had a significant lower alpha diversity due to the overriding abundance of *Bifidobacterium animalis* (Figure 37A). In terms of beta diversity, principal coordinate analysis showed a notable cluster effect of all dietary groups and psyllium and psyllium plus RS groups were relatively close, consistent with the previous experiment (Figure 37B).

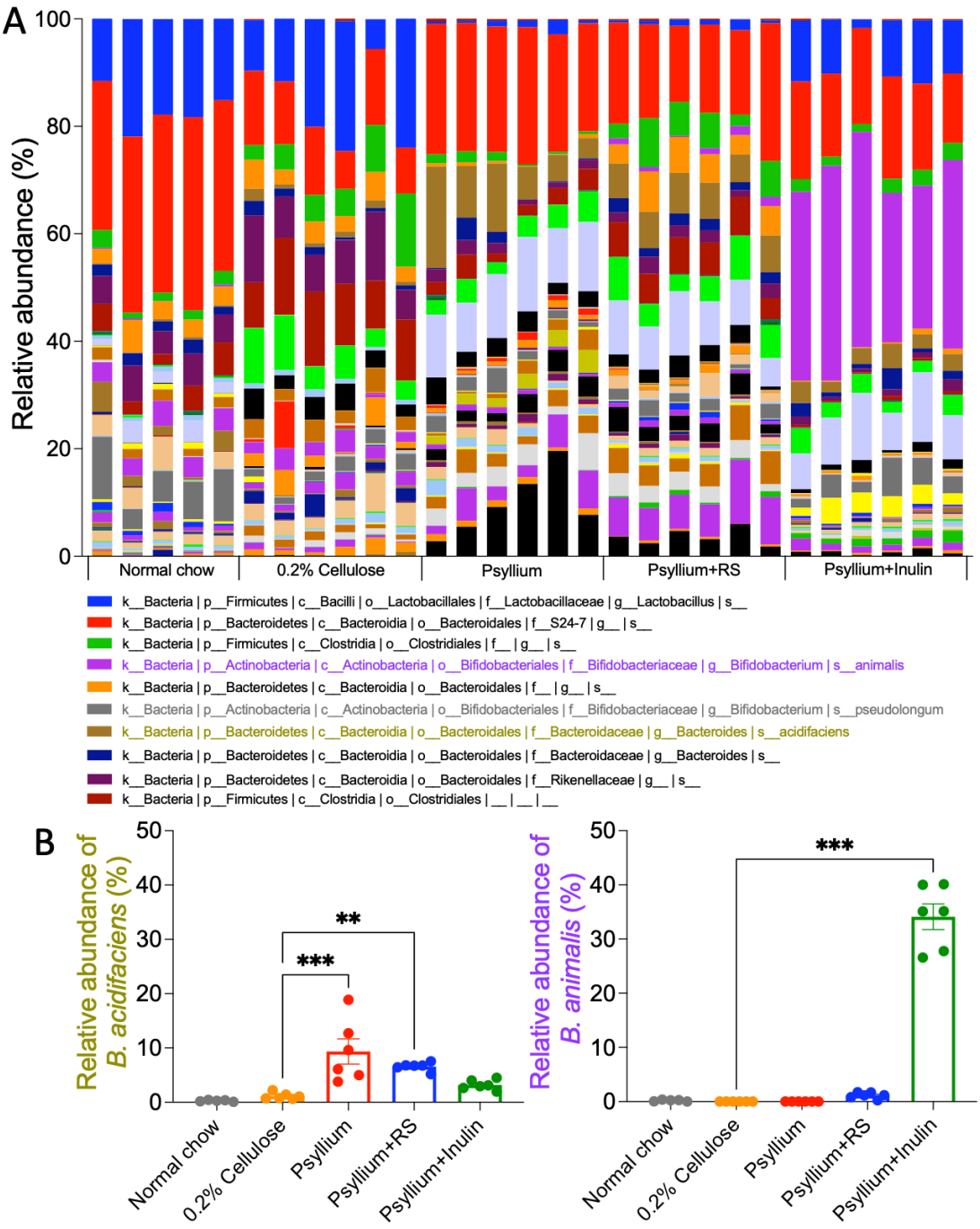


Figure 36 Phylogenetic composition of the faecal microbiota a at the species level. (A) Faecal samples were collected when tumours reached 100 mm^3 (n=6/group). (B) Relative abundance of *B. acidifaciens* and *B. animalis* of high fibre groups compared with 0.2% cellulose. One-way ANOVA with Dunnett's multiple comparison test was used to compare the means of different dietary groups. Error bars represent the standard error.

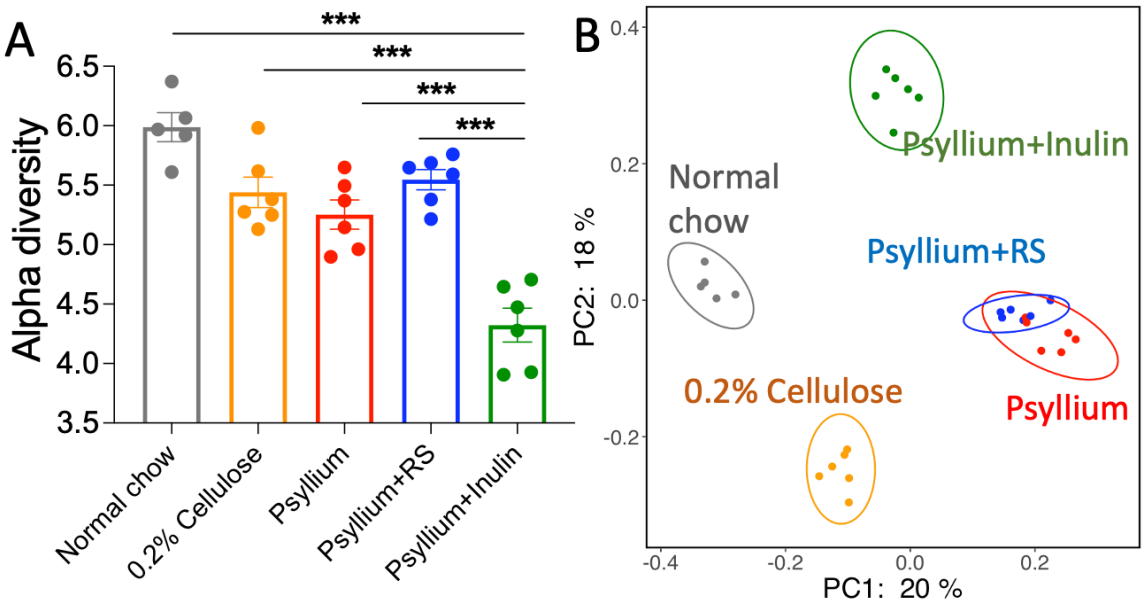


Figure 37 Alpha and beta diversity of the faecal microbiota. (A) Alpha diversity using Shannon index and (B) principal coordinate analysis of faecal microbiotas using Bray-Curtis dissimilarity. A notable clustering effect by diets was seen in the gut microbiota.

4.3.4 Untargeted metabolomics profiling of caecal contents

The PLS-DA plot showed a notable clustering effect of metabolite profiles by diet (Figure 38A). Consistent with the gut microbiota profile in Figure 37B, psyllium and psyllium plus RS were rather similar to each other compared to the other dietary groups. I ran an ANOVA analysis to compare the metabolites levels among 0.2% cellulose, psyllium, psyllium plus resistant starch or psyllium plus inulin groups (Figure 38B). The top 10 metabolites that had the lowest p-value among 126 analytes were listed in Figure 39. Myo-inositol 1-phosphate (P=7.09E-12) and sinapic acid (3.95E-11) were enriched in the 0.2% cellulose group. Psyllium and psyllium plus RS had higher levels of N-acetylneuraminic acid (P=7.05E-12) and caproic acid (P=3.53E-11) respectively. Among them, there were six metabolites increased in the psyllium plus inulin group, namely, N-acetyl ornithine (P=3.47E-13), homocitric acid (P=1.04E-12), maleic acid (P=1.87E-10), inosine (P=2.99E-10), gamma-glutamylalanine (P=9.23E-10) and methyl beta-D-glucopyranoside (P=2.91E-9).

Figure 40 shows the caecal metabolites enriched in the psyllium plus RS group including caproic acid (P=3.53E-11), D-phenyllactic acid (P=1.94E-6), beta-arabinose (P=1.98E-6), taurine (P=9.46E-5), allantoin (P=1.84E-4), hydroxyphenyllactic acid (P=4.14E-4), 5-hydroxyhexanoic acid (P=9.03E-4), 3-dehydroquinate (P=2.28E-3), p-cresol sulfate (P=2.99E-3), 5,7-dihydroxyflavone (P=3.63E-3), beta-citryl-L-glutamine (P=0.015) and butyric acid (P=0.015). A brief literature review of these metabolites is discussed in the section 4.5.

Figure 41 showed that psyllium plus inulin was enriched with the metabolisms of pyrimidine, purine, ascorbate and aldarate. Metabolites enriched in psyllium plus resistant starch were associated with the metabolism of tryptophan, amino sugars and nucleotide sugars, and purine (Figure 42).

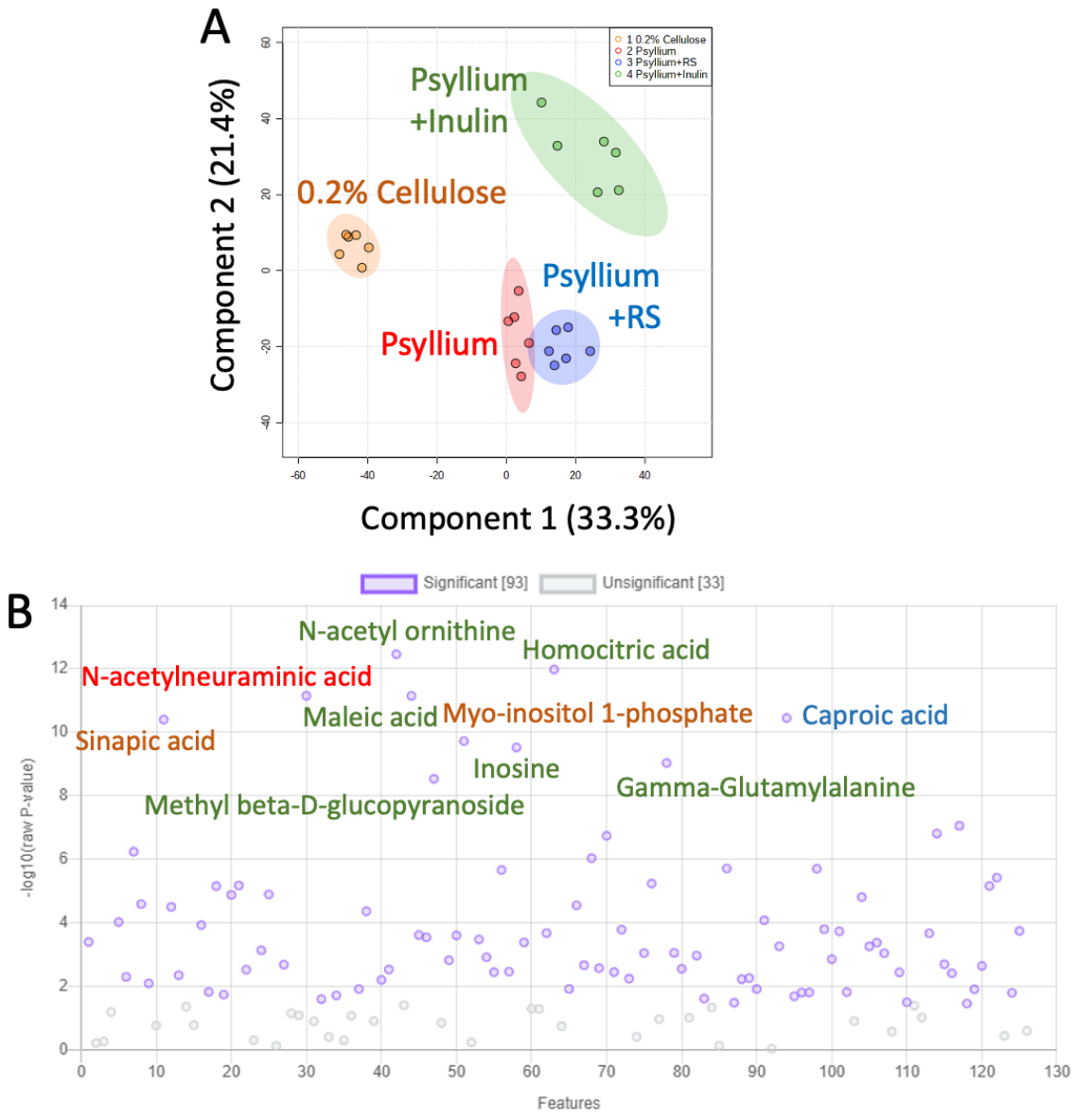


Figure 38 Untargeted metabolomics analysis of caecal contents in all dietary groups. (A) Partial least squares-discriminant analysis caecal metabolites of different dietary groups. A notable clustering effect by diets was seen in the metabolites. (B) The top ten metabolites which had the lowest p values in ANOVA test and (C) their relative levels among different dietary groups.

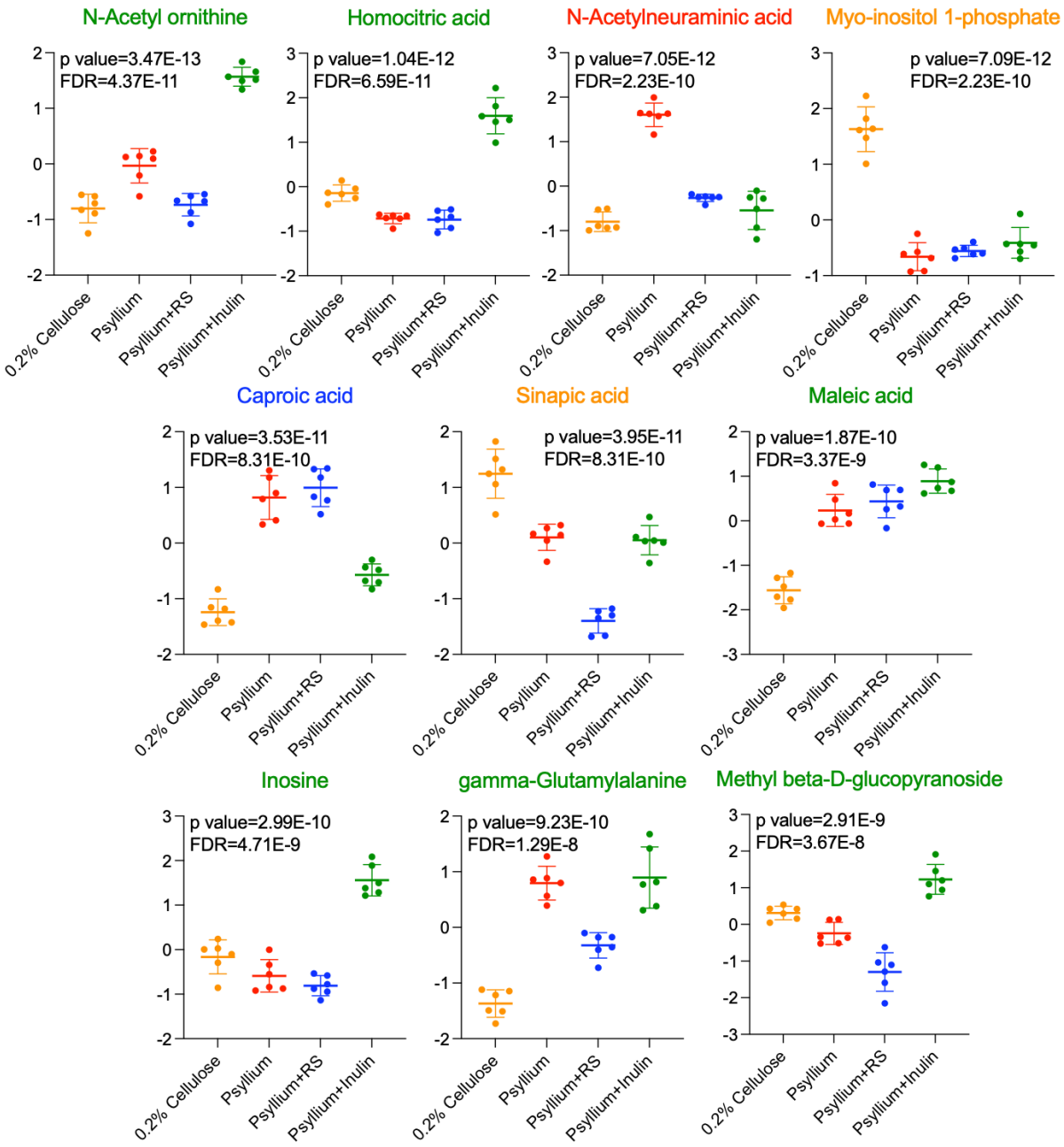


Figure 39 Caecal metabolites enriched in different dietary groups. The relative levels of the top 10 metabolites enriched in different dietary groups which had the lowest p values in an ANOVA test. Data is mean ± SEM.

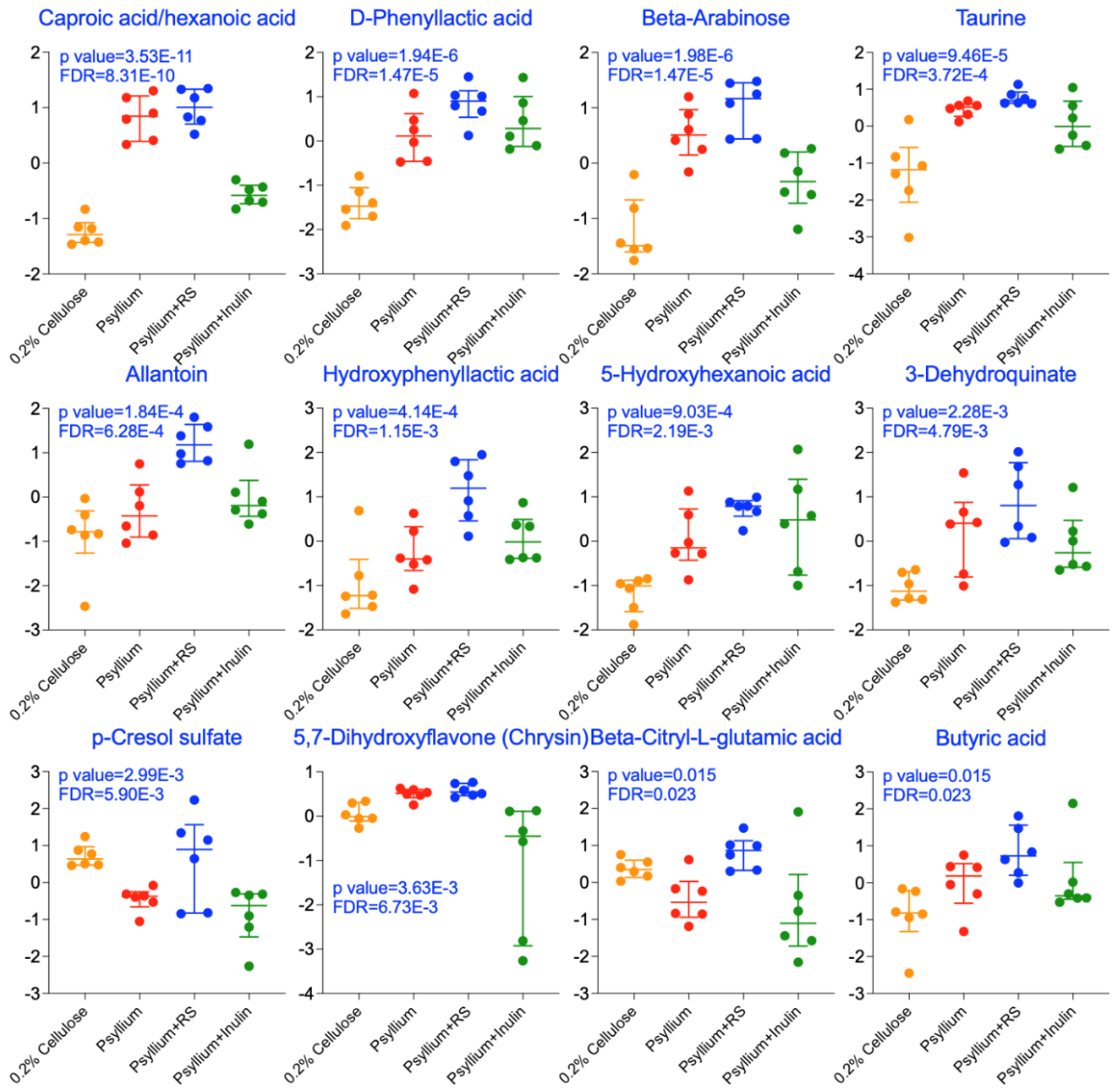


Figure 40 Caecal metabolites enriched in psyllium plus RS. The top 12 metabolites enriched in psyllium plus RS which had the lowest p values in an ANOVA test and their relative levels among different dietary groups. Data is mean ± SEM.

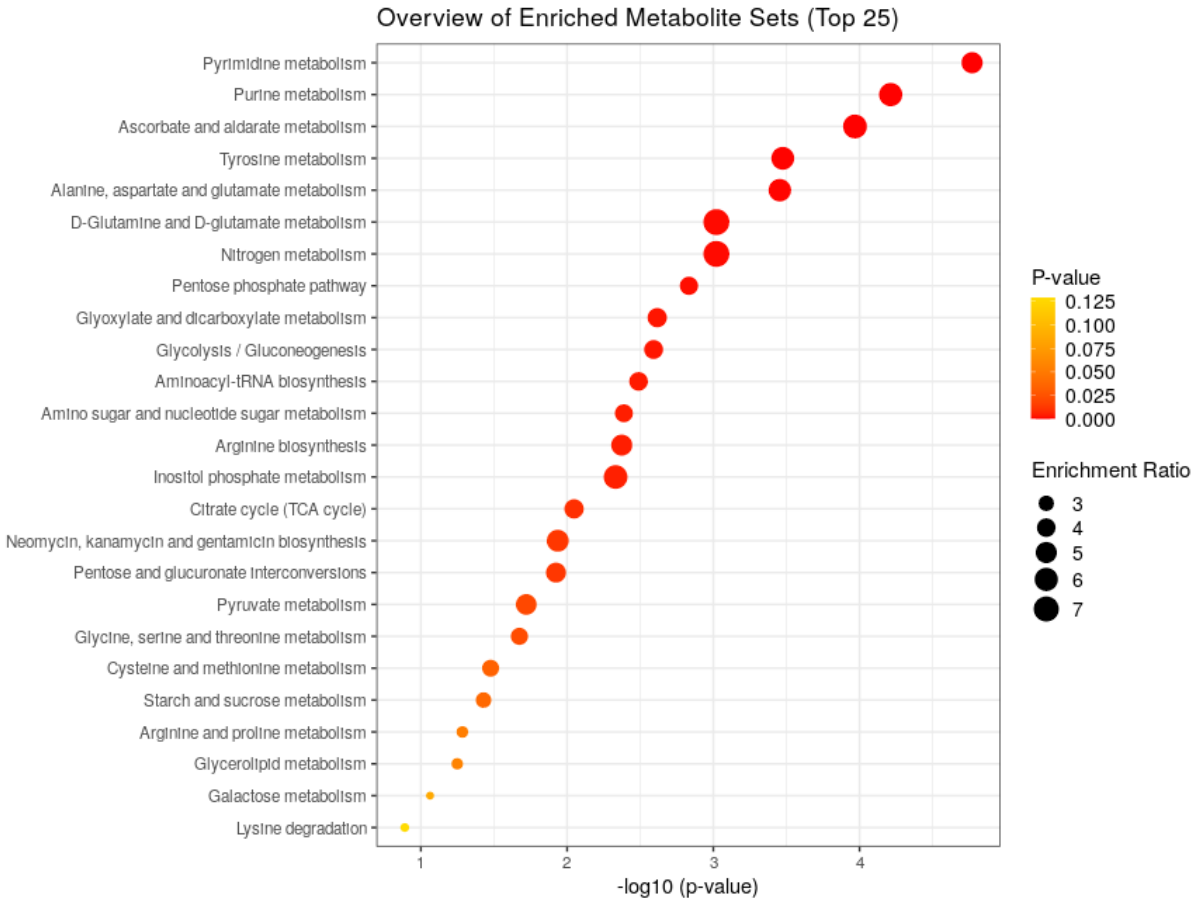


Figure 41 KEGG pathways of pyrimidine, purine and ascorbate and aldarate metabolism enriched in psyllium plus inulin. KEGG pathways enrichment analysis of metabolites enriched in psyllium plus inulin compared to psyllium. The intensity of colour denotes the P-value and the dot size denotes the enrichment ratio.



Figure 42 KEGG pathways of tryptophan, amino sugar and nucleotide sugar, and purine metabolism enriched in psyllium plus resistant starch. KEGG pathways enrichment analysis of metabolites enriched in psyllium plus RS compared to psyllium. The intensity of colour denotes the P-value and the dot size denotes the enrichment ratio.

4.4 Tumour growth following dietary fibre and ionising radiation

4.4.1 Overview

To study the radiosensitising effect of dietary fibre, I irradiated the subcutaneous flank tumours with 6 Gy IR when they reached 80-100 mm^3, with all other parameters as per the previous diet alone and UPPL1591 tumour experiment (Figure 43A). This experiment consisted of 60 mice in four groups (n=15 per group) fed diets comprising: 0.2% cellulose, 5% psyllium, 5% psyllium plus 10% RS and 5% psyllium plus 10% inulin either without (n=5) or with (n=10) irradiation. I sacrificed the mice when the tumours reached 700 mm^3 or at the end of experiment, day 40 post-tumour inoculation. Faeces, caecal contents, tumours, spleens, and plasma were taken to investigate the gut microbiota, metabolomics, and immune (see chapter 6) responses to dietary fibre and IR. 16S rRNA gene sequencing of faecal DNA was performed on a MiSeq platform to investigate the bacterial components of the mouse gut microbiota. The gut microbiota was analysed on a QIIME2 platform to identify the features (differentially abundant taxa or diversity index) that correlated to the phenotype. Caecal contents were used for untargeted metabolomics analysis to study the functional outcomes of dietary fibre and gut microbiota. Tumours, spleen, and plasma were taken to investigate the local and systemic immune responses.

4.4.2 Body weight changes of tumour-bearing mice fed with modified diets

Across the whole experiment, all mice stably gained weight in the low and high fibre diets groups (Figure 43B). All psyllium diets increased the rate of weight increase, especially psyllium plus RS ($P=0.047$) and psyllium plus inulin ($P<0.001$), compared to 0.2% cellulose. After receiving IR when the tumours reached 80-100 mm^3, IR cohorts of psyllium plus RS ($P=0.033$) or inulin ($P<0.001$) experienced slower rates of weight gain compared to their non-IR controls.

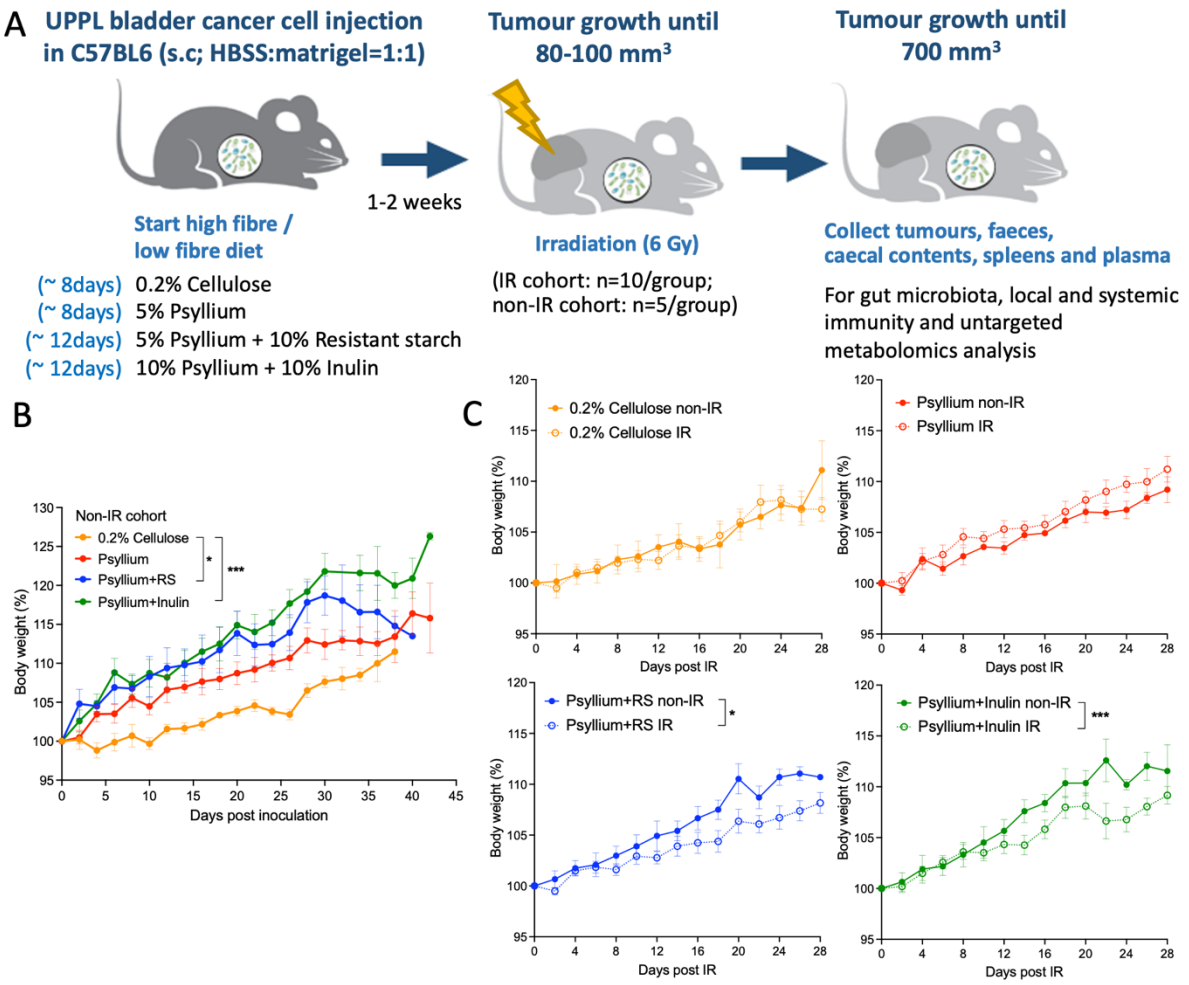


Figure 43 Overview of dietary fibre, IR and tumour growth experiment. (A) UPPL1591 bladder cancer cells were injected subcutaneously in the flank of C57BL/6 mice on the same day that they started on a low or high fibre diet (n=6/group). Tumours were irradiated with 6 Gy IR when they reached 80-100 mm^3 and monitored until 700 mm^3. (B) Body weight changes of mice fed with modified diets across the whole experiment. 100% was the weight on first day of tumour inoculation. (C) Body weight changes of non-IR and IR cohorts of each dietary groups after tumour reached 80-100 mm^3 for the mice that did not receive IR or following IR. Slopes of body weight curves were calculated by linear regression and compared by ANOVA test and Dunnett's multiple comparison test. Error bars represent the standard error.

4.4.3 Psyllium plus RS or psyllium plus inulin increased growth delay in bladder tumours

Within 24 days of tumour inoculation, psyllium plus RS (P=0.076) or psyllium plus inulin (P=0.004) delayed tumour growth compared to 0.2% cellulose (Figure 44A), which was consistent with the second set of diet and tumour experiments (Figure 35) where both of these diets had slower tumour growth rate compared to 0.2% cellulose. On day 18, all psyllium diet groups had smaller tumour volumes, especially psyllium plus inulin (P=0.046).

4.4.4 Psyllium plus RS or psyllium plus inulin combined with IR increased growth delay in bladder tumours

In all dietary groups, IR significantly delayed tumour growth compared with their non-IR controls (Figure 45A and B) (p-values were <0.001 for 0.2% cellulose, psyllium plus RS or psyllium plus inulin, and 0.039 for psyllium). In the IR cohorts, psyllium plus RS or psyllium plus inulin significantly delayed tumour growth compared with either 0.2% cellulose (P<0.001 for psyllium plus RS and =0.028 for psyllium plus inulin) or psyllium (P<0.001 for psyllium plus RS and =0.034 for psyllium plus inulin). This result showed the composite effect of high dietary fibre and IR in mediating tumour control.

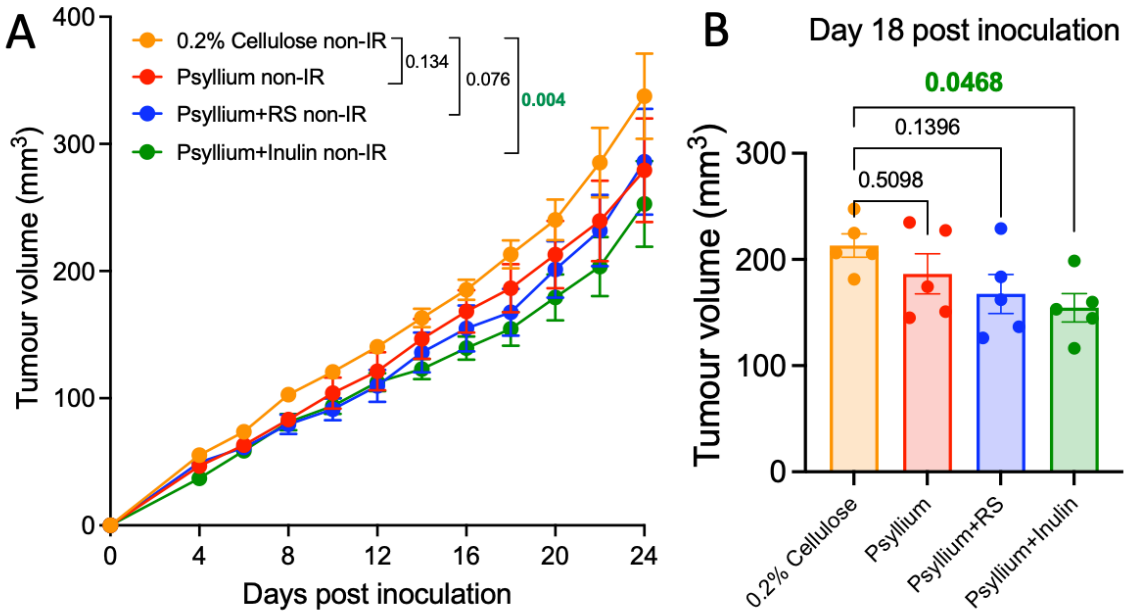


Figure 44 Psyllium plus RS and psyllium plus inulin cause increased tumour growth delay in bladder cancer cell allografts. (A) Treatment of UPPL1591 allografts with normal chow, low fibre (0.2% cellulose) and high fibre diets including psyllium, psyllium plus RS or inulin (n=6 for each group). Slopes of tumour curves were calculated by linear regression to represent tumour growth rates and compared by ANOVA test. (B) The tumour growth curves within 24 days and tumour sizes on day 18 after inoculation. The means were compared by ANOVA test and Dunnett's multiple comparison test. Error bars represent the standard error**.**

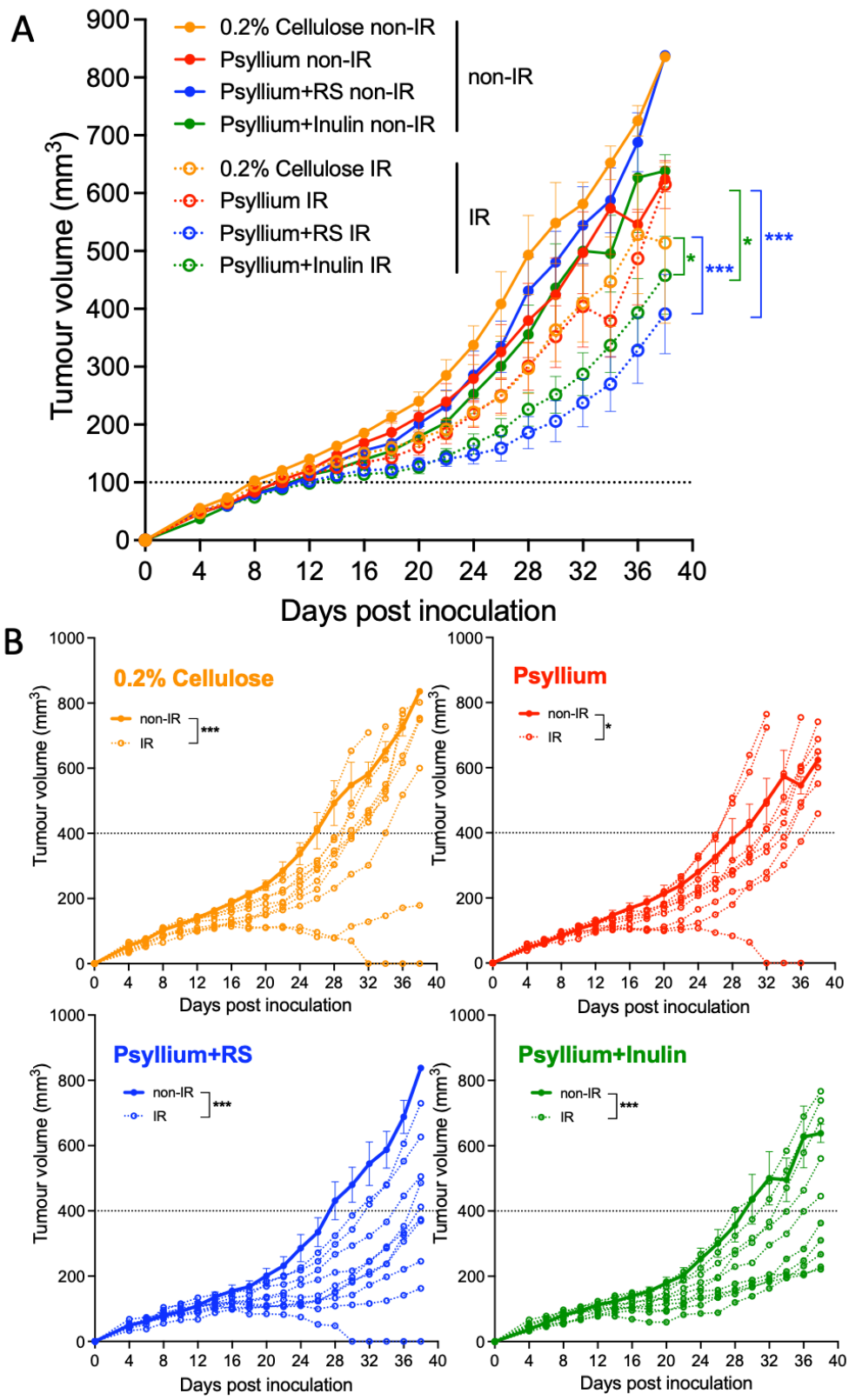

A
0.2% Cellulose non-IR
Psyllium non-IR
Psyllium+RS non-IR
Psyllium+Inulin non-IR
non-IR
0.2% Cellulose IR
Psyllium IR
Psyllium+RS IR
Psyllium+Inulin IR
IR
Tumour volume (mm3)
Days post inoculation
B
0.2% Cellulose
Psyllium
Psyllium+RS
Psyllium+Inulin
non-IR
IR

Figure 45 Psyllium plus RS or psyllium plus inulin enhanced tumour control combined with IR in bladder cancer cell allografts. (A) Treatment of UPPL1591 allografts with low fibre (0.2% cellulose) and high fibre diets including psyllium, psyllium plus RS or inulin (n=5 for each group). Tumours were irradiated with 6 Gy when they reached 80-100 mm^3 and monitored until 700 mm^3. (B) Individual tumour growth curves stratified into non-IR (solid line) and IR (dot line). Day 0 was the day of tumour inoculation and when the mice started taking modified diets. Data shown as mean and standard error. Slopes of tumour curves were calculated by linear regression to represent tumour growth rates and compared by ANOVA test and Dunnett's multiple comparison test.

4.4.5 Psyllium plus RS increased radiosensitivity of bladder tumour

To assess the specific radiosensitising effects of the high fibre diets (i.e. removing the effect of diet alone in delaying tumour growth), I aligned Day 0 to the day of tumours reaching 80-100mm^3 or receiving IR, and compared the tumour growth curves among different dietary groups (Figure 46A). Psyllium plus RS significantly radiosensitised bladder tumours compared to 0.2% cellulose ($P=0.004$) and psyllium ($P<0.001$). Based on two clear groups split for each diet at a tumour volume of around 400mm^3 at day 26 post IR, there were three responding mice who received 0.2% cellulose, five mice in the psyllium, eight mice in the psyllium plus RS and four mice in the psyllium plus inulin groups (Figure 46B).

4.4.6 Psyllium plus RS increased time to quadruple tumour volume

I further conducted survival analysis by using the time to quadruple in tumour volume as an endpoint (Figure 47A). Irradiated mice in all dietary groups had significantly longer median time for tumours to quadruple in volume compared to non-IR controls and the p-values were 0.021 for 0.2% cellulose, 0.034 for psyllium, <0.001 for psyllium plus RS and 0.004 for psyllium plus inulin (Figure 47B). These data reflect 6 Gy conferring some degree of survival advantage and demonstrate a greater impact of irradiation in the group fed psyllium plus resistant starch compared to psyllium plus inulin.

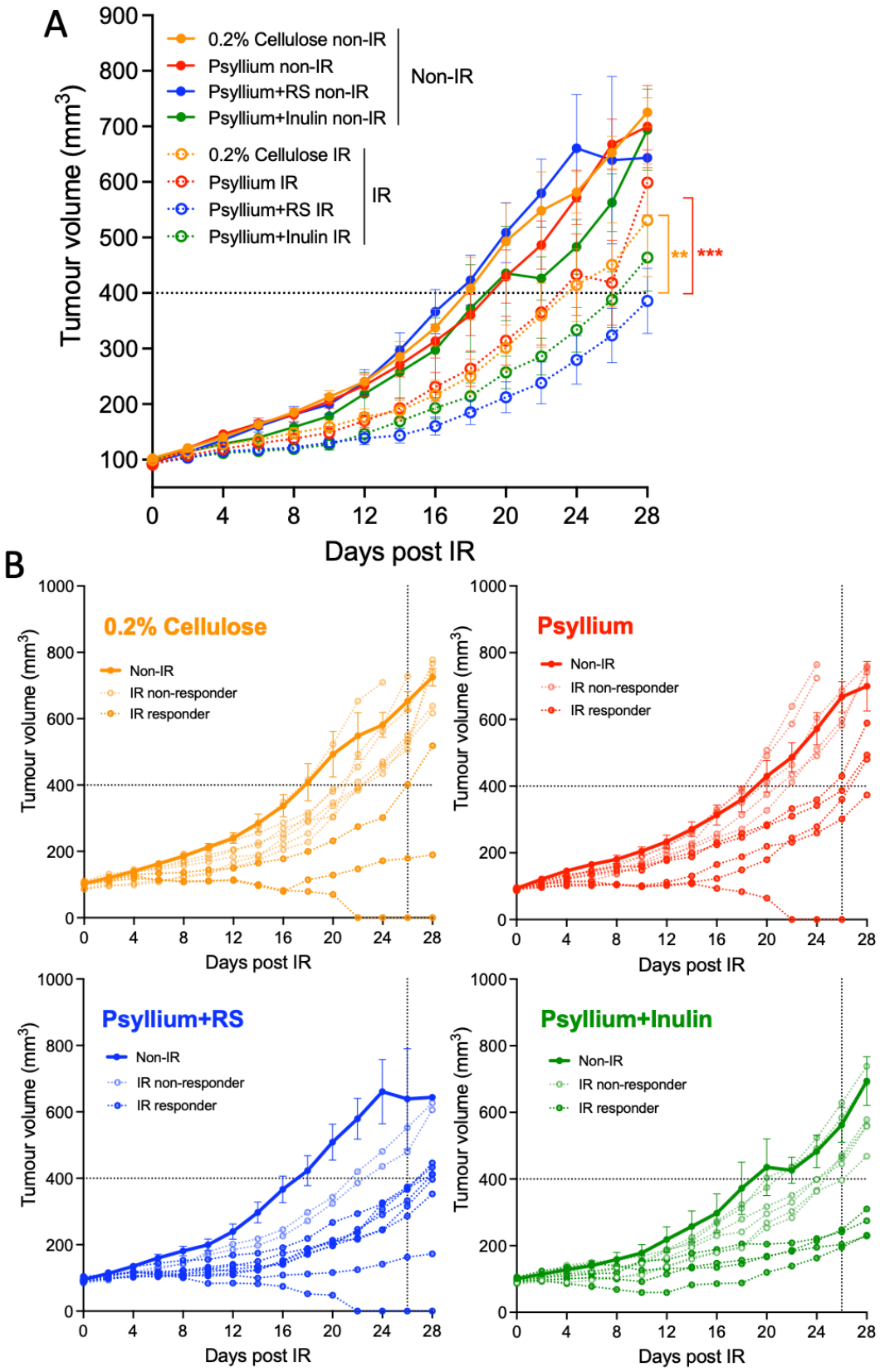

A
Tumour volume (mm3)
Days post IR
0.2% Cellulose non-IR
Psyllium non-IR
Psyllium+RS non-IR
Psyllium+Inulin non-IR
Non-IR
0.2% Cellulose IR
Psyllium IR
Psyllium+RS IR
Psyllium+Inulin IR
IR
**
***
B
0.2% Cellulose
Psyllium
Psyllium+RS
Psyllium+Inulin
Non-IR
IR non-responder
IR responder

Figure 46 Psyllium plus RS radiosensitised UPPL1591 bladder cancer cell allografts. (A) Treatment of irradiated (6 Gy) UPPL1591 allograft with 0.2% cellulose, psyllium, psyllium plus RS or inulin (n=5 for non-IR and n=10 for IR in each group). The growth curves of non-irradiated and irradiated mice were plotted in solid and dotted lines, respectively. Day 0 represents the day when tumours reached 80-100 mm^3 and received IR. Data shown as mean and standard error. Slopes of tumour curves were calculated by linear regression to represent tumour growth rates and compared by ANOVA test and Dunnett's multiple comparison test.

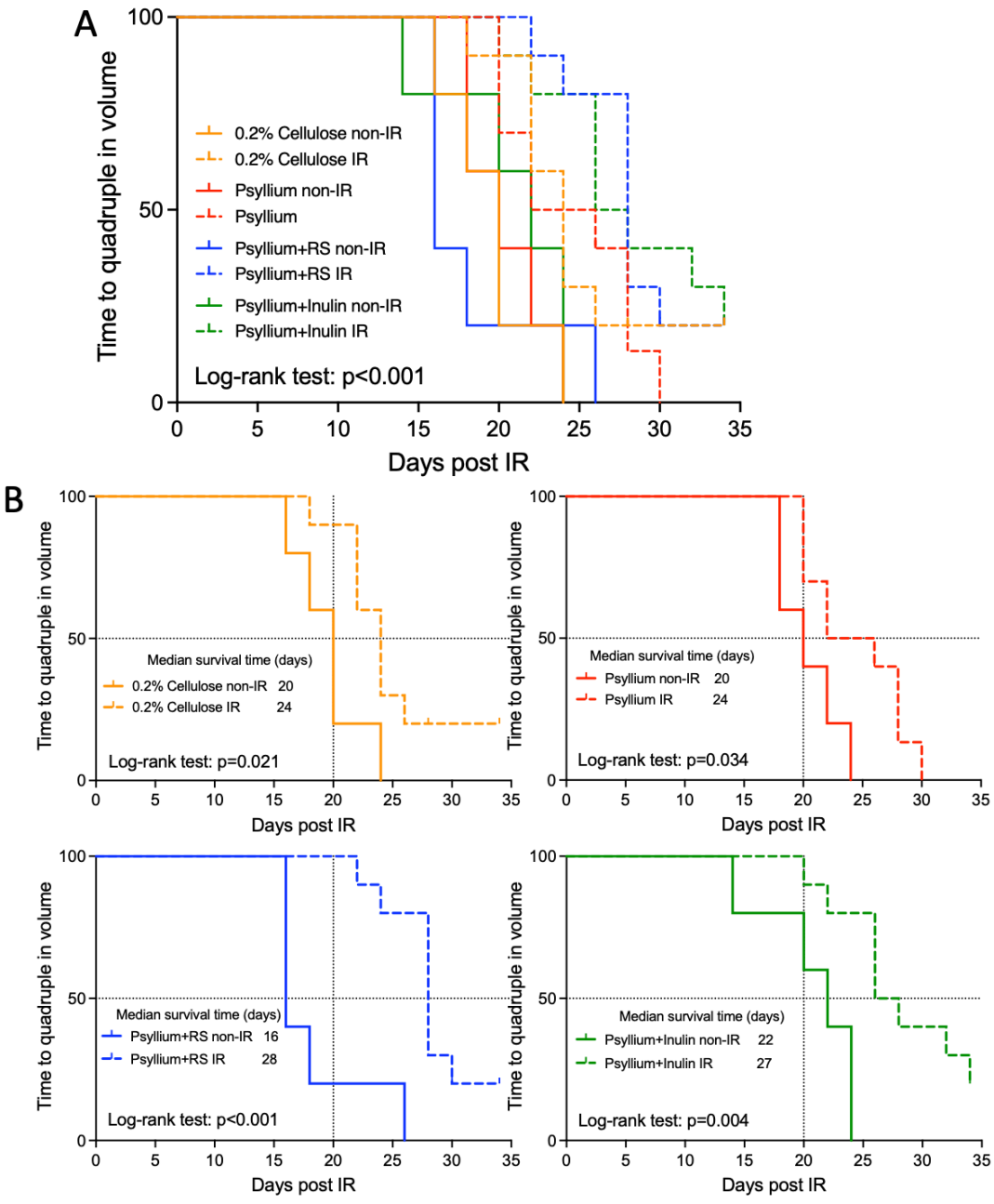


Figure 47 Survival analysis of tumour-bearing mice without and with IR in different dietary groups. (A) Overall and (B) individual Kaplan–Meier survival curve of mice with UPPL1591 allografts showing plots of time to quadruple in tumour volume.

4.4.7 The gut microbiota of tumour-bearing mice fed with low and high dietary fibre when the tumours reached 700 mm^3

Figure 48 shows the gut microbiota profiles from mice fed with low and high fibre diets. The legends for the top 20 taxa with the highest abundances were shown in Table A8 and A9. The Clostridiales unspecified species, *B. animalis, B. acidifaciens* and a *Bacteroides* unspecified species were still within the top 10 bacteria with the largest abundance among all the other bacteria species. The psyllium plus inulin group had a significant lower alpha diversity due to the overriding abundance of *B. animalis* (Figure 34B). In terms of beta diversity, principal coordinate analysis showed a notable clustering effect for all dietary groups and the psyllium and psyllium plus RS groups were relatively closest, which was consistent with the two previous experiments (Figure 32C and 37B). All psyllium diets shaped the gut microbiota into profiles that were significantly different from that 0.2% cellulose ($P<0.001$).

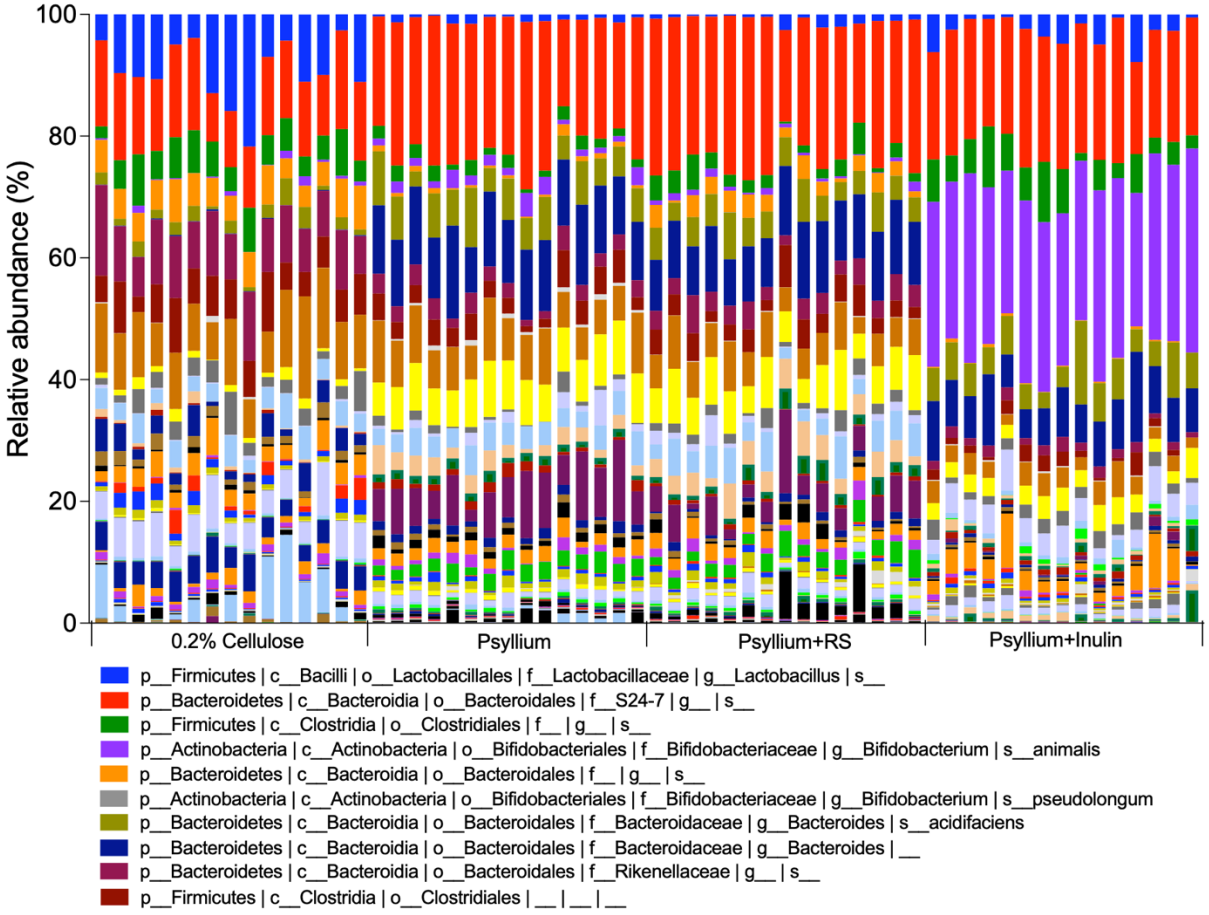


Figure 48 Phylogenetic composition of faecal microbiota at the species level. Faecal samples were collected when tumours reached 700 mm^3 (n=5/non-IR cohort, n=10/IR cohort in each dietary group).

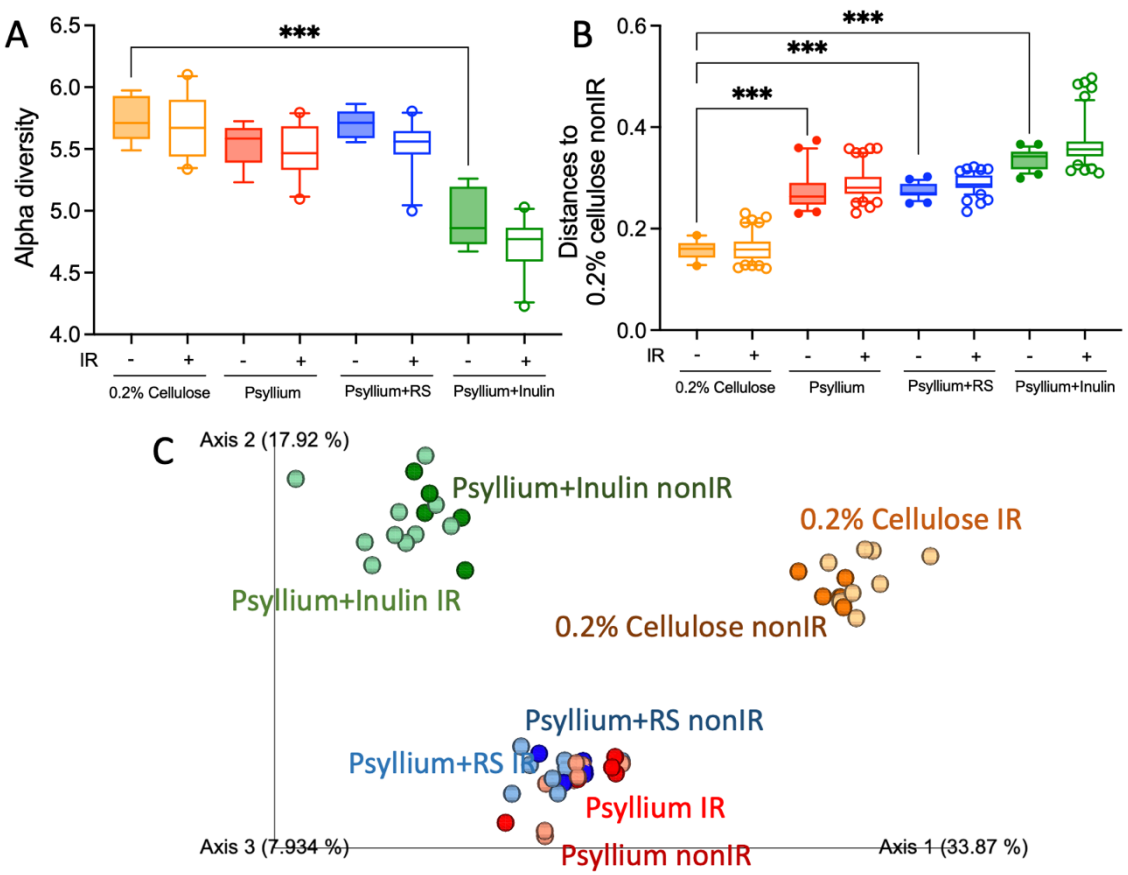


Figure 49 Alpha and beta diversity of faecal microbiota at the species level. Faecal samples were collected when tumours reached 700 mm^3 (n=5/non-IR cohort, n=10/IR cohort in each dietary group). (A) Alpha diversity using Shannon index, (B) beta diversity using PERMANOVA and (C) principal coordinate analysis using unweighted UniFrac of faecal microbiotas. A notable clustering effect by diets was seen in the gut microbiota. One-way ANOVA with Dunnett's multiple comparison test was used to compare the means of different dietary groups. Error bars represent the standard error.

4.4.8 Correlation between gut microbiota versus tumour responses

Mice in each dietary group responded very differently to radiotherapy. Based on two clear groups split for each diet at a tumour volume of around 400mm^3 at day 26 post IR, I classified them as responders and non-responders for further analysis. The responses to melanoma had been shown to be associated with the gut microbiota (Gopalakrishnan *et al.*, 2018).

To explore how specific bacterial taxa affect tumour control, I investigated the correlation between *Bacteroides* species and Lachnospiraceae family abundance versus tumour growth rate, because the *Bacteroides* species and Lachnospiraceae family were the 'top hits' for responders in the psyllium plus RS (Figure 50) and psyllium plus inulin (Figure 51) groups, respectively. I also investigated the Clostridiales order that has a higher taxonomy hierarchy that Lachnospiraceae family belong to.

An unspecified *Bacteroides* species colonised around 8 to 12 % of the gut microbiota in mice in the psyllium plus RS group. Its abundance was significantly negatively correlated with tumour growth ($P<0.001$). This unspecified *Bacteroides* species' abundance was higher in the IR cohort and it was associated with better tumour control ($P=0.003$), compared to the non-IR cohort (Figure 52). In contrast, S24-7 family was associated with worse tumour control in psyllium plus RS group ($P=0.049$, Figure 53).

In the psyllium plus inulin group, the abundance of the Clostridiales order negatively correlated with tumour growth in the IR cohort ($P=0.013$) but this was not seen in the non-IR cohort ($P=0.974$) (Figure 54). Although the Clostridiales order was enriched in the non-IR cohort, it was not associated with a slower rate of tumour growth. This suggested that IR is necessary for any tumour control mediated by the presence of the Clostridiales order in the gut microbiota.

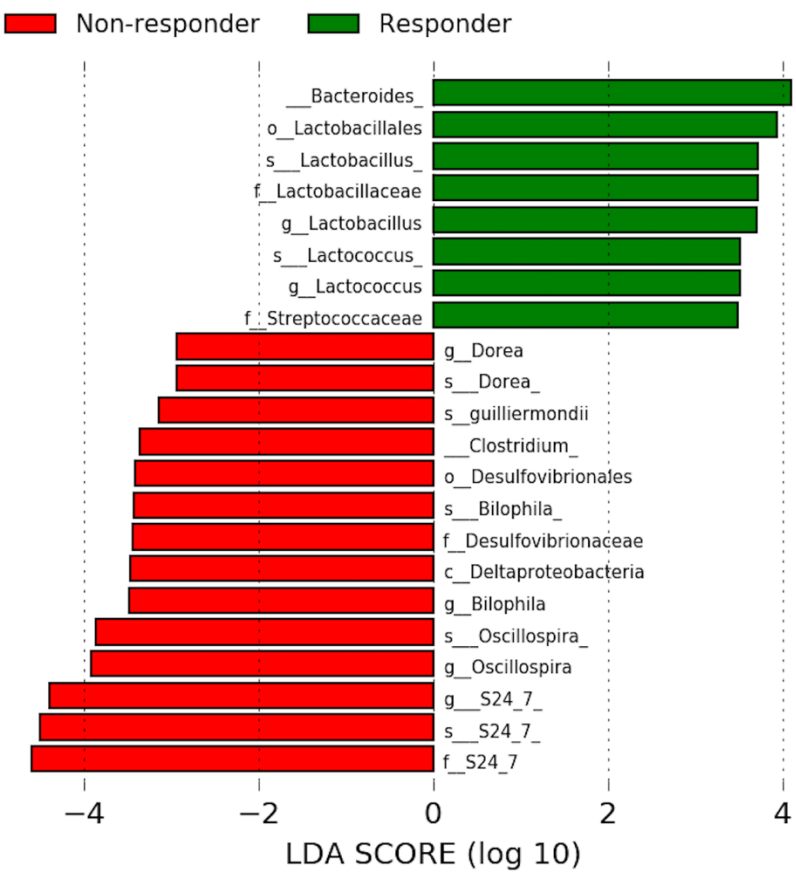


Figure 50 Differences in bacterial components in responders and non-responders in the psyllium plus RS group. Linear discriminant analysis (LDA) scores computed for differentially abundant taxa in the microbiomes of responders (green) and non-responders (red). Length indicates the effect size associated with a taxon and p = 0.05 for Kruskal-Wallis test.

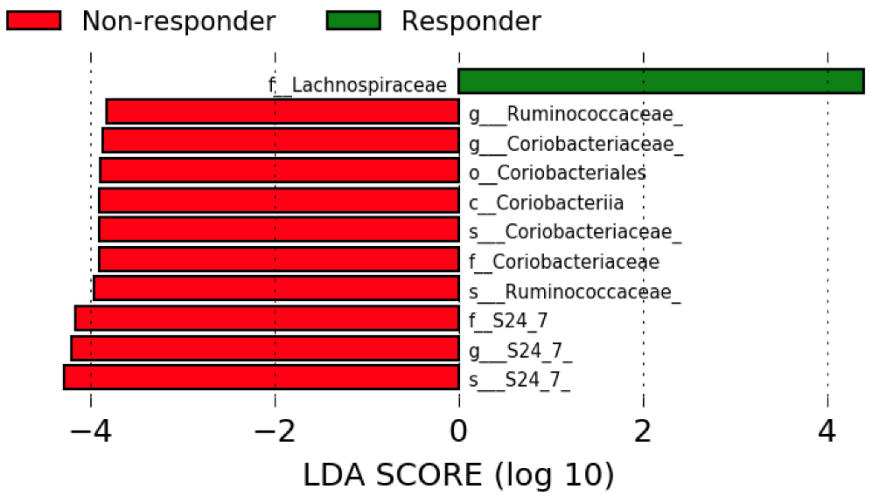


Figure 51 Differences in bacterial components in responders and non-responders in the psyllium plus inulin group. Linear discriminant analysis (LDA) scores computed for differentially abundant taxa in the microbiomes of responders (green) and non-responders (red). Length indicates the effect size associated with a taxon and p = 0.05 for Kruskal-Wallis test.

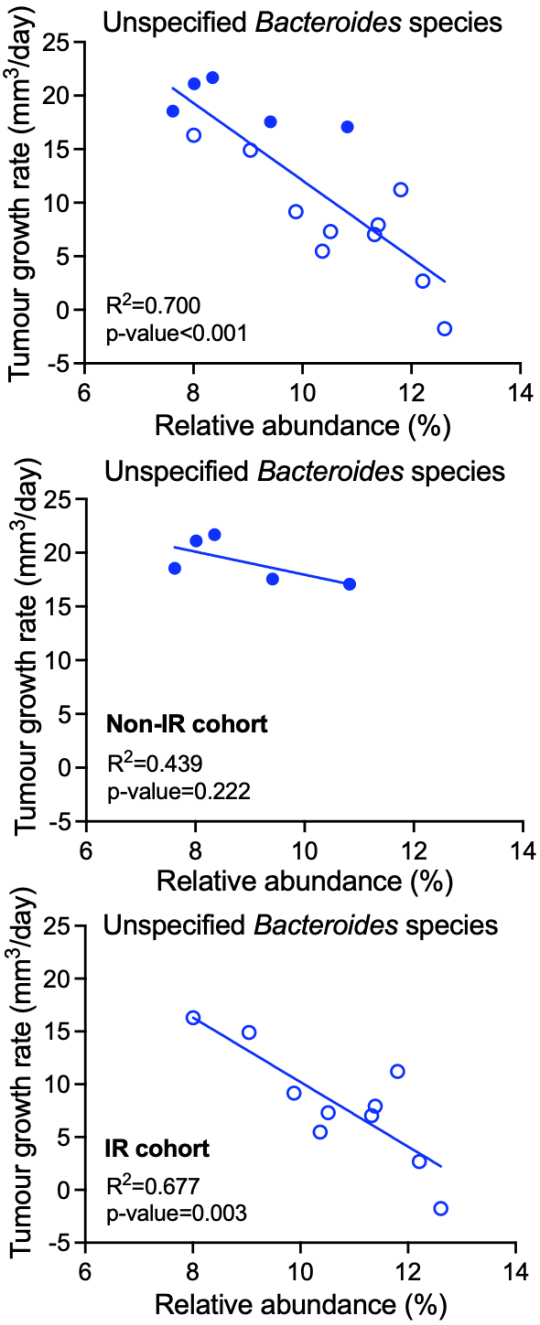


Figure 52 Unspecified *Bacteroides* species were associated with better tumour control in IR cohort of psyllium plus RS group. Correlation between the unspecified *Bacteroides* species versus the tumour growth in non-IR (solid symbols, R^2 = 0.439, P=0.222) and IR cohorts (open symbols, R^2 = 0.677, P=0.003) of psyllium plus RS. Tumour curve slopes were calculated by linear regression to represent tumour growth rates.

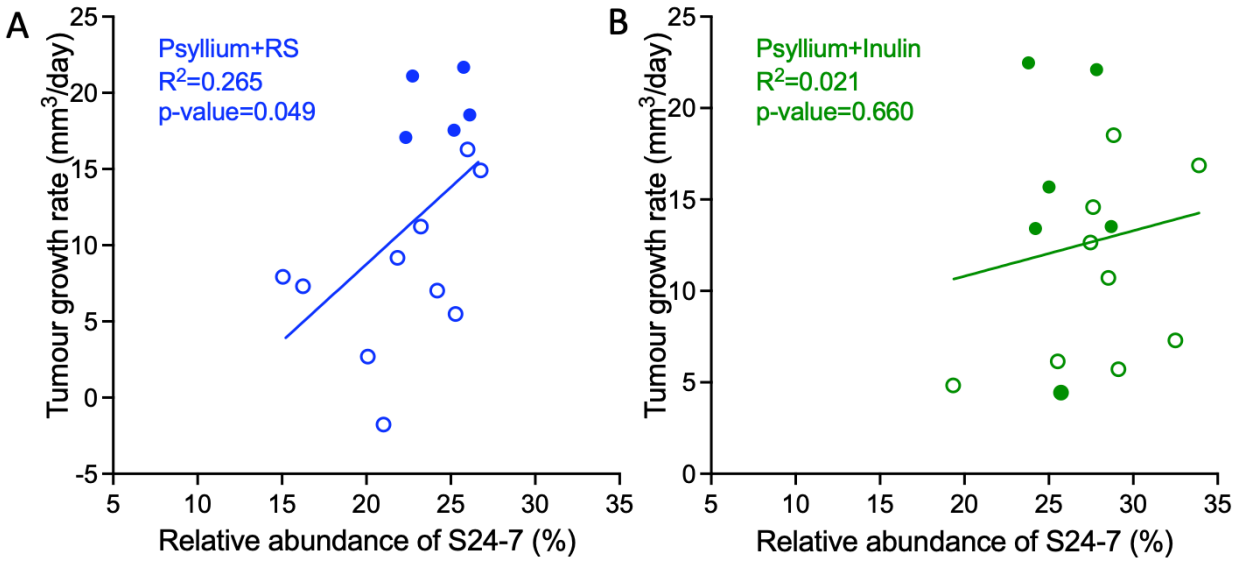


Figure 53 S24-7 family was associated with worse tumour control in psyllium plus RS group. Correlation between the S24-7 family versus the tumour growth in (A) psyllium plus RS and (B) psyllium plus inulin. Tumour curve slopes were calculated by linear regression to represent tumour growth rates.

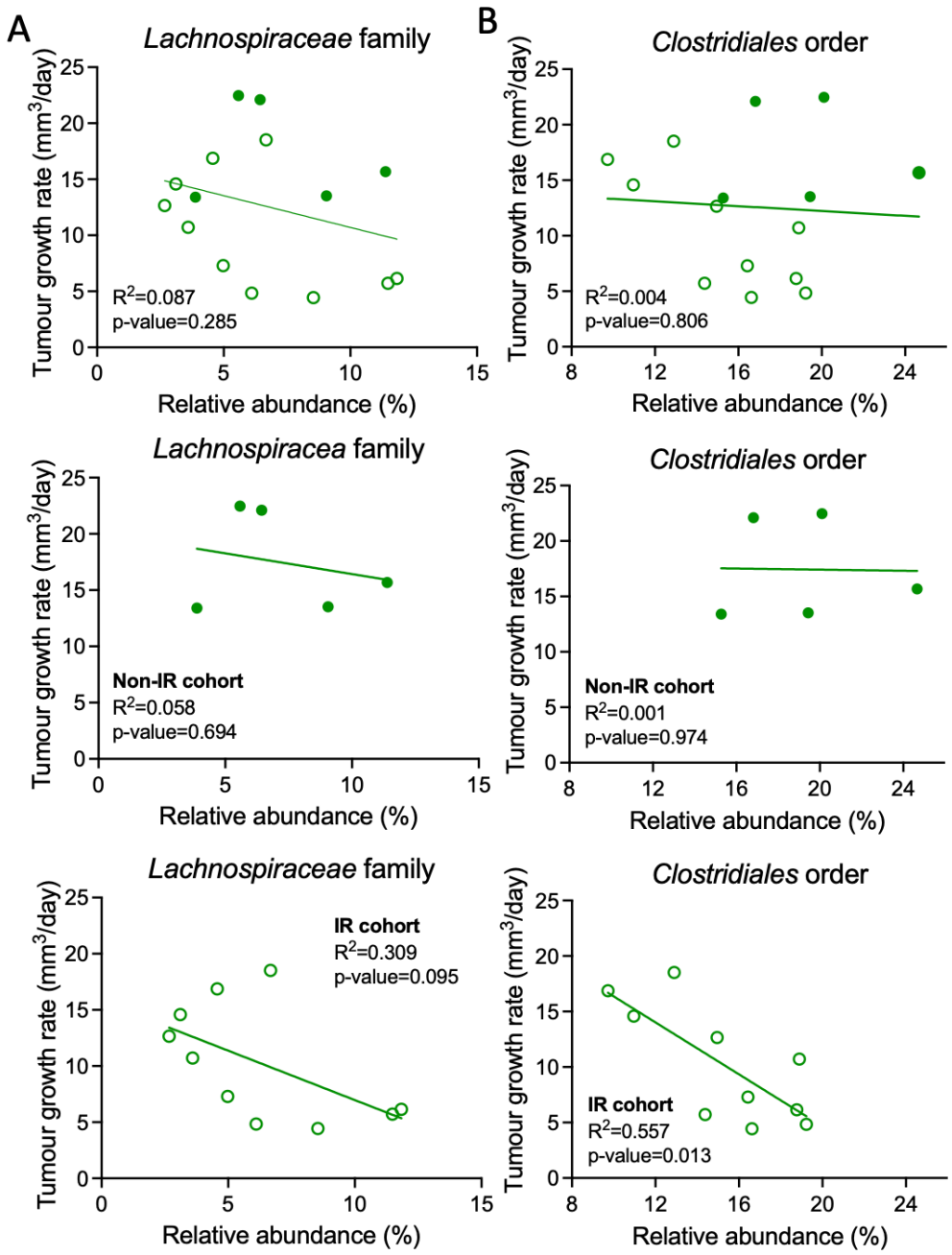


Figure 54 Lachnospiraceae family and Clostridiales order were associated with better tumour control in IR cohort of psyllium plus inulin group. Correlation between the (A) Lachnospiraceae family and (B) Clostridiales order versus the tumour growth in non-IR and IR cohorts of psyllium plus inulin. Tumour curve slopes were calculated by linear regression to represent tumour growth rates.

4.4.9 Untargeted metabolomics analysis

The untargeted metabolomics analysis showed that psyllium-containing diets increase the caecal butyrate levels compared to 0.2% cellulose (P=0.003 for psyllium+RS and =0.010 for psyllium+inulin) (Figure 55A), and it was associated with the tumour control while pooled the IR cohorts from all dietary groups (R^2 = 0.134, P=0.019) (Figure 55B). The caecal butyrate level also negatively correlated to the tumour growth in both non-IR and IR cohort of psyllium plus inulin group (R^2 = 0.325, P=0.041) (Figure 56). In addition to SCFAs, there are eight and three other metabolites significantly positively and negatively correlated with tumour growth (Table 10 and Table A4). The former eight metabolites were associated with taurine metabolism (Figure 57) that has been shown to activate cancer stem cells to drive relapse in hepatocellular carcinoma (Sun *et al.*, 2020) and to be a marker of colorectal cancer (Li *et al.*, 2019). Threitol has the lowest P value, and was associated with improved tumour control in the IR cohort of psyllium plus inulin (R^2 = 0.490, P=0.024) (Figure 58).

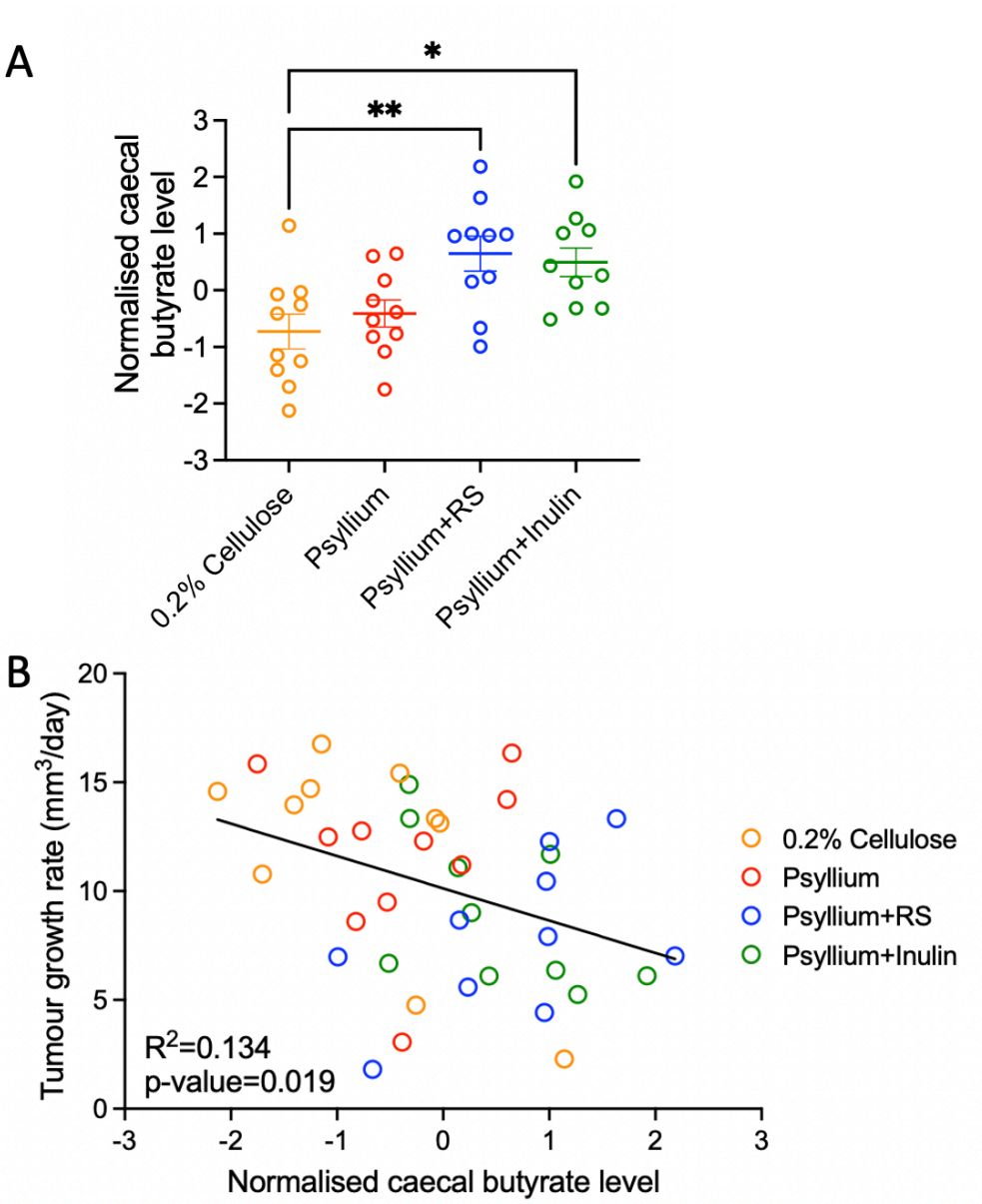


Figure 55 Psyllium plus resistant starch or psyllium plus inulin increased caecal butyrate levels. (A) Normalised caecal butyrate levels in all dietary groups. (B) Correlation between the caecal butyrate level versus the tumour growth while pooled the IR cohorts from all dietary groups (R^2=0.134, P=0.019). Data is mean ± SEM.

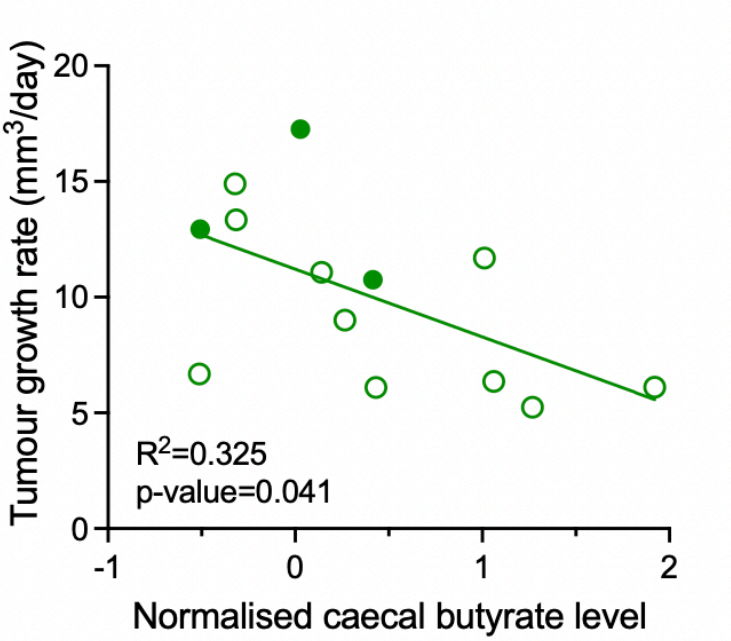


Figure 56 The caecal butyrate level was associated with better tumour control in non-IR and IR cohorts of psyllium plus inulin group. Correlation between the caecal butyrate level versus the tumour growth rate in non-IR (solid symbols) and IR cohorts (open symbols) of psyllium plus inulin (R^2 = 0.325, P=0.041).

Table 10 Metabolites that positively or negatively correlated to tumour growth in psyllium plus inulin.

Compound	Slope	R squared	P value
Hydantoin-5-propionic acid	0.08085	0.7188	0.0019
Cysteic acid	0.1542	0.6755	0.0035
p-Hydroxyphenylacetic acid	0.1593	0.6415	0.0054
Tyramine	0.1332	0.6179	0.007
Proline betaine	0.0572	0.5792	0.0106
Threitol	-0.0611	0.4901	0.0242
Adonitol (ribitol)	-0.0552	0.4637	0.0302
Quinic acid	0.09147	0.4445	0.0353
N-Propionylalanine	-0.05625	0.4114	0.0456
L-Homoserine	0.05477	0.4026	0.0488

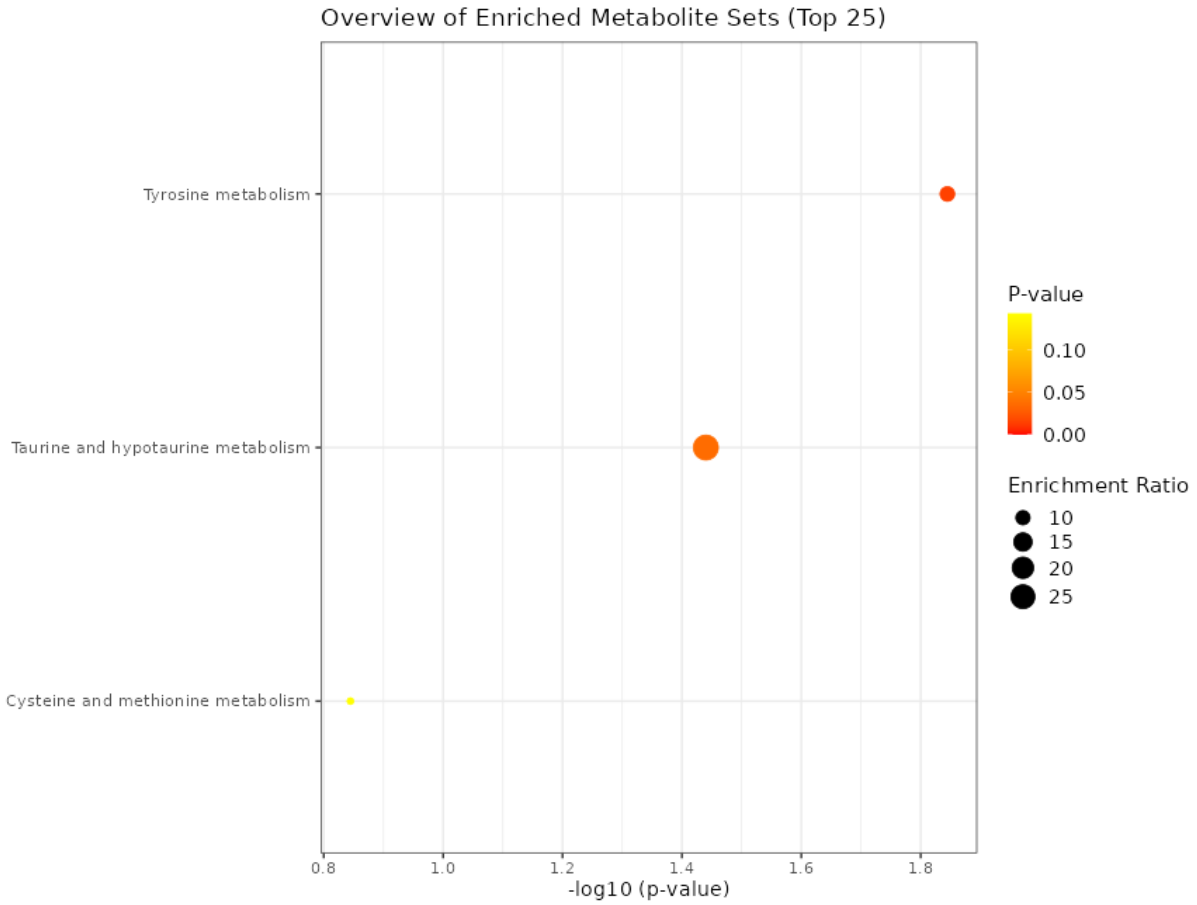


Figure 57 KEGG pathways of metabolites associated with worse tumour control in psyllium plus inulin. KEGG pathways enrichment analysis of metabolites that positively correlated to the tumour growth in psyllium plus inulin. The intensity of colour denotes the P-value and the dot size denotes the enrichment ratio.

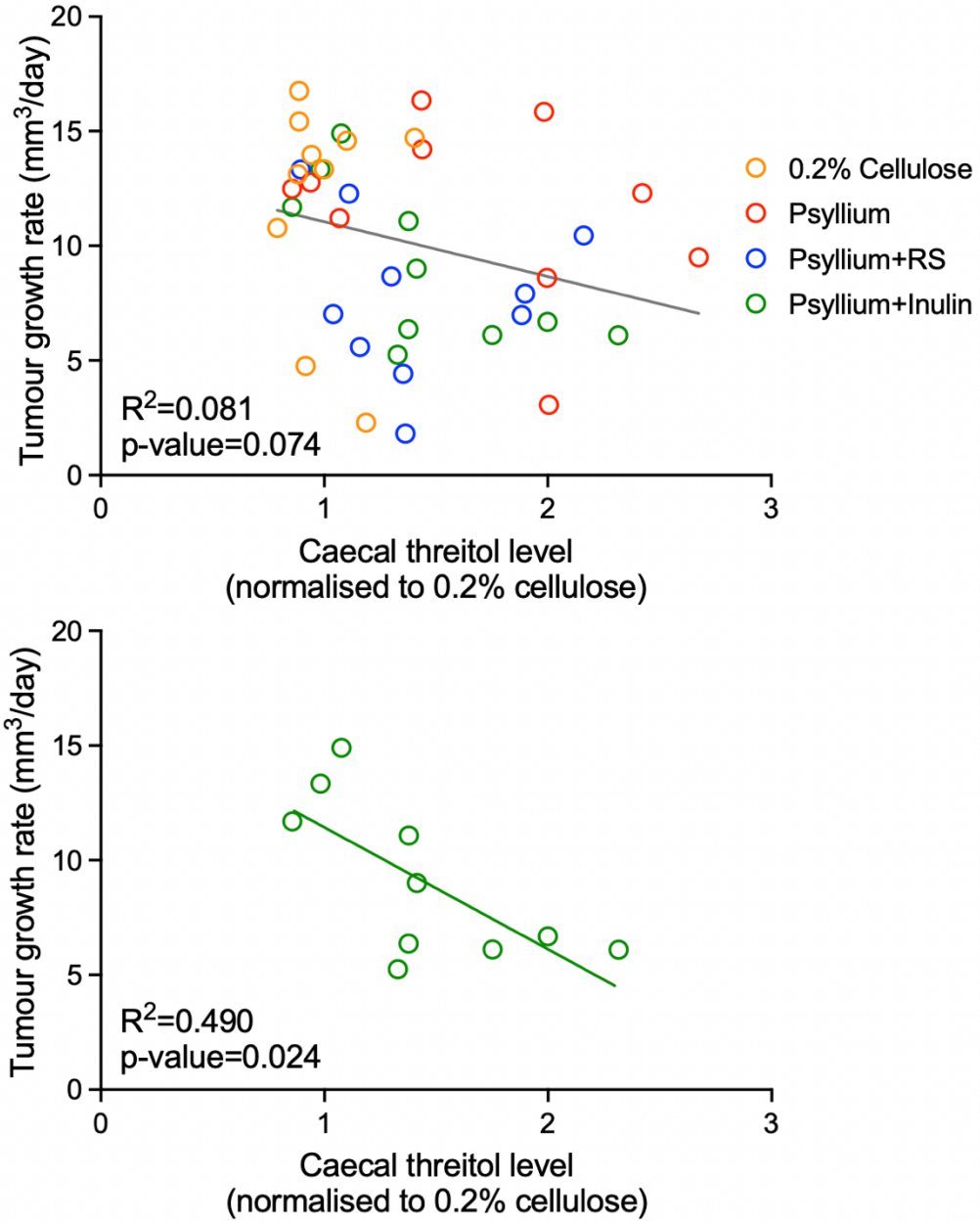


Figure 58 The caecal threitol level was associated with better tumour control in the IR cohort of psyllium plus inulin group. Correlation between the caecal threitol level versus the tumour growth rate in IR cohorts of all dietary groups and psyllium plus inulin only (R^2 = 0.490, P=0.024).

In the caecal metabolomes of psyllium plus resistant starch-treated mice, there are 17 and 2 metabolites significantly positively and negatively correlated to the tumour growth respectively (Table 11 and Table A5). The higher levels of the former 17 metabolites may result in worse tumour control. They were associated with the valine, leucine, isoleucine, glycine, serine and threonine metabolism that have been shown to be important for cancer cell survival and rapid proliferation (Figure 59) (Lieu *et al.*, 2020; Pan *et al.*, 2021; Sheen *et al.*, 2011). The latter two metabolites were N-acetyl-glucosamine-1-phosphate (Figure 60) and isoferulic acid (Figure 61) that were associated with better tumour control in the psyllium plus RS group. It is noted that, compared to 0.2% cellulose, the psyllium plus RS group had a significantly higher level of isoferulic acid (P=0.038; Figure 62) that has been shown to inhibit human leukemic cell growth (Long *et al.*, 2020).

Table 11 Metabolites that positively or negatively correlated to tumour growth in psyllium plus RS.

Compound	Slope	R squared	P value
Deoxyribose	0.05276	0.7083	0.0023
Pyruvic acid	0.05151	0.6562	0.0045
Caffeic acid	0.1056	0.6399	0.0055
Kynurenic acid	0.05434	0.6012	0.0084
Mevalonic acid	0.03273	0.5894	0.0095
Deoxyuridine	0.06813	0.5891	0.0095
3-Methyl-2-oxovaleric acid	0.109	0.5144	0.0196
Glycerol	0.03152	0.4993	0.0223
N-acetyl-glucosamine-1-phosphate	-0.192	0.4949	0.0232
Pantothenic acid	0.1045	0.4947	0.0233
Hydroxypyruvic acid	0.05516	0.481	0.0261
Isoferulic acid	-0.06201	0.4731	0.0279
2-Ketobutyric acid	0.07188	0.4721	0.0281
Pentanal	0.1105	0.4556	0.0322
3-(2,5-Dioxoimidazolidin-4-yl)propanoic acid	0.02649	0.4537	0.0327
Fructose 6-phosphate	0.1004	0.4294	0.0397
4-Acetamidobutanoic acid	0.08238	0.4242	0.0413
Maleic acid	0.08534	0.4236	0.0415
3-[3-(Sulfooxy)phenyl]propanoic acid	0.1006	0.4116	0.0456

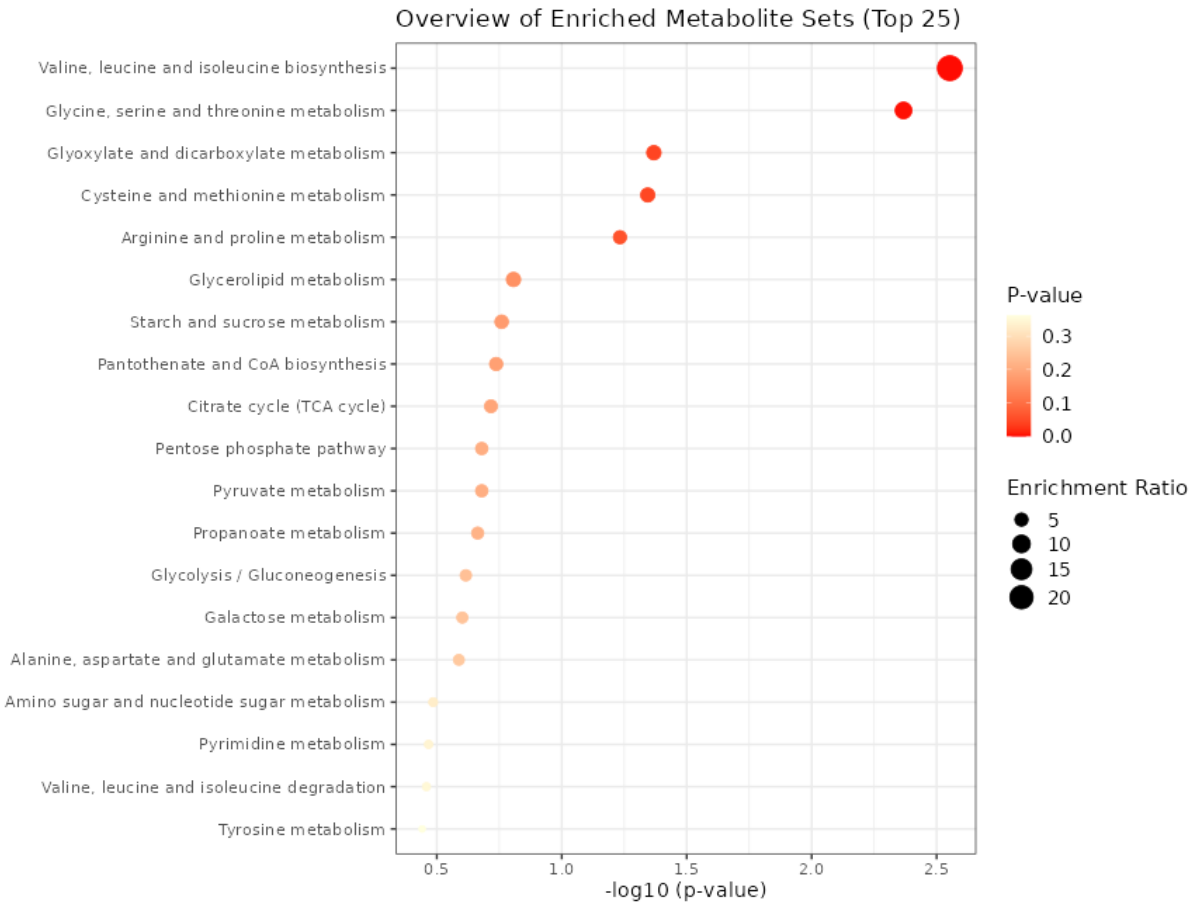


Figure 59 KEGG pathways of metabolites associated with worse tumour control in psyllium plus RS. KEGG pathways enrichment analysis of metabolites that positively correlated to the tumour growth in psyllium plus RS. The intensity of colour denotes the P-value and the dot size denotes the enrichment ratio.

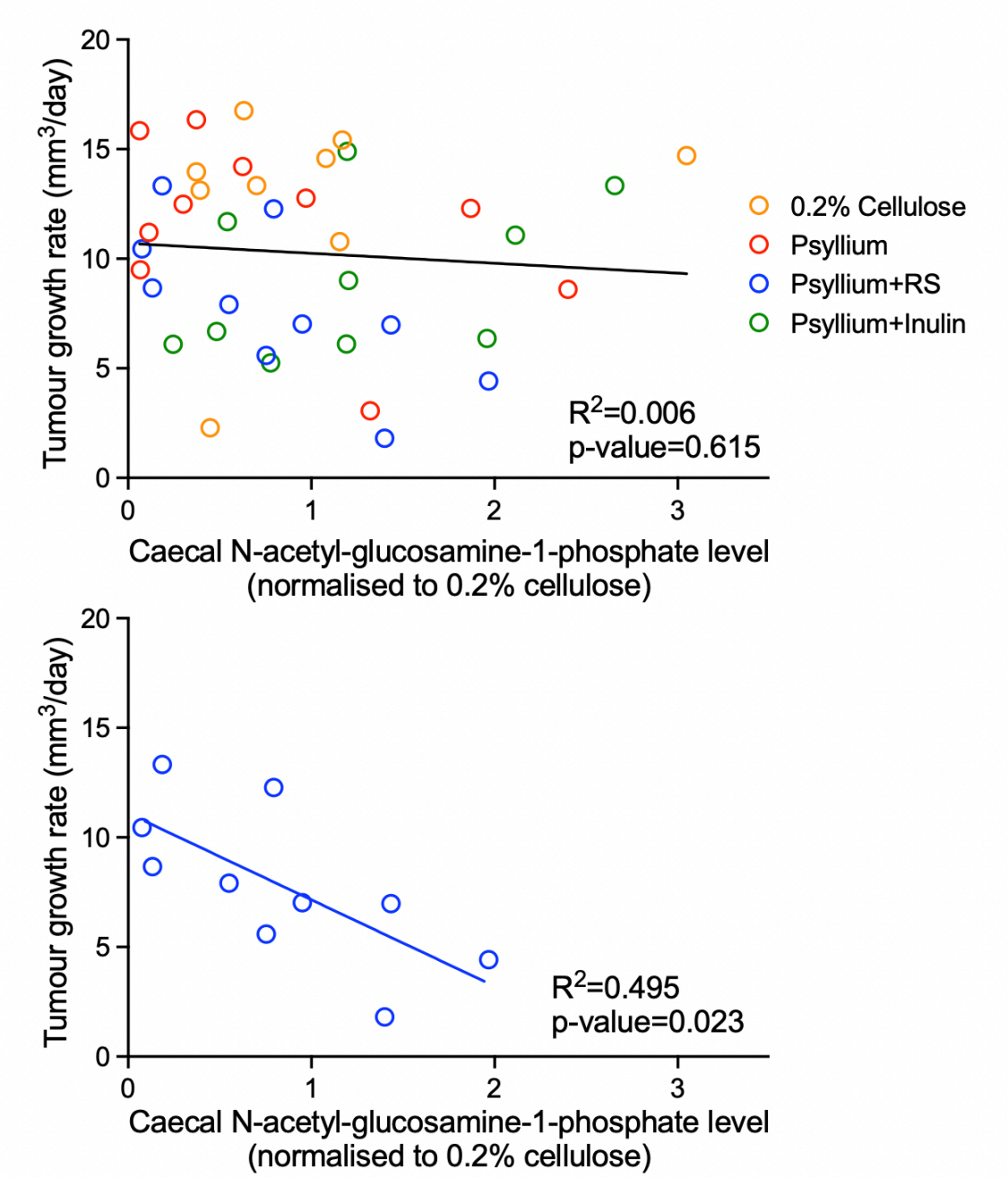


Figure 60 The caecal N-acetyl-glucosamine-1-phosphate level was associated with better tumour control in the IR cohort of psyllium plus resistant starch group. Correlation between the caecal N-acetyl-glucosamine-1-phosphate level versus the tumour growth rate in IR cohorts of all dietary groups and psyllium plus RS only (R^2 = 0.495, P=0.023).

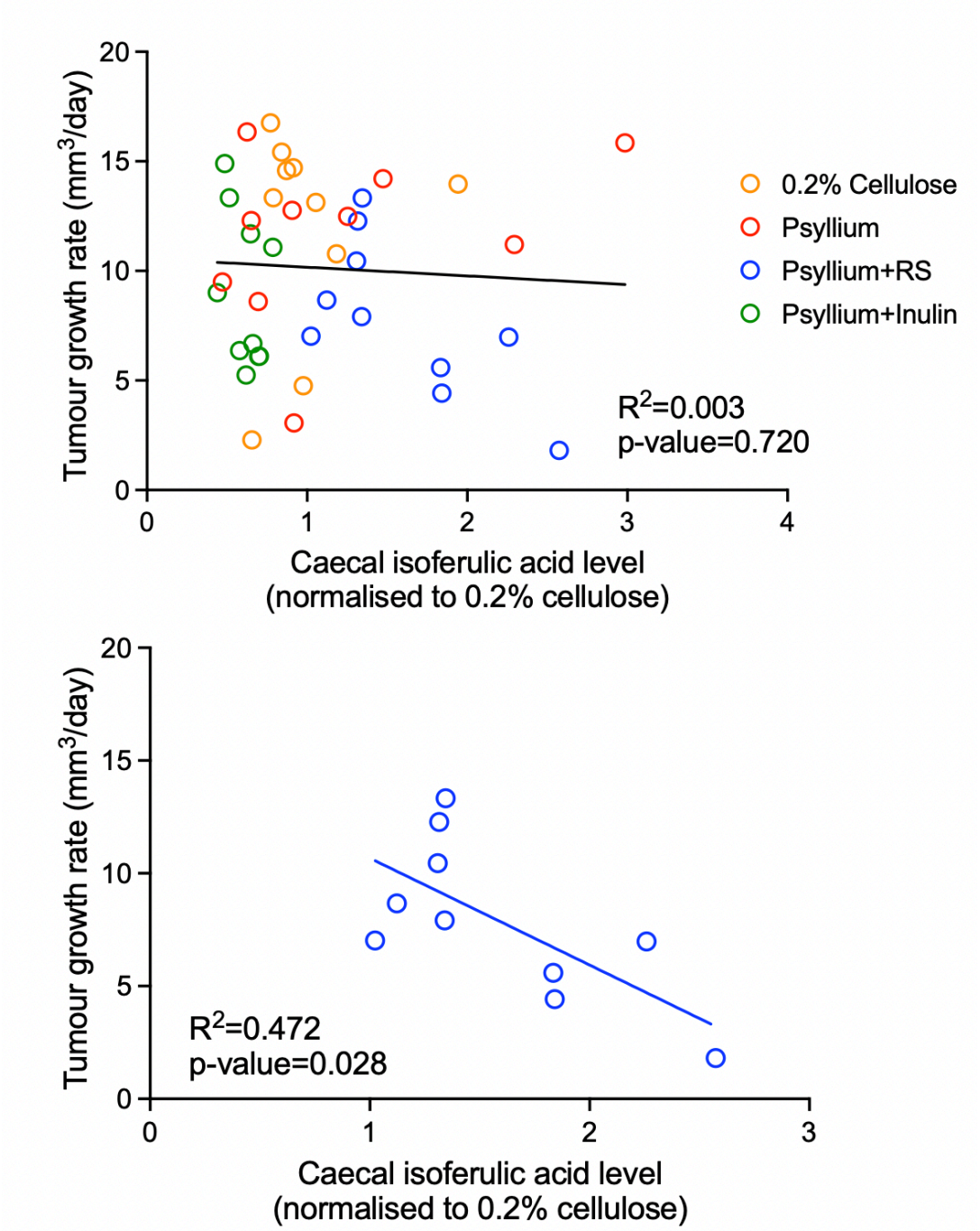


Figure 61 The caecal isoferulic acid level was associated with better tumour control in the IR cohort of psyllium plus resistant starch group. Correlation between the caecal isoferulic acid level versus tumour growth rate in IR cohorts of all dietary groups and psyllium plus inulin only (R^2 = 0.472, P=0.028).

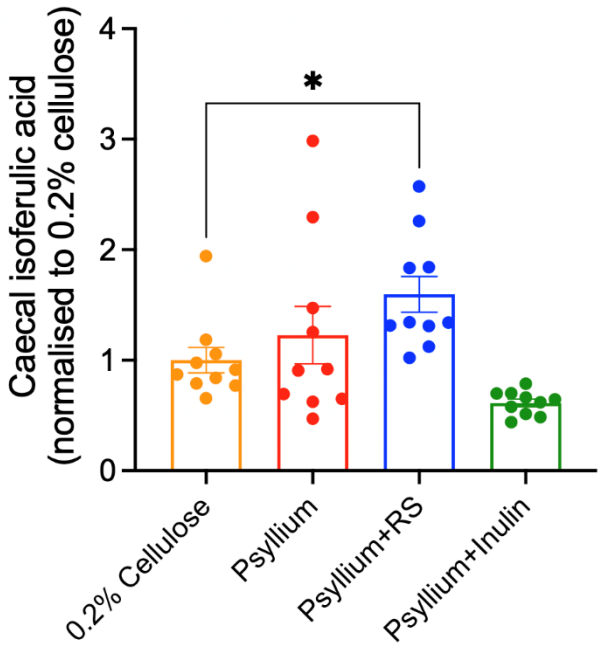


Figure 62 Psyllium plus resistant starch increased caecal isoferulic acid levels. Normalised caecal isoferulic acid levels in all dietary groups. Data is mean ± SEM.

4.5 Discussion

In the IR alone experiment in tumour-bearing mice, I found that 6 Gy was a sufficient radiation dose to achieve significant tumour control and that it was not markedly different to 8 Gy. Although 10 Gy had a stronger tumour control effect, 6 Gy was chosen because too high a radiation dose might mask the effects of a radiosensitiser. In addition, Figure 26 showed that only one out of five reached 400 mm^3 on day 20 in the 10 Gy group, but there were 4 out 5 in the 6 Gy group. Therefore, I did not use 10 Gy as would require longer experiments for the tumours to take off again.

Due to the large cell size of UPPL1591 compared to RT112 under the microscope, I increased the inoculation volume from 100 μL to 200 μL to allow the cells to have enough room to grow. As a 200 μL injection of Matrigel mixture with 50% Matrigel and 50% HBSS would form a visible, relatively large mass on the flank which could be a stress to the mouse, I diluted the HBSS:Matrigel ratio from 1:1 to 2:1. For the first set of experiments of diet (with corn starch) alone in tumour-bearing mice, I used cell mixtures in a HBSS:Matrigel ratio of 2:1 for tumour inoculation. This resulted in very low tumour take rates which made a tumour growth delay study combined with IR unfeasible. In addition, all diets contained corn starch that could potentially be resistant to upper gut digestion and the fermentation of partially indigestible corn starch might still occur in the colon (Achour *et al.*, 1997). A study has shown that corn starch increased faecal butyrate production compared to that of cabbage in rats (Weaver *et al.*, 1992). This increased butyrate generation might suppress the proliferation of cancer cells. Therefore, I used the HBSS:Matrigel ratio of 1:1 to increase the tumour take rate and replaced the corn starch with dextrose to avoid the possible enhancing effect of corn starch on butyrate production.

In the longer diet and IR experiment, the mice still tolerated the modified diets, as they stably maintained their body weight even after IR. It is noted that all psyllium diets significantly increased weight gain compared to 0.2% cellulose which was not seen in the other experiment. This might be due to the larger tumour sizes in the 0.2% cellulose group. In addition, the weight gain can be caused by the bulking effect of psyllium as it increased

the size of the caecum and the length of colon as seen in section 4.2.4 and in another study (Morita *et al.*, 1999).

In terms of tumour control, the second (section 4.2), third (section 4.3) and fourth (section 4.4) sets of experiments showed a consistent result in that psyllium plus inulin had the largest effect compared to 0.2% cellulose, psyllium, and psyllium plus RS. This result was supported by previous studies that inulin delayed tumour growth of breast cancer (Taper & Roberfroid, 1999) and enhanced tumour control combined with irradiation in mouse bladder tumours (Then *et al.*, 2020). In addition, a recent study also showed that inulin overcomes melanoma resistance to MEK inhibitor with increased dendritic cells, helper T and cytotoxic T cells (Li, Elmen*, et al.*, 2020). Altogether, this evidence has demonstrated anti-tumour effects of inulin in cancers outside the intestines, and that it can even enhance the efficacy of anti-cancer treatments. In the IR cohort of the fourth set of experiments, I did find that psyllium plus inulin increased tumour growth delay when combined with irradiation compared to 0.2% cellulose and psyllium. The tumour growth rate significantly negatively correlated with relative abundance of the Clostridiales order which emphasises the importance of gut microbiota modification in enhancing the tumour control.

Metabolites are the functional output of combined host-microorganism interactions. The untargeted metabolomics analysis showed that psyllium plus inulin increased caecal butyrate levels compared to 0.2% cellulose and psyllium. The caecal butyrate level was associated with tumour growth in both the IR and non-IR cohorts of the psyllium plus inulin group. In addition, there was another metabolite, threitol, also negatively correlated with tumour growth in the IR cohort. There are no published studies on the effects of threitol on tumours, but it is noted that threitol is part of the alkylating agent of the chemotherapy drug, Treosulfan (L-threitol- 1,4-bis-methanesulfonate, Ovastat) (Fichtner *et al.*, 2003; Kopf-Maier & Sass, 1996). Therefore, the result shows that gut microbiota modification and the resultant caecal metabolomes may be needed for tumour control seen when combining psyllium plus inulin and irradiation. However, consistent with our RT112 CD-1 nude experiment (Then *et al.*, 2020), SCFA in drinking water was not sufficient to attenuate tumour growth of

melanoma or bladder cancer (Li, Elmen*, et al.*, 2020). This could be due to: (1) short-chain fatty acids cannot act on the tumours as they have a very short half-life and they degrade very quickly after oral intake or (2) there might be a broad range of metabolites that need to work together with SCFAs to achieve tumour control. In our experiments, by using dietary fibre, we may have provided a stable production of SCFAs and other metabolites in the large intestine and the modified gut microbiota might be the key determinant of tumour control.

There are very limited studies about resistant starch and tumour growth outside colorectal cancer. Only one case-control study showed that high intake of resistant starch-containing food was associated with lower risk of breast cancer (Tajaddini *et al.*, 2015). In this thesis, I showed that although psyllium plus RS had a lesser tumour control compared to psyllium plus inulin, it conferred a significantly higher radiosensitising effect. The IR response in psyllium plus RS negatively correlated with unspecified *Bacteroides* species which suggested that the IR response was associated with the gut microbiota. From the non-targeted metabolomic analysis, four out of the top fifteen metabolites enriched in mice fed with psyllium plus resistant starch have previously been shown to have anti-tumourigenic effects. They are caproic acid in skin and cervical cancers (Narayanan *et al.*, 2015), taurine in lung cancer cells (Tu *et al.*, 2018), 5,7-dihydroxyflavone in leukaemia and cervical carcinoma cells (Zhang *et al.*, 2013), and butyrate in breast cancer cells (Salimi *et al.*, 2017). In the section 4.4, there are 17 and 2 metabolites positively and negatively correlated to the tumour growth in the IR cohort of psyllium plus resistant starch group. It is noted that the former 17 metabolites were predominantly associated with the valine, leucine, isoleucine, glycine, serine and threonine metabolism that has been shown to be important for cancer cell survival and rapid proliferation (Figure 58) (Lieu *et al.*, 2020; Pan *et al.*, 2021; Sheen *et al.*, 2011). The latter two metabolites were N-acetyl-glucosamine-1-phosphate (Figure 59) and isoferulic acid (Figure 60) that were associated with better tumour control in the psyllium plus RS group. It is noted that, compared to 0.2% cellulose, the psyllium plus RS group had a significantly higher level of isoferulic acid (P=0.038; Figure 61) that has been shown to inhibit human leukemic cell growth (Long *et al.*, 2020).

Chapter 5: Dietary fibre manipulation spares IR-induced normal tissue toxicities

Radiotherapy given to abdominal and pelvic cancers risks radiation-induced bowel injury, including the small intestine, colon, and rectum, leading to gastrointestinal side effects in most patients. One of the debilitating adverse effects of this treatment is the development of radiation enteritis (inflammation of the small or large intestine) and proctitis (inflammation of rectum). Both have acute (early) and chronic (late) manifestations.

Radiation enteritis refers to damage of the colon and small intestine occurring secondary to radiotherapy (Theis *et al.*, 2010). Acute radiation enteritis is common and occurs within 3 months. Up to 80% of patients receiving abdominal or pelvic radiotherapy experience the side effects of acute radiation-induced intestinal injury in the form of diarrhoea (79%), abdominal cramping (61%), bleeding (41%), incontinence (40%), and tenesmus (33%) (Hauer-Jensen *et al.*, 2014; Kozelsky *et al.*, 2003). The symptoms in most patients are usually self-limited and resolve within weeks of radiation therapy stopping. However, chronic radiation enteritis is a relentlessly progressive disease and develops after three months post-radiotherapy and lasts for months or even decades. Chronic intestinal radiation injury is a result of transmural damage of intestinal wall, leading to atrophy of the mucosa, fibrosis of the intestinal wall and microvascular sclerosis (Hauer-Jensen *et al.*, 2014).

Treatment of radiation intestinal toxicity is challenging. Diet modification and nutritional support play a very important role in relieving the symptoms. Administration of biotics can enhance production of key metabolites, particularly SCFAs, and butyrate reduces mucosal inflammation and promotes epithelial repair following injury in prostate cancer patients receiving RT (Hille *et al.*, 2008). A clinical study also showed that short-chain fatty acid enemas, containing acetate, propionate, and butyrate, decreased the rectal bleeding and accelerated the healing process in chronic radiation proctitis (Pinto *et al.*, 1999). In addition, gut commensal derived-valeric acid prevented radiation-induced intestinal inflammation and dysfunction, as indicated by colonic lengthening and increasing goblet cells in mice receiving

total abdominal irradiation (Li, Dong*, et al.*, 2020). Dietary supplements have been shown to be effective for relieving diarrhoea in our systematic review of clinical studies (Bartsch *et al.*, 2021).

There is always a clinical need to decrease normal tissue side effects and to increase tumour control in order to acheive a favourable radiotherapy therapeutic ratio. With the evidence of the benefits of SCFA in relieving radiation-induced symptoms, I wished to investigate whether dietary fibre could also achieve a favourable therapeutic ratio via its modified gut microbiota and metabolites by enhancing tumour cell kill by irradiation (Chapter 4) whilst sparing normal intestinal tissue toxicity (Chapter 5). To investigate this, I fed two cohorts of non-tumour bearing C57BL/6 mice modified diets for two weeks and irradiated their urinary bladder covering part of the intestine (Table 12). I then sacrificed the mice at 3.75 days and 24 weeks after IR to assess acute and late normal tissue toxicities.

Table 12 Overview of the study and sample sizes.

	Sample collected at	Diets		Radiation dose and sample size
1.	3.75 days after IR (N=84)	Dextrose	0.2% Cellulose Psyllium Psyllium+RS Psyllium+inulin	0 Gy (n=3/group) 10 Gy (n=6/group) 12 Gy (n=6/group) 14 Gy (n=6/group)
2.	24 weeks after IR (N=40)	Dextrose	0.2% Cellulose Psyllium Psyllium+RS Psyllium+inulin	0 Gy (n=5/group) 5 x 5 Gy (n=5/group)

In the acute toxicity experiment, the radiation was focused on the bladder and surrounding bowel to better mimic the human patient situation. Mice were treated supine with 10, 12 or 14 Gy of x-rays to the lower abdomen, including the lower small intestine using a Small Animal Radiation Research Platform (SARRP) irradiator (Xstrahl Ltd, Camberley, UK). Irradiation was delivered using a 356-degree arc treatment with a 13.7-mm circular collimator (at isocentre) at a dose rate of approximately 2 Gy per minute. Ten to 14 Gy irradiation was chosen because two previous studies of our laboratory showed that 10-14 Gy

caused crypt loss with 50% to 95% of crypts remaining 3.75 days after irradiation (Groselj *et al.*, 2013; Paillas *et al.*, 2020). The percentage mouse mortality raised from 40% to 80% when the mice received a total body irradiation dose of 14 Gy and 15 Gy, respectively, at day 20 (Booth *et al.*, 2012). Mice receiving 14 Gy showed denudation of the intestinal crypt and villus system but had only partially damaged marrow and at 15 Gy 25% of mice succumbed to death from the GI syndrome and 75% died of marrow failure. Therefore, I chose not to go up to 15 Gy or above.

For the late toxicity experiment, mice were treated using a SARRP with 5 Gy for 5 consecutive days, using a 356-degree arc treatment and 8.5-mm collimator, with the isocentre positioned at the posterior caudal bladder wall covering lower large intestine, to avoid the small intestine. I did not irradiate any small intestine at such high doses as this could be fatal (Vriesendorp *et al.*, 1992). The radiation was focused on the bladder and surrounding bowel to better mimic the human patient situation. I treated the mice head down to avoid irradiating their small intestine which is similar with the setting from previous studies encompassing the colorectum (Bull *et al.*, 2017; Malipatlolla *et al.*, 2019). In those studies, the radiation field was 3 × 3 cm^2, with the lower quadrant of the field placed to irradiate ~1.5 cm of the distal colon, avoiding the spinal cord and the testicles as much as possible to prevent dysmotility and hormonal interference.

Previous studies have investigated the acute and late histology of intestinal injury in mice and humans. In a mouse model treated with total body irradiation (TBI) to 0, 4, 8 and 12 Gy, the intestinal injuries were manifested in a radiation dose-dependent manner (Zhao *et al.*, 2021). For late effects, Malipatlolla *et al.* showed that mice irradiated to a small volume encompassing the colorectum with four fractions of 8 Gy per fraction had significant crypt loss from 6 weeks until 30 weeks post irradiation (Malipatlolla *et al.*, 2019).

To assess the histological changes of radiation-induced intestinal injury, the whole small intestine was made into a ‘Swiss roll’ which allows an overview of the whole intestine on one tissue slide, with the intestinal villi and the epithelial lining remain intact (Moolenbeek & Ruitenberg, 1981). Therefore, unlike the classical crypt assay where the whole abdomen of

the mouse is irradiated, our laboratory developed a modified crypt assay with some of the intestine is present at the radiation field edge, and therefore only receives 50% of the radiation dose.

Crypts contain the intestinal stem cells which intensively proliferate to renew the single-layer columnar epithelium of the small intestine. These intestinal stem cells are particularly sensitive to radiation damage because rapidly dividing cells are vulnerable and targeted by radiotherapy and chemotherapy. Our laboratory developed stringent criteria for assessment: each crypt had to contain >10 cells, have a distinct shape and boundary, no signs of apoptosis, and determined in regions with intact serosa, allowing a more objective method of assessing acute normal tissue toxicity in partially-irradiated intestine. This refined assay showed a log-linear dose response, consistent with previous studies (Hagemann *et al.*, 1971).

Since the bladder received high dose radiation of 5 x 5 Gy IR, I also evaluated its function by using a void spot assay, because the mice may experience lower urinary tract symptoms such as storage, voiding, and/or discharge after irradiation. This a simple, reproducible, non-invasive, and quantitative measure of spontaneous voiding function in mice (Yu *et al.*, 2014). A previous study showed that this assay detects abnormalities of voiding within a strain, whether caused by environment (induced diuresis), genetic mutation or aging.

5.1 Acute intestinal toxicity after IR

5.1.1 Overview

To determine whether dietary fibre supplementation can spare acute intestinal toxicity caused by radiation, I fed mice with 0.2% cellulose, 5% psyllium, 5% psyllium plus 10% RS and 5% psyllium plus 10% inulin for two weeks (Figure 63A). After that, I irradiated their lower abdomen, centred on the urinary bladder, and covering part of the small and large intestines, with 10, 12 and 14 Gy on SARRP platform using a 356-degree arc treatment with a 13.7-mm circular collimator at a dose rate (at isocentre) of 2 Gy per minute (Figure 63B). Faeces were collected one day before and two days after irradiation to study the baseline gut microbiota and its modification by the diets and any influence of ionising radiation. Mice were culled 3.75 days after IR, and the small intestine was made into Swiss rolls for the crypt assay and local gut immunity analysis. Spleens were used to investigate systemic immunity (Chapter 6). Caecal contents were collected for untargeted metabolomics analysis. Mice were sacrificed, and the tissues collected at 3.75 days after IR.

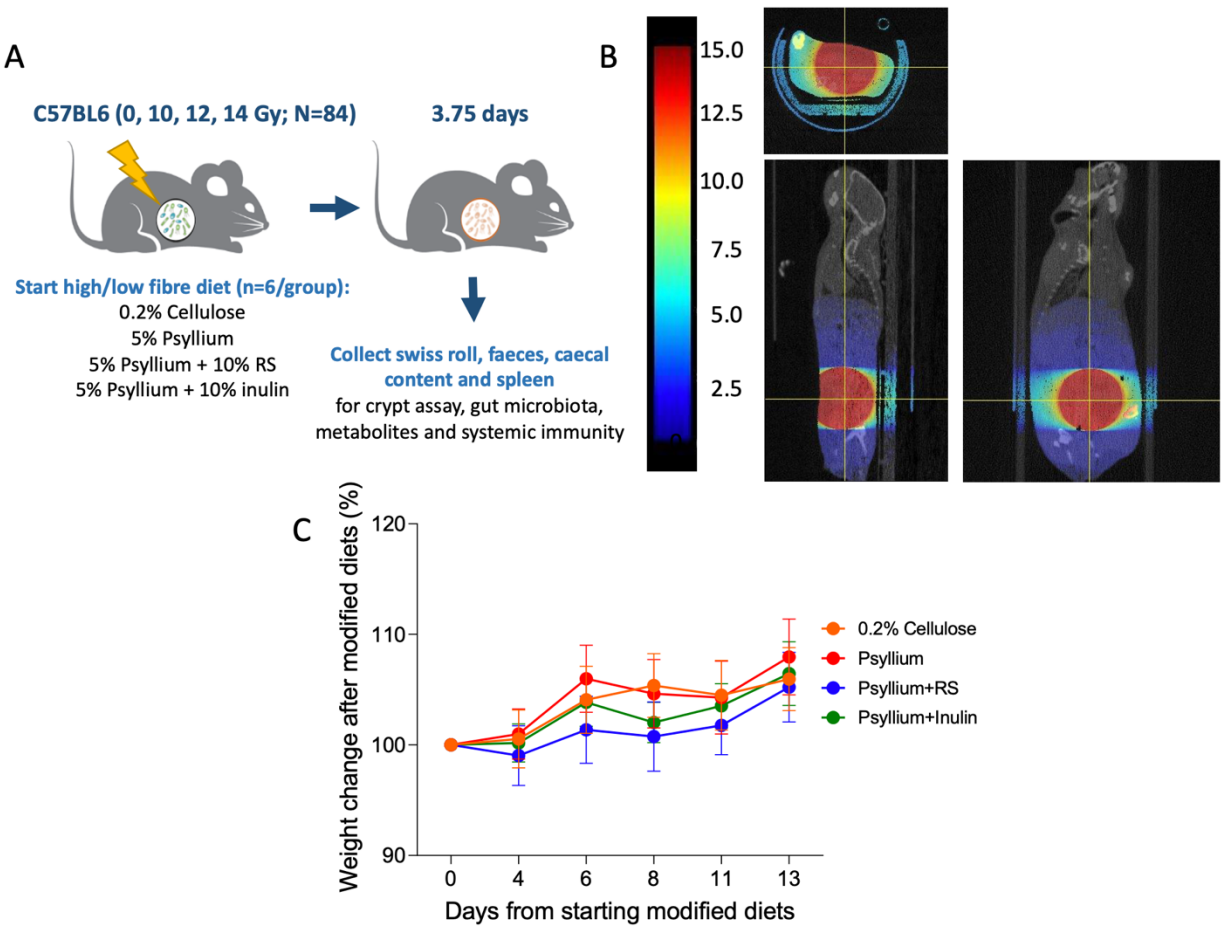


Figure 63 Overview of acute normal tissue toxicity experiment. (A) Two weeks after starting low or high fibre diets, C57BL/6 mice were treated supine with (B) 10-14 Gy SARRP IR to their lower abdomen (n=21/group). Tissues were collected 3.75 days after IR to assess the acute normal tissue responses. (C) The body weight change of non-tumour-bearing mice under modified diets across the whole experiment. Error bars represent the standard error.

5.1.2 The remaining crypts in small intestine and the length of large intestine after IR

I applied our modified crypt assay to investigate whether there was a protective effect conferred by the dietary fibre. Figure 64A showed that there was no difference among the different dietary groups when the mice received 10 and 12 Gy IR, but psyllium plus resistant starch (P=0.087) and psyllium plus inulin (P=0.007) increased the number of crypts remaining in mice receiving the higher 14 Gy dose of IR (Figure 64B and C).

The large intestine tended to be shorter in both the 0.2% cellulose and psyllium groups compared to psyllium plus RS and psyllium plus inulin groups regardless of whether the mice received IR or not. This implied that psyllium plus RS and psyllium plus inulin may prevent the large intestine shortening caused by lack of fermentable fibre in the diets.

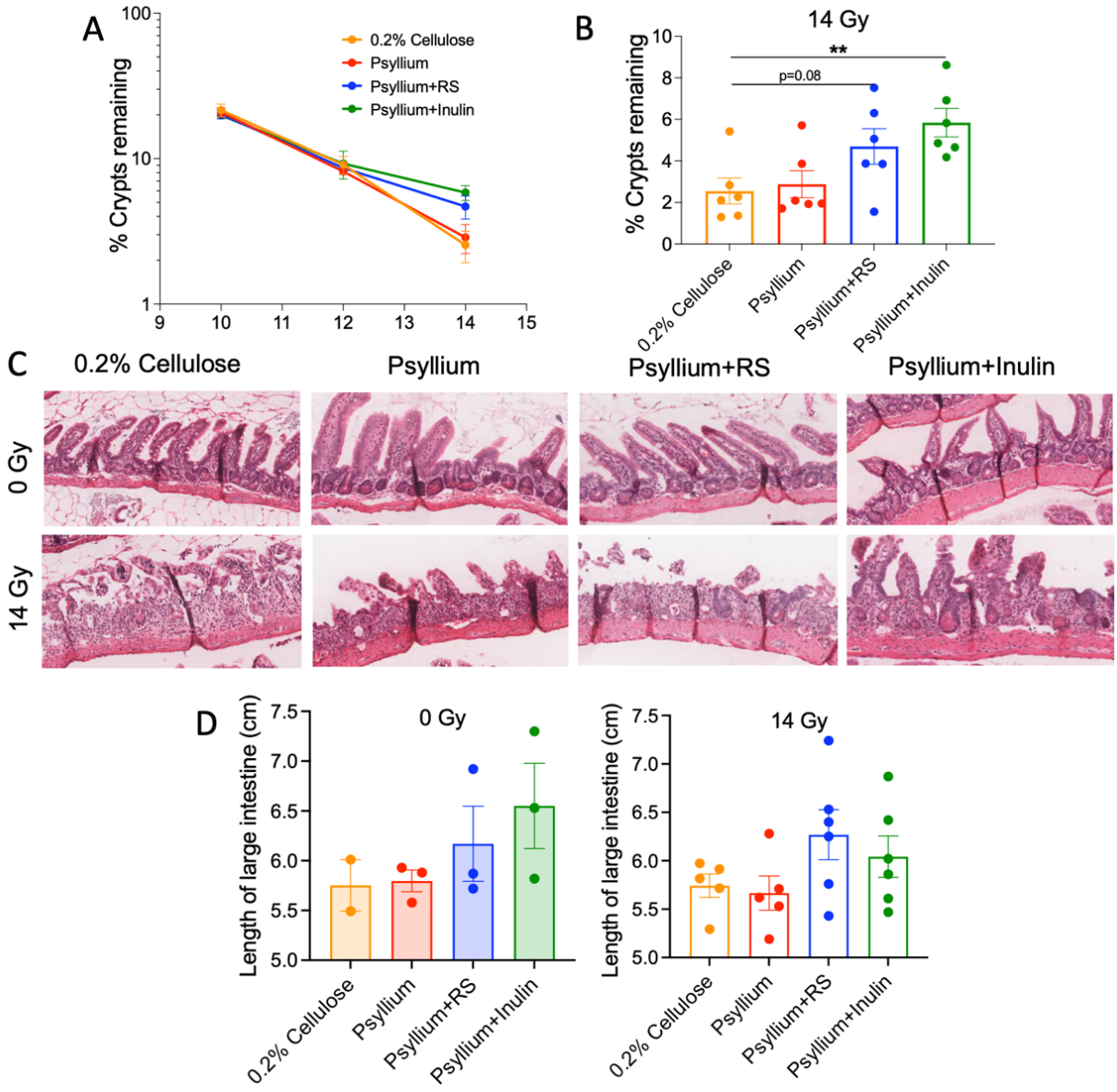


Figure 64 Psyllium plus RS or psyllium plus inulin mitigated the radiation injury from 14 Gy in intestinal crypt assays. (A & B) Small intestinal crypt assay survival for modified diets and IR (n=6 per group, except for 0 Gy IR: n=3). Data were normalised to mean crypts per mm of three mock samples. (C) Haematoxylin and eosin-stained sections of small intestinal Swiss rolls demonstrating crypt loss and regenerating crypts after 14 Gy IR. (D) The length of large intestine of non-tumour-bearing mice under 3-week modified diet with or without IR. All error bars represent ± standard error of the mean.

5.1.3 Body weight change after 2-week modified diets and after IR

A high fibre diet might not be tolerated by mice which may cause weight lost. Figure 65A showed the weight changes 3.75 days after three doses of IR in all dietary groups. Although weight loss was observed in all mice receiving radiation doses of 10, 12 and 14 Gy, there was no significant difference among the different diet groups. Figure 65B presented the weight changes of each dietary group within the 3.75 days after IR. Irradiated mice in the 0.2% cellulose group experienced significantly less weight gain compared to their non-IR control. This was seen in the psyllium plus inulin group only at one day after IR, but not in the psyllium or psyllium plus RS groups.

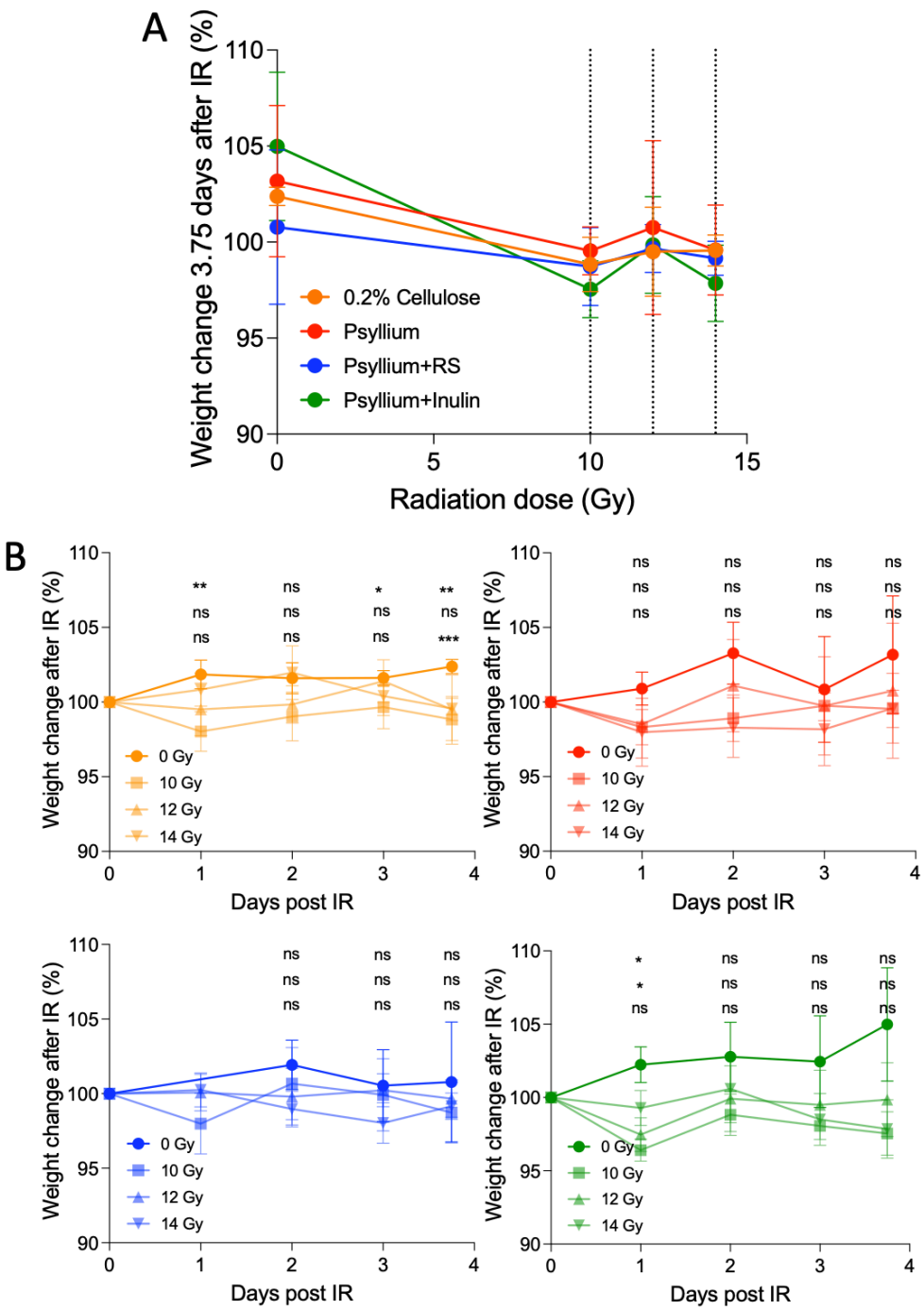


Figure 65 Body weight change 3.75 days after SARRP IR. (A) Overall comparison of body weight change of mice fed among different modified diets with or without IR at 3.75 days after IR. (B) Individual body weight changes of IR mice compared to their non-IR cohort in each dietary group within 3.75 days after IR. Two-way ANOVA tests were conducted for comparing IR cohort to non-IR cohort.

5.1.4 The gut microbiota of non-tumour bearing mice fed with low and high dietary fibre with or without IR

Figure 66 shows the gut microbiota profiles from mice fed with low and high fibre diets. The legends for the top 20 taxa with the highest abundances were shown in Table A10-A13. S24-7 family, unspecified Clostridiales species, *B. animalis, B. acidifaciens* and *Bacteroides* unspecified species were within the top 10 bacteria with the largest abundance. The relative abundance of *B. acidifaciens* was about 5-10% in all psyllium diets groups and it was higher, up to 20-30%, in the psyllium and psyllium plus inulin groups. These two high fibre groups had a significantly lower alpha diversity, due to the overriding abundance of *B. acidifaciens* (Figure 67). The alpha diversity slightly dropped after IR in the 0.2% cellulose and psyllium plus inulin groups. The phylogenetic composition showed that 0.2% cellulose had a more diverse gut microbiota and high fibre diets groups were overridden with several bacteria. The clustering effects of gut microbiota by diets suggests that dietary fibre can shape the gut microbiota from a diverse one to one where several gut bacteria predominate.

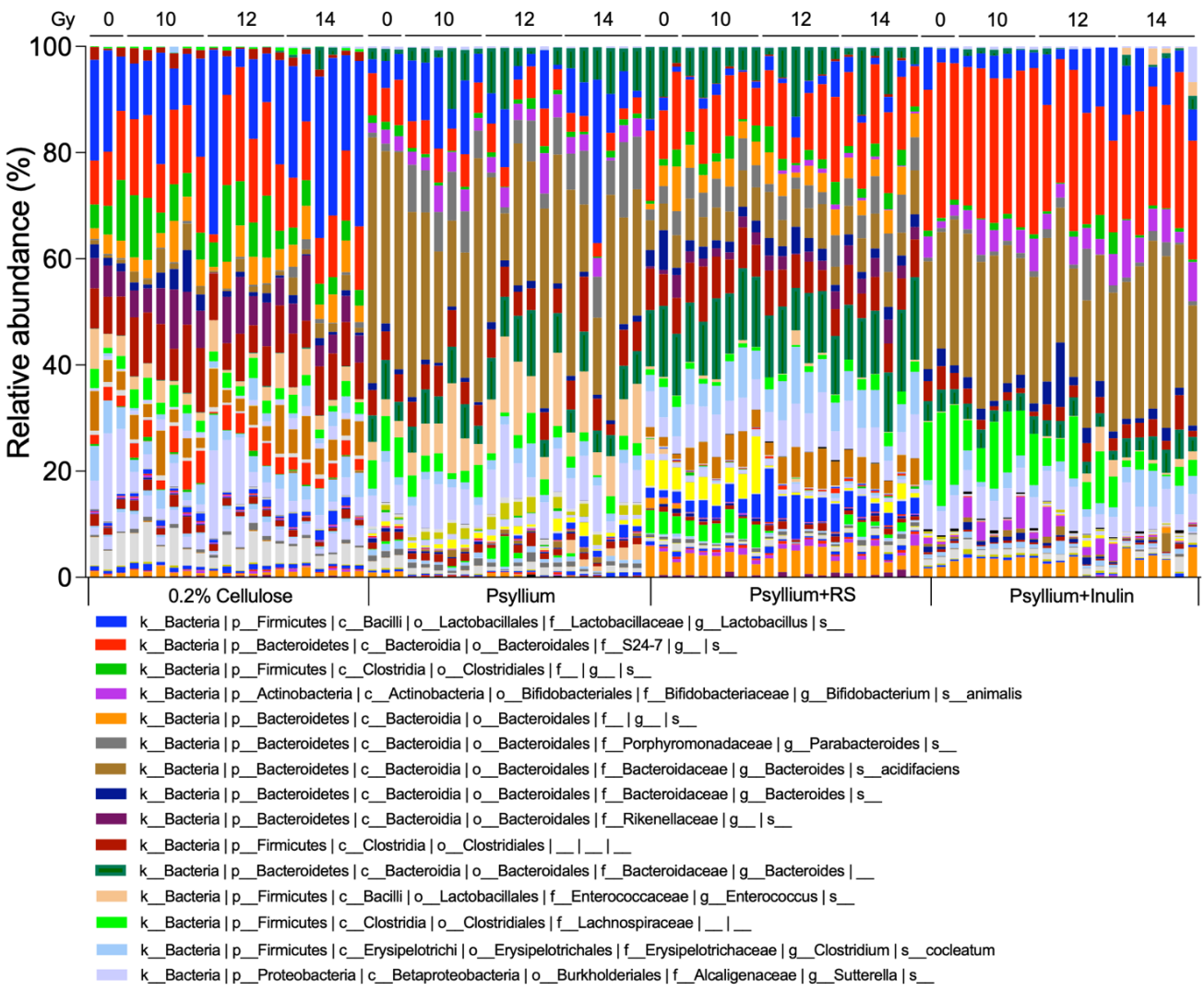


Figure 66 Phylogenetic composition of faecal microbiota a at the species level. Faecal samples were collected 3.75 days post IR (n=3/non-IR cohort, n=6/IR cohort in each IR doses and dietary group).

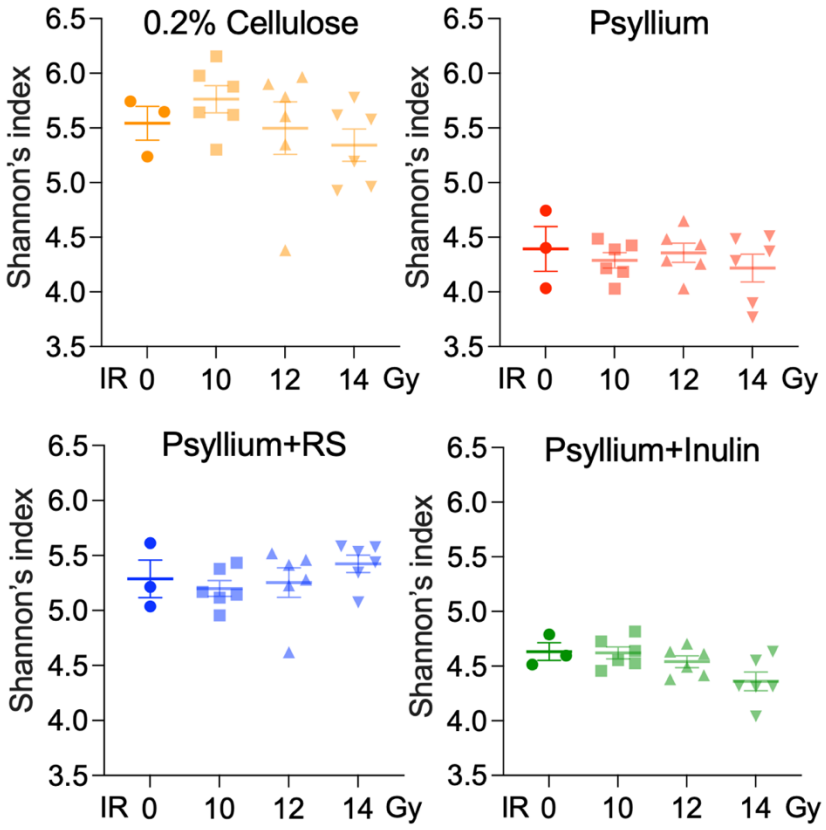


Figure 67 Alpha diversity of gut microbiota in non-tumour-bearing mice 3.75 days after SARRP IR. Alpha diversity using Shannon index of faecal microbiotas. One-way ANOVA with Dunnett's multiple comparison test was used to compare the means of different dietary groups. Error bars represent the standard error.

5.1.5 Beta diversity of gut microbiota in non-tumour-bearing mice 3.75 days after SARRP IR

In terms of beta diversity, principal coordinate analysis showed a notable cluster effect among the gut microbiota for all psyllium diets groups, especially psyllium plus RS which was the most different from 0.2% cellulose (Figure 68A). There was also higher similarity between psyllium and psyllium plus inulin and this trend was different from the previous experiments in tumour-bearing mice, where psyllium and psyllium plus RS were closer together.

Figure 68B shows the distances (from a dietary group to another) of gut microbiota in mice receiving different doses of SARRP IR within the same dietary group. I found that the higher the dose of IR, the larger the distance of gut microbiota compared with the non-IR (0 Gy) controls. All radiation doses significantly changed the gut microbiota in 0.2% cellulose ($P=0.018$, 0.003 and < 0.001), while for psyllium plus RS ($P=0.012$ for 12 Gy) or psyllium plus inulin ($P=0.010$ and < 0.001 for 12 and 14 Gy) only 12 Gy and 14 Gy caused changes.

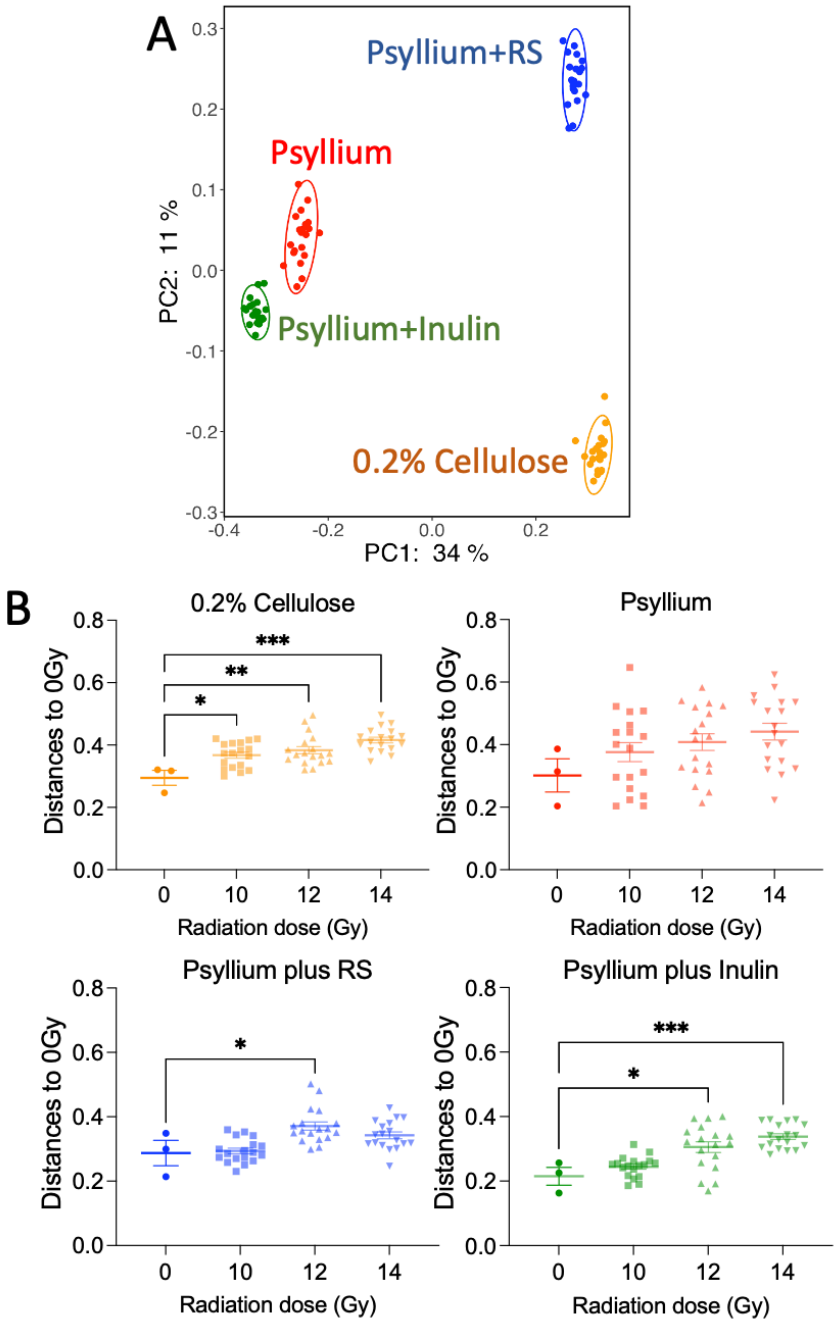


Figure 68 Beta diversity of gut microbiota in non-tumour-bearing mice 3.75 days after SARRP IR. (A) Principal coordinate analysis of faecal microbiota using Bray-Curtis dissimilarity. A notable clustering effect by diets was seen in the gut microbiota. (B) Distances of gut microbiota in mice compared to non-IR controls in each dietary groups using PERMANOVA.

5.1.6 Untargeted metabolomics profiling and SCFA levels of caecal contents

One of the major physiological functions of the gut microbiota is secretion of metabolites. I collected caecal contents at the end of experiment for the untargeted metabolomics analysis. The Partial Least-Squares Discriminant Analysis showed that psyllium and psyllium plus RS had more similar metabolomics profiles relative to psyllium plus inulin (Figure 69A) which was different from the trend of the gut microbiota profiles in Figure 37B. In addition, I saw that IR changed the metabolomic profiles, as the higher the IR dose, the more different the metabolomic profile compared to non-IR controls.

All psyllium diets significantly increased the caecal SCFA levels (normalised by median) after three-weeks of modified diet (Figure 69B). Psyllium significantly raised the acetate ($P<0.001$) and propionate ($P=0.002$) levels, and psyllium plus RS increased acetate ($P<0.001$ and $= 0.003$) and butyrate levels. Psyllium plus inulin resulted in the highest levels of acetate, propionate and butyrate among all dietary groups and the p-values were < 0.001 for all three SCFAs compared to 0.2% cellulose.

Figure 70 showed that psyllium plus inulin was enriched for metabolism of butyrate and pentose phosphate, and arginine biosynthesis. Metabolites enriched in psyllium plus resistant starch were associated with the metabolism of tryptophan, pentose phosphate, alanine, aspartate, and glutamate (Figure 71).

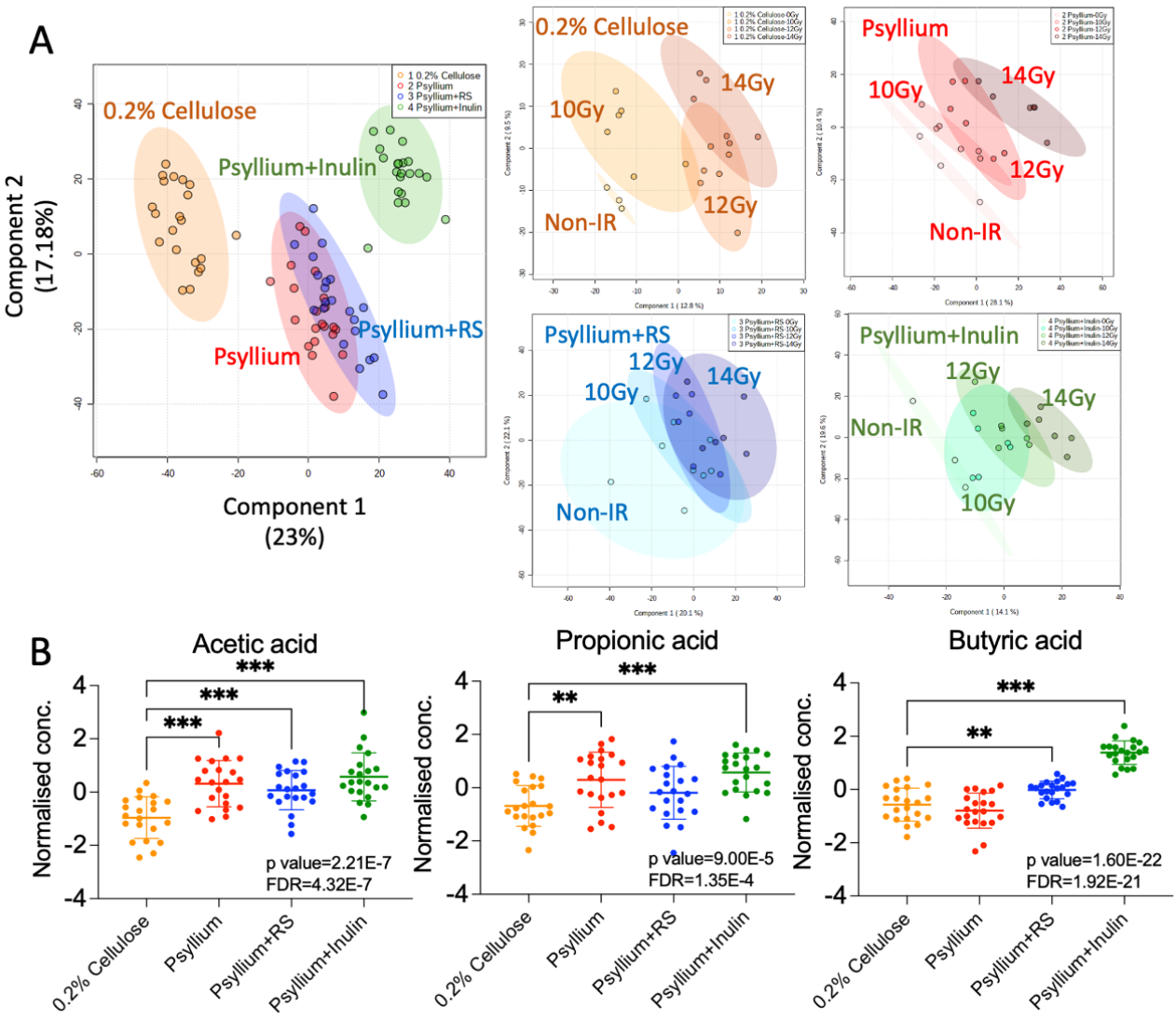


Figure 69 Untargeted metabolomics analysis of gut microbiota and caecal SCFAs in non-tumour-bearing mice after 3-week modified diet. (A) Principal coordinate analysis of gut microbiota in all and each dietary groups showing the higher the radiation dose, the more different the profiles compared to non-IR controls. The intensity of colour reflects the IR dose. (B) Relative levels of acetate, propionate, and butyrate in each dietary group pooling the mice from all IR doses.

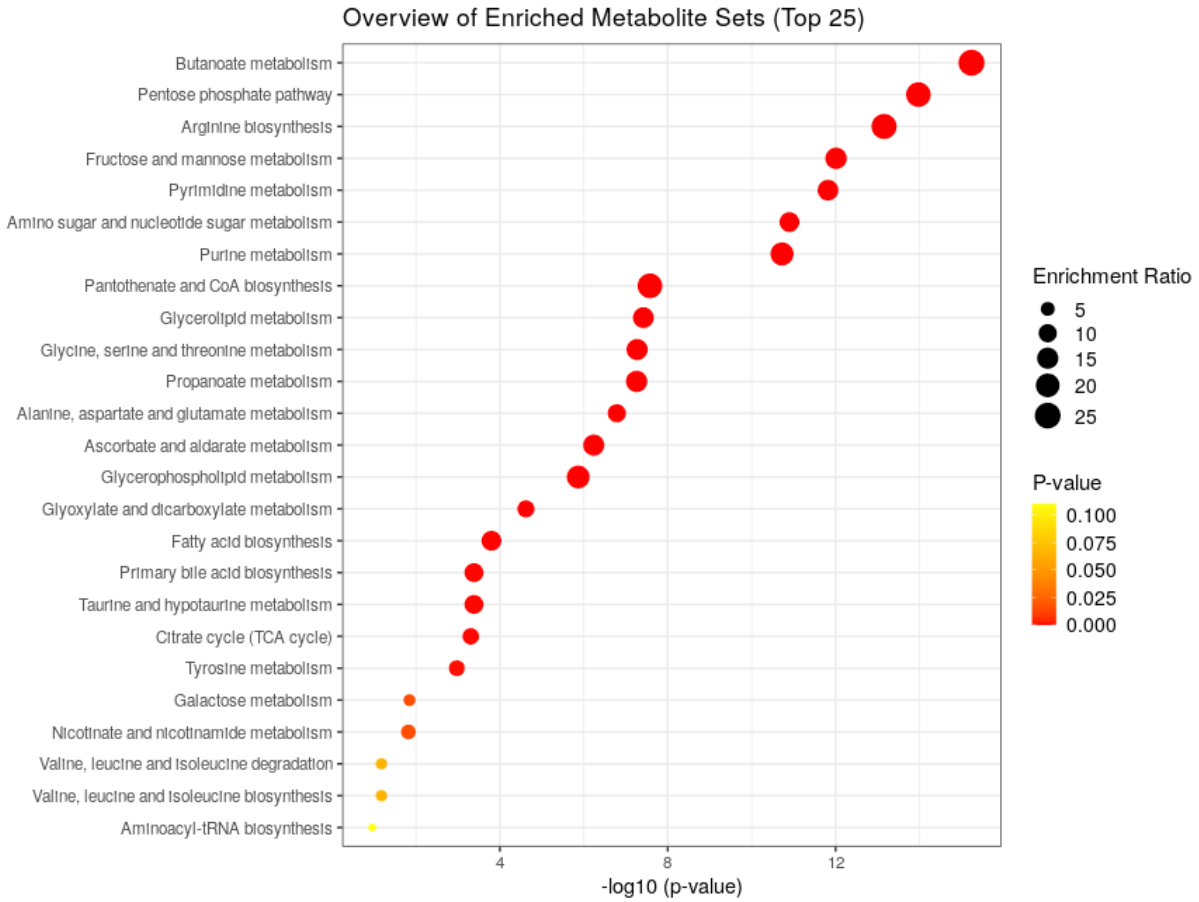


Figure 70 KEGG pathways enriched in psyllium plus inulin. KEGG pathways enrichment analysis of metabolites enriched in psyllium plus inulin compared to psyllium. The intensity of colour denotes the P-value and the dot size denotes the enrichment ratio.

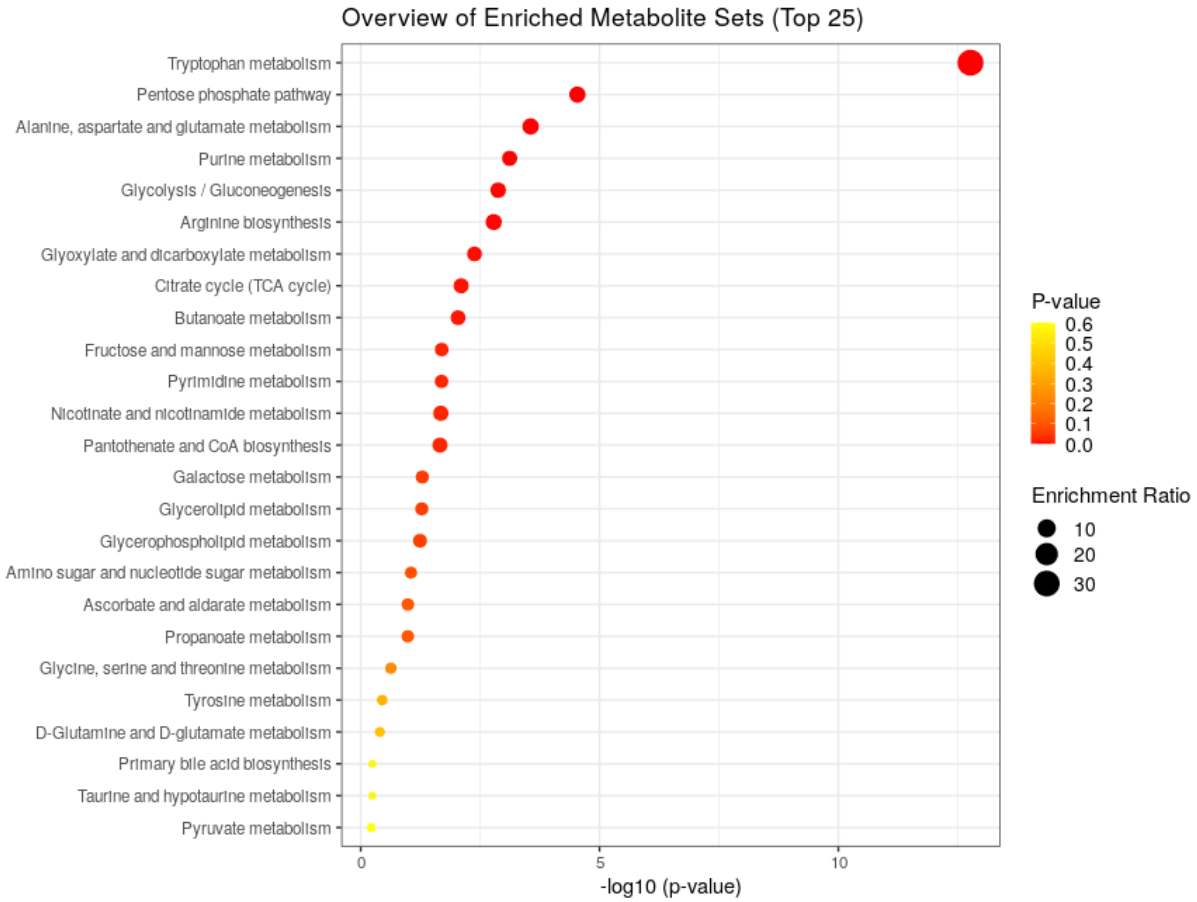


Figure 71 KEGG pathways enriched in psyllium plus resistant starch. KEGG pathways enrichment analysis of metabolites enriched in psyllium plus RS compared to psyllium. The intensity of colour denotes the P-value and the dot size denotes the enrichment ratio.

5.2 Late intestinal toxicity after IR

5.2.1 Overview

Patients may develop long-term side effects 3 months after receiving pelvic RT. To validate whether dietary fibre and the gut microbiota can protect the intestine from late radiation-induced injury, I performed an experiment irradiating the mice with 5 x 5Gy IR to the lower abdomen, including their urinary bladder and the lower part of the large intestine, avoiding the small intestine by treating the mice supine and head down, using a 356-degree arc treatment and 8.5-mm collimator. The mice would be followed up to 22 weeks (Figure 72). The stool and urine analyses were performed 7, 12 and 17 weeks after IR.

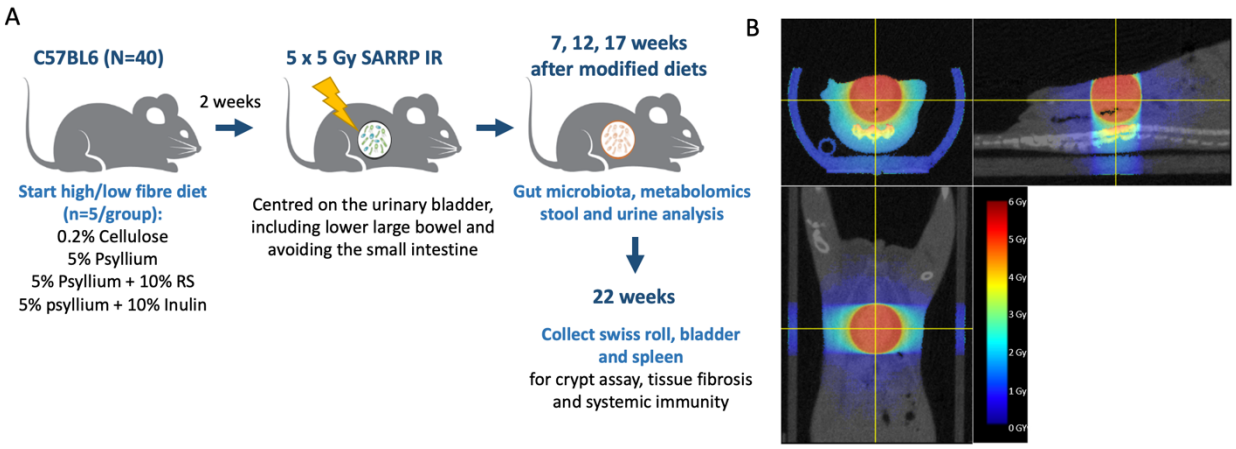


Figure 72 Overview of late normal tissue toxicity experiment. (A) C57BL/6 mice were treated supine with 5 Gy SARRP IR head down for 5 consecutive days to their lower abdomen after 2-weeks of modified diet. Stool and urine analyses were performed at the timepoints of 7-, 12- and 17-weeks post IR. (B) Treatment plans of CT images centred on the beam with mice positioned supine and head down. while mice were positioned upside down to avoid exposing small intestines to IR.

5.2.2 Body weight change after IR

Figure 73 showed the weight changes within 3 weeks after IR. The IR cohort in the 0.2% cellulose group experienced a delayed weight gain compared to their non-IR cohorts, not seen in the psyllium diet groups. The delayed weight gain in 0.2% cellulose was significant (P=0.0059) during the first week and gradually recovered subsequently.

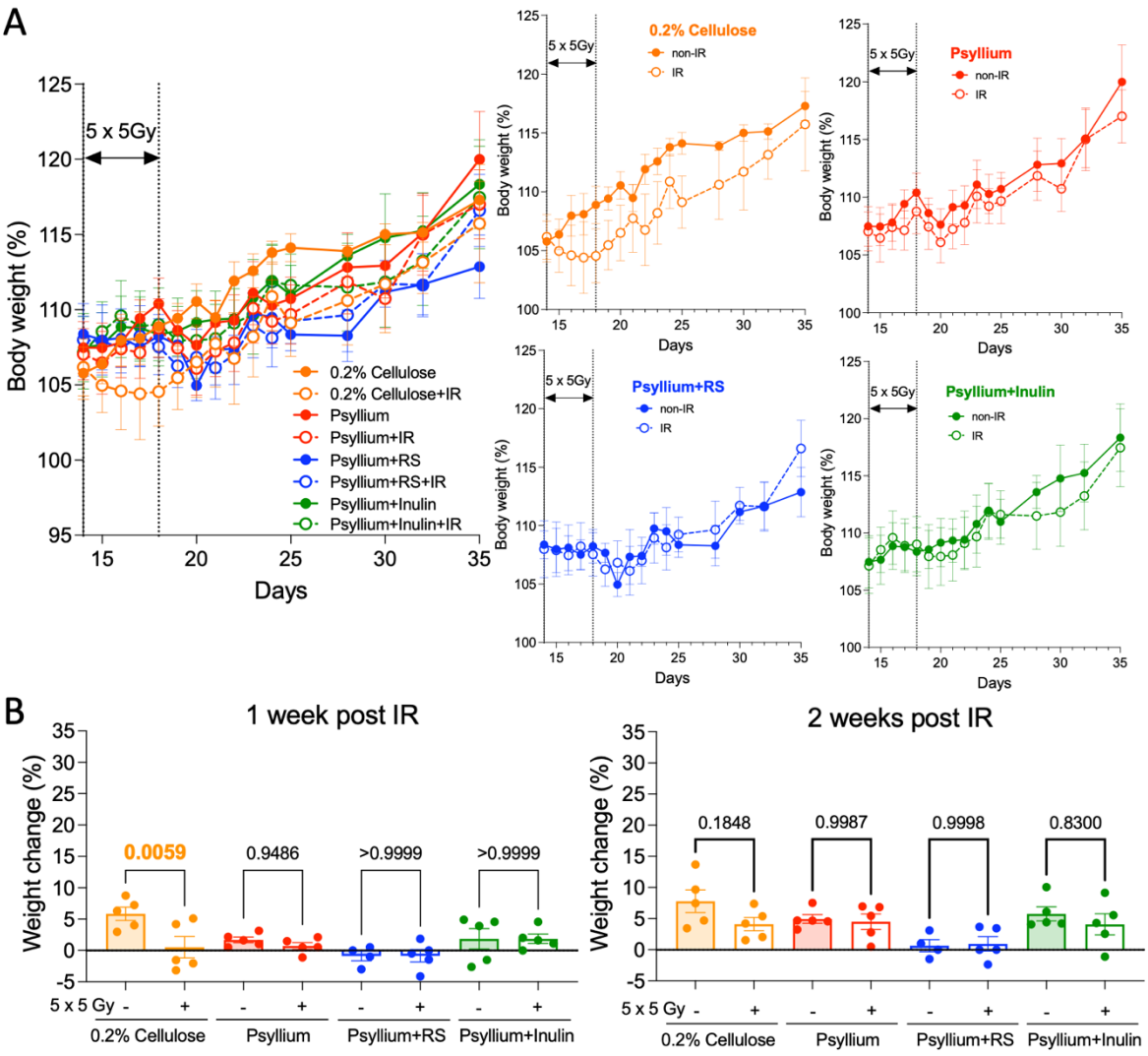


Figure 73 Body weight change within 2 weeks after SARRP IR. (A) Overall comparison of body weight change for mice fed different modified diets with or without IR. Individual body weight changes of IR mice compared to their non-IR cohort in each dietary group within 2 weeks after IR. The body weight (%) was the percentage of the weight of a specific day relative to the day when the mice started receiving modified diets. The x-axis was the days after starting the modified diets. (B) One-way ANOVA tests were conducted for comparison of IR cohorts to non-IR cohorts at 1- and 2-week post IR. The weight change (%) was the difference between the percentage of body weight of a specific day and the percentage of the day when the mice received irradiation.

5.2.3 Stool analysis

I measured the stool frequency by isolating the mice in individual cages for 24 hours (Figure 74). I measured the dry weight and calculated the number of faecal pellets which reflected the stool frequency (Paillas *et al.*, 2020). At the 7-week timepoint post IR, there was a greater stool frequency in all psyllium-containing diet groups compared to 0.2% cellulose with or without radiation, reflecting the increased fibre content. In the non-IR cohort, the P-values were <0.001 for all psyllium-containing diet groups compared to 0.2% cellulose. In IR cohort, the P-values were 0.08 for psyllium, <0.001 for psyllium plus RS and 0.03 for psyllium plus inulin. The stool frequencies increased at 12- and 17-weeks post IR compared to 7 weeks in non-irradiated mice of all dietary groups, which could be the consequence of reverting back to normal chow at the timepoint of 7-weeks post IR. At the latter two timepoints, there was no significantly difference of stool frequency among different dietary groups.

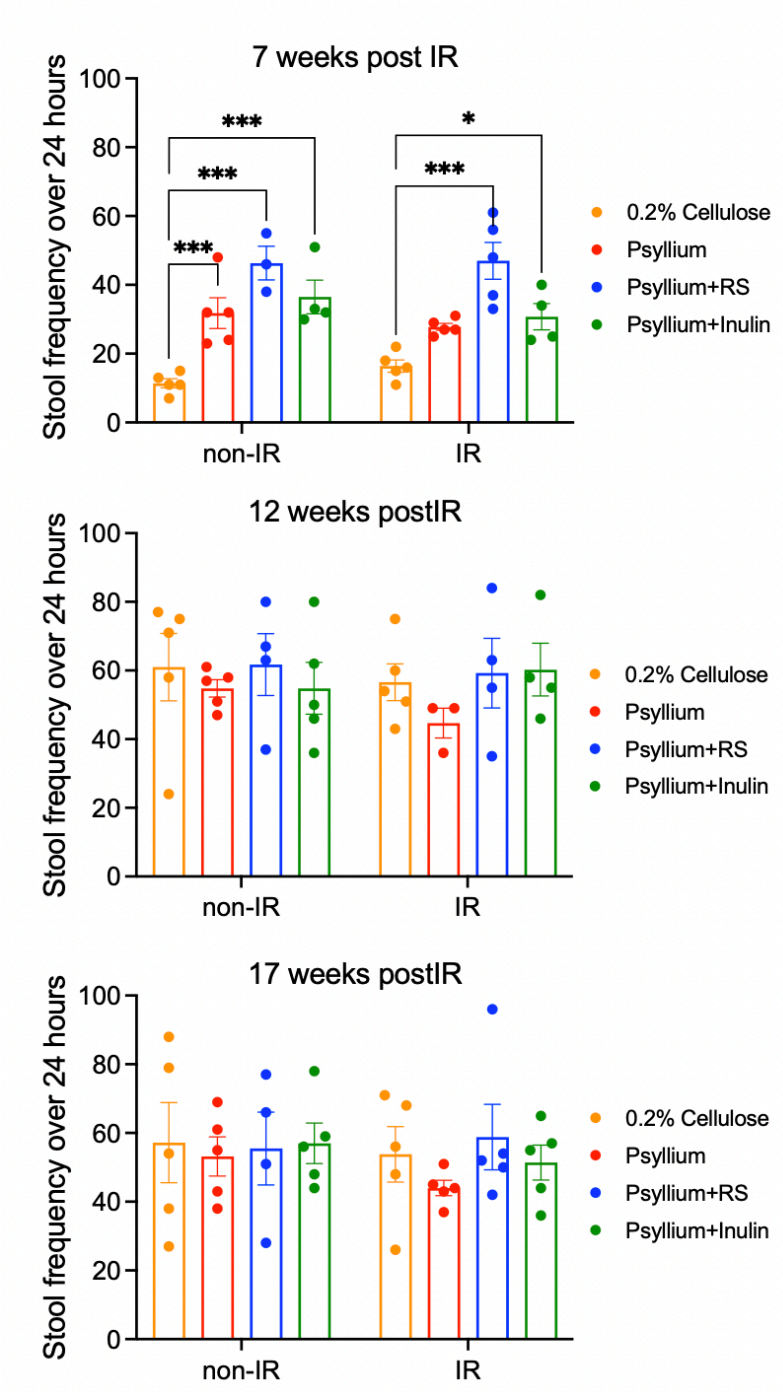


Figure 74 Stool frequency after SARRP IR. Overall stool frequency over 24 hours at 7-, 12- and 17-weeks post IR of all dietary groups. Data shown as mean and standard error.

5.2.4 Urine analysis

Since the SARRP radiation beam was centred on the urinary bladder, I assessed bladder function by measuring the voiding volume (Figure 75A) and frequency (Figure 75B) during 4 hours of isolation. I found that all mice in the IR cohorts tended to have lower urine outputs compared to their non-IR controls, especially in the psyllium plus inulin group at 17-weeks post IR (Figure 75A). Irradiated mice in the 0.2% cellulose group also tended to have higher voiding frequency, measured by the number of spots, compared to non-IR controls, but this was not seen in other mouse groups (Figure 75B).

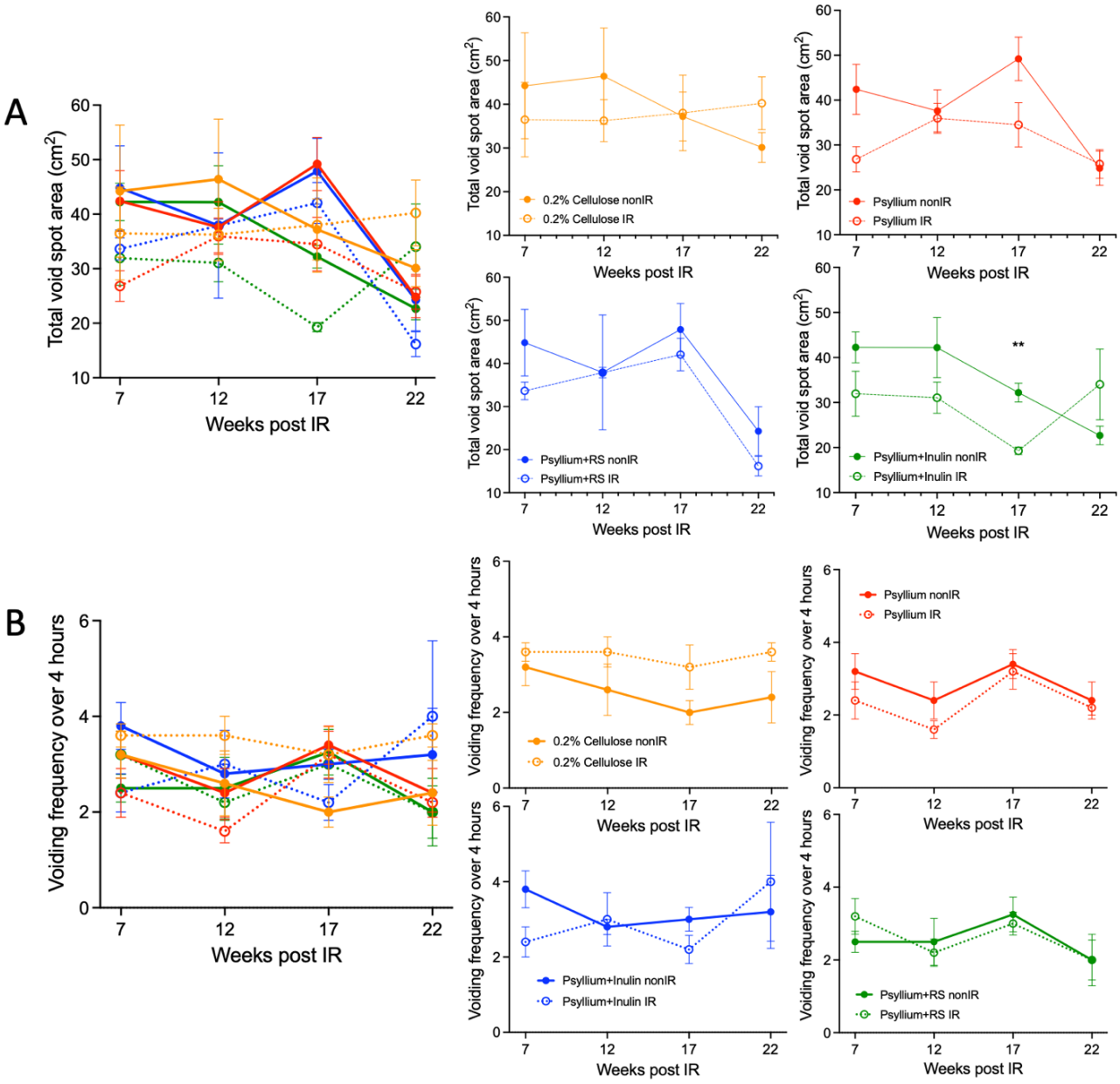


Figure 75 Voiding volume and frequency after SARRP IR. Overall voiding (A) area and (B) frequency over 24 hours at 7-, 12- and 17-weeks post IR of all dietary groups and the individual plots for each dietary group. Data shown as mean and standard error.

5.3 Discussion

Both acute and late toxicity experiments showed that irradiation caused a delayed weight gain only in the 0.2% cellulose within 1 week post irradiation. The phenomenon happened at the early stage after irradiation and may be caused by systemic inflammatory effects even though we were only irradiating the bladder and lower large intestine. A previous study showed that 15% oat bran in the diet significantly downregulated the systemic inflammation in mice receiving pelvic irradiation and this effect lasted for 1, 6 and 18 weeks after irradiation (Patel *et al.*, 2020). In our acute toxicity experiment, all psyllium diets significantly increased the caecal short-chain fatty acid levels that have been shown to exert anti-inflammatory effects in intestinal mucosa by histone deacetylases inhibition and activating the G protein coupled receptors present in intestinal epithelial cells and immune cells (Venegas *et al.*, 2019). These findings support that psyllium diets may protect the mice from the stress of systemic inflammation during the acute phase of IR.

In the acute toxicity experiment (section 5.1), psyllium plus RS or psyllium plus inulin increased the number of remaining crypts at the high irradiation dose of 14 Gy. Guo *et al.* found a negative association between increased abundances of Lachnospiraceae and Enterococcaceae and the gastrointestinal adverse effects of whole body radiation in leukemia patients (Guo *et al.*, 2020). In addition, the mouse metabolomics results revealed microbially-derived propionate and tryptophan in faeces can caused long-term radioprotection and mitigated gastrointestinal syndromes and proinflammatory responses. I found that there was significantly higher abundance of Lachnospiraceae in the gut microbiota and caecal SCFAs levels, including propionate, in mice fed with psyllium plus inulin, compared to 0.2% cellulose. Besides, tryptophan metabolism and SCFAs were enriched in the caecal contents of psyllium plus resistant starch-treated mice. These results imply that the radioprotective effects of psyllium plus inulin or psyllium plus resistant starch at high radiation doses may be mediated via modification of the gut microbiota and enhancement of specific metabolites. Further experiments are needed to prove the causal

effects of these bacterial taxa and metabolites on rescuing the crypts from radiation-induced injury.

Besides of the above-mentioned metabolites, there are also several metabolites enriched by psyllium plus resistant starch or psyllium plus inulin that may protect the gut from radiation injury, such as inosine and taurine. The untargeted metabolomics analysis of caecal contents (section 4.3.4) showed that the inosine levels increased in the psyllium plus inulin group (P=2.99E-10 for tumour-bearing mice and P=3.23E-12 for non-tumour bearing mice) and the taurine levels elevated in psyllium plus resistant starch (P=9.45E-5 for tumour-bearing mice). Hou *et al.* also demonstrated that inosine doses of 750 mmol/kg can prolong mouse survival time after a single dose of lethal total-body ionising radiation of 12Gy (Hou *et al.*, 2007). In addition, Li *et al.* showed that gut microbiota-produced inosine ameliorated dextran sulfate sodium (DSS)-induced colitis through enhancing adenosine 2A receptor/PPARγ-dependent mucosal barrier functions(Li *et al.*, 2021). Besides inosine, Yamashita *et al.* observed that taurine administration led to an early recovery of lymphocytes numbers after 7 Gy whole body irradiation in mice, although it did not improve survival (Yamashita *et al.*, 2019; Yamashita *et al.*, 2017). Yang *et al.* showed that high dose taurine (40mM) decreased radiation-induced apoptosis in mouse spermatocytes (Yang *et al.*, 2017).

Psyllium had been shown to be effective for radiation-induced diarrhoea (Murphy *et al.*, 2000) and is now prescribed for bladder and prostate cancer patients during radiotherapy for their acute diarrhoeal reaction. Murphy *et al.*'s finding supported that hypothesis psyllium might be able to maintain the consistency of stool in mice receiving irradiation to their lower abdomen. In the late toxicity experiment (section 5.2), 7 weeks post IR (10 weeks from starting the modified diets), the mice fed with psyllium-containing diets tended to have higher stool frequency, that was measured by the stool pellets, compared to 0.2% cellulose. This implies that the increased fibre content can indeed change the bowel habit. At later time points when the diets had been changed back to normal chow for 5 and 7 weeks (12- and 16-weeks post irradiation), there was still no significant difference of stool frequency among the non-IR and IR cohorts of different dietary groups. However, this assay may be too

crude. A definitive histopathology report also did not show significant changes of fibrosis for the non-IR and IR large intestine.

Overall, our data suggest that high dietary fibres protect the gut from radiation-caused injury, such as crypt loss and delayed weight gain, during the early phase post-radiotherapy, and the mice would recover in the later stages. Further experiments are needed to investigate the radioprotection role of psyllium plus resistant starch and psyllium plus inulin in terms of histological changes, DNA damage and repair and gut barrier function.

Chapter 6: Immunology

The immune context of a tumour determines its response to anti-cancer treatment. Furthermore, dietary fibre and the gut microbiota can modulate anti-tumour immune responses. Therefore, I explored how these factors affected the local tumour and systemic immune responses. In four sets of experiments from Chapter 4 and 5, I investigated how dietary fibre modulated the antitumour immune responses in tumour-bearing mice and local gut immune responses in non-tumour bearing mice after exposure to irradiation (Table 13).

Table 13 Immunology.

	Corresponding to experiment in:	Immune responses of interest
6.1	section 4.1 (tumour response for IR alone)	**Local tumour** immune responses
6.2	section 4.3 (tumour response for dietary fibre)	**Local tumour** and **systemic** immune responses
6.3	section 4.4 (tumour response for dietary fibre and IR)	**Local tumour** and **systemic** immune responses
6.4	section 5.1 (acute intestinal toxicity for dietary fibre and IR)	**Local gut** and **systemic** immune responses

Various immune cells reside in the tumour environment which can perform both pro- and anti-tumourigenic functions and even determine tumour response to treatment. Broadly, the immune cells fall into two categories: innate and adaptive immune cells (Anderson & Simon, 2020) (Table 14). Innate immunity is a non-specific defence mechanism that responds immediately to a foreign antigen entering the body. Natural killer (NK) cells, macrophages, neutrophils, and dendritic cells belong to the innate immune cells. Adaptive immunity is activated by innate immune cells and enhances more specific immune responses. The adaptive immune responses involve T cells and B cells.

Table 14 Functions of immune cells.

Innate immune cells	Function
Natural killer (NK) cells	Patrol the bloodstream, seek out and kill tumour cells.
Macrophages	Perform pathogen phagocytosis and antigen presentation. Can be categorised as either inflammatory M1 macrophages or immune-suppressive M2 macrophages.
Dendritic cells (DC)	Process antigen material and present it on the cell surface to T cells, thereby acting as messengers between the innate and adaptive immune systems.
Neutrophils	Make up to 70% of circulating leukocytes and provide the first line of defence against many pathogens.
Immature myeloid cells	Contribute greatly to tumour progression and promote tumour evasion from immune attack.
Adaptive immune cells	**Function**
CD8 (cytotoxic) T cells	Contain cytotoxic granules and promote apoptosis of target cells.
CD4 (helper) T cells	Secrete cytokines with different activities. -Produce IL-2 and IFN-γ and promote cellular immunity by acting on CD8+ cytotoxic T cells, NK cells and macrophages. -Produce IL-4, IL-5 and IL-13 and promote humoral immunity by acting on B cells.
B lymphocytes	Generate and present antibodies, cytokine production, and lymphoid tissue organisation.

Cytotoxic T cells (CD8+) are important effectors in anti-tumour immunity (Raskov *et al.*, 2021). They target tumour antigens expressed on cancer cells and eliminate them. Tumour infiltration with cytotoxic T cells is often associated with a positive prognosis in cancer patients (Blessin *et al.*, 2021). $CD4^+$ T cells differentiate into a variety of subtypes and further regulate a wide range of immune responses. T helper 1 (Th-1) cells are characterised as proinflammatory and support CD8+ cells through the secretion of interleukin-2 (IL-2) and IFN-γ.

Systemic immunity

The peripheral immune system is required to induce anti-tumour immune responses (Hiam-Galvez *et al.*, 2021). The localised anti-tumour immune response requires the continuous supply of myeloid cells from haematopoietic precursors in the bone marrow (Schultze *et al.*, 2019). In addition, T cell priming by dendritic cells takes place in lymphoid tissues. T helper cells are central to the development of immune responses (Masopust & Schenkel, 2013), and Th1 and Th2 are the two predominant Th cell subtypes that are critical for activating antigen-specific effector cells and recruiting cells of the innate immune system (Knutson & Disis, 2005). Th1 cells generate IFN-γ and IL-2 that are essential for the induction of cellular immunity, whereas Th2 cells produces IL-4, IL-5, and IL-10 that are required for humoral immunity. T helper 1 activation facilitates the induction of anti-tumour immunity via activation of antigen-presenting cells.

Local gut immunity

Effector immune cells reside diffusely throughout the intestinal epithelium and lamina propria. Under the intestinal epithelium, there are lymphoid aggregates that distribute in the mucosa and submucosa, which are known as gut-associated lymphoid tissue (GALT). They are the principal locations for priming adaptive immune responses working together with the draining lymph nodes in the small and large intestine. Peyer's patches are the components of the GALT found along the mucosa and submucosa of the small intestine and mainly contain CD4, CD8 T cells and IgA-producing B cells. Activated B cells in the Peyer's patches constantly supply IgA-producing plasma cells that are required to produce secretory IgA. It can either enter systemically into the mesenteric lymph system or protect the gut barrier from preventing pathogens from adhering to the intestinal surface.

Interaction between gut microbiota and local and systemic immunity

The gut microbiota modulates the immune system via their metabolites (SCFAs, aryl hydrocarbon receptor ligands or polyamines) or components (polysaccharide A, formyl peptides, HBPs) (Rooks & Garrett, 2016). SCFAs inactivate nuclear factor-KB and

downregulate pro-inflammatory cytokine tumour necrosis factor (TNF) via histone deacetylase inhibition in neutrophils (Vinolo *et al.*, 2011). In addition, the anti-inflammatory effects of HDAC inhibition conferred by SCFAs can also be extended to macrophages (Chang *et al.*, 2014) and dendritic cells (Singh *et al.*, 2010). Feeding the mice with high dietary fibre and SCFA-supplemented diets can also decrease colonic inflammation via increasing immunosuppressive effects of regulatory T cells (Furusawa *et al.*, 2013). The other microbial metabolites, AHR ligands, generated from the metabolism of tryptophan by *Lactobacilli* species, stimulate ILC3 and increase IL-22 and AMP production to inhibit the colonisation of pathogens, such as *Candida albicans*. The intestinal lumen contains high levels of polyamines which are critical in maintaining the integrity of gut barrier. For example, polyamines increase the tight junction proteins, namely, occludin, zonula occludens 1 and E-cadherin, which can reinforce epithelial barrier function (Liu *et al.*, 2009).

In terms of bacterial components, polysaccharide A, a polysaccharide mainly produced by *Bacteroides fragilis*, can act as a Toll-like receptor 2 on DCs and be presented to helper T cells (Wang *et al.*, 2006). In addition, PSA has also been shown to mediate the Th1/Th2 balance and to elicit appropriate cytokine production in germ-free mice, mechanisms which are important in reinforcing the host adaptive immune system (Mazmanian *et al.*, 2005).

6.1 Local tumour immune response following ionising radiation alone

To study the effect of IR on the local immune response in the tumour, I performed immunohistochemistry (IHC) staining of CD3 and CD8 to investigate the tumour-infiltrating general lymphocytes ($CD3^+$) and cytotoxic T cells ($CD8^+$). The result showed that only 10 Gy of IR tended to increase the number of $CD8^+$ cells compared to control (P=0.131; Figure 76).

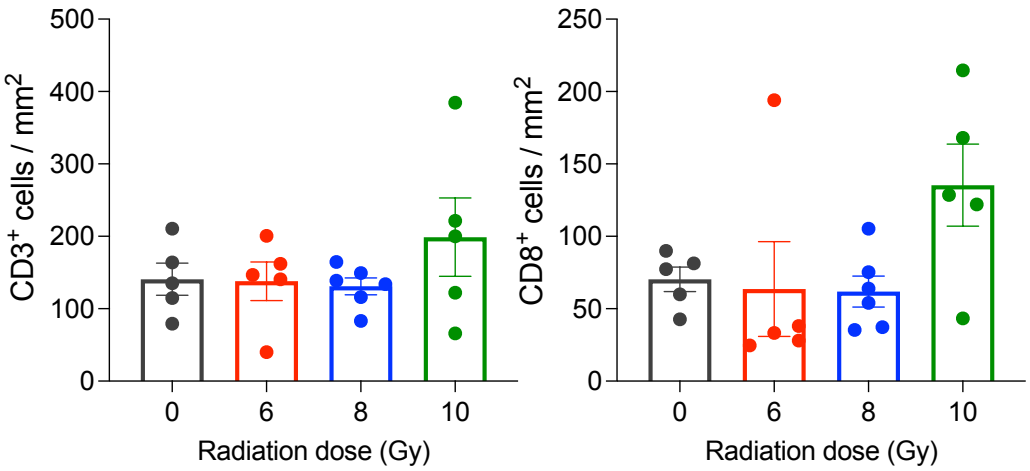


Figure 76 Ten Gy IR tended to increase intratumoural $CD8^+$ cell numbers.
Immunohistochemistry analysis of tumour-infiltrating general lymphocytes ($CD3^+$) and cytotoxic T cells ($CD8^+$) by IHC staining of CD3 and CD8 markers.

6.2 Local tumour and systemic immune responses to dietary fibre alone

6.2.1 Overview

Psyllium plus resistant starch or psyllium plus inulin delayed the tumour growth of UPPL1591 allografts (section 4.3). Several studies have shown that metabolites produced by the gut microbiota can increase the efficacy of immune checkpoint blockade via activation of $CD8^+$ cells (Mager *et al.*, 2020; Wang *et al.*, 2020). To see whether the immunomodulation of tumour was also affected by dietary fibre, I applied IHC staining, a nanoString assay of immune-related gene expression and flow cytometry analysis to investigate the local tumour and systemic immunity in UPPL1591 tumours responding to different dietary fibres.

6.2.2 Local intratumoural $CD8^+$ cells

It is acknowledged that the cytotoxic T cell is the most powerful effector cell in anti-tumour immunity (Raskov *et al.*, 2021). For all tumour samples, I performed IHC staining of CD8, a marker of cytotoxic T cells, and quantified the number of positively-stained cells in the tumour core to assess the intratumoural immune response (n=6/group; Figure 77A). In addition, for some representative samples (n=3/group), I extracted RNA from formalin-fixed paraffin-embedded tumour tissues and analysed immune-related gene expression on a nanoString platform (Figure 77B). Both results showed that the number of cytotoxic T cells was significantly increased by psyllium plus inulin (P=0.049 for IHC) but was decreased by psyllium plus RS compared to 0.2% cellulose. Immune cell profiling of the nanoString data also showed that psyllium plus inulin resulted in a significantly higher level of $CD8^+$/T cells compared to psyllium plus RS (Figure 77B). Also, $CD8^+$ cells were the only cell type enhanced by psyllium plus inulin among all the immune cells.

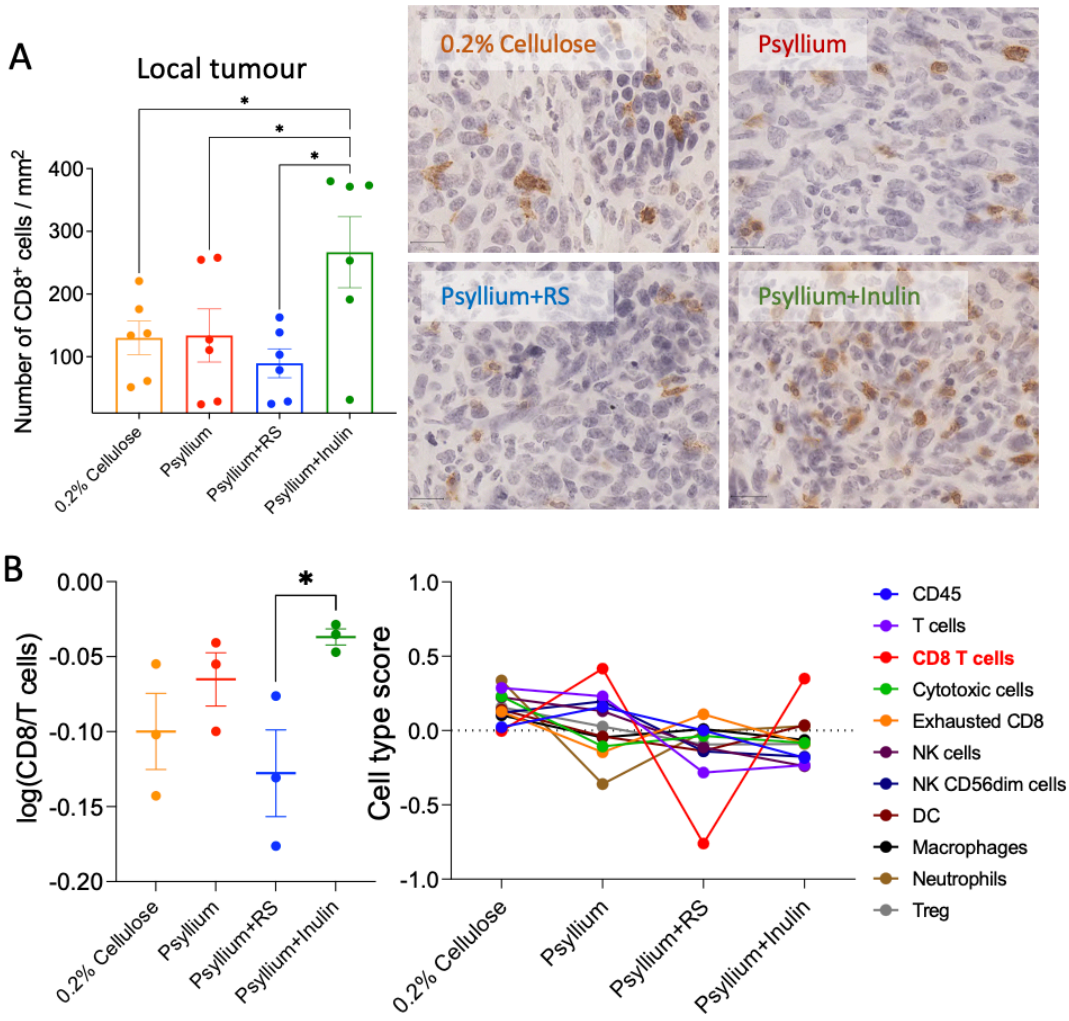


Figure 77 Intratumoural CD8⁺ cells increased by psyllium plus inulin, but decreased by psyllium plus RS. (A) IHC staining of CD8⁺ cells to assess the numbers of cytotoxic T cells and representative images. (B) Values of log (CD8⁺/T cells) and overall immune cell profiling evaluated on a nanoString platform. One-way ANOVA with Holm-Sidak's multiple comparison test was used to compare the means of different dietary groups. Error bars represent the standard error.

6.2.3 Systemic immunity

I assessed both myeloid (Figure 78A) and lymphoid (Figure 78B) immune cells using flow cytometry analysis, which consisted of dendritic cells, macrophages, helper T cells and cytotoxic T cells. I found that psyllium plus RS significantly increased the population of splenic macrophages compared to 0.2% cellulose (P=0.047). Psyllium plus inulin tended to have higher levels of systemic helper T (P=0.092) and cytotoxic T (P=0.103) cells compared to 0.2% cellulose, which was consistent with the findings of the IHC and nanoString analysis of the local tumour.

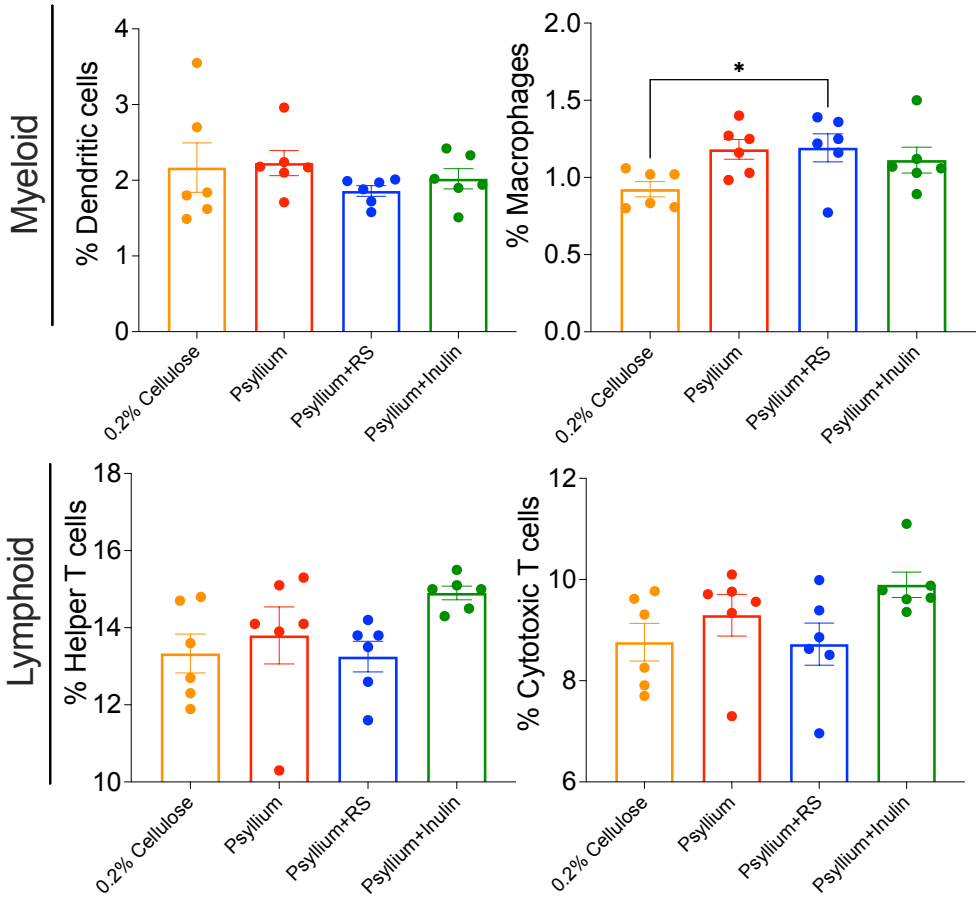


Figure 78 Systemic immune response. Percentages of splenic (A) dendritic cells, macrophages, (B) helper T and cytotoxic T cells measured by flow cytometry analysis. One-way ANOVA with Dunett's multiple comparison test was used to compare the means of different dietary groups. Error bars represent the standard error.

6.3 Local tumour and systemic immune responses following dietary fibre and ionising radiation

6.3.1 Overview

Section 4.4 showed that psyllium plus resistant starch and inulin enhanced tumour control when combined with irradiation. To further investigate whether this was mediated by immune responses, I applied the panCancer immune panel of a nanoString platform to investigate local tumour immune cell profiling and pathways. Flow cytometry analysis of splenocytes and multiplex plasma cytokine assays were performed to study the systemic immune responses to treatments.

Consistent with the intra-tumoural immune responses in the section 6.2 (Figure 77B), the number of CD8 cells was increased in the psyllium plus inulin but decreased in psyllium plus RS group (Figure 79A). In addition, the other immune cells, including neutrophils, cytotoxic T cells and NK CD56dim cells, were also elevated in the psyllium plus inulin group. Figure 79B shows the intensity of immune pathways normalised to 0.2% cellulose. High enrichment was seen in most of the pathways, especially humoral immunity, cytokines and receptors and interferon, in tumours of the psyllium plus inulin group.

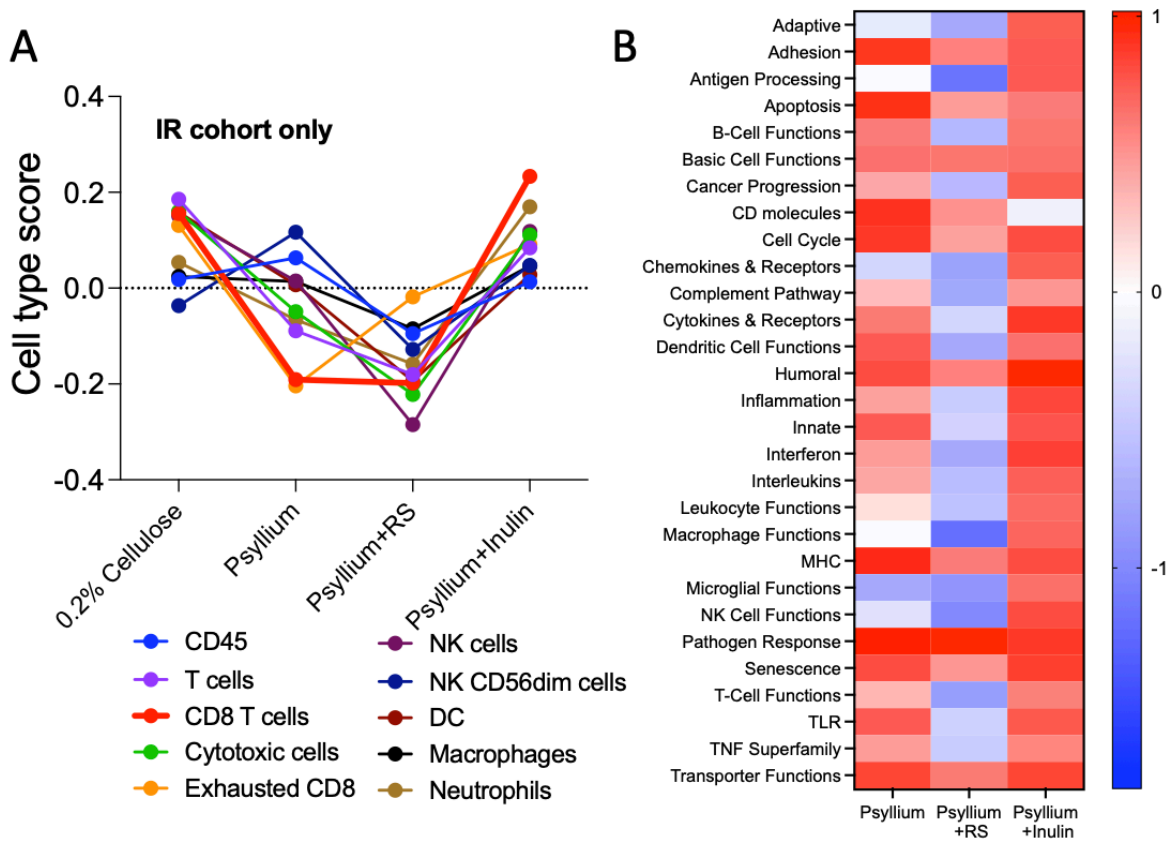


Figure 79 Local immune responses. (A) Immune cell profiling and (B) pathways of nanoString platform was used to study the local tumour immunity (n=6/group). Data shown as mean and standard error.

6.3.2 Systemic immune responses

Figure 80A and B shows the splenocytes populations and peripheral cytokines levels in different dietary groups. In the 0.2% cellulose and psyllium plus RS or psyllium plus inulin groups, IR tended to increase the number of splenic helper T and cytotoxic T cells, which was not statistically significant. In terms of plasma cytokine levels, IR also tended to raise IL-2 levels in the psyllium plus RS group and granulocyte-macrophage colony-stimulating factor (GM-CSF) levels in all psyllium diets groups.

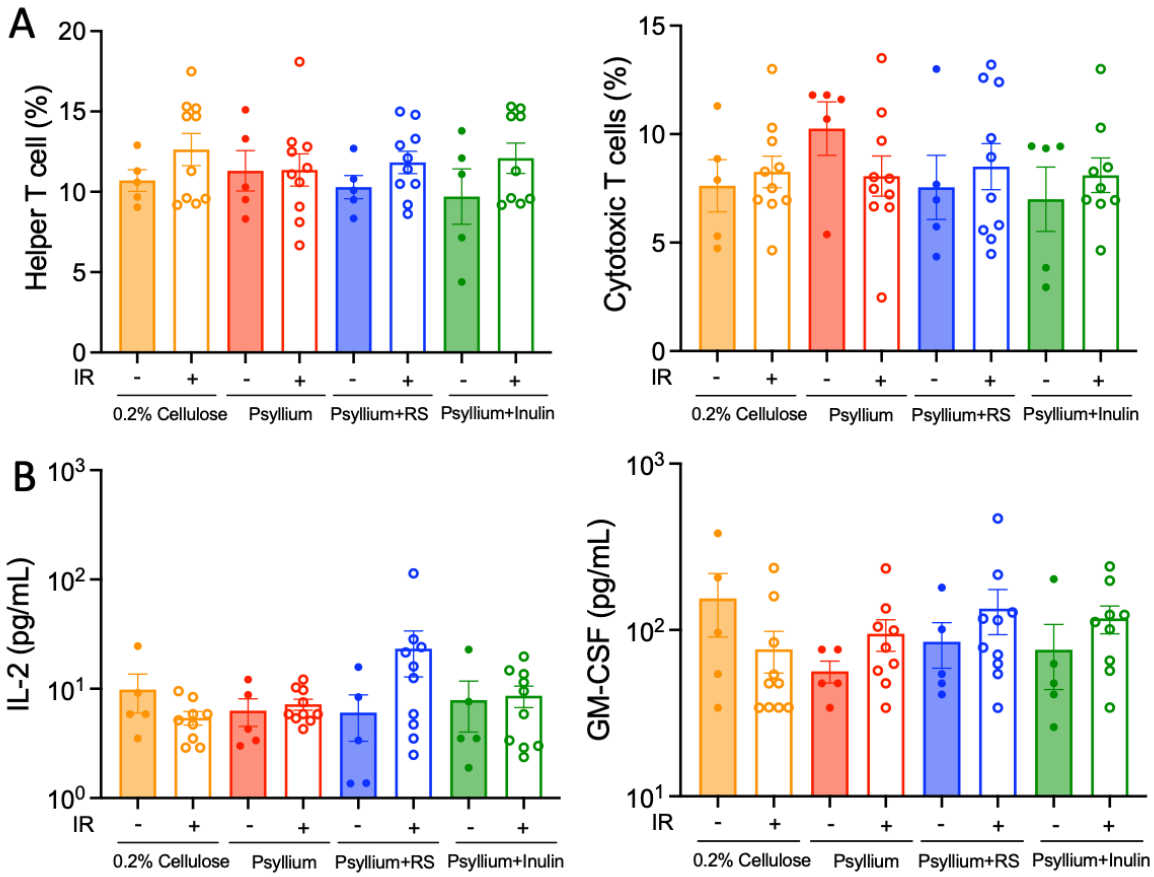


Figure 80 Systemic immune responses. (A) Flow cytometry analysis of splenic helper T and cytotoxic T cells, and (B) plasma cytokine assays of IL-2 and granulocyte-macrophage colony-stimulating factor (GM-CSF) were performed to investigate systemic immune response. Data shown as mean and standard error.

6.3.3 Local tumour and systemic immunity in psyllium plus inulin group by IR response

Since local tumour immune response was enhanced by psyllium plus inulin, I further validated whether the IR response was associated with local tumour (Figure 81) and/or systemic (Figure 82) immunity. Using the nanoString platform, on tumours, the number of exhausted CD8 cells significantly decreased in responders (P=0.043; black dots and connecting line), while the others, including NK cells, dendritic cells, NK CD56 dim cells and T cells, slightly increased (Figure 81A). In addition, the T cells functional pathways, and cytokines and receptors were enriched in responders to psyllium plus inulin (Figure 81B). For T cell function, the significantly up-regulated genes which had an adjusted p-value of <0.01 (to allow for multiple testing) were *Bcl10*, *Il2ra*, *Il18rap*, *Ca*rd11, *Cd5*, *Tnf*, *Dpp4*, *Il12b* and *Fasl*. For cytokines and receptors, there were six genes significantly up regulated, namely, *Traf3*, Il18r*ap*, *Card11*, *F2rl*, *Il1*2b, *Tnf* and *Fasl*, and *Il1r2* was downregulated. This implies that the up-regulation of genes related to T cell function, and also cytokines and relevant receptors may be needed for the tumour response to IR and psyllium plus inulin.

In terms of effector cells, splenic cytotoxic T cells tended to negatively correlate with tumour growth rate and to be increased by IR (Figure 82A). GM-CSF and IL-2 were two cytokines belonging to Th1 cytokine panel which have been used to improve the efficacy of radiotherapy by activations of immune cells and enhancement of antigen presentations (Palata *et al.*, 2019). There were negative correlations between these two cytokines and tumour growth (p-values 0.048 for GM-CSF and 0.071 for IL-2, respectively) (Figure 82B and C).

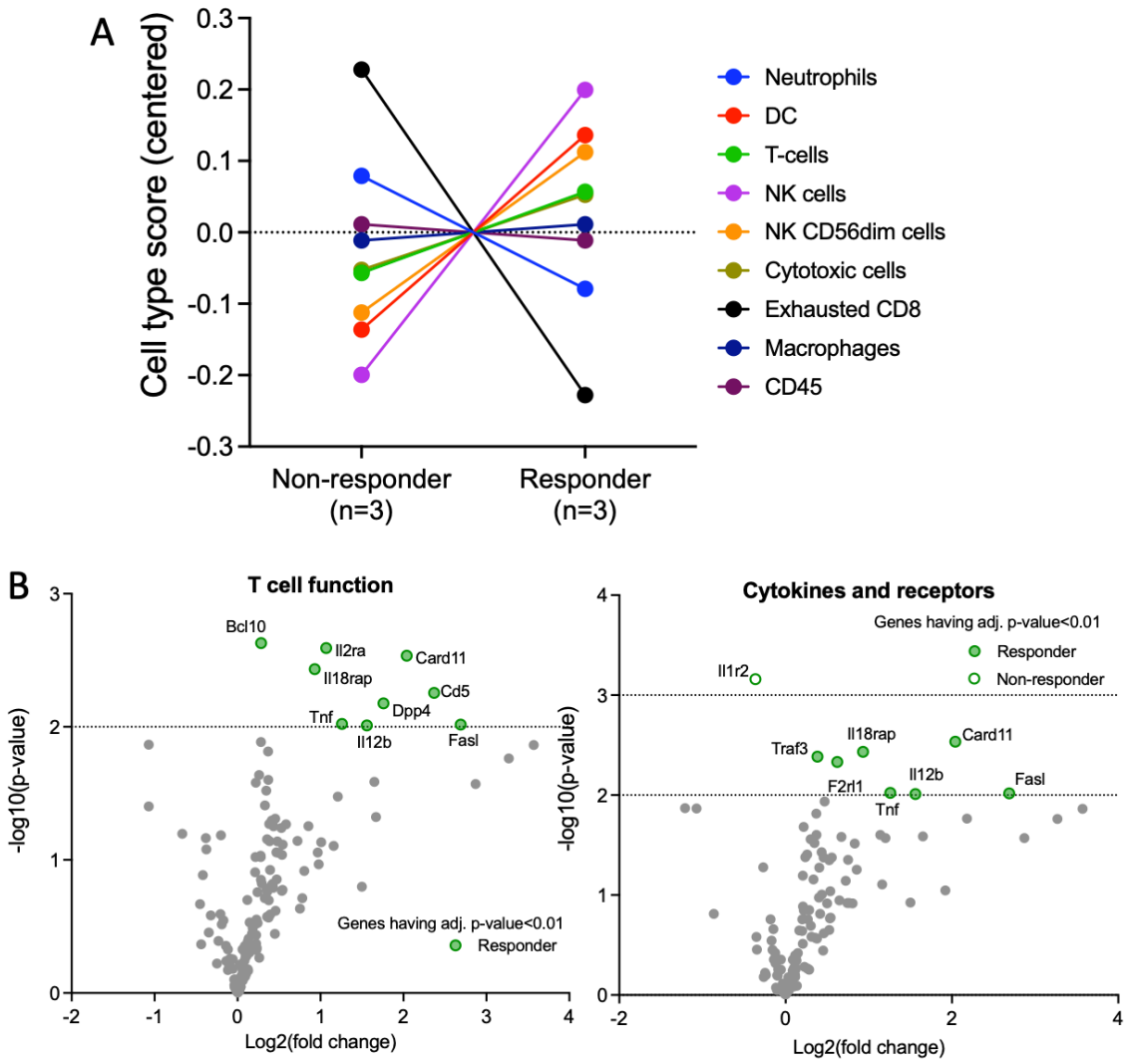


Figure 81 Local tumour immunity in psyllium plus inulin stratified by tumour response and IR. (A) Immune cell profiling and (B) gene sets of pathways of cytokines and receptors and T cell function on tumours in responders and non-responders in psyllium plus inulin groups (n=3/group).

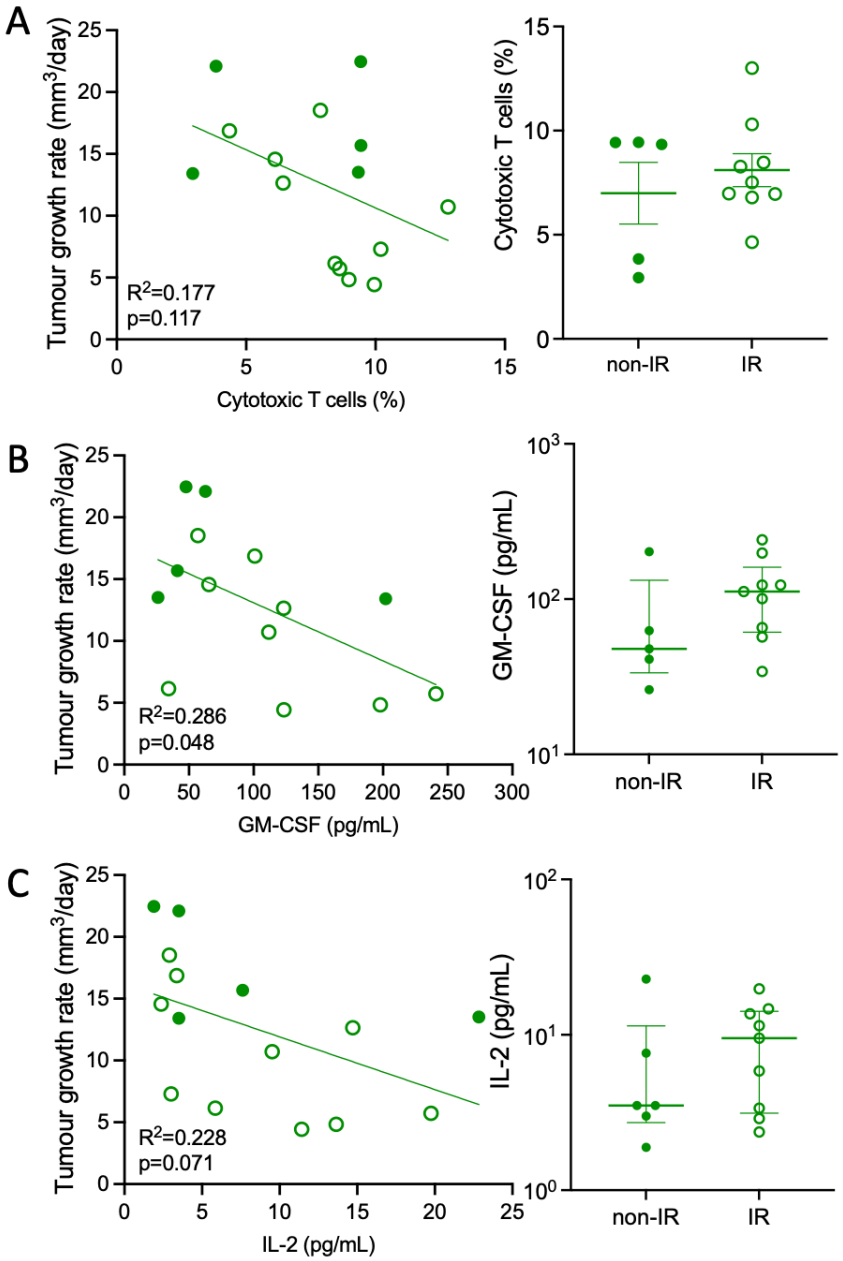


Figure 82 Systemic immunity in psyllium plus inulin stratified by tumour response and IR. Correlations of (A) splenic T cells and plasma Th1 cytokines, (B) GM-CSF and (C) IL-2, levels versus tumour growth rates in psyllium plus inulin and their percentages stratified by IR. Data shown as mean and standard error.

6.3.4 Correlation between gut microbiota and immune responses

To explore whether the tumour control-associated bacterial taxa modulate the systemic immune response, I assessed the correlation between *Bacteroides* species and Clostridiales order abundance and the splenic immune cells.

In the psyllium plus RS group, there were non-significant positive correlations between the *Bacteroides* species and leukocytes (R^2 = 0.149, P=0.269), cytotoxic T (R^2 = 0.217, P=0.174) and NK cells (R^2 = 0.330, P=0.082) (Figure 83A). In contrast, this bacterial taxon tended to positively correlate with the population of macrophages (R^2 = 0.342, P=0.075). In the psyllium plus inulin group, significant correlations were shown between the Clostridiales order and cytotoxic T cells (R^2 = 0.624, P=0.006) and macrophages (R^2 = 0.410, P=0.046) (Figure 83B). This implies that the dietary fibre-modified gut microbiota might be required to activate systemic immune responses.

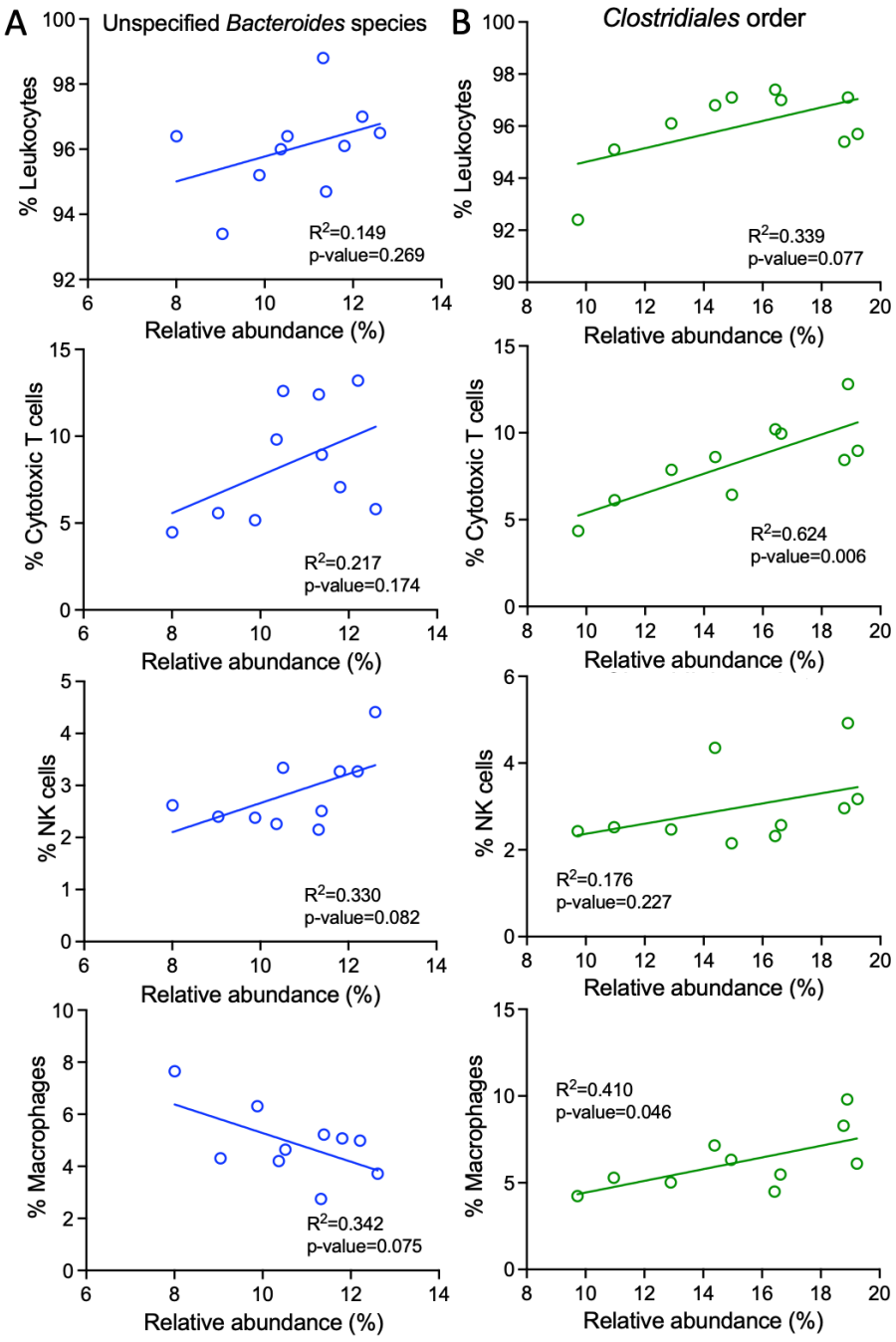


Figure 83 Unspecified *Bacteroides* species and Clostridiales order were associated with better tumour control in IR cohorts of psyllium plus RS or inulin groups. Correlations between (A) the unspecified *Bacteroides* species or (B) the Clostridiales order and the populations of leukocytes, cytotoxic T cells, natural killer cells and macrophages in the IR cohorts of psyllium plus RS or psyllium plus inulin groups.

6.4 Local gut and systemic immune responses for dietary fibre and ionising radiation

Dietary fibre and the gut microbiota can modulate local gut and systemic immunity in response to IR. Peyer's patches are the major secondary lymphoid tissue in the small intestine and they play important roles in gut health. After three-weeks of modified diet, I saw that the non-IR cohorts of psyllium plus RS or psyllium plus inulin-treated mice had more intact lymphoid tissue with a larger size (P=0.065 and 0.082) (Figure 84A) and non-statistically significantly higher populations of B cells (P=0.160 and 0.173; Figure 84B) compared to 0.2% cellulose and psyllium groups.

In terms of systemic immunity, all psyllium-treated mice had higher levels of splenic B cells compared to 0.2% cellulose, 3.75 days after receiving 12 and 14 Gy radiation to their lower abdomen (Figure 85). This suggests that dietary fibre is necessary for maintaining gut immunity, as smaller Peyer's patches were found in germ-free mice (Jain *et al.*, 2021). In addition, the psyllium plus inulin diet also significantly increased abundance of helper (P=0.004) and cytotoxic T (P<0.001) cells with 14 Gy IR compared with 0.2% cellulose.

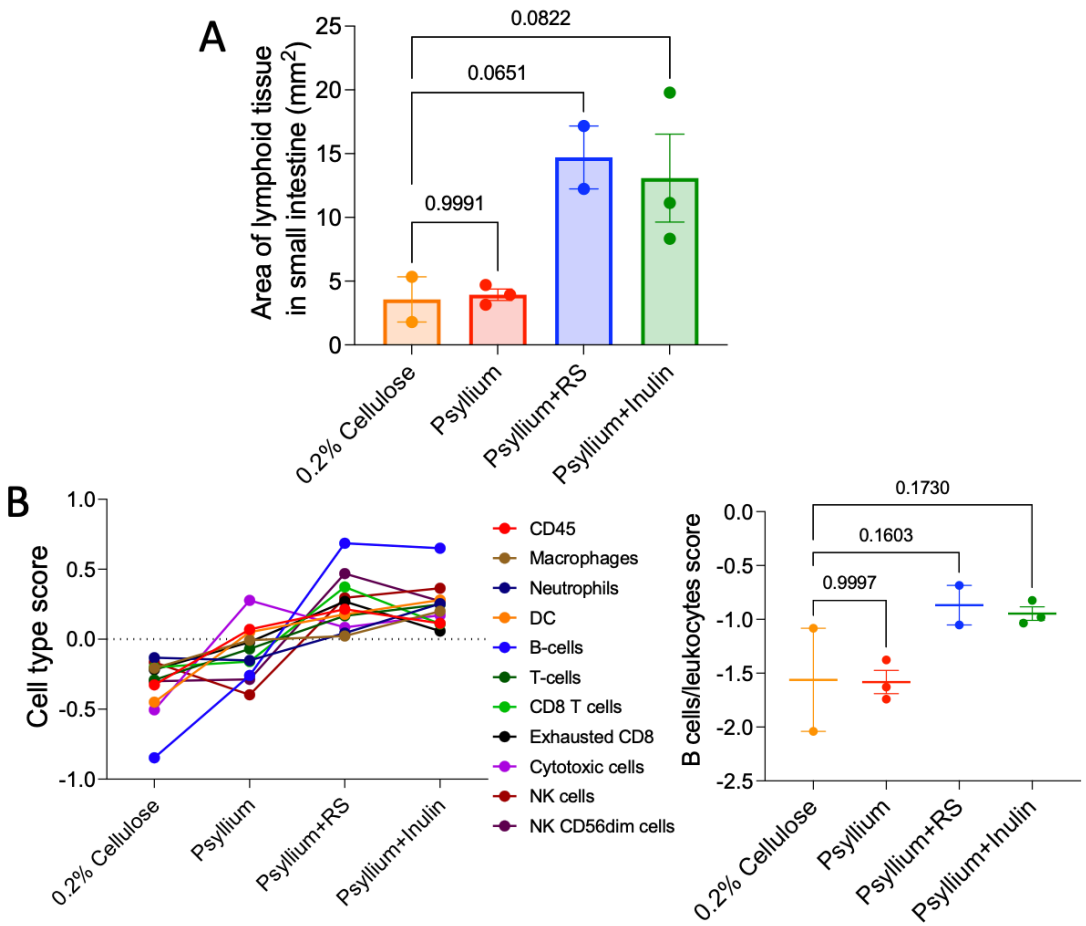


Figure 84 Local gut immunity in non-tumour-bearing mice after three-week modified diets. (A) Area of lymphoid tissue in small intestine quantified by image J and (B) cell type profiling of small intestine assessed by nanoString platform.

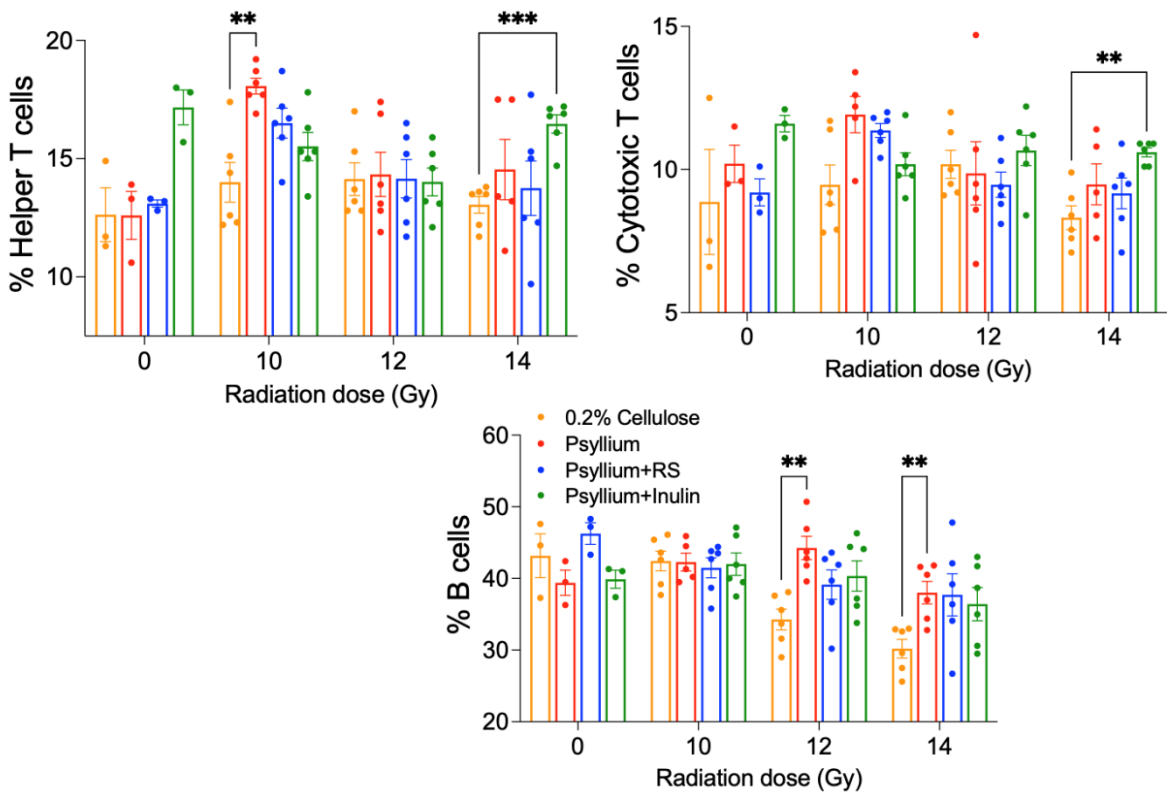


Figure 85 Systemic immunity in non-tumour-bearing mice 3.75 days after SARRP IR. Percentage of splenic lymphoid cells, helper T, cytotoxic T and B cells, evaluated by flow cytometry analysis.

6.5 Discussion

In section 6.1, the result showed that only 10 Gy tended to increase infiltrating $CD8^+$ cells in UPPL1591 tumours. This is consistent with a previous study that 10 Gy IR delayed tumour growth of melanoma with an increase of $CD8^+$ cells via dendritic cells activation in C57BL/6 mice (Gupta *et al.*, 2012). There was no difference of CD8+ cell numbers among non-IR and IR mice receiving 6 and 8 Gy. This implies that 6 or 8 Gy might be insufficient to mediate a T cell response, or the immune response could be delayed compared to 10 Gy. Another possible reason might be that the enhancement of $CD8^+$ cells could have occurred earlier and have waned by the time the tumour reached 700 mm^3.

In the experiment of section 4.3 without IR, only psyllium plus inulin increased intratumoural CD8 cells with a slight increase of splenic CD4 and CD8 cells compared to the other dietary groups. This result is consistent within both IHC and nanoString analysis. When combined with IR, as presented in section 4.4, enhanced local tumour immune responses with higher levels of $CD8^+$ cells, NK and cytotoxic cells were seen in the psyllium plus inulin group. These findings from the non-IR (section 4.3) and IR (section 4.4) experiments suggest that psyllium plus inulin modulates anti-tumour immune responses. In terms of the systemic immune responses, there were negative correlations between tumour growth and peripheral plasma cytokines, including IL-2 and GM-CSF, and the splenic cytotoxic T cells. This suggest that systemic immunomodulation might be necessary for the tumour control conferred by psyllium plus inulin.

Previous studies have shown that anti-tumour immune responses can be modulated by the gut microbiota or its metabolites. For examples, Gopalakrishnan *et al.* revealed that Clostridiales abundance was associated with the enhancement of systemic $CD8^+$ cells in mice receiving melanoma immunotherapy and this correlation (R^2=0.624, P=0.006) indeed existed in the irradiated mice fed with psyllium plus inulin in our experiment (section 6.3). In addition, untargeted metabolomics analysis showed that psyllium plus inulin increased the inosine levels in caecal contents. In 2020, there were two studies demonstrating that inosine produced by the gut microbiota can enhance immunotherapy efficacy via activation of

cytotoxic T cells (Mager *et al.*, 2020; Wang *et al.*, 2020). Although systemic inosine levels are found in the low micromolar range, relatively high local inosine levels in the gastrointestinal tract may be sufficient to modulate the immune cells residing in the gut.

There was a negative correlation between tumour growth and peripheral Th1 cytokines (P=0.048 for GM-CSF and 0.071 for IL-2) in psyllium plus inulin-treated mice, which was also increased by IR. These cytokines are GM-CSF and IL-2 that have been used in clinical trials to enhance the efficacy of radiotherapy in advanced cancers such as metastatic melanoma, renal cell carcinoma and non-small cell lung carcinoma (Palata *et al.*, 2019). GM-CSF has various functions in the immune response, such as stimulating the production of monocytes and neutrophils, and increasing antigen presentation by acting on dendritic cells (Choi *et al.*, 2006). IL-2 can induce the cytolytic activity of T cells and NK cells, which is needed for killing cancer cells (Arenas-Ramirez *et al.*, 2015). Altogether, the results suggest that the plasma cytokines GM-CSF and IL2 may be necessary for the tumour control seen with psyllium plus inulin, as they are negatively correlated with tumour response. It is noted that there was only a trend of association (not statistically significant) between the plasma GM-CSF level and tumour control, probably because it was too late to see effects other than in cytotoxic T cells when tumours reached 700 mm^3 in the tumour control experiments.

In contrast to psyllium plus inulin, both experiments in section 4.3 and 4.4 showed that the local tumour immune response was not enhanced, and was even suppressed, in mice fed with psyllium plus resistant starch. One possible reason could be the enhancement of tryptophan metabolism in mice fed with psyllium plus resistant starch (shown in the two experiments of section 4.3 and 5.1), as tryptophan can induce immunosuppression involving apoptosis of effector immune cells (Badawy, 2018). The suppression of immune response in psyllium plus RS suggests that its radiosensitising effect might be achieved via non-immune mechanisms.

Chapter 7: Gut microbiota-derived metabolites increase tumour radiosensitivity

The three major SCFAs produced by gut bacteria are acetate, propionate, and butyrate. SCFA exert different beneficial effects on the human energy metabolism, including glucose, lipid, and cholesterol metabolism in several tissue types. SCFAs have been shown to inhibit the proliferation of colorectal cancer cells and the other cancer cells outside of intestine, such as prostate cells. With no information on how SCFAs affected bladder cancer cells, I wished to determine how SCFAs, either singly or combination, affect the histone acetylation levels and proliferation of bladder cancer cells and further assess the concentrations required to achieve the phenotypes.

After fermentation, SCFAs can reach millimolar concentrations in the large intestine, from where they are absorbed by the colonic epithelium through passive and active transport (Deleu *et al.*, 2021). The acetate-propionate-butyrate concentrations are available in a relative molar ratio of approximately 60-30-10 respectively (Shukla *et al.*, 2017). The propionate and butyrate are mainly restricted to the intestinal mucosa, but acetate concentrations remain at higher levels after uptake in the peripheral blood. The transport mechanisms for SCFAs from the blood to different tissue types is still largely unknown, therefore, the question remains as to whether SCFAs can reach tumours outside the intestines. High fibre diets have been shown to increase butyrate levels in both plasma and tumour (Wei *et al.*, 2016). This supports the hypothesis that at least some of the SCFAs can reach the systemic circulation and tumour, although most of them are consumed by the gut epithelial and liver cells.

To explore the effects of SCFAs on bladder cancers, I used various assays of cell experiments, namely the MTT assay, clonogenic assay and Western blotting, to study single SCFAs or combinations in human bladder cancer cells lines RT112 and T24. The MTT assay is used to measure cell viability, proliferation, and cytotoxicity. Reduction of MTT to purple formazan crystals by metabolically active cells using NAD(P)H-dependent oxidoreductase enzymes

allows the quantification of viable cells after treatment. The clonogenic assay is the method of choice to determine cell reproductive death after treatment with ionising radiation but can also be used to determine the effectiveness of other cytotoxic agents. Western blotting of H3acK18 was used to assess histone acetylation levels which can be increased by histone deacetylase inhibition.

Bacterial strains isolated from human faecal specimens effectively kill leukaemic cells and cervical cancer and colorectal cancer cells (Zhou *et al.*, 2017). In addition, supernatant of *Lactobacillus rhamnosus*, a common probiotic, inhibited cell proliferation and induced apoptosis in colorectal cancer cell lines (Dehghani *et al.*, 2021). Therefore, I applied this approach to study the effect of supernatants of bacteria of interest on bladder cancer cells because these might contain diverse metabolites other than SCFA, which display anti-tumourigenic properties. Besides, there was very limited knowledge about a bacterium of interest, *B. acidifaciens*, found in our previous study. So, the study of bacterial supernatants allowed me to investigate its properties.

Immunofluorescence experiments and western blots of gamma-H2AX were used to compare the DNA damage after supernatant treatment and ionising radiation. γH2AX foci act as useful surrogate markers of DNA damage induced by these genotoxic agents. In the context of cancer therapy, quantitation of γH2AX is a particularly useful biomarker for evaluating the efficacy of radiation-modifying compounds. For example, the radiosensitising properties of histone deacetylase inhibitors (HDACi) have been widely investigated using γH2AX foci as an end point (Mah *et al.*, 2010).

7.1 Short-chain fatty acids mediated radiosensitisation

7.1.1 SCFAs conferred radiosensitivity in bladder cancer cells

I studied the radiosensitivity of SCFAs by irradiating the bladder cancer cells from 0-8 Gy. All SCFAs tended to increase radiosensitivity in the clonogenic assay, with butyrate having a statistically significant effect (P=0.002 for butyrate at 8Gy) (Figure 86A). In a cell viability assay, I used the combination of SCFAs in a 1:1:1 ratio and a physiological ratio in the gut (6:3:1) (Shukla *et al.*, 2017) to validate their effects on cell viability compared to each individual SCFA. SCFA mixtures conferred a stronger phenotype than single SCFAs at both ratios and this phenomenon existed in a time-dependent manner such that a longer incubation time decreased the cell viability (Figure 86B).

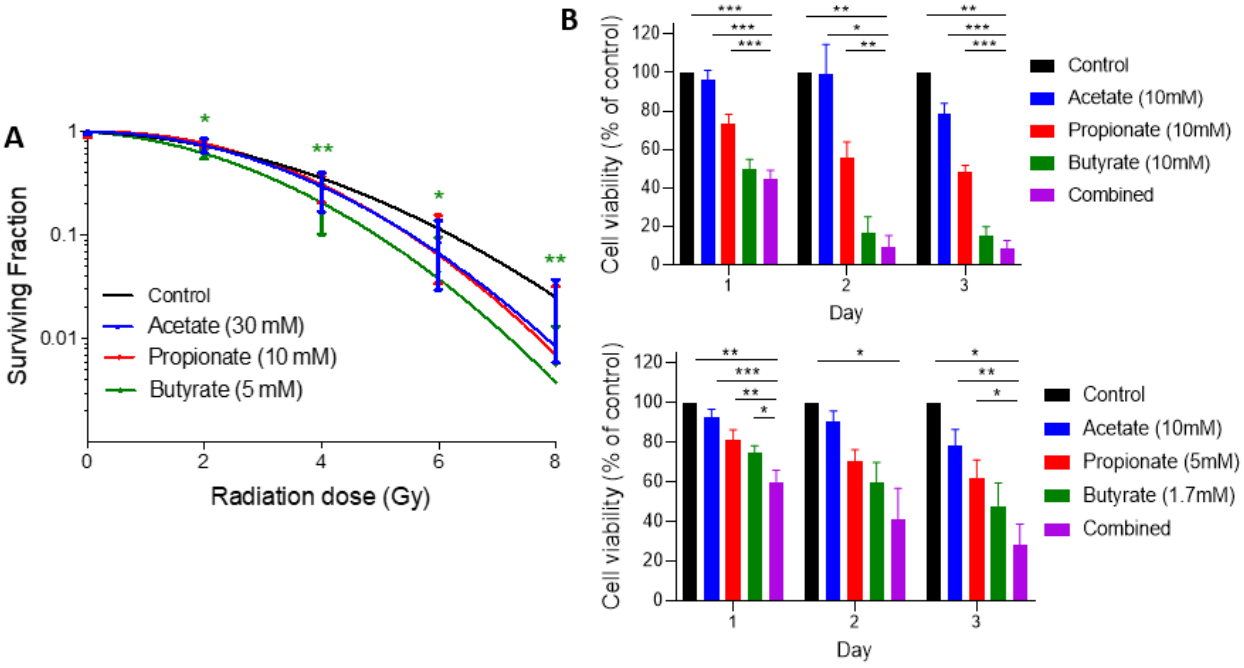


Figure 86 SCFAs conferred radiosensitivity of bladder cancer cells. (A) Linear quadratic survival curves of RT112 cells treated with IC10 (identified based on cell survival analysis) for 24 hours before receiving irradiation of 0-8 Gy (N=3). (B) Cell survival analysis of RT112 cells treated with single SCFA and combined SCFAs mixture (N=3). Combined (purple bar) denotes SCFA mixture of 10 mM for all SCFAs or 10 mM acetate plus 5 mM propionate plus 1.7 mM butyrate. Data are presented as mean ± SD. *P<0.05; **P<0.01; ***P<0.001.

7.1.2 SCFAs increased histone acetylation levels of bladder cancer cells

To validate the activity of histone deacetylase inhibition, I treated the RT112 human bladder cancer cell line with SCFAs to determine histone acetylation levels by western blot. The results showed that all three SCFAs increased histone acetylation (10 mM acetate $P=0.014$, 10 mM propionate $P=0.004$, 10 mM butyrate $P<0.001$) of RT112 bladder cancer cells (Figure 87A). Similar results for acetate and butyrate were found in the T24 human bladder cancer cell line in a time-dependent and dose-dependent manner (Figure 87B).

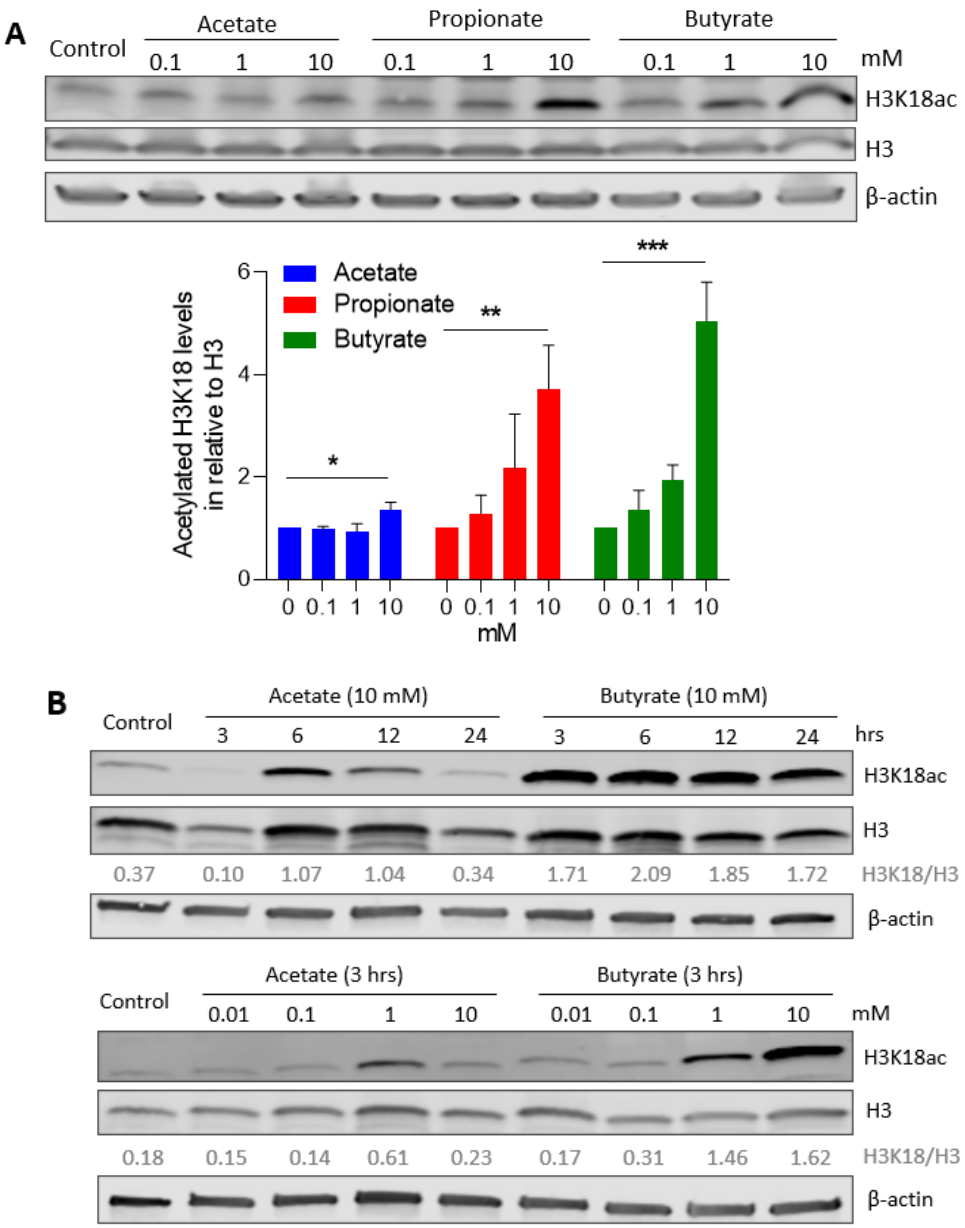


Figure 87 SCFAs increased histone acetylation levels in bladder cancer cells in a dose-dependent manner. Western blot analysis of histone acetylation levels of RT112 cells (A, N=3, incubation for 24 hours) and T24 cells (B, N=1) treated with SCFAs. Data are presented as mean ± SD. *P<0.05; **P<0.01; ***P<0.001.

7.2 Microbial metabolite-mediated radiosensitisation

7.2.1 Bacterial supernatants of co-cultures of *B. acidifaciens* and *F. prausnitzii* induced stronger cytotoxic response

In our previous study, the relative abundance of *B. acidifaciens* was enriched in responders to irradiation, and we proposed this species might be a potential radiosensitiser (Then *et al.*, 2020). To validate the anti-tumoural effects of *B. acidifaciens*, I treated the bladder tumour cells with bacterial supernatants of *B. acidifaciens* and its cross-feeding with *F. prausnitzii*, and compared the effects to *Bifidobacterium animalis* (an acetate-producer) and *F. prausnitzii* (a butyrate-producer) (Figure 88A). The pHs of GAM broth and all bacterial supernatants were neutralised to 7.2. The rationale for the cross-feeding of an acetate- and butyrate-producer is that the acetate is needed for butyrate production by the gut microbiota. Bacterial supernatants of *B. acidifaciens* and its co-culture with *F. prausnitzii* significantly increased the cytotoxic response of bladder tumour cells compared to the other supernatants. After 2 days of bacterial supernatant treatment, both 200 μL of *B. acidifaciens* ($P<0.001$ compared to control) and its cross-feeding with *F. prausnitzii* resulted in significantly lower cell viability levels (Figure 88B). After 2 days, significant results were found for four different volumes of bacterial supernatants, namely 25, 50, 100 and 200 μL (Figure 88C).

A

Gut microbiota	Metabolites
Bacteroides acidifaciens	?
Bifidobacterium	Acetate
Faecalibacterium prausnitzii	Butyrate
Co-culture of *BA+FP*	?
Co-culture of *Bif+FP*	Acetate & butyrate

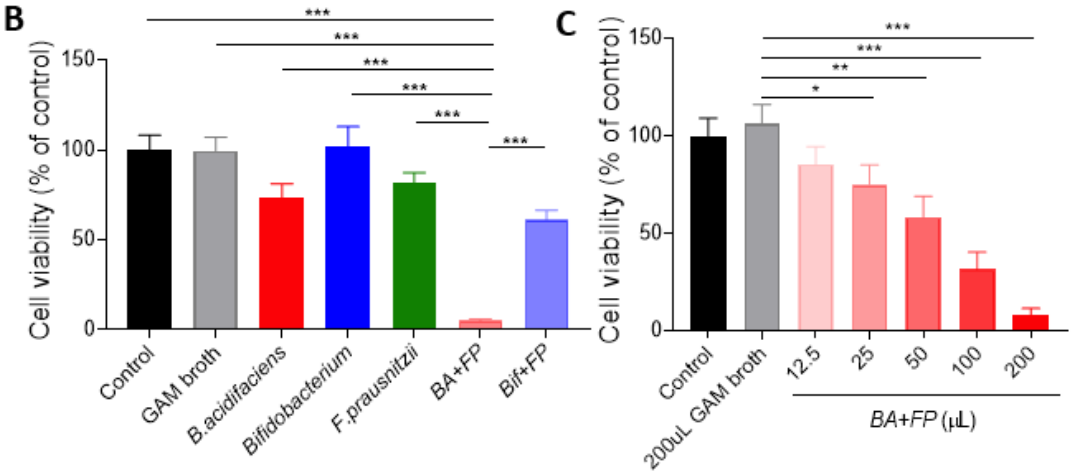


Figure 88 Bacterial supernatants from *B. acidifaciens* enhanced the cytotoxic response in bladder cancer cells. (A) The five bacterial supernatants used in this experiment. (B) The cell survival of RT112 cells treated with 200 µL of GAM broth or bacterial supernatants in 500 µL of medium in 24-well plate for 2 days(N=3). (C) The cell survival for 200 µL of GAM broth or different volumes of bacterial supernatants of *BA+FP* in 500 µL of medium in 24-well plate for 2 days (N=3). pHs of GAM broth and all bacterial supernatants were neutralised to 7.2. Control was just the cells in 500 µL of culture medium without any treatment. *BA+FP* denotes the co-culture of *B. acidifaciens* and *F. prausnitzii*, while *Bif+FP* denotes the co-culture of *B. animalis* and *F. prausnitzii.* Data are presented as mean ± SD. *P<0.05; **P<0.01; ***P<0.001.

7.2.2 Bacterial supernatants of co-cultures of *B. acidifaciens* and *F. prausnitzii* increased histone deacetylase inhibition and IR-induced DNA damage

Given that the histone deacetylase inhibition is a promising mechanism of radiosensitisation, I treated the RT112 human bladder cancer cell line with bacterial supernatants to determine the histone acetylation levels by western blot. The results showed that bacterial supernatants from the co-culture of *BA+FP* significantly increased histone acetylation of RT112 bladder cancer cells compared to blank GAM broth and the other supernatants (Figure 89A). Four hours after 5 Gy IR, there were significantly higher levels of DNA damage in *BA+FP* compared to their other supernatants as measured by γH2AX protein levels (Figure 89B).

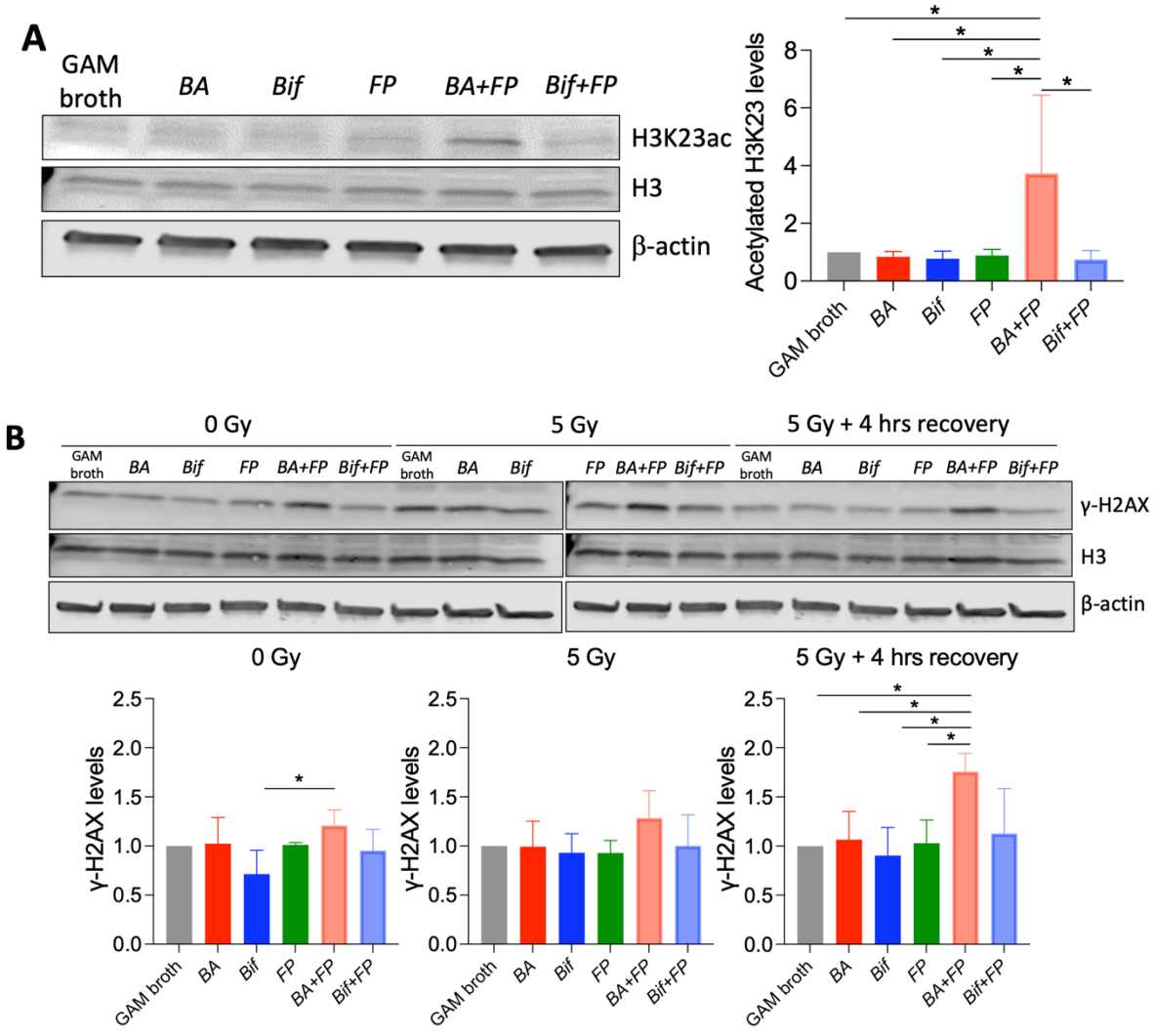


Figure 89 *BA+FP* increased histone acetylation levels and DNA damage in bladder cancer cells. Western blot analysis of histone acetylation (A, N=3) and γ-H2AX level (B, N=3) of RT112 cells treated with different bacterial supernatants in 6-well plate. Histone acetylation levels were determined after treating with 100 µL bacterial supernatants in 2 mL of medium for 24 hours. DNA damage was evaluated after treating with 5 Gy ionising radiation. pHs of GAM broth and all bacterial supernatants were neutralised to 7.2. *BA+FP* denotes the co-culture of *B. acidifaciens* and *F. prausnitzii*, while *Bif+FP* denotes the co-culture of *B. animalis* and *F. prausnitzii.* Data are presented as mean ± SD. *P<0.05; **P<0.01; ***P<0.001.

7.2.3 Bacterial supernatants of co-culture of *B. acidifaciens* and *F. prausnitzii* delayed IR-induced DNA damage repair in RT112 and T24 cell lines

Similar to the result in Figure 88B, treating RT112 cells with *BA+FP* supernatant demonstrated more γH2AX nuclear foci by immunofluorescence microscopy than each of the individual supernatants (Figure 90) and T24 (Figure 91). It is noted that the higher numbers of γH2AX nuclear foci in the *BA+FP* group compared to *BA* or *FP* occurred in a time-dependent manner and this implies the *BA+FP* causes delayed repair. The result also showed that *B. acidifaciens* conferred a stronger cytotoxic response (Figure 91A) and a delayed DNA damage repair (Figure 91B) compared to the other supernatants when combined with *F. prausnitzii* in T24 cells.

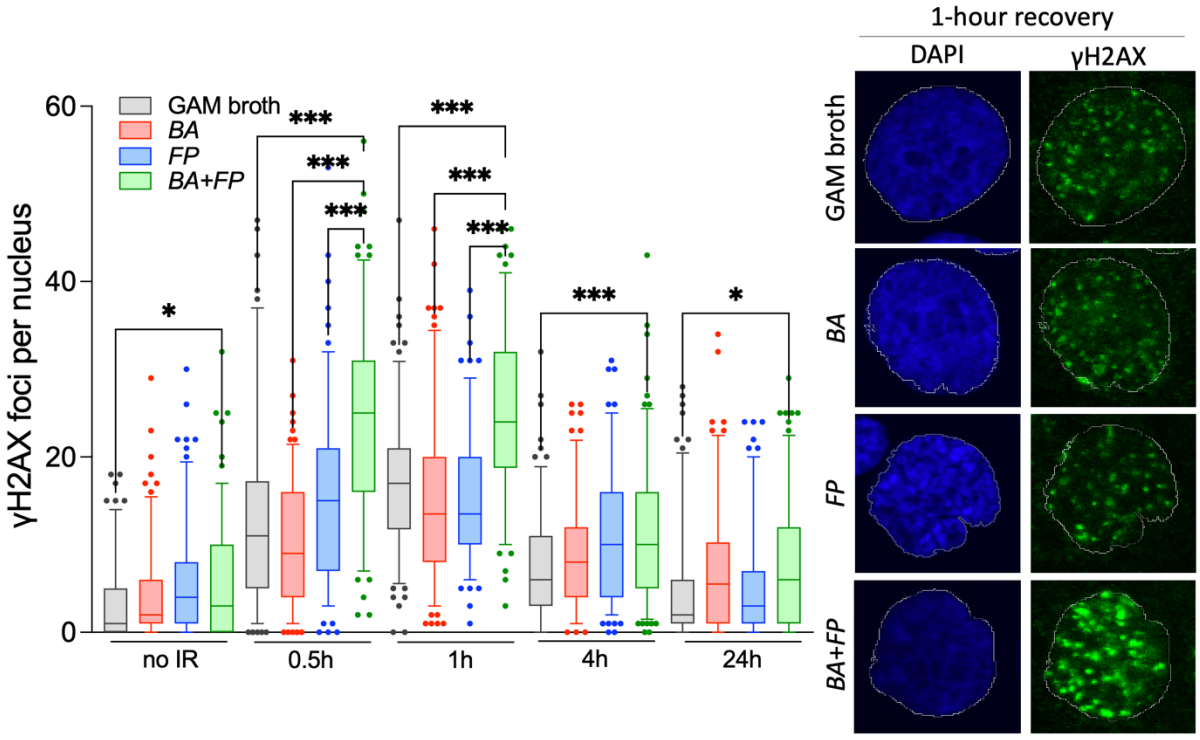


Figure 90 *BA+FP* increased histone acetylation levels and DNA damage in RT112 bladder cancer cells. Immunofluorescence microscopy analysis of γ-H2AX levels (N=3) in RT112 cells treated with 100 µL bacterial supernatants in 2 mL of medium in 6-well plate for 24 hours. DNA damage was evaluated after treating with 2 Gy IR. pHs of GAM broth and all bacterial supernatants were neutralised to 7.2. *BA+FP* denotes the co-culture of *B. acidifaciens* and *F. prausnitzii*, while *Bif+FP* denotes the co-culture of *B. animalis* and *F. prausnitzii.* Data are presented as mean ± SD. *P<0.05; **P<0.01; ***P<0.001.

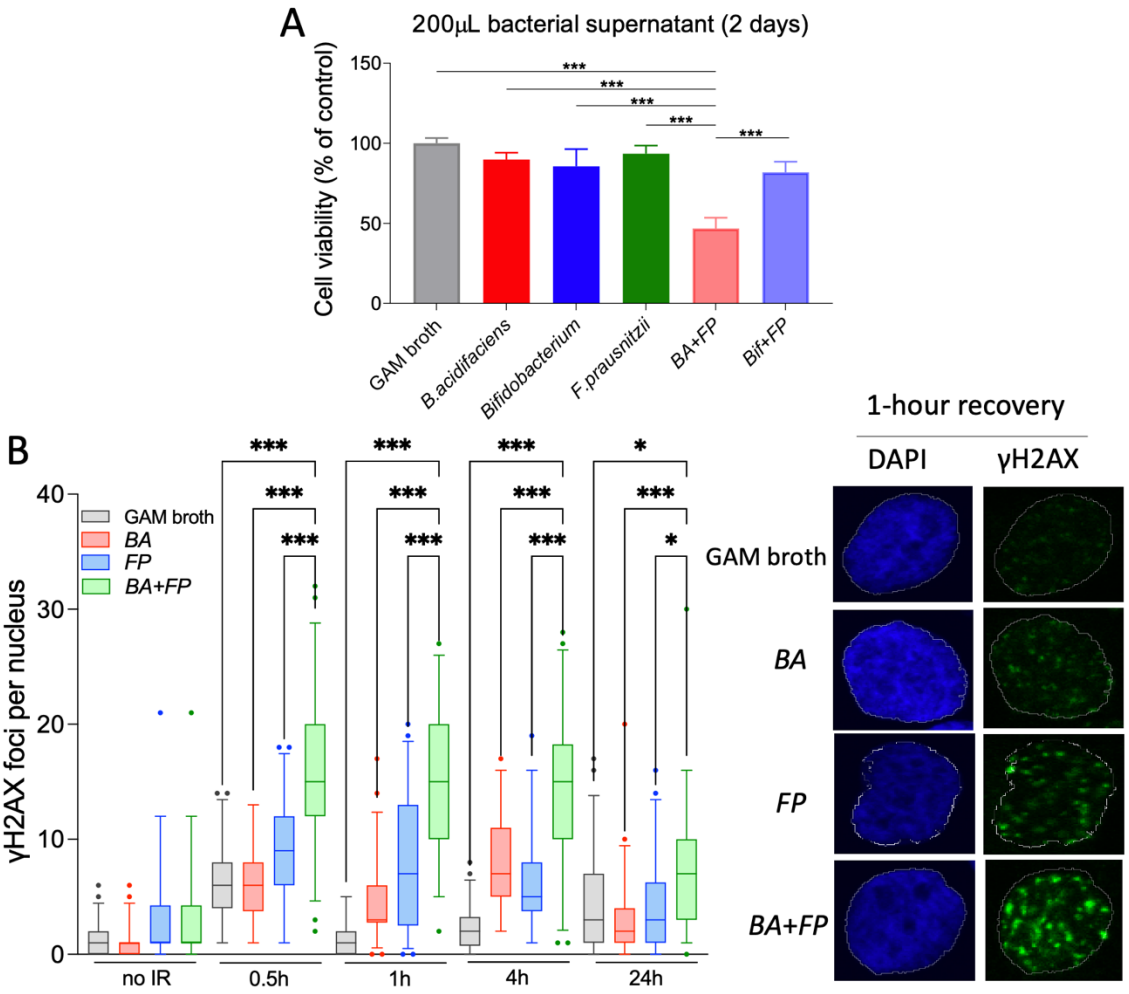


Figure 91 *BA+FP* increased histone acetylation levels and DNA damage in T24 bladder cancer cells. (A) The cell survival of T24 cells treated with 200 μL of GAM broth or bacterial supernatants in 500 μL of medium in 24-well plate for 2 days(N=3). (B) Immunofluorescence microscopy analysis of γ-H2AX levels (N=3) of T24 cells treated with 100 μL bacterial supernatants in 2 mL of medium in 6-well plate for 24 hours. DNA damage was evaluated after treating with 2 Gy ionising radiation. pHs of GAM broth and all bacterial supernatants were neutralised to 7.2. *BA+FP* denotes the co-culture of *B. acidifaciens* and *F. prausnitzii*, while *Bif+FP* denotes the co-culture of *B. animalis* and *F. prausnitzii.* Data are presented as mean ± SD. *P<0.05; **P<0.01; ***P<0.001.

7.2.4 Untargeted metabolomics analysis of bacterial supernatants

The PCA plot showed a notable clustering effect of metabolites profiling by bacteria (Figure 92). All supernatants were different from GAM broth, and *BA+FP* and *Bif+F*P were separated from the single bacterium alone. Butyrate (P=4.28E-10, FDR=9.26E-9), ADP P=2.8E-7, FDR=1.71E-6) and glutamylphenylalanine (P=7.41E-6, FDR=2.71E-5) were enriched in the supernatants of *BA+FP* and *Bif+FP* which had significantly higher cytotoxic responses shown in section 7.2.1, Figure 88B (Figure 93). There is currently no available literature on glutamylphenylalanine and cancer, but studies showed that gamma-glutamylphenylalanine was negatively associated with the risks of prostate cancer (Huang *et al.*, 2016) and chromophobe renal cell carcinoma (Priolo *et al.*, 2018).

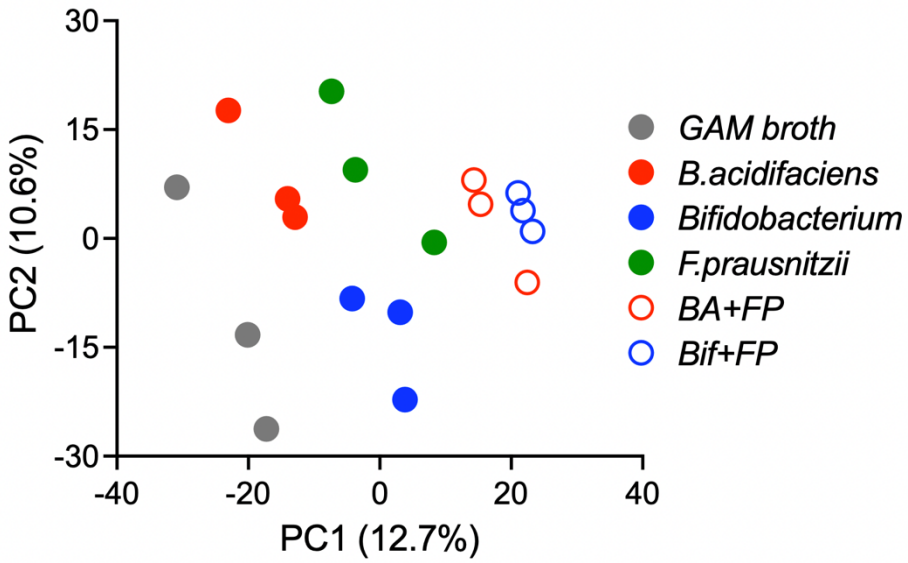


Figure 92 Principal component analysis of metabolomes in all bacterial groups. PCA plot of caecal metabolites in different bacterial supernatants, including GAM broth (solid grey), *B. acidifaciens* (solid red), *Bifidobacterium* (solid blue), *F. prausnitzii* (solid green), *BA+FP* (open red) and *Bif+FP* (open blue). A notable clustering effect by diets was seen in the metabolites. pHs of GAM broth and all bacterial supernatants were all neutralised to 7.2.

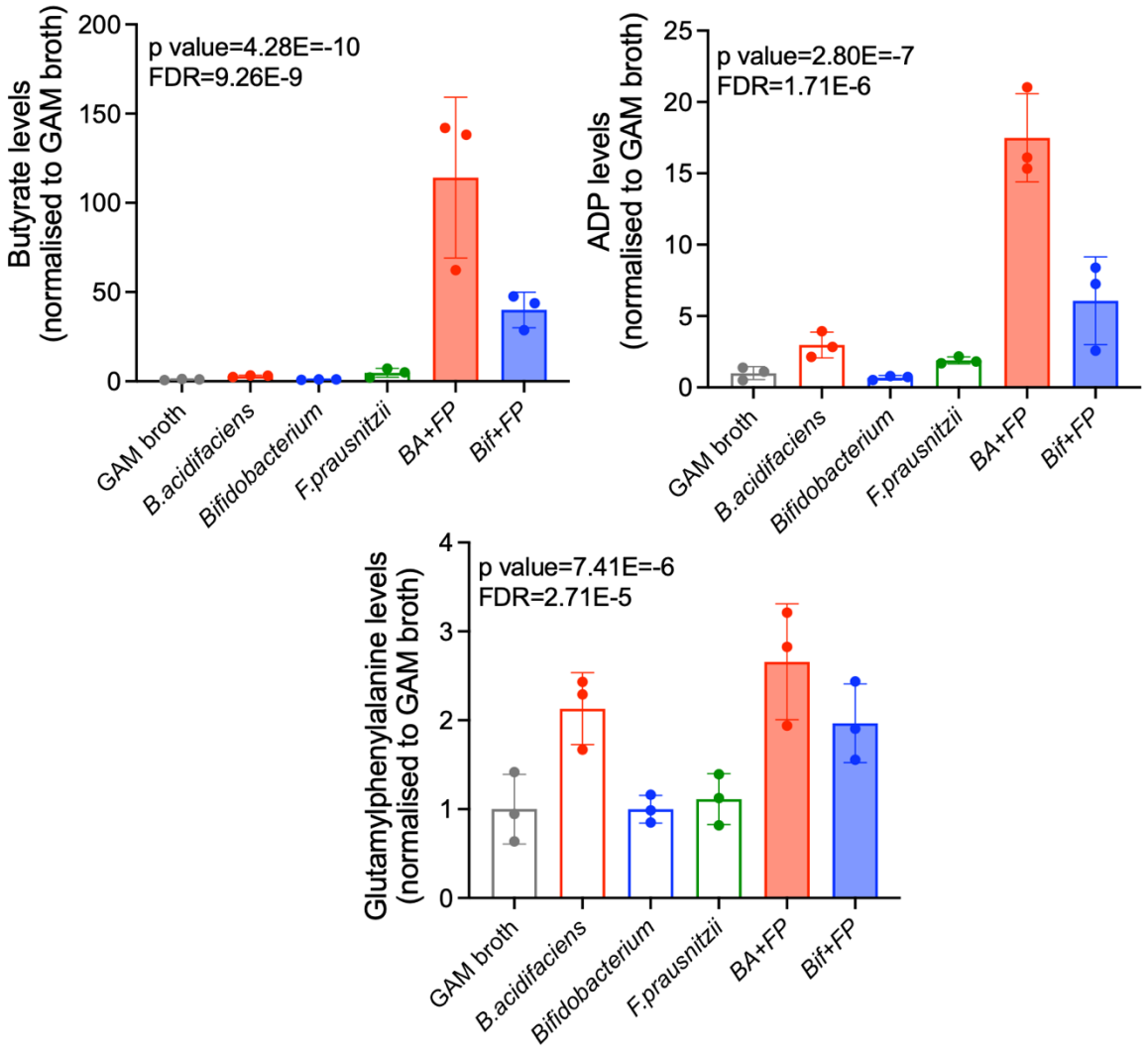


Figure 93 Metabolites enriched in the supernatant of *BA+FP*. Relative levels of (A) butyrate, (B) ADP and (C) glutamylphenylalanine in each bacterial supernatant. Data are presented as mean ± SD.

7.2.5 Bacterial supernatants conferred increased radiosensitivity in bladder cancer cells

I further studied the radiosensitising properties of bacterial supernatants of *BA+FP* by irradiating the bladder cancer cells from 0-8 Gy (Figure 94). Clonogenic assay showed that the supernatant can radiosensitise RT112 bladder cancer cells in a dose-dependent manner. It is noted that the concentration of 100 μL bacterial supernatant in 2 mL medium is the IC10 obtained from the cell viability assay.

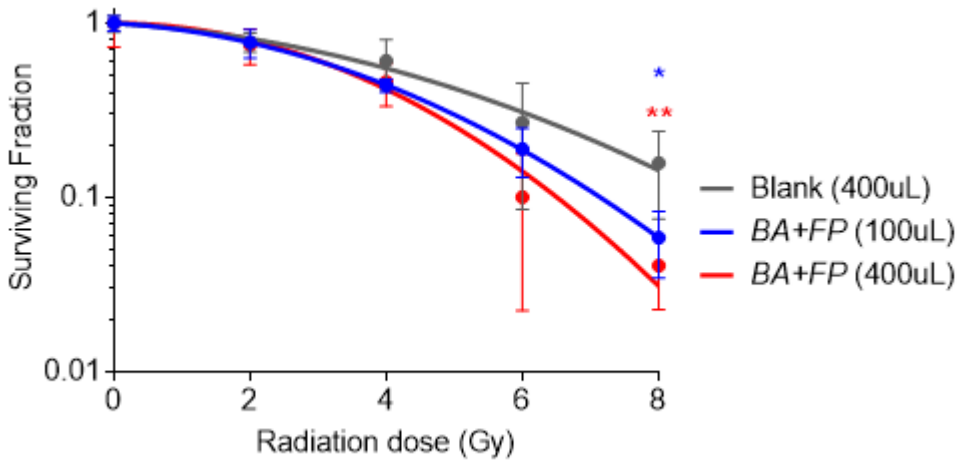


Figure 94 SCFAs conferred increased radiosensitivity in bladder cancer cells. (A) Linear quadratic survival curves of RT112 cells treated with 100 or 400 μL bacterial supernatant from *BA+FP* for 24 hours before receiving irradiation of 0-8 Gy (N=3). Data are presented as mean ± SD. *P<0.05; **P<0.01; ***P<0.001.

7.3 Discussion

Cell experiments showed that SCFAs reduce cell proliferation in liver cancer (Bindels *et al.*, 2012), induce apoptosis in lung cancer (Kim *et al.*, 2019), and do both in breast cancer (Semaan *et al.*, 2020). Consistent with the experiments in the other cancer cells, all three short-chain fatty acids inhibited the proliferation of bladder cancer cells. It is noted that the combination of SCFAs in a physiological ratio conferred a stronger phenotype. Both butyrate and propionate have been proposed to increase histone deacetylase inhibition (Silva *et al.*, 2018), which is a known mechanism of cellular radiosensitisation (Donohoe *et al.*, 2012). SCFAs also increased histone acetylation levels and increased tumour radiosensitivity in bladder cancer cells. As expected, butyrate had the strongest effect of these phenotype compared with propionate and acetate as shown in the previous study (Sunkara *et al.*, 2012).

Furthermore, *B. acidifaciens* was identified as a potential radiosensitiser because its abundance positively correlated with tumour response to radiation (Then *et al.*, 2020). Consistent with our findings, a high-fibre diet markedly increased the prevalence of *B. acidifaciens* (Li, Elmen*, et al.*, 2020; Marques *et al.*, 2017). Our recent data showed that the relative abundance of this bacterium can be increased by inulin in C57BL/6 and FVB mice and by psyllium and resistant starch (section 3.3.2). *B. acidifaciens* was first isolated in 2000 (Miyamoto & Itoh, 2000) and there is lack of the knowledge of this bacterium, particularly its anti-tumourigenic properties. The Bacteroides family are considered as acetate-producers (Miller, 1978; Robert *et al.*, 2007) and acetate is a necessary substrate for butyrate production. In my experiments, *B. acidifaciens* not only conferred a stronger phenotype of cytotoxic response compared to the well-known acetate producer (O'Callaghan & van Sinderen, 2016), *B. animalis*, or the butyrate producer, *Faecalibacterium prausnitzii*, but its co-culture with *FP* also outperformed the co-culture of *B. animalis* and *FP*. The metabolomics analysis showed that *B. acidifaciens* can produce more butyrate when co-cultured with *FP*, indicating a higher fermentation in this co-culture compared to either single bacterium alone or *B. animalis*+*F. prausnitzii*. However, studies suggest that a broad range of gut microbiota-derived metabolites can enhance anti-tumoural effects or tumour response to anti-cancer

treatments (Johnson *et al.*, 2016), so future work should include identifying radiosensitisers other than SCFAs with similar profiles from the global metabolomic analysis of *B. acidifaciens* or indeed a Clostridiales order that negatively correlated with tumour growth in the psyllium plus inulin group.

In our previous study, a predictive metagenomics study of the gut microbiota in responders with a higher abundance of *B. acidifaciens* was rich in carbohydrate metabolism pathways. This implies a higher level of fibre fermentation occurring in responders, reflecting the selection of bacteria more able to ferment carbohydrates. This could result in more SCFA production in the faeces. The result in section 7.2.4 showed that *B. acidifaciens* does indeed work much better together with *F. prausnitzii* (butyrate producer) compared to *B. animalis*, as the former co-culture produced a significantly higher level of butyrate. In addition, from the three experiments (section 4.3, 4.4 and 5.1) of this study, I demonstrated that high dietary fibre induced significantly higher caecal SCFAs levels and the caecal butyrate level was associated with tumour control in mice fed psyllium plus inulin.

One of the important qualities of the gut microbiota is that the bacteria always work together to achieve physiological function (Henriques *et al.*, 2020). Therefore, bacterial supernatants might be better tools to elucidate the radiosensitisation mechanism of gut microbiota on cancer cells rather than single metabolites. The major limitation of this cell experiment is that the metabolites levels that can be achieved in plasma and tumours remain to be determined, but I showed that some might have stronger effects than others. Metabolites might accumulate in cancer cells due to the Warburg effect, and furthermore, bacterial supernatants might influence a broad range of different immune cells and the tumour microenvironment which could not be studied in such cell experiments.

In our case, cell experiments showed that butyrate, among the other SCFAs, conferred the strongest cytotoxic and HDAC inhibiting effects on bladder cancer cells, and a mixture of SCFAs generated a stronger phenotype. Wei *et al.* also showed that high dietary fibre can increase butyrate level in plasma and also in lymphoma cells due to the Warburg effect (Wei *et al.*, 2016). This is the only study published to date regarding SCFAs levels in tumours

outside the intestine and our study supports this by showing the positive correlation between the caecal butyrate levels and tumour control in mice fed psyllium plus inulin. Further work is required to gain more knowledge regarding SCFA metabolism in non-gastrointestinal tumours. Besides SCFAs, there may be other metabolites present in a low concentrations in the tumour or blood circulation but still strong enough to have an effect on the cancer cells, which should be investigated in a future untargeted metabolomics study.

Chapter 8: Discussion

8.1 Novelty of dietary fibre and gut microbiota study for bladder cancer

There is an urgent clinical need to discover new radiosensitisers, as elderly patients with pelvic malignancies who receive chemoradiation may not always tolerate the toxicity of chemotherapeutic drugs. Dietary fibre and its resulting modified gut microbiota are ideal experimental targets, with mounting evidence showing their beneficial effects in increasing tumour control (Li, Elmen*, et al.*, 2020), enhancement of anti-cancer treatment efficacy (Spencer *et al.*, 2021), and even mitigation of radiotherapy side-effects (Murphy *et al.*, 2000). Dietary fibre, and the gut microbiota and their metabolites have been widely studied in immunotherapy (Gopalakrishnan *et al.*, 2018) and colorectal cancer (Yu *et al.*, 2017), but studies looking into their role in radiotherapy and cancers outsides of intestine are limited. There are only two studies using antibiotics as an approach to modify RT effectiveness, in melanoma, lung, and cervical cancer models (Uribe-Herranz *et al.*, 2020) and to diminish the RT effect in a breast cancer model (Shiao *et al.*, 2021). To my knowledge, we were the first to use dietary fibre to enhance radiosensitivity in an immunocompromised bladder tumour model (Then *et al.*, 2020). In addition, we also showed that dietary supplementation is effective in mitigating radiotherapy-induced diarrhoea in a systematic review (Bartsch *et al.*, 2021). However, our previous tumour experiment was done in an immunocompromised model and did not provide us with information on the involvement of immunomodulation and the metabolomes. In this thesis, I explored in depth that how dietary fibre, including psyllium, resistant starch, and inulin, and their subsequently modified gut microbiota enhanced bladder tumour response to RT (Chapter 4) and mitigated RT side effects (Chapter 5). I also explored the association with their metabolomic profiles (Chapter 4) and immune response (Chapter 6). In addition, I also investigated the effects of *B. acidifaciens*, a potential radiosensiting bacteria found in our previous project (Then *et al.*, 2020), on cell survival and radiosensitivity of bladder cancer cells.

8.2 Psyllium-containing diets are safe to use mice

In this thesis, there were four sets of experiments in non-tumour bearing mice and another three sets in tumour-bearing mice. They were fed with modified diets, namely, 0.2% cellulose, 5% psyllium, 5% psyllium plus 10% resistant starch, and 5% psyllium plus 10% inulin, from at least two weeks up to 9 weeks. No abnormalities of appearance or behaviour were observed throughout the experiments, and all stably maintained weight gain. Thus, the mice could well tolerate these high fibre diets and it is noted that the 5% psyllium plus 10% RS and 5% psyllium plus 10% inulin have not been used other mouse experiments before. Juan *et al.* showed that inulin lowered weight gain in rats (Rendon-Huerta *et al.*, 2012). A study of the influence of dietary fibre on intestinal and hepatic carbohydrate responses in C57BL/6 mice have shown that a combination of 5% cellulose plus 3.5% psyllium and 3.5% inulin did not slow down weight gain compared to 5% cellulose alone, 5% cellulose plus 7% psyllium, or 5% cellulose plus 7% inulin alone (Pontifex *et al.*, 2021). However, the physiology of preclinical mouse models can be different to humans (Holscher, 2017). Rodent trials frequently supplement fibre at 5–20% weight/weight of feed and the translation of these doses in humans is often an unattainable amount. For example, 5% of the diet as fibre is at least 20 grams/day for adult humans. It is noted that the Scientific Advisory Committee on Nutrition (SACN) recommends that human should be aiming for over 30 grams/day of dietary fibre intake (O'Connor & Crosswaite, 2018). If the fibre of interest is highly fermentable, e.g., inulin-type fibres, this dosage is near the top of the tolerable limit for human consumption. Consumption at this level is likely to result in unpleasant side effects such as gas, bloating, and diarrhoea (Grabitske & Slavin, 2009). Recently, Gunn *et al.* showed that 20 grams of psyllium can reduce gas production caused by 20 grams of inulin in a human MRI study whilst maintaining fermentation, found by *in vitro* testing (Gunn *et al.*, 2021). Other fibres, such as polydextrose and soluble corn fibre, have been shown to be tolerable up to 50 grams/day in clinical trials (Flood *et al.*, 2004). This suggests that adding psyllium together with inulin and resistant starch should be well tolerated in human patients, although further human volunteer studies are needed. This current study provides important knowledge that the

combinations of these high dietary fibres can be safely used in preclinical mouse models as they can enhance the production of short-chain fatty acids.

8.3 Psyllium-containing diets increased bacterial fermentations

Three of my studies all showed that psyllium and its combination with RS or inulin significantly increased caecal weight, which could be due the bulking effect of dietary fibre that increases water content (Morita *et al.*, 1999; Pontifex *et al.*, 2021). Notably, rodents are caecal fermenters, and this implies that higher levels of fermentation might occur in mice fed with psyllium containing diets. Psyllium containing diets increase acetate, propionate, and butyrate levels as shown sections 4.3.4 and 5.1.6. It is noted that they were even higher when given together with the high soluble fibres resistant starch and inulin. Psyllium plus inulin had the highest levels of all SCFAs, which is consistent with the gut microbiota profiles. In this, *B. animalis*, an acetate producer, overrides the other bacteria, and acetate is needed for butyrate production. Hoffman *et al.* also showed that inulin increased caecal size and both blood and caecal SCFAs production in a C57BL/6 mice Alzheimer's disease model (Hoffman *et al.*, 2019), which was consistent with my result that the psyllium plus inulin group had the highest levels of all SCFAs. In addition, enlargement of the caecum has been suggested to be a result of increased microbial content, which is also consistent with our findings (Kuo *et al.*, 2013). These results suggest that dietary supplementation with inulin causes increased fermentation in the caecum, leading to increased production of SCFAs.

In addition, Morita *et al.* found that caecal and faecal butyrate and total SCFAs concentrations were significantly higher in rats fed 5% high amylose corn starch (HAS) and 1.5% psyllium plus 5% HAS diets, compared to those fed the 0% HAS and 0% HAS plus 1.5% psyllium diets in the setting of 65% low amylose corn starch as the base diet (Morita *et al.*, 1999). The HAS/PS diet maintained higher butyrate concentrations throughout the large intestine while the butyrate and total SCFA concentrations in rats fed the HAS diet decreased along the length of the colon and faecal butyrate concentration was reduced to one-third of that in the caecum. This suggests that psyllium and high fermentable fibre can maintain SCFA production along the large intestine.

8.4 Psyllium plus inulin increased tumour control with or without IR, with enhancement of SCFAs and immune responses

In this study, I showed that psyllium plus inulin slowed tumour growth with or without irradiation in bladder tumours which was associated with both enhanced metabolite production and immunomodulation. It is noted that psyllium plus inulin significantly increased SCFAs levels, especially butyrate, and local tumour (particularly CD8 T cells) compared to the other dietary groups. The tumour response to IR was associated with the abundance of a Clostridiales order which supports the hypothesis that the tumour effect of dietary fibre could be via modification of gut microbiota. Consistent with this result, Li *et al.* also showed that 15% inulin inhibited tumour growth and increased MEK inhibitor efficacy in a mouse melanoma model (Li, Elmen*, et al.*, 2020). This was achieved by anti-tumour immune responses and the tumour control was associated with the enhancement of butyrate-producing bacteria. I also found that the Clostridiales order and the Lachnospiraceae family, positively associated with IR response in mice fed with psyllium plus inulin, were of the butyrate-producing taxon. Indeed, I found that this group of mice had the highest caecal butyrate levels. However, short-chain fatty acids administered in drinking water were not sufficient to confer delayed tumour growth. This could be due to lack of SCFAs reaching the large intestine to interact with immune cells as they can be absorbed in small intestine or degraded due to its very short plasma half-life (Miller *et al.*, 1987), emphasising the importance of the stable production of SCFAs production by dietary fibre and the gut microbiota in the colon. In addition, anti-tumour effects might be conferred by other key metabolites other than SCFAs, such as threitol (part of the chemotherapy drug, Treosulfan) and inosine (previously shown to increase immunotherapy efficacy via activation of CD8 T cells) (Mager *et al.*, 2020). Spencer *et al.* also showed that high dietary fibre increased the efficacy of melanoma immunotherapy in both mouse and human. This phenomenon was associated with the enhancement of T cell function, also seen in this study (section 6.3.2) (Spencer *et al.*, 2021). However, this effect was diminished when combining the dietary fibre with probiotics – *Lactobacillus* or *Bifidobacterium*. This led me to conclude that dominance of these probiotic species may have overridden the gut microbiota that

could have enhanced the efficacy of anti-cancer treatments. This evidence supports dietary fibre as a better approach to enhance the tumour control rather than a small number of specific bacteria, because it can shape the whole gut microbiota to a more favourable profile, with more diverse metabolites produced.

8.5 Psyllium plus RS increased tumour control combined with IR, with enhancement of SCFAs and other metabolites but not immune response

To date, there are limited studies related to the role of resistant starch in cancers outside of colorectal cancer. One showed a negative association between resistant starch and breast cancer risk (Tajaddini *et al.*, 2015) and the other showed that resistant starch decreased tumour size in a mouse pancreatic cancer model (Panebianco *et al.*, 2017). In this study, I showed that psyllium plus RS did not on its own cause tumour growth delay, but when IR was added the effect on tumour growth was more marked than that of psyllium plus inulin. Local tumour immune response was not enhanced by psyllium plus resistant starch, without or with irradiation, which suggests that immunomodulation is not the underlying mechanism of radiosensitisation. From the non-targeted metabolomic analysis, four out of the top fifteen metabolites enriched in mice fed with psyllium plus resistant starch have previously been shown to have anti-tumourigenic effects. They are caproic acid in skin and cervical cancers (Narayanan *et al.*, 2015), taurine in lung cancer cells (Tu *et al.*, 2018), 5,7-dihydroxyflavone in leukaemia and cervical carcinoma cells (Zhang *et al.*, 2013), and butyrate in breast cancer cells (Salimi *et al.*, 2017). Therefore, the radiosensitising effect of psyllium plus resistant starch was probably modulated by the enhancement of metabolites. Cell experiment showed that a combination of SCFAs can reduce cell viability more than a single SCFA alone. This implies that the metabolites may not need to reach to a high level to achieve HDAC inhibition, as they might act synergistically with a relatively low concentration of each individual metabolite or act on G-protein-coupled receptors that operate in a low concentration environment (Priyadarshini *et al.*, 2018).

8.6 Psyllium plus RS and psyllium plus inulin rescued crypt survival at high IR dose and all psyllium-containing diets prevented the delayed weight gain post IR

Psyllium plus resistant starch and psyllium plus inulin rescued more crypts from 14 Gy irradiation compared to the psyllium alone and 0.2% cellulose groups. This is consistent with a previous finding that 15% oat bran decreased the degenerating crypts and increased crypt fission, the division of a single crypt into two daughter crypts for normal tissue growth and maintenance, one week post irradiation with four fractions of 8 Gy (in total of 32 Gy) in C57BL/6 mice (Malipatlolla *et al.*, 2019). In addition, both acute (section 5.1) and late (section 5.2) toxicity experiments showed that irradiation caused a delayed weight gain in mice fed with 0.2% cellulose, but not in the other psyllium-containing diet groups. This delayed weight gain happened within one week post irradiation and resolved afterward. Romesser *et al.* found that the body weight of mice receiving 12 and 14.5 Gy whole abdominal irradiation dropped up to 30% within 2 weeks post irradiation (Romesser *et al.*, 2019), but there was only a slight weight loss within 5% in 0.2% cellulose group in our experiments, probably due to the irradiation being only focused at the lower pelvic area. Similar to human patients, mice exposed to high doses of radiation experience abnormal stool production as a result of damage to the intestinal epithelium (Levy *et al.*, 2020). The body weight loss could be an outcome of local gut and systemic inflammation as shown in colitic mice using a mouse model of ulcerative colitis (Engman *et al.*, 2018). It is noted that gastrointestinal inflammation is a common feature of both pelvic radiation disease and inflammatory bowel disease, so dietary fibre could protect the radiation-induced gut injury probably via suppression of inflammation. Malipatlolla *et al.* also showed that 15% oat bran managed to reduce the systemic pro-inflammatory cytokine levels from one to 18 weeks post irradiation of the colorectal region (Patel *et al.*, 2020). In addition, Ji *et al.* showed that 1% inulin increased SCFA-producing bacterial abundance and faecal SCFAs concentration, and successfully mitigated the radiation-induced colonic fibrosis in C57BL/6J mice (Ji *et al.*, 2022). Therefore, the result in the current study demonstrated that high dietary fibre diets provide benefits to mice in the early stages post-irradiation probably due to the reduction of

local gut and systemic inflammation and it was probably associated with the increased caecal SCFAs levels.

I also noted that delayed weight gain occurred in mice fed with 0.2% cellulose with bigger tumours. Previous studies showed that the tumour-bearing status of mice caused body weight loss and increased levels of cytokine expression of spleen cells (Gomez-Ambrosi *et al.*, 2002; Murray *et al.*, 1997) which implies that the body weight loss could be due to systemic inflammation. High fibre diets in mice significantly increased production of SCFAs that have anti-inflammatory properties (Eslick *et al.*, 2022). This means that high dietary fibre may prevent the mice from experiencing stress, which presents as weight loss. In addition, the delayed weight gain which occurred in the 0.2% cellulose group could also be due to the poorer tumour control or the smaller caecal size. Therefore, further studies are needed to determine the detailed mechanisms of how dietary fibre can protect tumour-bearing mice from weight loss.

8.7 The role of butyrate in cancers outside the intestine

Cell experiments showed that SCFAs conferred radiosensitisation in bladder cancer cells (Then *et al.*, 2020). It remains unclear whether butyrate or butyrate-producing bacteria or the other gut microbiota can enhance or abrogate the efficacy of radiotherapy. Park *et al.* showed that butyrate enhanced radiation-induced cell death of colorectal cancer patient-derived organoids (Park *et al.*, 2020). Shiao *et al.* also showed that an antibiotic cocktail of ampicillin, imipenem, cilastatin, and vancomycin reduced the efficacy of radiotherapy in mouse mammary tumours (Shiao *et al.*, 2021), but Yang *et al.* found that reduction of butyrate-producing bacteria by vancomycin can increase anti-tumour immune responses to IR in mouse colorectal tumours (Yang *et al.*, 2021). This evidence together suggested that, in colorectal cancer, butyrate was associated with increasing RT efficacy in cell experiments but reduced RT efficacy in the mouse immunocompetent model. However, this might not be applicable to cancer models outsides the gastrointestinal tract since butyrate might not be able to accumulate in tumours to the high levels seen in colorectal tumours that are directly exposed to the gut lumen. There was only one study showing that butyrate can accumulate

in lymphoma (Wei *et al.*, 2016). Our results in section 4.4.9 showed the significant negative association between caecal butyrate levels and tumour growth in both the IR and non-IR cohorts of mice fed with psyllium plus inulin. This association however does not provide direct evidence to support butyrate or butyrate-producing bacteria being involved in the tumour control or radiosensitisation, so more evidence is needed to make conclusion, for example, an oral gavage experiment of butyrate-producing fibre and bacteria in specific pathogen-free (SPF) mice.

8.8 Different gut microbiota profiles between tumour-bearing and non-tumour bearing mice

In this current study, tumour-bearing and non-tumour bearing mice had different gut microbiota profiles when fed with either psyllium or psyllium plus RS. It has been noted that there is a complex crosstalk between the gut microbiota and systemic immunity as the antimicrobial peptides, cytokines and the other components of innate immune system can determine the colonisation of gut bacteria (Zheng *et al.*, 2020). This suggests that tumour status affects the gut microbiota, probably due to systemic alterations in immunity, as peripheral solid tumours often induce a systemic inflammatory state that correlates with tumour growth in mouse models and cancer patients (Diakos *et al.*, 2014; Rutkowski *et al.*, 2015). Although the psyllium group had more similar gut microbiota profiles to psyllium plus inulin in non-tumour bearing mice, psyllium still had a more similar metabolomics profile to psyllium plus RS, as seen in both tumour-bearing and non-tumour bearing mice. This implies that the dietary fibre might be a dominant factor for the metabolite production. In addition, higher levels of SCFAs and better tumour control were observed in psyllium plus RS, a butyrate-producing fibre, compared to psyllium although they had similar gut microbiota profiles. Both psyllium plus resistant starch and psyllium plus inulin had better outcomes in terms of tumour control and mitigation of RT-induced sides effect compared to psyllium alone. This suggests that both the prebiotics (i.e dietary fibre) and the probiotics (i.e gut microbiota) are important for achieving better outcomes.

8.9 Limitations

One of the major limitations of this thesis was that all mouse experiments used a subcutaneous flank tumour model instead of an orthotopic model.

The orthotopic model would have presented some difficulties. The growth of BBN-induced orthotopic bladder tumours in K5.Stat3 mouse was highly heterogenous which required a very large sample size. In addition, it took 4 weeks to develop carcinoma in situ and 8 weeks to develop muscle-invasive bladder tumour which was highly time consuming. The only way to monitor orthotopic bladder tumours was to perform ultrasound scanning at 8 weeks post BBN treatment which was time- and cost-consuming for a big mouse experiment.

In light of these, I chose a flank subcutaneous mouse tumour model that was more feasible for a 3-years DPhil project. I hypothesised that the tumour control was achieved by the effects of systemic metabolites and systemic immune responses which can be validated in a subcutaneous model.

In addition to the limitation above, I also realised that the gut microbiota was different between tumour-bearing and non-tumour bearing mice. This can be due to the systemic immune effects of the tumour status, so the normal tissue toxicity experiment using the non-tumour bearing mice may not recapitulate the clinical situation of the gut tissue of cancer patients receiving radiotherapy. Therefore, I hope to use a tumour-bearing mouse model where we can irradiate the lower abdomen and flank tumour simultaneously in the future.

8.10 Co-culture of *B. acidifaciens* and *F. prausnitzii* increased bacterial fermentation and conferred stronger phenotypes compared to other bacteria

B. acidifaciens was identified as a potential radiosensitiser in our previous study because its abundance was positively correlated with tumour response to irradiation (Then *et al.*, 2020). Cell experiments showed that co-cultures of *B. acidifaciens* and *F. prausnitzii* produced significantly higher levels of SCFAs and conferred stronger phenotypes of cytotoxicity compared to each single bacterium alone, or indeed the other well-known acetate producer, *B. animalis*. This bacterium was first isolated in 2000 and got its name because the isolates reduced the pH level of peptone-yeast broth with Fildes' digest (Miyamoto & Itoh, 2000). Another study also revealed that *B. acidifaciens* was enriched in normal humans, compared to patients with inflammatory bowel disease (Ott *et al.*, 2004). The effect of this bacterium on tumour growth is still controversial. A study showed that increasing *B. acidifaciens* was seen in hepatocellular carcinoma which was induced by a streptozotocin-high fat diet (Xie *et al.*, 2016). However, *B. acidifaciens* reduces isoflavones, a chemical that is associated with increased risk of breast cancer (Renouf & Hendrich, 2011). In contrast, *B. acidifaciens* has been shown to contribute to the anti-tumour effect of medicinal Gynostemma saponins (Chen *et al.*, 2015). In my studies, I provided direct evidence that *B. acidifaciens* has anti-tumourigenic properties and it works better together with butyrate-producing bacteria compared to the other acetate producer. This also suggests the need to build a collection of combinations of bacteria, including *B. acidifaciens* and other butyrate producers, to pursue a better response instead of using a single bacterium alone. This was shown in a previous study of a consortium of 11-strains, primarily rare, low-abundance components of the human microbiota, which enhanced the therapeutic efficacy of immunotherapy in a mouse colorectal cancer model (Tanoue *et al.*, 2019).

8.11 Other evidence for and against the role of the gut microbiota in radiotherapy

To date there have been two main strategies, namely, using antibiotics or dietary fibre, in studying the role of the gut microbiota in the efficacy of anti-cancer treatment in preclinical cancer models of extra-gastrointestinal tumours. Both these strategies have been explored in immunotherapy of mainly melanoma. In studies involving radiotherapy and extra-gastrointestinal tumours, Shiao *et al.* used an antibiotics approach to diminish the RT effect in a breast cancer model (Shiao *et al.*, 2021) and Uribe-Herranz *et al.* used antibiotics to modify RT effectiveness in melanoma, lung, and cervical cancer models (Uribe-Herranz *et al.*, 2020), while our RT112 CD-1 nude and UPPL1591 C57BL/6 experiments were two using dietary fibre to modify the gut microbiota. In this latter study, I not only confirmed the beneficial effects of inulin on tumour control, but I also showed that psyllium plus resistant starch and psyllium plus inulin were favourable dietary fibre combinations to improve radiotherapy efficacy and also mitigate the side effects of RT at an early stage. In terms of dietary fibre, pectin is a potential candidate as it has all the properties of being highly fermentable, highly soluble, and highly viscous, that were found in the combination of psyllium plus RS and psyllium plus inulin. The dietary fibre pectin promotes high faecal bacterial diversity, growth of bacteria with anti-inflammatory properties, and butyrate (SCFA) production (Lewis *et al.*, 2019; Xie *et al.*, 2020).

8.12 Importance of the work and how it could lead to patient benefits

In this thesis, the results showed that psyllium plus either resistant starch or inulin not only increased tumour growth delay combined with irradiation, but also prevented the delay in time to gain weight and increased the remaining small intestinal crypts post-irradiation. This suggests that these dietary fibres achieve a more favourable therapeutic ratio compared to 0.2% cellulose and psyllium alone by increasing tumour response and mitigating the IR-induced side effects. An in-depth understanding of the mechanisms involved immunity and metabolomes will ultimately help take our findings forward to a clinical trial in radiotherapy

patients. This approach has the potential to improve patient outcomes at a low cost and minimal distress to patients.

Conclusions

I demonstrated that dietary fibre supplements increased the radiation response of bladder tumours, with associated gut microbiota modification and enhancement of immune responses and metabolite levels. Since psyllium plus either RS or inulin achieved a more favourable therapeutic ratio with improved tumour control with decreased side effects, I propose that dietary fibre supplements may be useful adjuncts to radiotherapy in patients with pelvic malignancy.

Future work

In this study, psyllium plus resistant starch and psyllium plus inulin have been proven to enhance tumour control when combined with irradiation and to mitigate IR-induced intestinal side effects. It is noted that these phenotypes were associated with modified gut microbiota, metabolomes, and immune responses. With these promising findings, future studies are still needed to clarify the in-depth mechanisms, to provide evidence of the causal effects of the gut microbiota, the metabolome and immunity, and to explore the other potential dietary fibres (such as pectin) or combinations to maximise the therapeutic ratio of radiotherapy.

The results showed that immunomodulation is not likely to be involved in the radiosensitising effects of psyllium plus RS, as the local immune response was not enhanced, and was even suppressed, in both the dietary fibre and UPPL1591 tumour without and with irradiation experiments. Further experiments are needed to discover the key critical metabolites for radiosensitisation. In addition, we also need to investigate whether resistant starch or inulin alone is sufficient to enhance the IR responses and whether a combination of RS and inulin could be another promising approach. Besides resistant starch and inulin, pectin is also another potential candidate as it has all the advantages of dietary fibre as it is highly soluble, viscous, and fermentable (Table 15). After identifying the best fibre regimen to enhance the RT efficacy, a human trial should be performed to study if it can achieve the same outcomes as seen in mice.

Table 15 Physiochemical characteristics of common dietary fibres.

Fibre type	Common sources	Physiochemical characteristics		
		Solubility	Viscosity	Fermentability
Cellulose	All green plant cell walls	Insoluble	Non-viscous	Low
Psyllium	Seeds of Plantago	Low to medium	Medium	Low
Resistant starch (RS-2)	Cereals, raw legumes, raw fruits, vegetables	Low	Non-viscous	High
Inulin	Cereals, fruits, vegetables	Medium to high	Low to high	High
Pectin	Fruits, vegetables, legumes	High	Medium to high	Medium to high

In addition, it is also important to investigate the detailed local tumour immune response, particularly at an early timepoint (i.e. 3 and 7 days) as immune cells, such as macrophages, neutrophils, and NK cells, may wane by the time tumours grow to 700 mm^3. A previous study has shown that the tumour control was due to the early initiation of immune response by anti-cancer treatments (O'Brien *et al.*, 2021). The information on the early immune response may allow us to maximise the tumour control by introducing more specific gut bacteria, metabolites or immunomodulatory molecules, or by adjusting the IR doses.

To prove the causal relationship between the gut microbiota and radiosensitisation, we need to perform oral gavage of specific gut bacteria in SPF mice. *B. acidifaciens*, other human SCFA-producers and inosine-producing bacteria could be potential first candidates. Cell experiments showed that higher levels of cytotoxic responses and DNA damage can be caused by the co-culture of *B. acidifaciens* with butyrate-producing bacteria (i.e. *F. prausnitzii*). This suggests that the co-operation or cross-feeding of gut microbiota might be needed. Besides, several studies show that the gut microbiota can produce inosine that enhances the efficacy of immunotherapy (Mager *et al.*, 2020; Wang *et al.*, 2020). It is worth identifying the inosine-producing bacteria and gavage these bacteria into mice, to see whether they can also modulate the anti-tumour immune response and enhance the efficacy of psyllium plus inulin and RT. Alternatively, faecal transplantation of responding mice or human patients to IR in germ-free mice can be another approach to prove the causal relationship between gut microbiota and radiosensitisation.

We used two different mouse models, namely subcutaneous model for the tumour responses and SARRP IR to the lower abdomen for normal tissue toxicity. To mirror the clinical setting, a tumour-bearing mouse model should be developed where mice are irradiated to the lower abdomen and flank tumour simultaneously and crypt assay performed at 3.75 days as per the normal tissue experiments. This will allow capture of early immune effects and also to determine the normal tissue effects simultaneously, in the presence of tumour, as this was absent in the crypt assay in section 5.1 as the presence of tumour may influence any immune-mediated normal tissue effects. This will also avoid the

issue of the difference of the gut microbiota and metabolomes between tumour-bearing and non-tumour bearing mice (details are discussed in section 8.7).

List of publications

1. **Then, C. K.**, Paillas, S., Wang, X., Hampson, A. & Kiltie, A. E. (2020). Association of *Bacteroides acidifaciens* relative abundance with high-fibre diet-associated radiosensitisation. *BMC Biol*, 18(1), 102.
2. Bartsch, B *., **Then, C. K.** *, Harriss, E., Kartsonaki, C. & Kiltie, A. E. (2021). The role of dietary supplements, including biotics, glutamine, polyunsaturated fatty acids and polyphenols, in reducing gastrointestinal side effects in patients undergoing pelvic radiotherapy: A systematic review and meta-analysis. *Clin Transl Radiat Oncol*, *29*, 11-19. * These authors contributed equally to this work..
3. Paillas, S., **Then, C. K.**, Kilgas, S., Ruan, J. L., Thompson, J., Elliott, A., Smart, S. & Kiltie, A. E. (2020). The histone deacetylase inhibitor romidepsin spares normal tissues while acting as an effective radiosensitizer in bladder tumors in Vivo. *Int J Radiat Oncol Biol Phys*, 107(1), 212-221.
4. Na, J., Newman, J. A., **Then, C. K.**, Syed, J., Vendrell, I., Torrecilla, I., Ellermann, S., Ramadan, K., Fischer, R. & Kiltie, A. E. (2021). SPRTN protease-cleaved MRE11 decreases DNA repair and radiosensitises cancer cells. Cell Death Dis, 12(2), 165.
5. Kilgas, S., Singh, A. N., Paillas, S., **Then, C. K.**, Torrecilla, I., Nicholson, J., Browning, L., Vendrell, I., Konietzny, R., Kessler, B. M., Kiltie, A. E. & Ramadan, K. (2021). p97/VCP inhibition causes excessive MRE11-dependent DNA end resection promoting cell killing after ionizing radiation. *Cell Rep*, 35(8), 109153.
6. Eaton, S. E., Kaczmarek, J., Mahmood, D., McDiarmid, A. M., Norarfan, A.N., Scott, E. G., **Then, C. K.**, Tsui, H. Y., Kiltie, A. K. (2022) Exploiting dietary fibre and the gut microbiota in pelvic radiotherapy patients. *Br J Cancer*. Accepted.
7. Ruan, J. L., Lee, C., Wouters, S., Tullis, I. D. C., Verslegers, M., Mysara, M., **Then, C. K.**, Smart, S. C., Hill, M. A., Muschel, R. J., Giaccia, A. J., Vojnovic, B., Kiltie, A. E. & Petersson, K. (2021). Irradiation at Ultra-High (FLASH) Dose Rates Reduces Acute Normal Tissue Toxicity in the Mouse Gastrointestinal System. *Int J Radiat Oncol Biol Phys*, 111(5), 1250-1261.

List of oral presentations

1. **Then, C. K.**, Paillas, S., Wang, X., Misheva, M., McCullagh, J., Foster, K. R., & Kiltie, A. E. Can the gut microbiota both radiosensitise tumours and spare normal tissue toxicity? Presented at: 4th Bladder cancer translational research meeting; 31 March 2022; King's College London, UK (1st prize).
2. **Then, C. K.**, Paillas, S., Wang, X., Misheva, M., McCullagh, J., Foster, K. R., & Kiltie, A. E. Can the gut microbiota both radiosensitise tumours and spare normal tissue toxicity? Presented at: Department of Oncology internal seminar; 30 March 2022; University of Oxford, UK.
3. **Then, C. K.**, Paillas, S., Wang, X., Misheva, M., McCullagh, J., Foster, K. R., & Kiltie, A. E. Can the gut microbiota both radiosensitise tumours and spare normal tissue toxicity? Presented at: 2021 International Symposium on Gut Microbiology; 13 - 15 October 2021; National Research Institute for Agriculture, Food and Environment, France, and University of Aberdeen, UK.
4. **Then, C. K.**, Paillas, S., Wang, X., Foster, K. R., & Kiltie, A. E. Can the gut microbiota act as an endogenous radiosensitiser? Presented at: 2020 Department of Oncology Student Symposium; 11 June 2020; University of Oxford, UK (Best presentation).

List of poster presentations

1. **Then, C. K.**, Paillas, S., Wang, X., Misheva, M., McCullagh, J., Foster, K. R., & Kiltie, A. E. Can the gut microbiota both radiosensitise tumours and spare normal tissue toxicity? Presented at: AACR annual meeting; 8-13 April 2022; New Orleans, USA.
2. **Then, C. K.**, Paillas, S., Wang, X., Misheva, M., McCullagh, J., Foster, K. R., & Kiltie, A. E. Can the gut microbiota both radiosensitise tumours and spare normal tissue toxicity? Presented at: NCRI Cancer Conference; 8-12 November 2021; virtual (pre-recorded talk).
3. **Then, C. K.**, Paillas, S., Wang, X., Foster, K. R., & Kiltie, A. E. Radiosensitisation of bladder cancer cells via short-chain fatty acids and/or other metabolites produced by the gut microbiota. Presented at: NCRI Cancer Conference; 2 - 3 November 2020; virtual, UK.
4. **Then, C. K.**, Paillas, S., Wang, X., Foster, K. R., & Kiltie, A. E. Radiosensitisation of bladder cancer cells via short-chain fatty acids and/or other metabolites produced by the gut microbiota. Presented at: NCRI Cancer Conference; 21 - 23 October 2020; University of Cambridge, UK.
5. **Then, C. K.**, Paillas, S., Wang, X., Foster, K. R., & Kiltie, A. E. Radiosensitisation of bladder cancer cells via short-chain fatty acids and/or other metabolites produced by the gut microbiota. Presented at: International Bladder Cancer Network meeting; 17 October 2020; virtual.
6. **Then, C. K.**, Paillas, S., Wang, X., Foster, K. R., & Kiltie, A. E. Relative abundance of *Bacteroides acidifaciens* is associated with radiosensitisation of tumour xenografts in nude mice fed a high fibre diet. Presented at: Bladder Cancer Translational Research Meeting; 6 March 2020; University of Birmingham, UK (Best poster).
7. **Then, C. K.**, Paillas, S., Wang, X., Foster, K. R., & Kiltie, A. E. Relative abundance of *Bacteroides acidifaciens* is associated with radiosensitisation of tumour xenografts in nude mice fed a high fibre diet. Presented at: Exploring Human Host-Microbiota Interactions in Health and Disease; 23 - 25 October 2019; University of Cambridge, UK.(Bursary award winner).

8. **Then, C. K.**, Paillas, S., Wang, X., Foster, K. R., & Kiltie, A. E. Can the gut microbiota act as an endogenous radiosensitiser? Presented at: Department of Oncology Student Symposium; 5 June 2019; University of Oxford, UK (Best poster).

References

Achour, L., Flourie, B., Briet, F., Franchisseur, C., Bornet, F., Champ, M., Rambaud, J. C., & Messing, B. (1997). Metabolic effects of digestible and partially indigestible cornstarch: a study in the absorptive and postabsorptive periods in healthy humans. *American Journal of Clinical Nutrition*, *66*(5), 1151-1159.

Action Bladder Cancer UK. (2022). https://actionbladdercanceruk.org/about-us/

Adjemian, S., Oltean, T., Martens, S., Wiernicki, B., Goossens, V., Vanden Berghe, T., Cappe, B., Ladik, M., Riquet, F. B., Heyndrickx, L., Bridelance, J., Vuylsteke, M., Vandecasteele, K., & Vandenabeele, P. (2020). Ionizing radiation results in a mixture of cellular outcomes including mitotic catastrophe, senescence, methuosis, and iron-dependent cell death. *Cell Death Dis*, *11*(11), 1003.

Aguilera, T. A., Rafat, M., Castellini, L., Shehade, H., Kariolis, M. S., Hui, A. B., Stehr, H., von Eyben, R., Jiang, D., Ellies, L. G., Koong, A. C., Diehn, M., Rankin, E. B., Graves, E. E., & Giaccia, A. J. (2016). Reprogramming the immunological microenvironment through radiation and targeting Axl. *Nat Commun*, *7*, 13898.

Ahmed, W., & Rashid, S. (2019). Functional and therapeutic potential of inulin: A comprehensive review. *Crit Rev Food Sci Nutr*, *59*(1), 1-13.

Anderson, M. J. (2001). A new method for non-parametric multivariate analysis of variance. *Austral Ecology*, *26*(1), 32-46.

Anderson, M. J., Ellingsen, K. E., & McArdle, B. H. (2006). Multivariate dispersion as a measure of beta diversity. *Ecology Letters*, *9*(6), 683-693.

Anderson, N. M., & Simon, M. C. (2020). The tumor microenvironment. *Current Biology*, *30*(16), R921-R925.

Andreyev, J. (2005). Gastrointestinal complications of pelvic radiotherapy: are they of any importance? *Gut*, *54*(8), 1051-1054.

Arenas-Ramirez, N., Woytschak, J., & Boyman, O. (2015). Interleukin-2: Biology, Design and Application. *Trends Immunol*, *36*(12), 763-777.

Arpaia, N., Campbell, C., Fan, X. Y., Dikiy, S., van der Veeken, J., deRoos, P., Liu, H., Cross, J. R., Pfeffer, K., Coffer, P. J., & Rudensky, A. Y. (2013). Metabolites produced by commensal bacteria promote peripheral regulatory T-cell generation. *Nature*, *504*(7480), 451-+.

Arundel, C. M., Glicksman, A. S., & Leith, J. T. (1985). Enhancement of Radiation-Injury in Human-Colon Tumor-Cells by the Maturational Agent Sodium-Butyrate (Nab). *Radiation Research*, *104*(3), 443-448.

Badawy, A. A. B. (2018). Targeting tryptophan availability to tumors: the answer to immune escape? *Immunology and Cell Biology*, *96*(10), 1026-1034.

Balvociute, M., & Huson, D. H. (2017). SILVA, RDP, Greengenes, NCBI and OTT - how do these taxonomies compare? *Bmc Genomics*, *18*.

Bartsch, B., Then, C. K., Harriss, E., Kartsonaki, C., & Kiltie, A. E. (2021). The role of dietary supplements, including biotics, glutamine, polyunsaturated fatty acids and polyphenols, in reducing gastrointestinal side effects in patients undergoing pelvic

radiotherapy: A systematic review and meta-analysis. *Clin Transl Radiat Oncol*, *29*, 11-19.

Baxter, N. T., Schmidt, A. W., Venkataraman, A., Kim, K. S., Waldron, C., & Schmidt, T. M. (2019). Dynamics of Human Gut Microbiota and Short-Chain Fatty Acids in Response to Dietary Interventions with Three Fermentable Fibers. *Mbio*, *10*(1).

Bayne, L. J., & Vonderheide, R. H. (2013). Multicolor flow cytometric analysis of immune cell subsets in tumor-bearing mice. *Cold Spring Harb Protoc*, *2013*(10), 955-960.

Begg, A. C., Stewart, F. A., & Vens, C. (2011). Strategies to improve radiotherapy with targeted drugs. *Nat Rev Cancer*, *11*(4), 239-253.

Bi, H., Tian, Y., Song, C., Li, J. R., Liu, T. T., Chen, Z., Chen, C., Huang, Y., & Zhang, Y. Y. (2019). Urinary microbiota - a potential biomarker and therapeutic target for bladder cancer. *Journal of Medical Microbiology*, *68*(10), 1471-1478.

Bindels, L. B., Porporato, P., Dewulf, E. M., Verrax, J., Neyrinck, A. M., Martin, J. C., Scott, K. P., Buc Calderon, P., Feron, O., Muccioli, G. G., Sonveaux, P., Cani, P. D., & Delzenne, N. M. (2012). Gut microbiota-derived propionate reduces cancer cell proliferation in the liver. *Br J Cancer*, *107*(8), 1337-1344.

Biragyn, A., & Ferrucci, L. (2018). Gut dysbiosis: a potential link between increased cancer risk in ageing and inflammaging. *Lancet Oncology*, *19*(6), E295-E304.

Birt, D. F., Boylston, T., Hendrich, S., Jane, J. L., Hollis, J., Li, L., McClelland, J., Moore, S., Phillips, G. J., Rowling, M., Schalinske, K., Scott, M. P., & Whitley, E. M. (2013). Resistant Starch: Promise for Improving Human Health. *Advances in Nutrition*, *4*(6), 587-601.

Bishehsari, F., Engen, P. A., Preite, N. Z., Tuncil, Y. E., Naqib, A., Shaikh, M., Rossi, M., Wilber, S., Green, S. J., Hamaker, B. R., Khazaie, K., Voigt, R. M., Forsyth, C. B., & Keshavarzian, A. (2018). Dietary Fiber Treatment Corrects the Composition of Gut Microbiota, Promotes SCFA Production, and Suppresses Colon Carcinogenesis. *Genes*, *9*(2).

Blessin, N. C., Li, W. C., Mandelkow, T., et al. (2021). Prognostic role of proliferating CD8(+) cytotoxic Tcells in human cancers. *Cellular Oncology*, *44*(4), 793-803.

Boffa, L. C., Vidali, G., Mann, R. S., & Allfrey, V. G. (1978). Suppression of Histone Deacetylation Invivo and Invitro by Sodium Butyrate. *Journal of Biological Chemistry*, *253*(10), 3364-3366.

Bolden, J. E., Peart, M. J., & Johnstone, R. W. (2006). Anticancer activities of histone deacetylase inhibitors. *Nat Rev Drug Discov*, *5*(9), 769-784.

Booth, C., Tudor, G., Tudor, J., Katz, B. P., & MacVittie, T. J. (2012). Acute gastrointestinal syndrome in high-dose irradiated mice. *Health Phys*, *103*(4), 383-399.

Bourassa, M. W., Alim, I., Bultman, S. J., & Ratan, R. R. (2016). Butyrate, neuroepigenetics and the gut microbiome: Can a high fiber diet improve brain health? *Neuroscience Letters*, *625*, 56-63.

Boustani, J., Bertaut, A., Galsky, M. D., et al. (2018). Radical cystectomy or bladder preservation with radiochemotherapy in elderly patients with muscle-invasive bladder cancer: Retrospective International Study of Cancers of the Urothelial Tract (RISC) Investigators. *Acta Oncol*, *57*(4), 491-497.

Brandmaier, A., & Formenti, S. C. (2020). The Impact of Radiation Therapy on Innate and Adaptive Tumor Immunity. *Seminars in Radiation Oncology*, *30*(2), 139-144.

Bray, F., Ferlay, J., Soerjomataram, I., Siegel, R. L., Torre, L. A., & Jemal, A. (2018). Global cancer statistics 2018: GLOBOCAN estimates of incidence and mortality worldwide for 36 cancers in 185 countries. *CA Cancer J Clin*, *68*(6), 394-424.

Bull, C., Malipatlolla, D., Kalm, M., Sjoberg, F., Alevronta, E., Grander, R., Sultanian, P., Persson, L., Bostrom, M., Eriksson, Y., Swanpalmer, J., Wold, A. E., Blomgren, K., Bjork-Eriksson, T., & Steineck, G. (2017). A novel mouse model of radiation-induced cancer survivorship diseases of the gut. *Am J Physiol Gastrointest Liver Physiol*, *313*(5), G456-G466.

Burkholder, B., Huang, R. Y., Burgess, R., Luo, S., Jones, V. S., Zhang, W., Lv, Z. Q., Gao, C. Y., Wang, B. L., Zhang, Y. M., & Huang, R. P. (2014). Tumor-induced perturbations of cytokines and immune cell networks. *Biochim Biophys Acta*, *1845*(2), 182-201.

Camilleri, M., Lyle, B. J., Madsen, K. L., Sonnenburg, J., Verbeke, K., & Wu, G. D. (2019). Role for diet in normal gut barrier function: developing guidance within the framework of food-labeling regulations. *American Journal of Physiology-Gastrointestinal and Liver Physiology*, *317*(1), G17-G39.

Cancer Genome Atlas Research, N. (2014). Comprehensive molecular characterization of urothelial bladder carcinoma. *Nature*, *507*(7492), 315-322.

Cancer Research UK Bladder cancer statistics. https://www.cancerresearchuk.org/health-professional/cancer-statistics/statistics-by-cancer-type/bladder-cancer

Candido, E. P. M., Reeves, R., & Davie, J. R. (1978). Sodium Butyrate Inhibits Histone Deacetylation in Cultured-Cells. *Cell*, *14*(1), 105-113.

Caporaso, J. G., Lauber, C. L., Walters, W. A., Berg-Lyons, D., Huntley, J., Fierer, N., Owens, S. M., Betley, J., Fraser, L., Bauer, M., Gormley, N., Gilbert, J. A., Smith, G., & Knight, R. (2012). Ultra-high-throughput microbial community analysis on the Illumina HiSeq and MiSeq platforms. *ISME J*, *6*(8), 1621-1624.

Carpenter, A. R., Becknell, M. B., Ching, C. B., Cuaresma, E. J., Chen, X., Hains, D. S., & McHugh, K. M. (2016). Uroplakin 1b is critical in urinary tract development and urothelial differentiation and homeostasis. *Kidney International*, *89*(3), 612-624.

Carvalho, H. A., & Villar, R. C. (2018). Radiotherapy and immune response: the systemic effects of a local treatment. *Clinics (Sao Paulo)*, *73*(suppl 1), e557s.

Castellarin, M., Warren, R. L., Freeman, J. D., Dreolini, L., Krzywinski, M., Strauss, J., Barnes, R., Watson, P., Allen-Vercoe, E., Moore, R. A., & Holt, R. A. (2012). Fusobacterium nucleatum infection is prevalent in human colorectal carcinoma. *Genome Research*, *22*(2), 299-306.

Cekic, C., Sag, D., Li, Y., Theodorescu, D., Strieter, R. M., & Linden, J. (2012). Adenosine A2B receptor blockade slows growth of bladder and breast tumors. *Journal of Immunology*, *188*(1), 198-205.

Chang, P. V., Hao, L. M., Offermanns, S., & Medzhitov, R. (2014). The microbial metabolite butyrate regulates intestinal macrophage function via histone deacetylase inhibition. *Proceedings of the National Academy of Sciences of the United States of America*, *111*(6), 2247-2252.

Chaplin, D. D. (2010). Overview of the immune response. *Journal of Allergy and Clinical Immunology*, *125*(2), S3-S23.

Chelakkot, C., Ghim, J., & Ryu, S. H. (2018). Mechanisms regulating intestinal barrier integrity and its pathological implications. *Experimental and Molecular Medicine*, *50*.

Chen, D., Ye, Y. L., Guo, S. J., & Yao, K. (2021). Progress in the Research and Targeted Therapy of ErbB/HER Receptors in Urothelial Bladder Cancer. *Frontiers in Molecular Biosciences*, *8*.

Chen, L., Tai, W. C., Brar, M. S., Leung, F. C., & Hsiao, W. L. (2015). Tumor grafting induces changes of gut microbiota in athymic nude mice in the presence and absence of medicinal Gynostemma saponins. *Plos One*, *10*(5), e0126807.

Chen, Z., Hui, P. C., Hui, M., Yeoh, Y. K., Wong, P. Y., Chan, M. C. W., Wong, M. C. S., Ng, S. C., Chan, F. K. L., & Chan, P. K. S. (2019). Impact of Preservation Method and 16S rRNA Hypervariable Region on Gut Microbiota Profiling. *mSystems*, *4*(1).

Choi, K. J., Kim, J. H., Lee, Y. S., Kim, J., Suh, B. S., Kim, H., Cho, S., Sohn, J. H., Kim, G. E., & Yun, C. O. (2006). Concurrent delivery of GM-CSF and B7-1 using an oncolytic adenovirus elicits potent antitumor effect. *Gene Therapy*, *13*(13), 1010-1020.

Choi, W., Czemiak, B., Ochoa, A., Su, X. P., Siefker-Radtke, A., Dinney, C., & McConkey, D. J. (2014). Intrinsic basal and luminal subtypes of muscle-invasive bladder cancer. *Nature Reviews Urology*, *11*(7), 400-410.

Choi, W., Porten, S., Kim, S., et al. (2014). Identification of distinct basal and luminal subtypes of muscle-invasive bladder cancer with different sensitivities to frontline chemotherapy. *Cancer Cell*, *25*(2), 152-165.

Chutkan, R., Fahey, G., Wright, W. L., & McRorie, J. (2012). Viscous versus nonviscous soluble fiber supplements: mechanisms and evidence for fiber-specific health benefits. *J Am Acad Nurse Pract*, *24*(8), 476-487.

Collado, M. C., Derrien, M., & Isolauri, E. (2007). Intestinal integrity and Akkermansia muciniphila, a mucin-degrading member of the intestinal microbiota present in infants, adults, and the elderly. *Applied and Environmental Microbiology*, *73*(23), 7767-7770.

Colquhoun, A. J., & Mellon, J. K. (2002). Epidermal growth factor receptor and bladder cancer. *Postgraduate Medical Journal*, *78*(924), 584-589.

Daillere, R., Vetizou, M., Waldschmitt, N., et al. (2016). Enterococcus hirae and Barnesiella intestinihominis Facilitate Cyclophosphamide-Induced Therapeutic Immunomodulatory Effects. *Immunity*, *45*(4), 931-943.

Damrauer, J. S., Hoadley, K. A., Chism, D. D., Fan, C., Tiganelli, C. J., Wobker, S. E., Yeh, J. J., Milowsky, M. I., Iyer, G., Parker, J. S., & Kim, W. Y. (2014). Intrinsic subtypes of high-grade bladder cancer reflect the hallmarks of breast cancer biology. *Proceedings of the National Academy of Sciences of the United States of America*, *111*(8), 3110-3115.

Daro-Faye, M., Kassouf, W., Souhami, L., Marcq, G., Cury, F., Niazi, T., & Sargos, P. (2021). Combined radiotherapy and immunotherapy in urothelial bladder cancer: harnessing the full potential of the anti-tumor immune response. *World J Urol*, *39*(5), 1331-1343.

David, L. A., Maurice, C. F., Carmody, R. N., Gootenberg, D. B., Button, J. E., Wolfe, B. E., Ling, A. V., Devlin, A. S., Varma, Y., Fischbach, M. A., Biddinger, S. B., Dutton, R. J., &

Turnbaugh, P. J. (2014). Diet rapidly and reproducibly alters the human gut microbiome. *Nature*, *505*(7484), 559-563.

Davie, J. R. (2003). Inhibition of histone deacetylase activity by butyrate. *J Nutr*, *133*(7 Suppl), 2485S-2493S.

DeGraff, D. J., Clark, P. E., Cates, J. M., Yamashita, H., Robinson, V. L., Yu, X. P., Smolkin, M. E., Chang, S. S., Cookson, M. S., Herrick, M. K., Shariat, S. F., Steinberg, G. D., Frierson, H. F., Wu, X. R., Theodorescu, D., & Matusik, R. J. (2012). Loss of the Urothelial Differentiation Marker FOXA1 Is Associated with High Grade, Late Stage Bladder Cancer and Increased Tumor Proliferation. *Plos One*, *7*(5).

Dehghan, P., Gargari, B. P., & Jafar-Abadi, M. A. (2014). Oligofructose-enriched inulin improves some inflammatory markers and metabolic endotoxemia in women with type 2 diabetes mellitus: A randomized controlled clinical trial. *Nutrition*, *30*(4), 418-423.

Dehghani, N., Tafvizi, F., & Jafari, P. (2021). Cell cycle arrest and anti-cancer potential of probiotic Lactobacillus rhamnosus against HT-29 cancer cells. *Bioimpacts*, *11*(4), 245-252.

Deleu, S., Machiels, K., Raes, J., Verbeke, K., & Vermeire, S. (2021). Short chain fatty acids and its producing organisms: An overlooked therapy for IBD? *EBioMedicine*, *66*, 103293.

Demidenko, E. (2010). Three endpoints of in vivo tumour radiobiology and their statistical estimation. *International Journal of Radiation Biology*, *86*(2), 164-173.

Demirer, S., Aydintug, S., Aslim, B., Kepenekci, I., Sengul, N., Evirgen, O., Gerceker, D., Andrieu, M. N., Ulusoy, C., & Karahuseyinoglu, S. (2006). Effects of probiotics on radiation-induced intestinal injury in rats. *Nutrition*, *22*(2), 179-186.

Desai, M. S., Seekatz, A. M., Koropatkin, N. M., Kamada, N., Hickey, C. A., Wolter, M., Pudlo, N. A., Kitamoto, S., Terrapon, N., Muller, A., Young, V. B., Henrissat, B., Wilmes, P., Stappenbeck, T. S., Nunez, G., & Martens, E. C. (2016). A Dietary Fiber-Deprived Gut Microbiota Degrades the Colonic Mucus Barrier and Enhances Pathogen Susceptibility. *Cell*, *167*(5), 1339-+.

DeSantis, T. Z., Hugenholtz, P., Larsen, N., Rojas, M., Brodie, E. L., Keller, K., Huber, T., Dalevi, D., Hu, P., & Andersen, G. L. (2006). Greengenes, a chimera-checked 16S rRNA gene database and workbench compatible with ARB. *Applied and Environmental Microbiology*, *72*(7), 5069-5072.

Desouky, O., Ding, N., & Zhou, G. M. (2015). Targeted and non-targeted effects of ionizing radiation. *Journal of Radiation Research and Applied Sciences*, *8*(2), 247-254.

DeSouza, K., Chowdhury, S., & Hughes, S. (2014). Prompt diagnosis key in bladder cancer. *Practitioner*, *258*(1767), 23-27, 23.

Dhingra, D., Michael, M., Rajput, H., & Patil, R. T. (2012). Dietary fibre in foods: a review. *Journal of Food Science and Technology-Mysore*, *49*(3), 255-266.

Diakos, C. I., Charles, K. A., McMillan, D. C., & Clarke, S. J. (2014). Cancer-related inflammation and treatment effectiveness. *Lancet Oncology*, *15*(11), E493-E503.

Dikeman, C. L., & Fahey, G. C. (2006). Viscosity as related to dietary fiber: A review. *Critical Reviews in Food Science and Nutrition*, *46*(8), 649-663.

Do, N. L., Nagle, D., & Poylin, V. Y. (2011). Radiation proctitis: current strategies in management. *Gastroenterol Res Pract*, *2011*, 917941.

Donohoe, D. R., Collins, L. B., Wali, A., Bigler, R., Sun, W., & Bultman, S. J. (2012). The Warburg Effect Dictates the Mechanism of Butyrate-Mediated Histone Acetylation and Cell Proliferation. *Molecular Cell*, *48*(4), 612-626.

DuRoss, A. N., Neufeld, M. J., Rana, S., Thomas, C. R., & Sun, C. (2019). Integrating nanomedicine into clinical radiotherapy regimens. *Advanced Drug Delivery Reviews*, *144*, 35-56.

Efstathiou, J. A., Spiegel, D. Y., Shipley, W. U., Heney, N. M., Kaufman, D. S., Niemierko, A., Coen, J. J., Skowronski, R. Y., Paly, J. J., McGovern, F. J., & Zietman, A. L. (2012). Long-Term Outcomes of Selective Bladder Preservation by Combined-Modality Therapy for Invasive Bladder Cancer: The MGH Experience. *European Urology*, *61*(4), 705-711.

El-Awady, R. A., Dikomey, E., & Dahm-Daphi, J. (2003). Radiosensitivity of human tumour cells is correlated with the induction but not with the repair of DNA double-strand breaks. *British Journal of Cancer*, *89*(3), 593-601.

Engman, C., Garciafigueroa, Y., Phillips, B. E., Trucco, M., & Giannoukakis, N. (2018). Co-Stimulation-Impaired Bone Marrow-Derived Dendritic Cells Prevent Dextran Sodium Sulfate-Induced Colitis in Mice. *Frontiers in Immunology*, *9*.

Erickson, B. A., Otterson, M. F., Moulder, J. E., & Sarna, S. K. (1994). Altered motility causes the early gastrointestinal toxicity of irradiation. *Int J Radiat Oncol Biol Phys*, *28*(4), 905-912.

Erlich, A., & Zlotta, A. R. (2016). Treatment of bladder cancer in the elderly. *Investig Clin Urol*, *57 Suppl 1*, S26-35.

Eslick, S., Thompson, C., Berthon, B., & Wood, L. (2022). Short-chain fatty acids as anti-inflammatory agents in overweight and obesity: a systematic review and meta-analysis. *Nutrition Reviews*, *80*(4), 838-856.

Fan, X. Z., Alekseyenko, A. V., Wu, J., Peters, B. A., Jacobs, E. J., Gapstur, S. M., Purdue, M. P., Abnet, C. C., Stolzenberg-Solomon, R., Miller, G., Ravel, J., Hayes, R. B., & Ahn, J. (2018). Human oral microbiome and prospective risk for pancreatic cancer: a population-based nested case-control study. *Gut*, *67*(1), 120-127.

Fichtner, I., Becker, M., & Baumgart, J. (2003). Antileukaemic activity of treosulfan in xenografted human acute lymphoblastic leukaemias (ALL). *European Journal of Cancer*, *39*(6), 801-807.

Finotello, F., Mastrorilli, E., & Di Camillo, B. (2018). Measuring the diversity of the human microbiota with targeted next-generation sequencing. *Briefings in Bioinformatics*, *19*(4), 679-692.

Flood, M. T., Auerbach, M. H., & Craig, S. A. S. (2004). A review of the clinical toleration studies of polydextrose in food. *Food and Chemical Toxicology*, *42*(9), 1531-1542.

Franken, N. A., Rodermond, H. M., Stap, J., Haveman, J., & van Bree, C. (2006). Clonogenic assay of cells in vitro. *Nat Protoc*, *1*(5), 2315-2319.

Freedman, N. D., Silverman, D. T., Hollenbeck, A. R., Schatzkin, A., & Abnet, C. C. (2011). Association Between Smoking and Risk of Bladder Cancer Among Men and Women (vol 306, pg 737, 2011). *Jama-Journal of the American Medical Association*, *306*(20), 2220-2220.

Fridman, R., Giaccone, G., Kanemoto, T., Martin, G. R., Gazdar, A. F., & Mulshine, J. L. (1990). Reconstituted Basement-Membrane (Matrigel) and Laminin Can Enhance the

Tumorigenicity and the Drug-Resistance of Small-Cell Lung-Cancer Cell-Lines. *Proceedings of the National Academy of Sciences of the United States of America*, *87*(17), 6698-6702.

Fridman, R., Kibbey, M. C., Royce, L. S., Zain, M., Sweeney, T. M., Jicha, D. L., Yannelli, J. R., Martin, G. R., & Kleinman, H. K. (1991). Enhanced Tumor-Growth of Both Primary and Established Human and Murine Tumor-Cells in Athymic Mice after Coinjection with Matrigel. *Jnci-Journal of the National Cancer Institute*, *83*(11), 769-774.

Friswell, M. K., Gika, H., Stratford, I. J., Theodoridis, G., Telfer, B., Wilson, I. D., & McBain, A. J. (2010). Site and strain-specific variation in gut microbiota profiles and metabolism in experimental mice. *Plos One*, *5*(1), e8584.

Fuentes-Zaragoza, E., Sanchez-Zapata, E., Sendra, E., Sayas, E., Navarro, C., Fernandez-Lopez, J., & Perez-Alvarez, J. A. (2011). Resistant starch as prebiotic: A review. *Starch-Starke*, *63*(7), 406-415.

Furrie, E., Macfarlane, S., Kennedy, A., Cummings, J. H., Walsh, S. V., O'Neil, D. A., & Macfarlane, G. T. (2005). Synbiotic therapy (Bifidobacterium longum/Synergy 1) initiates resolution of inflammation in patients with active ulcerative colitis: a randomised controlled pilot trial. *Gut*, *54*(2), 242-249.

Furusawa, Y., Obata, Y., Fukuda, S., et al. (2013). Commensal microbe-derived butyrate induces the differentiation of colonic regulatory T cells. *Nature*, *504*(7480), 446-+.

Garcia-Peris, P., Velasco, C., Hernandez, M., Lozano, M. A., Paron, L., de la Cuerda, C., Breton, I., Camblor, M., & Guarner, F. (2016). Effect of inulin and fructo-oligosaccharide on the prevention of acute radiation enteritis in patients with gynecological cancer and impact on quality-of-life: a randomized, double-blind, placebo-controlled trial. *European Journal of Clinical Nutrition*, *70*(2), 170-174.

Gatta, L. B., Melocchi, L., Bugatti, M., Missale, F., Lonardi, S., Zanetti, B., Cristinelli, L., Belotti, S., Simeone, C., Ronca, R., Grillo, E., Licini, S., Bresciani, D., Tardanico, R., Chan, S. R., Giurisato, E., Calza, S., & Vermi, W. (2019). Hyper-Activation of STAT3 Sustains Progression of Non-Papillary Basal-Type Bladder Cancer via FOSL1 Regulome. *Cancers*, *11*(9).

Geller, L. T., Barzily-Rokni, M., Danino, T., et al. (2017). Potential role of intratumor bacteria in mediating tumor resistance to the chemotherapeutic drug gemcitabine. *Science*, *357*(6356), 1156-1160.

Geng, H. W., Yin, F. Y., Zhang, Z. F., Gong, X., & Yang, Y. (2021). Butyrate Suppresses Glucose Metabolism of Colorectal Cancer Cells via GPR109a-AKT Signaling Pathway and Enhances Chemotherapy. *Frontiers in Molecular Biosciences*, *8*.

Gibson, G. R., Hutkins, R., Sanders, M. E., Prescott, S. L., Reimer, R. A., Salminen, S. J., Scott, K., Stanton, C., Swanson, K. S., Cani, P. D., Verbeke, K., & Reid, G. (2017). The International Scientific Association for Probiotics and Prebiotics (ISAPP) consensus statement on the definition and scope of prebiotics. *Nature Reviews Gastroenterology & Hepatology*, *14*(8), 491-502.

Gill, S. K., Rossi, M., Bajka, B., & Whelan, K. (2021). Dietary fibre in gastrointestinal health and disease. *Nature Reviews Gastroenterology & Hepatology*, *18*(2), 101-116.

Gomez-Ambrosi, J., Zabalegui, N., Bing, C., Tisdale, M. J., Trayhurn, P., & Williams, G. (2002). Weight loss in tumour-bearing mice is not associated with changes in resistin gene

expression in white adipose tissue. *Hormone and Metabolic Research*, *34*(11-12), 674-677.

Gopalakrishnan, V., Spencer, C. N., Nezi, L., et al. (2018). Gut microbiome modulates response to anti-PD-1 immunotherapy in melanoma patients. *Science*, *359*(6371), 97-103.

Grabitske, H., & Slavin, J. (2009). Gastrointestinal Effects of Low-Digestible Carbohydrates. *Critical Reviews in Food Science and Nutrition*, *49*(4), 327-360.

Groselj, B., Kerr, M., & Kiltie, A. E. (2013). Radiosensitisation of bladder cancer cells by panobinostat is modulated by Ku80 expression. *Radiother Oncol*, *108*(3), 429-433.

Groselj, B., Ruan, J. L., Scott, H., Gorrill, J., Nicholson, J., Kelly, J., Anbalagan, S., Thompson, J., Stratford, M. R. L., Jevons, S. J., Hammond, E. M., Scudamore, C. L., Kerr, M., & Kiltie, A. E. (2018). Radiosensitization In Vivo by Histone Deacetylase Inhibition with No Increase in Early Normal Tissue Radiation Toxicity. *Mol Cancer Ther*, *17*(2), 381-392.

Grossman, H. B., Natale, R. B., Tangen, C. M., Speights, V. O., Vogelzang, N. J., Trump, D. L., deVere White, R. W., Sarosdy, M. F., Wood, D. P., Jr., Raghavan, D., & Crawford, E. D. (2003). Neoadjuvant chemotherapy plus cystectomy compared with cystectomy alone for locally advanced bladder cancer. *N Engl J Med*, *349*(9), 859-866.

Guancial, E. A., Roussel, B., Bergsma, D. P., Bylund, K. C., Sahasrabudhe, D., Messing, E., Mohile, S. G., & Fung, C. (2015). Bladder cancer in the elderly patient: challenges and solutions. *Clinical Interventions in Aging*, *10*.

Gunn, D., Abbas, Z., Harris, H. C., Major, G., Hoad, C., Gowland, P., Marciani, L., Gill, S. K., Warren, F. J., Rossi, M., Remes-Troche, J. M., Whelan, K., & Spiller, R. C. (2021). Psyllium reduces inulin-induced colonic gas production in IBS: MRI and in vitro fermentation studies. *Gut*, 10.1136/gutjnl-2021-324784.

Guo, H., Chou, W. C., Lai, Y., et al. (2020). Multi-omics analyses of radiation survivors identify radioprotective microbes and metabolites. *Science*, *370*(6516).

Gupta, A., Probst, H. C., Vuong, V., Landshammer, A., Muth, S., Yagita, H., Schwendener, R., Pruschy, M., Knuth, A., & van den Broek, M. (2012). Radiotherapy promotes tumor-specific effector CD8+ T cells via dendritic cell activation. *Journal of Immunology*, *189*(2), 558-566.

Hagemann, R. F., Sigdestad, C. P., & Lesher, S. (1971). Intestinal Crypt Survival and Total and Per Crypt Levels of Proliferative Cellularity Following Irradiation - Single X-Ray Exposures. *Radiation Research*, *46*(3), 533-+.

Hall, M., & Beiko, R. G. (2018). 16S rRNA Gene Analysis with QIIME2. *Methods Mol Biol*, *1849*, 113-129.

Hallert, C., Bjorck, I., Nyman, M., Pousette, A., Granno, C., & Svensson, H. (2003). Increasing fecal butyrate in ulcerative colitis patients by diet: Controlled pilot study. *Inflammatory Bowel Diseases*, *9*(2), 116-121.

Han, R., Nusbaum, O., Chen, X. Y., & Zhu, Y. (2020). Valeric Acid Suppresses Liver Cancer Development by Acting as a Novel HDAC Inhibitor. *Molecular Therapy-Oncolytics*, *19*, 8-18.

Han, R., Yang, H., Li, Y., Ling, C., & Lu, L. (2022). Valeric Acid acts as a novel HDAC3 inhibitor against Prostate Cancer. *Research Square (preprint)*, https://doi.org/10.21203/rs.3.rs-1806155/v1.

Harrington, K. J., Billingham, L. J., Brunner, T. B., Burnet, N. G., Chan, C. S., Hoskin, P., Mackay, R. I., Maughan, T. S., Macdougall, J., McKenna, W. G., Nutting, C. M., Oliver, A., Plummer, R., Stratford, I. J., Illidge, T., & Radiot, N. C. T. (2011). Guidelines for preclinical and early phase clinical assessment of novel radiosensitisers. *British Journal of Cancer*, *105*(5), 628-639.

Hauer-Jensen, M., Denham, J. W., & Andreyev, H. J. (2014). Radiation enteropathy--pathogenesis, treatment and prevention. *Nat Rev Gastroenterol Hepatol*, *11*(8), 470-479.

Hautmann, R. E., de Petriconi, R. C., Pfeiffer, C., & Volkmer, B. G. (2012). Radical Cystectomy for Urothelial Carcinoma of the Bladder Without Neoadjuvant or Adjuvant Therapy: Long-Term Results in 1100 Patients. *European Urology*, *61*(5), 1039-1047.

Hayashi, K., Nikolos, F., Lee, Y. C., Jain, A., Tsouko, E., Gao, H., Kasabyan, A., Leung, H. E., Osipov, A., Jung, S. Y., Kurtova, A. V., & Chan, K. S. (2020). Tipping the immunostimulatory and inhibitory DAMP balance to harness immunogenic cell death. *Nat Commun*, *11*(1), 6299.

He, Y., Fu, L., Li, Y., Wang, W., Gong, M., Zhang, J., Dong, X., Huang, J., Wang, Q., Mackay, C. R., Fu, Y. X., Chen, Y., & Guo, X. (2021). Gut microbial metabolites facilitate anticancer therapy efficacy by modulating cytotoxic CD8(+) T cell immunity. *Cell Metab*, *33*(5), 988-1000 e1007.

Hendry, J. H., & West, C. M. L. (1997). Apoptosis and mitotic cell death: Their relative contributions to normal-tissue and tumour radiation response. *International Journal of Radiation Biology*, *71*(6), 709-719.

Henriques, S. F., Dhakan, D. B., Serra, L., Francisco, A. P., Carvalho-Santos, Z., Baltazar, C., Elias, A. P., Anjos, M., Zhang, T., Maddocks, O. D. K., & Ribeiro, C. (2020). Metabolic cross-feeding in imbalanced diets allows gut microbes to improve reproduction and alter host behaviour. *Nature Communications*, *11*(1).

Hiam-Galvez, K. J., Allen, B. M., & Spitzer, M. H. (2021). Systemic immunity in cancer. *Nature Reviews Cancer*, *21*(6), 345-359.

Hill, C., Guarner, F., Reid, G., Gibson, G. R., Merenstein, D. J., Pot, B., Morelli, L., Canani, R. B., Flint, H. J., Salminen, S., Calder, P. C., & Sanders, M. E. (2014). The International Scientific Association for Probiotics and Prebiotics consensus statement on the scope and appropriate use of the term probiotic. *Nature Reviews Gastroenterology & Hepatology*, *11*(8), 506-514.

Hille, A., Herrmann, M. K., Kertesz, T., Christiansen, H., Hermann, R. M., Pradier, O., Schmidberger, H., & Hess, C. F. (2008). Sodium butyrate enemas in the treatment of acute radiation-induced proctitis in patients with prostate cancer and the impact on late proctitis. A prospective evaluation. *Strahlenther Onkol*, *184*(12), 686-692.

Hoffman, J. D., Yanckello, L. M., Chlipala, G., Hammond, T. C., McCulloch, S. D., Parikh, I., Sun, S., Morganti, J. M., Green, S. J., & Lin, A. L. (2019). Dietary inulin alters the gut microbiome, enhances systemic metabolism and reduces neuroinflammation in an APOE4 mouse model. *Plos One*, *14*(8), e0221828.

Holscher, H. D. (2017). Dietary fiber and prebiotics and the gastrointestinal microbiota. *Gut Microbes*, *8*(2), 172-184.

Hou, B., Xu, Z. W., Yang, C. W., Gao, Y., Zhao, S. F., & Zhang, C. G. (2007). Protective effects of inosine on mice subjected to lethal total-body ionizing irradiation. *Journal of Radiation Research*, *48*(1), 57-62.

Huang, J. Q., Mondul, A. M., Weinstein, S. J., Koutros, S., Derkach, A., Karoly, E., Sampson, J. N., Moore, S. C., Berndt, S. I., & Albanes, D. (2016). Serum metabolomic profiling of prostate cancer risk in the prostate, lung, colorectal, and ovarian cancer screening trial. *British Journal of Cancer*, *115*(9), 1087-1095.

Human Microbiome Project, C. (2012a). A framework for human microbiome research. *Nature*, *486*(7402), 215-221.

Human Microbiome Project, C. (2012b). Structure, function and diversity of the healthy human microbiome. *Nature*, *486*(7402), 207-214.

Huttenhower, C., Gevers, D., Knight, R., et al. (2012). Structure, function and diversity of the healthy human microbiome. *Nature*, *486*(7402), 207-214.

Iida, N., Dzutsev, A., Stewart, C. A., et al. (2013). Commensal Bacteria Control Cancer Response to Therapy by Modulating the Tumor Microenvironment. *Science*, *342*(6161), 967-970.

Ingersoll, M. A., & Albert, M. L. (2013). From infection to immunotherapy: host immune responses to bacteria at the bladder mucosa. *Mucosal Immunology*, *6*(6), 1041-1053.

Intensity Modulated Radiation Therapy Collaborative Working, G. (2001). Intensity-modulated radiotherapy: current status and issues of interest. *Int J Radiat Oncol Biol Phys*, *51*(4), 880-914.

Ito, H., Takemura, N., Sonoyama, K., Kawagishi, H., Topping, D. L., Conlon, M. A., & Morita, T. (2011). Degree of Polymerization of Inulin-Type Fructans Differentially Affects Number of Lactic Acid Bacteria, Intestinal Immune Functions, and Immunoglobulin A Secretion in the Rat Cecum. *Journal of Agricultural and Food Chemistry*, *59*(10), 5771-5778.

Itoh, Y., Mizuno, M., Ikeda, M., Nakahara, R., Kubota, S., Ito, J., Okada, T., Kawamura, M., Kikkawa, F., & Naganawa, S. (2015). A Randomized, Double-Blind Pilot Trial of Hydrolyzed Rice Bran versus Placebo for Radioprotective Effect on Acute Gastroenteritis Secondary to Chemoradiotherapy in Patients with Cervical Cancer. *Evidence-Based Complementary and Alternative Medicine*, *2015*.

Jackson, S. P., & Bartek, J. (2009). The DNA-damage response in human biology and disease. *Nature*, *461*(7267), 1071-1078.

Jain, T., Sharma, P., Are, A. C., Vickers, S. M., & Dudeja, V. (2021). New Insights Into the Cancer-Microbiome-Immune Axis: Decrypting a Decade of Discoveries. *Front Immunol*, *12*, 622064.

Jalanka, J., Major, G., Murray, K., Singh, G., Nowak, A., Kurtz, C., Silos-Santiago, I., Johnston, J. M., de Vos, W. M., & Spiller, R. (2019). The Effect of Psyllium Husk on Intestinal Microbiota in Constipated Patients and Healthy Controls. *Int J Mol Sci*, *20*(2).

James, N. D., Hussain, S. A., Hall, E., Jenkins, P., Tremlett, J., Rawlings, C., Crundwell, M., Sizer, B., Sreenivasan, T., Hendron, C., Lewis, R., Waters, R., Huddart, R. A., & Investigators, B. (2012). Radiotherapy with or without Chemotherapy in Muscle-Invasive Bladder Cancer. *New England Journal of Medicine*, *366*(16), 1477-1488.

Ji, K., Zhang, M., Du, L., Liu, Y., Xu, C., He, N., Wang, Q., Wang, J., Gu, Y., Song, H., Sun, X., Wang, Y., & Liu, Q. (2022). Targeting the gut microbiota with inulin: a novel approach for the management of irradiation-induced colonic fibrosis. *Research Square (preprint)*.

Jiang, F., & Zhou, X. M. (1997). A model of orthotopic murine bladder (MBT-2) tumor implants. *Urological Research*, *25*(3), 179-182.

Jiang, L., Amir, A., Morton, J. T., Heller, R., Arias-Castro, E., & Knight, R. (2017). Discrete False-Discovery Rate Improves Identification of Differentially Abundant Microbes. *mSystems*, *2*(6).

Johnson, C. H., Spilker, M. E., Goetz, L., Peterson, S. N., & Siuzdak, G. (2016). Metabolite and Microbiome Interplay in Cancer Immunotherapy. *Cancer Research*, *76*(21), 6146-6152.

Jones, K. I., Tiersma, J., Yuzhalin, A. E., Gordon-Weeks, A. N., Buzzelli, J., Im, J. H., & Muschel, R. J. (2018). Radiation combined with macrophage depletion promotes adaptive immunity and potentiates checkpoint blockade. *EMBO Mol Med*, *10*(12).

Kamoun, A., de Reynies, A., Allory, Y., et al. (2020). A Consensus Molecular Classification of Muscle-invasive Bladder Cancer. *Eur Urol*, *77*(4), 420-433.

Kang, J. E., Kim, H. D., Park, S. Y., Pan, J. G., Kim, J. H., & Yum, D. Y. (2018). Dietary Supplementation With a Bacillus Superoxide Dismutase Protects Against gamma-Radiation-induced Oxidative Stress and Ameliorates Dextran Sulphate Sodium-induced Ulcerative Colitis in Mice. *Journal of Crohns & Colitis*, *12*(7), 860-869.

Kelly-Quagliana, K. A., Nelson, P. D., & Buddington, R. K. (2003). Dietary oligofructose and inulin modulate immune functions in mice. *Nutrition Research*, *23*(2), 257-267.

Kim, C. H. (2021). Control of lymphocyte functions by gut microbiota-derived short-chain fatty acids. *Cellular & Molecular Immunology*, *18*(5), 1161-1171.

Kim, C. K., Yang, V. W., & Bialkowska, A. B. (2017). The Role of Intestinal Stem Cells in Epithelial Regeneration Following Radiation-Induced Gut Injury. *Current Stem Cell Reports*, *3*(4), 320-332.

Kim, K., Kwon, O., Ryu, T. Y., Jung, C. R., Kim, J., Min, J. K., Kim, D. S., Son, M. Y., & Cho, H. S. (2019). Propionate of a microbiota metabolite induces cell apoptosis and cell cycle arrest in lung cancer. *Mol Med Rep*, *20*(2), 1569-1574.

Kim, M., Morrison, M., & Yu, Z. T. (2011). Evaluation of different partial 16S rRNA gene sequence regions for phylogenetic analysis of microbiomes. *Journal of Microbiological Methods*, *84*(1), 81-87.

Kim, S., Shen, S. H., Moore, D. F., Shih, W., Lin, Y., Li, H., Dolan, M., Shao, Y. H., & Lu-Yao, G. L. (2011). Late Gastrointestinal Toxicities Following Radiation Therapy for Prostate Cancer. *European Urology*, *60*(5), 908-916.

Kiriluk, K. J., Prasad, S. M., Patel, A. R., Steinberg, G. D., & Smith, N. D. (2012). Bladder cancer risk from occupational and environmental exposures. *Urologic Oncology-Seminars and Original Investigations*, *30*(2), 199-211.

Klepinina, L., Klepinin, A., Truu, L., Chekulayev, V., Vija, H., Kuus, K., Teino, I., Pook, M., Maimets, T., & Kaambre, T. (2021). Colon cancer cell differentiation by sodium butyrate modulates metabolic plasticity of Caco-2 cells via alteration of phosphotransfer network. *Plos One*, *16*(1).

Knochelmann, H. M., Dwyer, C. J., Bailey, S. R., Amaya, S. M., Elston, D. M., Mazza-McCrann, J. M., & Paulos, C. M. (2018). When worlds collide: Th17 and Treg cells in cancer and autoimmunity. *Cellular & Molecular Immunology*, *15*(5), 458-469.

Knutson, K. L., & Disis, M. L. (2005). Tumor antigen-specific T helper cells in cancer immunity and immunotherapy. *Cancer Immunology Immunotherapy*, *54*(8), 721-728.

Kopf-Maier, P., & Sass, G. (1996). Antitumor activity of treosulfan in human lung carcinomas. *Cancer Chemother Pharmacol*, *37*(3), 211-221.

Korsten, S. G. P. J., Peracic, L., van Groeningen, L. M. B., Diks, M. A. P., Vromans, H., Garssen, J., & Willemsen, L. E. M. (2022). Butyrate Prevents Induction of CXCL10 and Non-Canonical IRF9 Expression by Activated Human Intestinal Epithelial Cells via HDAC Inhibition. *International Journal of Molecular Sciences*, *23*(7).

Kotwal, S., Choudhury, A., Johnston, C., Paul, A. B., Whelan, P., & Kiltie, A. E. (2008). Similar treatment outcomes for radical cystectomy and radical radiotherapy in invasive bladder cancer treated at a United Kingdom specialist treatment center. *International Journal of Radiation Oncology Biology Physics*, *70*(2), 456-463.

Kozelsky, T. F., Meyers, G. E., Sloan, J. A., Shanahan, T. G., Dick, S. J., Moore, R. L., Engeler, G. P., Frank, A. R., McKone, T. K., Urias, R. E., Pilepich, M. V., Novotny, P. J., & Martenson, J. A. (2003). Phase III double-blind study of glutamine versus placebo for the prevention of acute diarrhea in patients receiving pelvic radiation therapy. *Journal of Clinical Oncology*, *21*(9), 1669-1674.

Krautkramer, K. A., Fan, J., & Backhed, F. (2021). Gut microbial metabolites as multi-kingdom intermediates. *Nat Rev Microbiol*, *19*(2), 77-94.

Kuo, S. M., Merhige, P. M., & Hagey, L. R. (2013). The Effect of Dietary Prebiotics and Probiotics on Body Weight, Large Intestine Indices, and Fecal Bile Acid Profile in Wild Type and IL10-/- Mice. *Plos One*, *8*(3).

Laboratory Mice and Rats. (2012). https://www.labome.com/method/Laboratory-Mice-and-Rats.html

Lambin, P., Malaise, E. P., & Joiner, M. C. (1994). The Effect of Very-Low Radiation-Doses on the Human Bladder-Carcinoma Cell-Line Rt112. *Radiotherapy and Oncology*, *32*(1), 63-72.

Langille, M. G., Zaneveld, J., Caporaso, J. G., McDonald, D., Knights, D., Reyes, J. A., Clemente, J. C., Burkepile, D. E., Vega Thurber, R. L., Knight, R., Beiko, R. G., & Huttenhower, C. (2013). Predictive functional profiling of microbial communities using 16S rRNA marker gene sequences. *Nat Biotechnol*, *31*(9), 814-821.

Lawrie, T. A., Green, J. T., Beresford, M., Wedlake, L., Burden, S., Davidson, S. E., Lal, S., Henson, C. C., & Andreyev, H. J. N. (2018). Interventions to reduce acute and late adverse gastrointestinal effects of pelvic radiotherapy for primary pelvic cancers. *Cochrane Database Syst Rev*, *1*, CD012529.

Le Bastard, Q., Chapelet, G., Javaudin, F., Lepelletier, D., Batard, E., & Montassier, E. (2020). The effects of inulin on gut microbial composition: a systematic review of evidence from human studies. *European Journal of Clinical Microbiology & Infectious Diseases*, *39*(3), 403-413.

Lecerf, J. M., Depeint, F., Clerc, E., Dugenet, Y., Niamba, C. N., Rhazi, L., Cayzeele, A., Abdelnour, G., Jaruga, A., Younes, H., Jacobs, H., Lambrey, G., Abdelnour, A. M., &

Pouillart, P. R. (2012). Xylo-oligosaccharide (XOS) in combination with inulin modulates both the intestinal environment and immune status in healthy subjects, while XOS alone only shows prebiotic properties. *British Journal of Nutrition*, *108*(10), 1847-1858.

Lenis, A. T., Lec, P. M., Chamie, K., & Mshs, M. D. (2020). Bladder Cancer: A Review. *JAMA*, *324*(19), 1980-1991.

Levy, K., Natarajan, S., Wang, J. H., et al. (2020). Abdominal FLASH irradiation reduces radiation-induced gastrointestinal toxicity for the treatment of ovarian cancer in mice. *Scientific Reports*, *10*(1).

Lewis, G., Wang, B., Shafiei Jahani, P., et al. (2019). Dietary Fiber-Induced Microbial Short Chain Fatty Acids Suppress ILC2-Dependent Airway Inflammation. *Front Immunol*, *10*, 2051.

Li, D., Feng, Y., Tian, M., Ji, J., Hu, X., & Chen, F. (2021). Gut microbiota-derived inosine from dietary barley leaf supplementation attenuates colitis through PPARgamma signaling activation. *Microbiome*, *9*(1), 83.

Li, J. K., Li, J., Wang, H., Qi, L. W., Zhu, Y. M., & Lai, M. D. (2019). Tyrosine and Glutamine-Leucine Are Metabolic Markers of Early-Stage Colorectal Cancers. *Gastroenterology*, *157*(1), 257-+.

Li, Q. R., Cao, L. J., Tian, Y., Zhang, P., Ding, C. J., Lu, W. J., Jia, C. X., Shao, C., Liu, W. Y., Wang, D., Ye, H., & Hao, H. P. (2018). Butyrate Suppresses the Proliferation of Colorectal Cancer Cells via Targeting Pyruvate Kinase M2 and Metabolic Reprogramming. *Molecular & Cellular Proteomics*, *17*(8), 1531-1545.

Li, Y., Dong, J., Xiao, H., Zhang, S., Wang, B., Cui, M., & Fan, S. (2020). Gut commensal derived-valeric acid protects against radiation injuries. *Gut Microbes*, *11*(4), 789-806.

Li, Y., Elmen, L., Segota, I., Xian, Y., Tinoco, R., Feng, Y., Fujita, Y., Segura Munoz, R. R., Schmaltz, R., Bradley, L. M., Ramer-Tait, A., Zarecki, R., Long, T., Peterson, S. N., & Ronai, Z. A. (2020). Prebiotic-Induced Anti-tumor Immunity Attenuates Tumor Growth. *Cell Rep*, *30*(6), 1753-1766 e1756.

Li, Y., Ishiguro, H., Kawahara, T., Kashiwagi, E., Izumi, K., & Miyamoto, H. (2014). Loss of GATA3 in bladder cancer promotes cell migration and invasion. *Cancer Biology & Therapy*, *15*(4), 428-435.

Liang, L., Liu, L., Zhou, W., Yang, C., Mai, G., Li, H., & Chen, Y. (2022). Gut microbiota-derived butyrate regulates gut mucus barrier repair by activating the macrophage/WNT/ERK signaling pathway. *Clin Sci (Lond)*, *136*(4), 291-307.

Lieu, E. L., Nguyen, T., Rhyne, S., & Kim, J. (2020). Amino acids in cancer. *Experimental and Molecular Medicine*, *52*(1), 15-30.

Lim, B. O., Yamada, K., Nonaka, M., Kuramoto, Y., Hung, P., & Sugano, M. (1997). Dietary fibers modulate indices of intestinal immune function in rats. *Journal of Nutrition*, *127*(5), 663-667.

Liu, H., Wang, J., He, T., Becker, S., Zhang, G. L., Li, D. F., & Ma, X. (2018). Butyrate: A Double-Edged Sword for Health? *Advances in Nutrition*, *9*(1), 21-29.

Liu, L., Guo, X., Rao, J. N., Zou, T. T., Xiao, L., Yu, T. X., Timmons, J. A., Turner, D. J., & Wang, J. Y. (2009). Polyamines regulate E-cadherin transcription through c-Myc modulating

intestinal epithelial barrier function. *American Journal of Physiology-Cell Physiology*, *296*(4), C801-C810.

Long, Z. G., Feng, G. J., Zhao, N., Wu, L., & Zhu, H. B. (2020). Isoferulic acid inhibits human leukemia cell growth through induction of G2/M-phase arrest and inhibition of Akt/mTOR signaling. *Molecular Medicine Reports*, *21*(3), 1035-1042.

Loskog, A., Dzojic, H., Vikman, S., Ninalga, C., Essand, M., Korsgren, O., & Totterman, T. H. (2004). Adenovirus CD40 ligand gene therapy counteracts immune escape mechanisms in the tumor Microenvironment. *Journal of Immunology*, *172*(11), 7200-7205.

Luu, M., Riester, Z., Baldrich, A., et al. (2021). Microbial short-chain fatty acids modulate CD8(+) T cell responses and improve adoptive immunotherapy for cancer. *Nat Commun*, *12*(1), 4077.

Lycke, N. Y., & Bemark, M. (2017). The regulation of gut mucosal IgA B-cell responses: recent developments. *Mucosal Immunol*, *10*(6), 1361-1374.

Ma, C., Han, M. J., Heinrich, B., et al. (2018). Gut microbiome-mediated bile acid metabolism regulates liver cancer via NKT cells. *Science*, *360*(6391).

Madison, B. B., & Nakagawa, H. (2011). Delta force in intestinal crypts. *Gastroenterology*, *140*(4), 1135-1139.

Mager, L. F., Burkhard, R., Pett, N., Cooke, N. C. A., Brown, K., Ramay, H., Paik, S., Stagg, J., Groves, R. A., Gallo, M., Lewis, I. A., Geuking, M. B., & McCoy, K. D. (2020). Microbiome-derived inosine modulates response to checkpoint inhibitor immunotherapy. *Science*, *369*(6510), 1481-1489.

Mah, L. J., El-Osta, A., & Karagiannis, T. C. (2010). gammaH2AX: a sensitive molecular marker of DNA damage and repair. *Leukemia*, *24*(4), 679-686.

Majchrzak, K., Nelson, M. H., Bailey, S. R., Bowers, J. S., Yu, X. Z., Rubinstein, M. P., Himes, R. A., & Paulos, C. M. (2016). Exploiting IL-17-producing CD4+ and CD8+ T cells to improve cancer immunotherapy in the clinic. *Cancer Immunol Immunother*, *65*(3), 247-259.

Malipatlolla, D. K., Patel, P., Sjoberg, F., Devarakonda, S., Kalm, M., Angenete, E., Lindskog, E. B., Grander, R., Persson, L., Stringer, A., Wildearng, U., Swanpalmer, J., Kuhn, H. G., Steineck, G., & Bull, C. (2019). Long-term mucosal injury and repair in a murine model of pelvic radiotherapy. *Scientific Reports*, *9*.

Mandal, S., Van Treuren, W., White, R. A., Eggesbo, M., Knight, R., & Peddada, S. D. (2015). Analysis of composition of microbiomes: a novel method for studying microbial composition. *Microb Ecol Health Dis*, *26*, 27663.

Mao, W. P., Huang, X., Wang, L. S., Zhang, Z. W., Liu, M. N., Li, Y., Luo, M., Yao, X. D., Fan, J., & Geng, J. (2019). Circular RNA hsa_circ_0068871 regulates FGFR3 expression and activates STAT3 by targeting miR-181a-5p to promote bladder cancer progression. *Journal of Experimental & Clinical Cancer Research*, *38*.

Mao, Z. Y., Bozzella, M., Seluanov, A., & Gorbunova, V. (2008). Comparison of nonhomologous end joining and homologous recombination in human cells. *DNA Repair*, *7*(10), 1765-1771.

Marconi, R., Serafini, A., Giovanetti, A., Bartoleschi, C., Pardini, M. C., Bossi, G., & Strigari, L. (2019). Cytokine Modulation in Breast Cancer Patients Undergoing Radiotherapy: A

Revision of the Most Recent Studies. *International Journal of Molecular Sciences*, *20*(2).

Marques, F. Z., Mackay, C. R., & Kaye, D. M. (2018). Beyond gut feelings: how the gut microbiota regulates blood pressure. *Nature Reviews Cardiology*, *15*(1), 20-32.

Marques, F. Z., Nelson, E., Chu, P. Y., Horlock, D., Fiedler, A., Ziemann, M., Tan, J. K., Kuruppu, S., Rajapakse, N. W., El-Osta, A., Mackay, C. R., & Kaye, D. M. (2017). High-Fiber Diet and Acetate Supplementation Change the Gut Microbiota and Prevent the Development of Hypertension and Heart Failure in Hypertensive Mice. *Circulation*, *135*(10), 964-977.

Marshall, J. S., Warrington, R., Watson, W., & Kim, H. L. (2018). An introduction to immunology and immunopathology. *Allergy Asthma and Clinical Immunology*, *14*.

Masopust, D., & Schenkel, J. M. (2013). The integration of T cell migration, differentiation and function. *Nature Reviews Immunology*, *13*(5), 309-320.

Massari, F., Ciccarese, C., Santoni, M., Iacovelli, R., Mazzucchelli, R., Piva, F., Scarpelli, M., Berardi, R., Tortora, G., Lopez-Beltran, A., Cheng, L., & Montironi, R. (2016). Metabolic phenotype of bladder cancer. *Cancer Treat Rev*, *45*, 46-57.

Matson, V., Fessler, J., Bao, R., Chongsuwat, T., Zha, Y., Alegre, M. L., Luke, J. J., & Gajewski, T. F. (2018). The commensal microbiome is associated with anti-PD-1 efficacy in metastatic melanoma patients. *Science*, *359*(6371), 104-108.

Mazmanian, S. K., Liu, C. H., Tzianabos, A. O., & Kasper, D. L. (2005). An immunomodulatory molecule of symbiotic bacteria directs maturation of the host immune system. *Cell*, *122*(1), 107-118.

Miller, A. A., Kurschel, E., Osieka, R., & Schmidt, C. G. (1987). Clinical-Pharmacology of Sodium-Butyrate in Patients with Acute-Leukemia. *European Journal of Cancer & Clinical Oncology*, *23*(9), 1283-1287.

Miller, T. L. (1978). The pathway of formation of acetate and succinate from pyruvate by Bacteroides succinogenes. *Archives of Microbiology*, *117*(2), 145-152.

Miyamoto, Y., & Itoh, K. (2000). Bacteroides acidifaciens sp. nov., isolated from the caecum of mice. *Int J Syst Evol Microbiol*, *50 Pt 1*, 145-148.

Modena, B. D., Milam, R., Harrison, F., Cheeseman, J. A., Abecassis, M. M., Friedewald, J. J., Kirk, A. D., & Salomon, D. R. (2017). Changes in Urinary Microbiome Populations Correlate in Kidney Transplants With Interstitial Fibrosis and Tubular Atrophy Documented in Early Surveillance Biopsies. *American Journal of Transplantation*, *17*(3).

Moolenbeek, C., & Ruitenberg, E. J. (1981). The Swiss Roll - a Simple Technique for Histological Studies of the Rodent Intestine. *Laboratory Animals*, *15*(1), 57-59.

Morita, T., Kasaoka, S., Hase, K., & Kiriyama, S. (1999). Psyllium shifts the fermentation site of high-amylose cornstarch toward the distal colon and increases fecal butyrate concentration in rats. *Journal of Nutrition*, *129*(11), 2081-2087.

Mowat, A. M., & Agace, W. W. (2014). Regional specialization within the intestinal immune system. *Nature Reviews Immunology*, *14*(10), 667-685.

Murphy, J., Stacey, D., Crook, J., Thompson, B., & Panetta, D. (2000). Testing control of radiation-induced diarrhea with a psyllium bulking agent: a pilot study. *Canadian Oncology Nursing Journal*, *10*(3), 96-100.

Murray, S., Schell, K., McCarthy, D. O., & Albertini, M. R. (1997). Tumor growth, weight loss and cytokines in SCID mice. *Cancer Letters*, *111*(1-2), 111-115.

Narayanan, A., Baskaran, S. A., Amalaradjou, M. A., & Venkitanarayanan, K. (2015). Anticarcinogenic properties of medium chain fatty acids on human colorectal, skin and breast cancer cells in vitro. *Int J Mol Sci*, *16*(3), 5014-5027.

Nearing, J. T., Douglas, G. M., Comeau, A. M., & Langille, M. G. I. (2018). Denoising the Denoisers: an independent evaluation of microbiome sequence error-correction approaches. *Peerj*, *6*.

Nikolos, F., Hayashi, K., Hoi, X. P., Alonzo, M. E., Mo, Q. X., Kasabyan, A., Furuya, H., Trepel, J., Di Vizio, D., Guarnerio, J., Theodorescu, D., Rosser, C., Apolo, A., Galsky, M., & Chan, K. S. (2022). Cell death-induced immunogenicity enhances chemoimmunotherapeutic response by converting immune-excluded into T-cell inflamed bladder tumors. *Nature Communications*, *13*(1).

O'Brien, S. A., Orf, J., Skrzypczynska, K. M., Tan, H., Kim, J., DeVoss, J., Belmontes, B., & Egen, J. G. (2021). Activity of tumor-associated macrophage depletion by CSF1R blockade is highly dependent on the tumor model and timing of treatment. *Cancer Immunology Immunotherapy*, *70*(8), 2401-2410.

O'Callaghan, A., & van Sinderen, D. (2016). Bifidobacteria and Their Role as Members of the Human Gut Microbiota. *Frontiers in Microbiology*, *7*.

O'Connor, A., & Crosswaite, S. (2018). Can healthy motivated British adults achieve the revised UK government fibre recommendations of 30 g per day? Results from a preliminary study. *Nutr Health*, *24*(4), 211-215.

O'Donnell, M. A., Luo, Y., Hunter, S. E., Chen, X. H., Hayes, L. L., & Clinton, S. K. (2004). Interleukin-12 immunotherapy of murine transitional cell carcinoma of the bladder: Dose dependent tumor eradication and generation of protective immunity. *Journal of Urology*, *171*(3), 1330-1335.

O'Toole, P. W., & Jeffery, I. B. (2015). Gut microbiota and aging. *Science*, *350*(6265), 1214-1215.

Ogata, M., Ogita, T., Tari, H., Arakawa, T., & Suzuki, T. (2017). Supplemental psyllium fibre regulates the intestinal barrier and inflammation in normal and colitic mice. *Br J Nutr*, *118*(9), 661-672.

Okumura, R., & Takeda, K. (2018). Maintenance of intestinal homeostasis by mucosal barriers. *Inflamm Regen*, *38*, 5.

Olcina, M. M., & Giaccia, A. J. (2016). Reducing radiation-induced gastrointestinal toxicity - the role of the PHD/HIF axis. *J Clin Invest*, *126*(10), 3708-3715.

Oronsky, B. T., Knox, S. J., & Scicinski, J. (2011). Six Degrees of Separation: The Oxygen Effect in the Development of Radiosensitizers. *Translational Oncology*, *4*(4), 256-265.

Ott, S. J., Musfeldt, M., Wenderoth, D. F., Hampe, J., Brant, O., Folsch, U. R., Timmis, K. N., & Schreiber, S. (2004). Reduction in diversity of the colonic mucosa associated bacterial microflora in patients with active inflammatory bowel disease. *Gut*, *53*(5), 685-693.

Ozawa, A., Tanji, N., Kikugawa, T., Sasaki, T., Yanagihara, Y., Miura, N., & Yokoyama, M. (2010). Inhibition of bladder tumour growth by histone deacetylase inhibitor. *BJU Int*, *105*(8), 1181-1186.

Paillas, S., Then, C. K., Kilgas, S., Ruan, J. L., Thompson, J., Elliott, A., Smart, S., & Kiltie, A. E. (2020). The Histone Deacetylase Inhibitor Romidepsin Spares Normal Tissues While Acting as an Effective Radiosensitizer in Bladder Tumors in Vivo. *Int J Radiat Oncol Biol Phys*, *107*(1), 212-221.

Palata, O., Hradilova Podzimkova, N., Nedvedova, E., Umprecht, A., Sadilkova, L., Palova Jelinkova, L., Spisek, R., & Adkins, I. (2019). Radiotherapy in Combination With Cytokine Treatment. *Front Oncol*, *9*, 367.

Pan, S. J., Fan, M., Liu, Z. N., Li, X., & Wang, H. J. (2021). Serine, glycine and one-carbon metabolism in cancer (Review). *International Journal of Oncology*, *58*(2), 158-170.

Panebianco, C., Adamberg, K., Adamberg, S., Saracino, C., Jaagura, M., Kolk, K., Di Chio, A. G., Graziano, P., Vilu, R., & Pazienza, V. (2017). Engineered Resistant-Starch (ERS) Diet Shapes Colon Microbiota Profile in Parallel with the Retardation of Tumor Growth in In Vitro and In Vivo Pancreatic Cancer Models. *Nutrients*, *9*(4).

Pang, Z. Q., Chong, J., Zhou, G. Y., Morais, D. A. D., Chang, L., Barrette, M., Gauthier, C., Jacques, P. E., Li, S. Z., & Xia, J. G. (2021). MetaboAnalyst 5.0: narrowing the gap between raw spectra and functional insights. *Nucleic Acids Research*, *49*(W1), W388-W396.

Paris, F., Fuks, Z., Kang, A., Capodieci, P., Juan, G., Ehleiter, D., Haimovitz-Friedman, A., Cordon-Cardo, C., & Kolesnick, R. (2001). Endothelial apoptosis as the primary lesion initiating intestinal radiation damage in mice. *Science*, *293*(5528), 293-297.

Park, J. S., Lee, E. J., Lee, J. C., Kim, W. K., & Kim, H. S. (2007). Anti-inflammatory effects of short chain fatty acids in IFN-gamma-stimulated RAW 264.7 murine macrophage cells: involvement of NF-kappaB and ERK signaling pathways. *Int Immunopharmacol*, *7*(1), 70-77.

Park, M., Kwon, J., Shin, H. J., Moon, S. M., Kim, S. B., Shin, U. S., Han, Y. H., & Kim, Y. (2020). Butyrate enhances the efficacy of radiotherapy via FOXO3A in colorectal cancer patientderived organoids. *Int J Oncol*, *57*(6), 1307-1318.

Parsonnet, J., Friedman, G. D., Vandersteen, D. P., Chang, Y., Vogelman, J. H., Orentreich, N., & Sibley, R. K. (1991). Helicobacter pylori infection and the risk of gastric carcinoma. *N Engl J Med*, *325*(16), 1127-1131.

Patel, P., Malipatlolla, D. K., Devarakonda, S., Bull, C., Rascon, A., Nyman, M., Stringer, A., Tremaroli, V., Steineck, G., & Sjoberg, F. (2020). Dietary Oat Bran Reduces Systemic Inflammation in Mice Subjected to Pelvic Irradiation. *Nutrients*, *12*(8).

Pearce, M. M., Hilt, E. E., Rosenfeld, A. B., Zilliox, M. J., Thomas-White, K., Fok, C., Kliethermes, S., Schreckenberger, P. C., Brubaker, L., Gai, X. W., & Wolfe, A. J. (2014). The Female Urinary Microbiome: a Comparison of Women with and without Urgency Urinary Incontinence. *Mbio*, *5*(4).

Peng, L. Y., Li, Z. R., Green, R. S., Holzman, I. R., & Lin, J. (2009). Butyrate Enhances the Intestinal Barrier by Facilitating Tight Junction Assembly via Activation of AMP-Activated Protein Kinase in Caco-2 Cell Monolayers. *Journal of Nutrition*, *139*(9), 1619-1625.

Peng, T. C., Wang, G., Cheng, S. T., Xiong, Y. Y., Cao, R., Qian, K. Y., Ju, L. G., Wang, X. H., & Xiao, Y. (2020). The role and function of PPAR gamma in bladder cancer. *Journal of Cancer*, *11*(13), 3965-3975.

Pettenati, C., & Ingersoll, M. A. (2018). Mechanisms of BCG immunotherapy and its outlook for bladder cancer. *Nature Reviews Urology*, *15*(10), 615-625.

Philippou, Y., Sjoberg, H. T., Murphy, E., et al. (2020). Impacts of combining anti-PD-L1 immunotherapy and radiotherapy on the tumour immune microenvironment in a murine prostate cancer model. *Br J Cancer*, *123*(7), 1089-1100.

Pierre, F., Perrin, P., Champ, M., Bornet, F., Meflah, K., & Menanteau, J. (1997). Short-chain fructo-oligosaccharides reduce the occurrence of colon tumors and develop gut-associated lymphoid tissue in Min mice. *Cancer Research*, *57*(2), 225-228.

Pinto, A., Fidalgo, P., Cravo, M., Midoes, J., Chaves, P., Rosa, J., dos Anjos Brito, M., & Leitao, C. N. (1999). Short chain fatty acids are effective in short-term treatment of chronic radiation proctitis: randomized, double-blind, controlled trial. *Dis Colon Rectum*, *42*(6), 788-795; discussion 795-786.

Pontifex, M. G., Mushtaq, A., Le Gall, G., Rodriguez-Ramiro, I., Blokker, B. A., Hoogteijling, M. E. M., Ricci, M., Pellizzon, M., Vauzour, D., & Muller, M. (2021). Differential Influence of Soluble Dietary Fibres on Intestinal and Hepatic Carbohydrate Response. *Nutrients*, *13*(12).

Popovic, V. B., Situm, M., Chow, C. E. T., Chan, L. S., Roje, B., & Terzic, J. (2018). The urinary microbiome associated with bladder cancer. *Scientific Reports*, *8*.

Potten, C. S. (1977). Extreme Sensitivity of Some Intestinal Crypt Cells to X and Gamma-Irradiation. *Nature*, *269*(5628), 518-521.

Potten, C. S., & Grant, H. H. (1998). The relationship between ionizing radiation-induced apoptosis and stem cells in the small and large intestine. *British Journal of Cancer*, *78*(8), 993-1003.

Priolo, C., Khabibullin, D., Reznik, E., Filippakis, H., Ogorek, B., Kavanagh, T. R., Nijmeh, J., Herbert, Z. T., Asara, J. M., Kwiatkowski, D. J., Wu, C. L., & Henske, E. P. (2018). Impairment of gamma-glutamyl transferase 1 activity in the metabolic pathogenesis of chromophobe renal cell carcinoma. *Proceedings of the National Academy of Sciences of the United States of America*, *115*(27), E6274-E6282.

Priyadarshini, M., Kotlo, K. U., Dudeja, P. K., & Layden, B. T. (2018). Role of Short Chain Fatty Acid Receptors in Intestinal Physiology and Pathophysiology. *Comprehensive Physiology*, *8*(3), 1091-1115.

Pushalkar, S., Hundeyin, M., Daley, D., et al. (2018). The Pancreatic Cancer Microbiome Promotes Oncogenesis by Induction of Innate and Adaptive Immune Suppression. *Cancer Discovery*, *8*(4), 403-416.

Rafter, J., Bennett, M., Caderni, G., Clune, Y., Hughes, R., Karlsson, P. C., Klinder, A., O'Riordan, M., O'Sullivan, G. C., Pool-Zobel, B., Rechkemmer, G., Roller, M., Rowland, I., Salvadori, M., Thijs, H., Van Loo, J., Watzl, B., & Collins, J. K. (2007). Dietary synbiotics reduce cancer risk factors in polypectomized and colon cancer patients. *American Journal of Clinical Nutrition*, *85*(2), 488-496.

Ramirez, D., Gupta, A., Canter, D., Harrow, B., Dobbs, R. W., Kucherov, V., Mueller, E., Streeper, N., Uhlman, M. A., Svatek, R. S., Messing, E. M., & Lotan, Y. (2016). Microscopic haematuria at time of diagnosis is associated with lower disease stage in patients with newly diagnosed bladder cancer. *BJU Int*, *117*(5), 783-786.

Raskov, H., Orhan, A., Christensen, J. P., & Gogenur, I. (2021). Cytotoxic CD8(+) T cells in cancer and cancer immunotherapy. *Br J Cancer*, *124*(2), 359-367.

Reis Ferreira, M., Andreyev, H. J. N., Mohammed, K., Truelove, L., Gowan, S. M., Li, J., Gulliford, S. L., Marchesi, J. R., & Dearnaley, D. P. (2019). Microbiota- and Radiotherapy-Induced Gastrointestinal Side-Effects (MARS) Study: A Large Pilot Study of the Microbiome in Acute and Late-Radiation Enteropathy. *Clin Cancer Res*, *25*(21), 6487-6500.

Reisz, J. A., Bansal, N., Qian, J., Zhao, W. L., & Furdui, C. M. (2014). Effects of Ionizing Radiation on Biological Molecules-Mechanisms of Damage and Emerging Methods of Detection. *Antioxidants & Redox Signaling*, *21*(2), 260-292.

Rendon-Huerta, J. A., Juarez-Flores, B., Pinos-Rodriguez, J. M., Aguirre-Rivera, J. R., & Delgado-Portales, R. E. (2012). Effects of different sources of fructans on body weight, blood metabolites and fecal bacteria in normal and obese non-diabetic and diabetic rats. *Plant Foods Hum Nutr*, *67*(1), 64-70.

Renouf, M., & Hendrich, S. (2011). Bacteroides uniformis is a putative bacterial species associated with the degradation of the isoflavone genistein in human feces. *J Nutr*, *141*(6), 1120-1126.

Robert, C., Chassard, C., Lawson, P. A., & Bernalier-Donadille, A. (2007). Bacteroides cellulosilyticus sp nov., a cellulolytic bacterium from the human gut microbial community. *International Journal of Systematic and Evolutionary Microbiology*, *57*, 1516-1520.

Robinson, A., Keely, S., Karhausen, J., Gerich, M. E., Furuta, G. T., & Colgan, S. P. (2008). Mucosal protection by hypoxia-inducible factor prolyl hydroxylase inhibition. *Gastroenterology*, *134*(1), 145-155.

Roediger, W. E. (1980). Role of anaerobic bacteria in the metabolic welfare of the colonic mucosa in man. *Gut*, *21*(9), 793-798.

Romesser, P. B., Kim, A. S., Jeong, J., Mayle, A., Dow, L. E., & Lowe, S. W. (2019). Preclinical murine platform to evaluate therapeutic countermeasures against radiation-induced gastrointestinal syndrome. *Proceedings of the National Academy of Sciences of the United States of America*, *116*(41), 20672-20678.

Rooks, M. G., & Garrett, W. S. (2016). Gut microbiota, metabolites and host immunity. *Nature Reviews Immunology*, *16*(6), 341-352.

Rossi, M., Corradini, C., Amaretti, A., Nicolini, M., Pompei, A., Zanoni, S., & Matteuzzi, D. (2005). Fermentation of fructooligosaccharides and inulin by bifidobacteria: a comparative study of pure and fecal cultures. *Applied and Environmental Microbiology*, *71*(10), 6150-6158.

Routy, B., Le Chatelier, E., Derosa, L., et al. (2018). Gut microbiome influences efficacy of PD-1-based immunotherapy against epithelial tumors. *Science*, *359*(6371), 91-+.

Ruan, J. L., Lee, C., Wouters, S., Tullis, I. D. C., Verslegers, M., Mysara, M., Then, C. K., Smart, S. C., Hill, M. A., Muschel, R. J., Giaccia, A. J., Vojnovic, B., Kiltie, A. E., & Petersson, K. (2021). Irradiation at Ultra-High (FLASH) Dose Rates Reduces Acute Normal Tissue Toxicity in the Mouse Gastrointestinal System. *Int J Radiat Oncol Biol Phys*, *111*(5), 1250-1261.

Rutkowski, M. R., Svoronos, N., Perales-Puchalt, A., & Conejo-Garcia, J. R. (2015). The Tumor Macroenvironment: Cancer-Promoting Networks Beyond Tumor Beds. *Immunotherapy of Cancer*, *128*, 235-262.

Saito, R., Smith, C. C., Utsumi, T., Bixby, L. M., Kardos, J., Wobker, S. E., Stewart, K. G., Chai, S., Manocha, U., Byrd, K. M., Damrauer, J. S., Williams, S. E., Vincent, B. G., & Kim, W. Y. (2018). Molecular Subtype-Specific Immunocompetent Models of High-Grade Urothelial Carcinoma Reveal Differential Neoantigen Expression and Response to Immunotherapy. *Cancer Res*, *78*(14), 3954-3968.

Salimi, V., Shahsavari, Z., Safizadeh, B., Hosseini, A., Khademian, N., & Tavakoli-Yaraki, M. (2017). Sodium butyrate promotes apoptosis in breast cancer cells through reactive oxygen species (ROS) formation and mitochondrial impairment. *Lipids in Health and Disease*, *16*.

Sanli, O., Dobruch, J., Knowles, M. A., Burger, M., Alemozaffar, M., Nielsen, M. E., & Lotan, Y. (2017). Bladder cancer. *Nat Rev Dis Primers*, *3*, 17022.

Savage, D. C. (1977). Microbial ecology of the gastrointestinal tract. *Annu Rev Microbiol*, *31*, 107-133.

Schauber, J., Svanholm, C., Termen, S., Iffland, K., Menzel, T., Scheppach, W., Melcher, R., Agerberth, B., Luhrs, H., & Gudmundsson, G. H. (2003). Expression of the cathelicidin LL-37 is modulated by short chain fatty acids in colonocytes: relevance of signalling pathways. *Gut*, *52*(5), 735-741.

Schley, P. D., & Field, C. J. (2002). The immune-enhancing effects of dietary fibres and prebiotics. *British Journal of Nutrition*, *87*, S221-S230.

Schulthess, J., Pandey, S., Capitani, M., Rue-Albrecht, K. C., Arnold, I., Franchini, F., Chomka, A., Ilott, N. E., Johnston, D. G. W., Pires, E., McCullagh, J., Sansom, S. N., Arancibia-Carcamo, C. V., Uhlig, H. H., & Powrie, F. (2019). The Short Chain Fatty Acid Butyrate Imprints an Antimicrobial Program in Macrophages. *Immunity*, *50*(2), 432-+.

Schultze, J. L., Mass, E., & Schlitzer, A. (2019). Emerging Principles in Myelopoiesis at Homeostasis and during Infection and Inflammation. *Immunity*, *50*(2), 288-301.

Schwiertz, A., Lehmann, U., Jacobasch, G., & Blaut, M. (2002). Influence of resistant starch on the SCFA production and cell counts of butyrate-producing Eubacterium spp. in the human intestine. *J Appl Microbiol*, *93*(1), 157-162.

Segain, J. P., de la Bletiere, D. R., Bourreille, A., Leray, V., Gervois, N., Rosales, C., Ferrier, L., Bonnet, C., Blottiere, H. M., & Galmiche, J. P. (2000). Butyrate inhibits inflammatory responses through NF kappa B inhibition: implications for Crohn's disease. *Gut*, *47*(3), 397-403.

Segata, N., Izard, J., Waldron, L., Gevers, D., Miropolsky, L., Garrett, W. S., & Huttenhower, C. (2011). Metagenomic biomarker discovery and explanation. *Genome Biol*, *12*(6), R60.

Semaan, J., El-Hakim, S., Ibrahim, J. N., Safi, R., Elnar, A. A., & El Boustany, C. (2020). Comparative effect of sodium butyrate and sodium propionate on proliferation, cell cycle and apoptosis in human breast cancer cells MCF-7. *Breast Cancer*, 10.1007/s12282-020-01063-6.

Sethi, V., Kurtom, S., Tarique, M., Lavania, S., Malchiodi, Z., Hellmund, L., Zhang, L., Sharma, U., Giri, B., Garg, B., Ferrantella, A., Vickers, S. M., Banerjee, S., Dawra, R., Roy, S.,

Ramakrishnan, S., Saluja, A., & Dudeja, V. (2018). Gut Microbiota Promotes Tumor Growth in Mice by Modulating Immune Response. *Gastroenterology*, *155*(1), 33-+.

Shadad, A. K., Sullivan, F. J., Martin, J. D., & Egan, L. J. (2013). Gastrointestinal radiation injury: symptoms, risk factors and mechanisms. *World J Gastroenterol*, *19*(2), 185-198.

Sheen, J. H., Zoncu, R., Kim, D., & Sabatini, D. M. (2011). Defective Regulation of Autophagy upon Leucine Deprivation Reveals a Targetable Liability of Human Melanoma Cells In Vitro and In Vivo. *Cancer Cell*, *19*(5), 613-628.

Shi, F. Q., Li, Y., Han, R., Fu, A., Wang, R. H., Nusbaum, O., Qin, Q., Chen, X. Y., Hou, L., & Zhu, Y. (2021). Valerian and valeric acid inhibit growth of breast cancer cells possibly by mediating epigenetic modifications. *Scientific Reports*, *11*(1).

Shiao, S. L., & Coussens, L. M. (2010). The tumor-immune microenvironment and response to radiation therapy. *J Mammary Gland Biol Neoplasia*, *15*(4), 411-421.

Shiao, S. L., Kershaw, K. M., Limon, J. J., et al. (2021). Commensal bacteria and fungi differentially regulate tumor responses to radiation therapy. *Cancer Cell*, *39*(9), 1202-1213 e1206.

Shoaib, M., Shehzad, A., Omar, M., Rakha, A., Raza, H., Sharif, H. R., Shakeel, A., Ansari, A., & Niazi, S. (2016). Inulin: Properties, health benefits and food applications. *Carbohydrate Polymers*, *147*, 444-454.

Shokryazdan, P., Jahromi, M. F., Navidshad, B., & Liang, J. B. (2017). Effects of prebiotics on immune system and cytokine expression. *Medical Microbiology and Immunology*, *206*(1), 1-9.

Shou, J. F., Zhang, Q., & Zhang, D. H. (2021). The prognostic effect of metastasis patterns on overall survival in patients with distant metastatic bladder cancer: a SEER population-based analysis. *World Journal of Urology*, *39*(11), 4151-4158.

Shukla, S. D., Budden, K. F., Neal, R., & Hansbro, P. M. (2017). Microbiome effects on immunity, health and disease in the lung. *Clin Transl Immunology*, *6*(3), e133.

Silva, L. G., Ferguson, B. S., Avila, A. S., & Faciola, A. P. (2018). Sodium propionate and sodium butyrate effects on histone deacetylase (HDAC) activity, histone acetylation, and inflammatory gene expression in bovine mammary epithelial cells. *J Anim Sci*, *96*(12), 5244-5252.

Sims, T. T., El Alam, M. B., Karpinets, T. V., et al. (2021). Gut microbiome diversity is an independent predictor of survival in cervical cancer patients receiving chemoradiation. *Communications Biology*, *4*(1).

Singh, N., Thangaraju, M., Prasad, P. D., Martin, P. M., Lambert, N. A., Boettger, T., Offermanns, S., & Ganapathy, V. (2010). Blockade of Dendritic Cell Development by Bacterial Fermentation Products Butyrate and Propionate through a Transporter (Slc5a8)-dependent Inhibition of Histone Deacetylases. *Journal of Biological Chemistry*, *285*(36), 27601-27608.

Sirichoat, A., Sankuntaw, N., Engchanil, C., Buppasiri, P., Faksri, K., Namwat, W., Chantratita, W., & Lulitanond, V. (2021). Comparison of different hypervariable regions of 16S rRNA for taxonomic profiling of vaginal microbiota using next-generation sequencing. *Archives of Microbiology*, *203*(3), 1159-1166.

Sivan, A., Corrales, L., Hubert, N., Williams, J. B., Aquino-Michaels, K., Earley, Z. M., Benyamin, F. W., Lei, Y. M., Jabri, B., Alegre, M. L., Chang, E. B., & Gajewski, T. F. (2015). Commensal Bifidobacterium promotes antitumor immunity and facilitates anti-PD-L1 efficacy. *Science*, *350*(6264), 1084-1089.

Soltanian, N., Janghorbani, M., & Adibib, P. (2018). Effects of psyllium vs. placebo on constipation, weight, glycemia, and lipids: A randomized trial in patients with type 2 diabetes and chronic constipation. *Complementary Therapies in Medicine*, *40*, 1-7.

Sonnenburg, E. D., Smits, S. A., Tikhonov, M., Higginbottom, S. K., Wingreen, N. S., & Sonnenburg, J. L. (2016). Diet-induced extinctions in the gut microbiota compound over generations. *Nature*, *529*(7585), 212-U208.

Spakowicz, D., Bibi, A., Muniak, M., Williams, N. F., Hoyd, R., & Presley, C. J. (2021). The aging microbiome and response to immunotherapy: Considerations for the treatment of older adults with cancer. *Journal of Geriatric Oncology*, *12*(6), 985-989.

Spencer, C. N., McQuade, J. L., Gopalakrishnan, V., et al. (2021). Dietary fiber and probiotics influence the gut microbiome and melanoma immunotherapy response. *Science*, *374*(6575), 1632-1640.

Sternberg, C. N., Bellmunt, J., Sonpavde, G., Siefker-Radtke, A. O., Stadler, W. M., Bajorin, D. F., Dreicer, R., George, D. J., Milowsky, M. I., Theodorescu, D., Vaughn, D. J., Galsky, M. D., Soloway, M. S., Quinn, D. I., & International Consultation on Urologic Disease-European Association of Urology Consultation on Bladder, C. (2013). ICUD-EAU International Consultation on Bladder Cancer 2012: Chemotherapy for urothelial carcinoma-neoadjuvant and adjuvant settings. *Eur Urol*, *63*(1), 58-66.

Stobbe, C. C., Park, S. J., & Chapman, J. D. (2002). The radiation hypersensitivity of cells at mitosis. *International Journal of Radiation Biology*, *78*(12), 1149-1157.

Summerhayes, I. C., & Franks, L. M. (1979). Effects of donor age on neoplastic transformation of adult mouse bladder epithelium in vitro. *J Natl Cancer Inst*, *62*(4), 1017-1023.

Sun, L., Zhang, L., Chen, J., Li, C. Q., Sun, H. Q., Wang, J. R., & Xiao, H. (2020). Activation of Tyrosine Metabolism in CD13(+) Cancer Stem Cells Drives Relapse in Hepatocellular Carcinoma. *Cancer Research and Treatment*, *52*(2), 604-621.

Sunkara, L. T., Jiang, W., & Zhang, G. (2012). Modulation of antimicrobial host defense peptide gene expression by free fatty acids. *Plos One*, *7*(11), e49558.

Tajaddini, A., Pourzand, A., Sanaat, Z., & Pirouzpanah, S. (2015). Dietary resistant starch contained foods and breast cancer risk: a case-control study in northwest of Iran. *Asian Pac J Cancer Prev*, *16*(10), 4185-4192.

Tan, J., McKenzie, C., Potamitis, M., Thorburn, A. N., Mackay, C. R., & Macia, L. (2014). The role of short-chain fatty acids in health and disease. *Adv Immunol*, *121*, 91-119.

Taniguchi, C. M., Miao, Y. R., Diep, A. N., Wu, C., Rankin, E. B., Atwood, T. F., Xing, L., & Giaccia, A. J. (2014). PHD Inhibition Mitigates and Protects Against Radiation-Induced Gastrointestinal Toxicity via HIF2. *Science Translational Medicine*, *6*(236).

Tanoue, T., Morita, S., Plichta, D. R., et al. (2019). A defined commensal consortium elicits CD8 T cells and anti-cancer immunity. *Nature*, *565*(7741), 600-605.

Taper, H. S., & Roberfroid, M. (1999). Influence of inulin and oligofructose on breast cancer and tumor growth. *J Nutr*, *129*(7 Suppl), 1488S-1491S.

Theis, V. S., Sripadam, R., Ramani, V., & Lal, S. (2010). Chronic radiation enteritis. *Clin Oncol (R Coll Radiol)*, *22*(1), 70-83.

Then, C. K., Paillas, S., Wang, X., Hampson, A., & Kiltie, A. E. (2020). Association of Bacteroides acidifaciens relative abundance with high-fibre diet-associated radiosensitisation. *BMC Biol*, *18*(1), 102.

Thursby, E., & Juge, N. (2017). Introduction to the human gut microbiota. *Biochemical Journal*, *474*(11), 1823-1836.

Tomayko, M. M., & Reynolds, C. P. (1989). Determination of Subcutaneous Tumor Size in Athymic (Nude) Mice. *Cancer Chemotherapy and Pharmacology*, *24*(3), 148-154.

Tran, L., Xiao, J. F., Agarwal, N., Duex, J. E., & Theodorescu, D. (2021). Advances in bladder cancer biology and therapy. *Nat Rev Cancer*, *21*(2), 104-121.

Tran, M. N., Choi, W., Wszolek, M. F., Navai, N., Lee, I. L. C., Nitti, G., Wen, S. J., Flores, E. R., Siefker-Radtke, A., Czerniak, B., Dinney, C., Barton, M., & McConkey, D. J. (2013). The p63 Protein Isoform Delta Np63 alpha Inhibits Epithelial-Mesenchymal Transition in Human Bladder Cancer Cells ROLE OF MIR-205. *Journal of Biological Chemistry*, *288*(5), 3275-3288.

Trompette, A., Gollwitzer, E. S., Pattaroni, C., Lopez-Mejia, I. C., Riva, E., Pernot, J., Ubags, N., Fajas, L., Nicod, L. P., & Marsland, B. J. (2018). Dietary Fiber Confers Protection against Flu by Shaping Ly6c(-) Patrolling Monocyte Hematopoiesis and CD8(+) T Cell Metabolism. *Immunity*, *48*(5), 992-+.

Tu, S., Zhang, X. L., Wan, H. F., Xia, Y. Q., Liu, Z. Q., Yang, X. H., & Wan, F. S. (2018). Effect of taurine on cell proliferation and apoptosis human lung cancer A549 cells. *Oncology Letters*, *15*(4), 5473-5480.

Turina, M., Mulhall, A. M., Mahid, S. S., Yashar, C., & Galandiuk, S. (2008). Frequency and surgical management of chronic complications related to pelvic radiation. *Arch Surg*, *143*(1), 46-52; discussion 52.

Turnbaugh, P. J., Ley, R. E., Hamady, M., Fraser-Liggett, C. M., Knight, R., & Gordon, J. I. (2007). The Human Microbiome Project. *Nature*, *449*(7164), 804-810.

Uribe-Herranz, M., Rafail, S., Beghi, S., Gil-de-Gomez, L., Verginadis, I., Bittinger, K., Pustylnikov, S., Pierini, S., Perales-Linares, R., Blair, I. A., Mesaros, C. A., Snyder, N. W., Bushman, F., Koumenis, C., & Facciabene, A. (2020). Gut microbiota modulate dendritic cell antigen presentation and radiotherapy-induced antitumor immune response. *Journal of Clinical Investigation*, *130*(1), 466-479.

Vacchelli, E., Aranda, F., Bloy, N., Buque, A., Cremer, I., Eggermont, A., Fridman, W. H., Fucikova, J., Galon, J., Spisek, R., Zitvogel, L., Kroemer, G., & Galluzzi, L. (2016). Trial Watch-Immunostimulation with cytokines in cancer therapy. *Oncoimmunology*, *5*(2), e1115942.

van der Hee, B., & Wells, J. M. (2021). Microbial Regulation of Host Physiology by Short-chain Fatty Acids. *Trends Microbiol*, *29*(8), 700-712.

Venegas, D. P., De la Fuente, M. K., Landskron, G., Gonzalez, M. J., Quera, R., Dijkstra, G., Harmsen, H. J. M., Faber, K. N., & Hermoso, M. A. (2019). Short Chain Fatty Acids (SCFAs)-Mediated Gut Epithelial and Immune Regulation and Its Relevance for Inflammatory Bowel Diseases (vol 10, 277, 2019). *Frontiers in Immunology*, *10*.

Vernia, P., Fracasso, P. L., Casale, V., Villotti, G., Marcheggiano, A., Stigliano, V., Pinnaro, P., Bagnardi, V., & Caprilli, R. (2000). Topical butyrate for acute radiation proctitis: randomised, crossover trial. *Lancet*, *356*(9237), 1232-1235.

Viaud, S., Saccheri, F., Mignot, G., et al. (2013). The intestinal microbiota modulates the anticancer immune effects of cyclophosphamide. *Science*, *342*(6161), 971-976.

Vinolo, M. A., Rodrigues, H. G., Hatanaka, E., Hebeda, C. B., Farsky, S. H., & Curi, R. (2009). Short-chain fatty acids stimulate the migration of neutrophils to inflammatory sites. *Clin Sci (Lond)*, *117*(9), 331-338.

Vinolo, M. A., Rodrigues, H. G., Hatanaka, E., Sato, F. T., Sampaio, S. C., & Curi, R. (2011). Suppressive effect of short-chain fatty acids on production of proinflammatory mediators by neutrophils. *J Nutr Biochem*, *22*(9), 849-855.

Vriesendorp, H. M., Vigneulle, R. M., Kitto, G., Pelky, T., Taylor, P., & Smith, J. (1992). Survival after Total-Body Irradiation - Effects of Irradiation of Exteriorized Small-Intestine. *Radiotherapy and Oncology*, *23*(3), 160-169.

Walsby-Tickle, J., Gannon, J., Hvinden, I., Bardella, C., Abboud, M. I., Nazeer, A., Hauton, D., Pires, E., Cadoux-Hudson, T., Schofield, C. J., & McCullagh, J. S. O. (2020). Anion-exchange chromatography mass spectrometry provides extensive coverage of primary metabolic pathways revealing altered metabolism in IDH1 mutant cells. *Commun Biol*, *3*(1), 247.

Wang, K., & Tepper, J. E. (2021). Radiation therapy-associated toxicity: Etiology, management, and prevention. *CA Cancer J Clin*, *71*(5), 437-454.

Wang, Q., McLoughlin, R. M., Cobb, B. A., Charrel-Dennis, M., Zaleski, K. J., Golenbock, D., Tzianabos, A. O., & Kasper, D. L. (2006). A bacterial carbohydrate links innate and adaptive responses through Toll-like receptor 2. *Journal of Experimental Medicine*, *203*(13), 2853-2863.

Wang, T., Gnanaprakasam, J. N. R., Chen, X., et al. (2020). Inosine is an alternative carbon source for CD8(+)-T-cell function under glucose restriction. *Nat Metab*, *2*(7), 635-647.

Wang, Y. F., Deng, W. Y., Li, N., Neri, S. Y., Sharma, A., Jiang, W., & Lin, S. H. (2018). Combining Immunotherapy and Radiotherapy for Cancer Treatment Current Challenges and Future Directions. *Frontiers in Pharmacology*, *9*.

Ward, D. V., Gevers, D., Giannoukos, G., et al. (2012). Evaluation of 16S rDNA-Based Community Profiling for Human Microbiome Research. *Plos One*, *7*(6).

Ward, J. F. (2000). Complexity of damage produced by ionizing radiation. *Cold Spring Harb Symp Quant Biol*, *65*, 377-382.

Weaver, G. A., Krause, J. A., Miller, T. L., & Wolin, M. J. (1992). Cornstarch Fermentation by the Colonic Microbial Community Yields More Butyrate Than Does Cabbage Fiber Fermentation - Cornstarch Fermentation Rates Correlate Negatively with Methanogenesis. *American Journal of Clinical Nutrition*, *55*(1), 70-77.

Wei, W., Sun, W., Yu, S., Yang, Y., & Ai, L. (2016). Butyrate production from high-fiber diet protects against lymphoma tumor. *Leuk Lymphoma*, *57*(10), 2401-2408.

Wei, Z. H., Wang, H., Chen, X. Y., Wang, B. S., Rong, Z. X., Wang, B. S., Su, B. H., & Chen, H. Z. (2009). Time- and dose-dependent effect of psyllium on serum lipids in mild-to-moderate hypercholesterolemia: a meta-analysis of controlled clinical trials. *European Journal of Clinical Nutrition*, *63*(7), 821-827.

Wong, J. M., de Souza, R., Kendall, C. W., Emam, A., & Jenkins, D. J. (2006). Colonic health: fermentation and short chain fatty acids. *J Clin Gastroenterol*, *40*(3), 235-243.

Wu, L., Zeng, T. S., Zinellu, A., Rubino, S., Kelvin, D. J., & Carru, C. (2019). A Cross-Sectional Study of Compositional and Functional Profiles of Gut Microbiota in Sardinian Centenarians. *mSystems*, *4*(4).

Wu, P., Zhang, G. H., Zhao, J., Chen, J. W., Chen, Y., Huang, W. N., Zhong, J. L., & Zeng, J. R. (2018). Profiling the Urinary Microbiota in Male Patients With Bladder Cancer in China. *Frontiers in Cellular and Infection Microbiology*, *8*.

Xiao, H. W., Cui, M., Li, Y., Dong, J. L., Zhang, S. Q., Zhu, C. C., Jiang, M., Zhu, T., Wang, B., Wang, H. C., & Fan, S. J. (2020). Gut microbiota-derived indole 3-propionic acid protects against radiation toxicity via retaining acyl-CoA-binding protein. *Microbiome*, *8*(1), 69.

Xie, G., Wang, X., Liu, P., Wei, R., Chen, W., Rajani, C., Hernandez, B. Y., Alegado, R., Dong, B., Li, D., & Jia, W. (2016). Distinctly altered gut microbiota in the progression of liver disease. *Oncotarget*, *7*(15), 19355-19366.

Xie, J., Yu, R., Qi, J., Zhang, G., Peng, X., & Luo, J. (2020). Pectin and inulin stimulated the mucus formation at a similar level: An omics-based comparative analysis. *J Food Sci*, *85*(6), 1939-1947.

Yamashita, T., Kato, T., Isogai, T., Gu, Y., & Ma, N. (2019). Protective Effects of Taurine on the Radiation Exposure Induced Cellular Damages in the Mouse Intestine. *Adv Exp Med Biol*, *1155*, 443-450.

Yamashita, T., Kato, T., Tunekawa, M., Gu, Y., Wang, S., & Ma, N. (2017). Effect of Radiation on the Expression of Taurine Transporter in the Intestine of Mouse. *Adv Exp Med Biol*, *975 Pt 2*, 729-740.

Yan, Y., Kolachala, V., Dalmasso, G., Nguyen, H., Laroui, H., Sitaraman, S. V., & Merlin, D. (2009). Temporal and spatial analysis of clinical and molecular parameters in dextran sodium sulfate induced colitis. *Plos One*, *4*(6), e6073.

Yang, K., Hou, Y., Zhang, Y., Liang, H., Sharma, A., Zheng, W., Wang, L., Torres, R., Tatebe, K., Chmura, S. J., Pitroda, S. P., Gilbert, J. A., Fu, Y. X., & Weichselbaum, R. R. (2021). Suppression of local type I interferon by gut microbiota-derived butyrate impairs antitumor effects of ionizing radiation. *Journal of Experimental Medicine*, *218*(3).

Yang, W. J., Huang, J. F., Xiao, B., Liu, Y., Zhu, Y. Q., Wang, F., & Sun, S. H. (2017). Taurine Protects Mouse Spermatocytes from Ionizing Radiation-Induced Damage Through Activation of Nrf2/HO-1 Signaling. *Cellular Physiology and Biochemistry*, *44*(4), 1629-1639.

Yarza, P., Yilmaz, P., Pruesse, E., Glockner, F. O., Ludwig, W., Schleifer, K. H., Whitman, W. B., Euzeby, J., Amann, R., & Rossello-Mora, R. (2014). Uniting the classification of cultured and uncultured bacteria and archaea using 16S rRNA gene sequences. *Nature Reviews Microbiology*, *12*(9), 635-645.

Yu, T. C., Guo, F. F., Yu, Y. N., Sun, T. T., Ma, D., Han, J. X., Qian, Y., Kryczek, I., Sun, D. F., Nagarsheth, N., Chen, Y. X., Chen, H. Y., Hong, J., Zou, W. P., & Fang, J. Y. (2017). Fusobacterium nucleatum Promotes Chemoresistance to Colorectal Cancer by Modulating Autophagy. *Cell*, *170*(3), 548-+.

Yu, W., Ackert-Bicknell, C., Larigakis, J. D., MacIver, B., Steers, W. D., Churchill, G. A., Hill, W. G., & Zeidel, M. L. (2014). Spontaneous voiding by mice reveals strain-specific lower urinary tract function to be a quantitative genetic trait. *Am J Physiol Renal Physiol*, *306*(11), F1296-1307.

Yuille, S., Reichardt, N., Panda, S., Dunbar, H., & Mulder, I. E. (2018). Human gut bacteria as potent class I histone deacetylase inhibitors in vitro through production of butyric acid and valeric acid. *Plos One*, *13*(7).

Zasloff, M. (2007). Antimicrobial peptides, normally sterile urinary innate immunity, and the tract. *Journal of the American Society of Nephrology*, *18*(11), 2810-2816.

Zhang, S., Bai, J. Q., Ren, S. Y., Wang, R., Zhang, L., & Zuo, Y. F. (2012). Sodium butyrate restores ASC expression and induces apoptosis in LS174T cells. *International Journal of Molecular Medicine*, *30*(6), 1431-1437.

Zhang, Z. Z., Ye, T. M., Cai, X. T., Yang, J., Lu, W. G., Hu, C. P., Wang, Z. G., Wang, X. N., & Cao, P. (2013). 5,7-Dihydroxyflavone Enhances the Apoptosis-Inducing Potential of TRAIL in Human Tumor Cells via Regulation of Apoptosis-Related Proteins. *Evidence-Based Complementary and Alternative Medicine*, *2013*.

Zhao, T. S., Xie, L. W., Cai, S., Xu, J. Y., Zhou, H., Tang, L. F., Yang, C., Fang, S. G., Li, M., & Tian, Y. (2021). Dysbiosis of Gut Microbiota Is Associated With the Progression of Radiation-Induced Intestinal Injury and Is Alleviated by Oral Compound Probiotics in Mouse Model. *Frontiers in Cellular and Infection Microbiology*, *11*.

Zheng, D. P., Liwinski, T., & Elinav, E. (2020). Interaction between microbiota and immunity in health and disease. *Cell Research*, *30*(6), 492-506.

Zhou, Y. J., Zhao, D. D., Liu, H. D., et al. (2017). Cancer killers in the human gut microbiota: diverse phylogeny and broad spectra. *Oncotarget*, *8*(30), 49574-49591.

Zhu, J. N., Huang, Z. X., Zhang, M. Z., Wang, W. Y., Liang, H., Zeng, J., Wu, K. J., Wang, X. Y., Hsieh, J. T., Guo, P., & Fan, J. H. (2018). HIF-1 alpha promotes ZEB1 expression and EMT in a human bladder cancer lung metastasis animal model. *Oncology Letters*, *15*(3), 3482-3489.

Ziai, S. A., Larijani, B., Akhondzadeh, S., Fakhrzadeh, H., Dastpak, A., Bandarian, F., Rezai, A., Badi, H. N., & Emami, T. (2005). Psyllium decreased serum glucose and glycosylated hemoglobin significantly in diabetic outpatients. *Journal of Ethnopharmacology*, *102*(2), 202-207.

Zindler, J. D., Thomas, C. R., Hahn, S. M., Hoffmann, A. L., Troost, E. G. C., & Lambin, P. (2016). Increasing the Therapeutic Ratio of Stereotactic Ablative Radiotherapy by Individualized Isotoxic Dose Prescription. *Jnci-Journal of the National Cancer Institute*, *108*(2).

Appendix

Table A1 Rodent diets used in the study with varying levels of cellulose, psyllium, resistant starch or inulin per 4000 kcal.

	Low fibre		High fibre (Psyllium)		High fibre (Resistant Starch)		High fibre (Inulin)	
	2 gm Cellulose/3850kcal		50 gm Psyllium/3850kcal		100 gm RS/3850kcal		100 gm Inulin/3850kcal	
	gm%	kcal%	gm%	kcal%	gm%	kcal%	gm%	kcal%
Protein	21	20	21	20	19	20	20	20
Carbohydrate	67	64	63	64	56	59	59	60
Fat	7	16	7	16	7	16	7	16
Total		100		100		100		96
kcal/gm	4.20		4.05		3.99		3.95	
Ingredient	**gm**	**kcal**	**gm**	**kcal**	**gm**	**kcal**	**gm**	**kcal**
Casein	200	800	200	800	200	800	200	800
L-Cystein	3	12	3	12	3	12	3	12
Corn starch	397.49	1590	384.99	1540	272.19	1089	359.99	1440
Dextrose, Monohydrate	0	0	0	0	0	0	0	0
Hi-Maize Corn Starch 260 (56% RS)	0	0	0	0	179	501	0	0
Maltodextrin 10	132	528	132	528	132	528	132	528
Sucrose	100	400	100	400	100	400	100	400
Cellulose, BM200	2	0	100	0	0	0	0	0
Inulin	0	0	0	0	100	0	100	150
Psyllium	0	0	50	50	0	0	0	0
Soybean oil	70	630	70	630	70	630	70	630
t-Butylhydroquinone	0.014	0	0.014	0	0.014	0	0.014	0
Mineral mix S10022G	35	0	35	0	35	0	35	0
Vitamin mix V10037	10	40	10	40	10	40	10	40
Choline bitartrate	2.5	0	2.5	0	2.5	0	2.5	0
Total	**952**	**4000**	**987.5**	**4000**	**1003.71**	**4000**	**1012.5**	**4000**
Cellulose (gm/kg diet)	2.1		0		0		0	
Psyllium (gm/kg diet)	0		50.6		0		0	
Resistant starch (gm/kg diet)	0		0		100		0	
Inulin (gm/kg diet)	0		0		0		98.8	

These diets were formulated by Jia-Yu Ke at Research Diets, Inc. on 31/3/2020.

The content of resistant starch is based on the CoA of Hi-Maize Corn Starch, which has 62.8% TDF-dry basis and 11.7% moisture. The content may change based on the batch of Hi-Maize Corn Starch used.

Table A2 Rodent diets used in the study with varying levels of psyllium plus resistant starch or inulin per 4000 kcal.

	High fibre (Psyllium+5%RS)		High fibre (Psyllium+10%RS)		High fibre (Psyllium+Inulin)	
	50gm Psyllium + 50 gm RS/4000kcal		50gm Psyllium + 100 gm RS/4000kcal		50gm Psyllium + 100 gm Inulin/4000kcal	
	gm%	kcal%	gm%	kcal%	gm%	kcal%
Protein	20	20	19	20	19	20
Carbohydrate	64	64	65	64	56	59
Fat	7	16	7	16	7	16
Total		100		100		95
kcal/gm	3.94		3.84		3.81	
Ingredient	**gm**	**kcal**	**gm**	**kcal**	**gm**	**kcal**
Casein	200	800	200	800	200	800
L-Cystein	3	12	3	12	3	12
Corn starch	322.69	1291	256.69	1039	347.49	1390
Dextrose, Monohydrate	0	0	0	0	0	0
Hi-Maize Corn Starch 260 (56% RS)	89	249	179	501	0	0
Maltodextrin 10	132	528	132	528	132	528
Sucrose	100	100	100	100	100	400
Cellulose, BM200	0	0	0	0	0	0
Inulin	0	0	0	0	100	150
Psyllium	50	50	50	50	50	50
Soybean oil	70	70	70	70	70	630
t-Butylhydroquinone	0.014	0.014	0.014	0.014	0.014	0
Mineral mix S10022G	35	35	35	35	35	0
Vitamin mix V10037	10	10	10	10	10	40
Choline bitartrate	2.5	2.5	2.5	2.5	2.5	0
Total	**1014.21**	**4000**	**1041.21**	**4000**	**1050**	**4000**
Cellulose (gm/kg diet)	0		0		0	
Psyllium (gm/kg diet)	49.3		48		47.6	
Resistant starch (gm/kg diet)	49		96		0	
Inulin (gm/kg diet)	0		0		95.2	

These diets were formulated by Jia-Yu Ke at Research Diets, Inc. on 11/6/2018.

Table A3 Rodent diets without corn starch used in the study with varying levels of cellulose, psyllium, psyllium plus resistant starch, or inulin per 4000 kcal.

	Low fibre		High fibre (Psyllium)		High fibre (Psyllium+RS)		High fibre (Psyllium+Inulin)	
	2 gm Cellulose/4000kcal		50 gm Psyllium/4000kcal		50 gm Psyllium + 100 gm RS/4000kcal		50 gm Psyllium + 100 gm Inulin/4000kcal	
	gm%	kcal%	gm%	kcal%	gm%	kcal%	gm%	kcal%
Protein	21	20	21	20	19	20	19	20
Carbohydrate	67	64	63	64	65	64	56	59
Fat	7	16	7	16	7	16	7	16
Total		100		100		100		95
kcal/gm	4.20		4.05		3.84		3.81	
Ingredient	**gm**	**kcal**	**gm**	**kcal**	**gm**	**kcal**	**gm**	**kcal**
Casein	200	800	200	800	200	800	200	800
L-Cystein	3	12	3	12	3	12	3	12
Corn starch	0	0	0	0	0	0	0	0
Dextrose, Monohydrate	397.49	1590	384.99	1540	322.69	1291	347.49	1390
Hi-Maize Corn Starch 260 (56% RS)	0	0	0	0	179	501	0	0
Maltodextrin 10	132	528	132	528	132	528	132	528
Sucrose	100	400	100	400	100	400	100	400
Cellulose, BM200	2	0	100	0	0	0	0	0
Inulin	0	0	0	0	0	0	100	150
Psyllium	0	0	50	50	50	50	50	50
Soybean oil	70	630	70	630	70	630	70	630
t-Butylhydroquinone	0.014	0	0.014	0	0.014	0	0.014	0
Mineral mix S10022G	35	0	35	0	35	0	35	0
Vitamin mix V10037	10	40	10	40	10	40	10	40
Choline bitartrate	2.5	0	2.5	0	2.5	0	2.5	0
Total	**952**	**4000**	**987.5**	**4000**	**1041.21**	**4000**	**1031.25**	**4000**
Cellulose (gm/kg diet)	2.1		0		0		0	
Psyllium (gm/kg diet)	0		50.6		48		47.6	
Resistant starch (gm/kg diet)	0		0		96		100	
Inulin (gm/kg diet)	0		0		0		0	

These diets were formulated by Vijay Indukuri at Research Diets, Inc. on 16/11/2020.

The content of resistant starch is based on the CoA of Hi-Maize Corn Starch, which has 62.8% TDF-dry basis and 11.7% moisture. The content may change based on the batch of Hi-Maize Corn Starch used.

Table 16 Metabolites that positively or negatively correlated with tumour growth in psyllium plus inulin-treated mice.

Compound	Fold-change (relative to 0.2% cellulose)	Slope	R squared	P value
Hydantoin-5-propionic acid	0.449	0.081	0.719	0.002
Cysteic acid	1.144	0.154	0.676	0.004
p-Hydroxyphenylacetic acid	0.274	0.159	0.642	0.005
Tyramine	0.090	0.133	0.618	0.007
Proline betaine	0.176	0.057	0.579	0.011
Threitol	1.448	-0.061	0.490	0.024
Adonitol (ribitol)	1.604	-0.055	0.464	0.030
Quinic acid	0.030	0.091	0.445	0.035
N-Propionylalanine	0.535	-0.056	0.411	0.046
L-Homoserine	0.206	0.055	0.403	0.049
Niacinamide	0.456	0.190	0.374	0.060
3-Dehydroquinate	0.923	-0.048	0.345	0.074
Quinolinic acid	0.106	0.188	0.324	0.086
Taurine	2.697	0.055	0.319	0.089
Allantoin	12.345	-0.098	0.313	0.093
4,5-Dihydroorotic acid	0.195	0.047	0.312	0.093
Prostaglandin E2	0.361	0.096	0.305	0.098
Methionyl-Threonine	13.832	-0.159	0.305	0.098
3-[3-(Sulfooxy)phenyl]propanoic acid	0.063	0.099	0.293	0.106
Homogentisic acid	0.122	0.047	0.291	0.108
Thymine	1.923	0.049	0.288	0.110
N-Acetyltaurine	0.628	0.085	0.282	0.115
N-Formyl-DL-ethionine	0.777	0.055	0.280	0.116
Asparaginyl-Hydroxyproline	0.013	-0.282	0.279	0.117
2-Hydroxy-4-phenylbutanoic acid	0.099	0.043	0.276	0.119
N-Acetyl-D-glucosamine	0.379	0.038	0.273	0.122
Glucose	0.357	0.016	0.270	0.124
Homovanillic acid	1.126	-0.087	0.269	0.125
Deoxyuridine	0.708	0.065	0.262	0.130
Sebacic acid	0.375	0.041	0.261	0.132
Butyric acid	0.878	-0.032	0.257	0.135
4-Hydroxyproline	0.272	-0.055	0.245	0.146
Glyceric acid	1.422	0.036	0.244	0.147
3-Hydroxypicolinic acid	0.431	0.018	0.222	0.170
1-Hydroxyibuprofen	0.185	0.082	0.221	0.170
Orotic acid	0.055	0.058	0.220	0.171
EDTA	0.475	0.030	0.219	0.172
Beta-Citryl-L-glutamic acid	0.314	-0.071	0.212	0.180
N-Acetylvaline	0.471	-0.058	0.206	0.187

Pentanal	0.359	0.059	0.204	0.190
D-Aspartic acid	0.169	-0.077	0.203	0.191
Chlorogenic acid	0.003	0.737	0.189	0.210
Ribose	0.858	-0.031	0.178	0.225
3,4-dihydroxyphenyl acetic acid	1.196	0.041	0.175	0.228
4-Acetylbutyrate	0.202	-0.234	0.164	0.245
Dimethyl fumarate	0.372	0.014	0.162	0.250
5-Hydroxymethyl-2'-deoxyuridine	3.641	0.035	0.161	0.250
4-Hydroxypyrrolidinone	1.154	0.030	0.159	0.253
Cyclohexanecarboxylic acid	0.228	0.042	0.155	0.260
NAD+	0.146	-1.045	0.147	0.275
Cysteine-S-sulfate	0.380	-0.126	0.143	0.281
3-methoxyphenylacetic acid	0.063	-0.141	0.143	0.281
2-Ketobutyric acid	0.349	0.057	0.140	0.287
Phenylalanyl-Aspartate	4.038	-0.160	0.139	0.289
Methylglutaric acid	2.550	0.035	0.135	0.297
Tyramine-O-sulfate	0.066	0.075	0.131	0.304
Cysteine	1.576	0.028	0.131	0.305
Isoferulic acid	0.616	-0.017	0.124	0.319
Hydroxyisoheptanoic acid	11.813	-0.049	0.123	0.321
Vanillylmandelic acid	2.490	0.022	0.122	0.324
Sinapic acid	0.181	0.017	0.120	0.327
Ophthalmic Acid	0.117	-0.076	0.119	0.328
Malondialdehyde	0.758	0.013	0.119	0.328
Pectic acid	0.268	-0.057	0.118	0.331
Pantothenic acid	0.789	0.031	0.117	0.335
N-Acetyl proline	0.744	-0.065	0.112	0.346
Phenyl acetate	0.584	-0.024	0.111	0.347
N-Formyl-methionine	0.301	-0.073	0.105	0.361
Methyl phenylacetate	0.101	-0.100	0.104	0.364
Dihydroxyacetone phosphate	23.411	-0.107	0.103	0.367
Ribothymidine	2.098	-0.058	0.102	0.370
N-Acetylmannosamine (ManNac)	1.019	0.040	0.100	0.374
Methylisocitric acid	0.892	-0.022	0.099	0.377
cis-Aconitic acid	0.530	0.037	0.094	0.389
Prolylglycine	0.419	-0.143	0.093	0.393
Acetoacetate	0.919	-0.023	0.091	0.397
N-Acetylglutamate	0.379	-0.017	0.090	0.401
Gluconate	1.021	-0.025	0.087	0.408
Sorbitol-6-phosphate	1.251	-0.071	0.087	0.408
3-Hydroxysuberic acid	0.277	-0.020	0.087	0.408
Kynurenine	0.603	-0.180	0.087	0.408
Succinic acid	12.907	-0.028	0.083	0.419
Pyruvic acid	0.629	-0.038	0.081	0.425

dAMP	0.397	0.103	0.079	0.430
Adipate semialdehyde	0.067	-0.044	0.079	0.430
Oxoadipic acid	0.327	0.008	0.079	0.432
Citrulline	-	-0.073	0.079	0.432
2-Hydroxybutyric acid	1.313	-0.035	0.078	0.435
Sedoheptulose 1-phosphate	6.131	-0.117	0.077	0.438
N-Alpha-acetyllysine	-	-0.079	0.077	0.439
3,4-Dihydroxyhydrocinnamic acid	1.980	-0.047	0.075	0.443
Hydroxyoctanoic acid	0.319	-0.026	0.075	0.444
Succinyl-Homoserine	0.772	0.034	0.074	0.447
Erythrose 4-phosphate	139770.907	-0.095	0.074	0.447
Galacturonic acid	2.573	-0.029	0.070	0.459
Tyrosyl-Glutamine	4.047	-1.440	0.070	0.460
Gluconolactone	0.348	-0.016	0.070	0.461
3-Methyl-2-oxovaleric acid	0.337	0.035	0.067	0.469
Acetylglycine	0.185	0.013	0.067	0.471
Pimelic acid	0.340	0.022	0.066	0.475
Thiamine monophosphate	0.077	0.055	0.066	0.475
Ketoleucine	0.164	0.020	0.064	0.480
6-phosphonoglucono-lactone	27.357	-0.079	0.063	0.484
Glycyl-Methionine	3.050	-0.038	0.062	0.489
3-Nitrotyrosine	1.763	-0.044	0.061	0.491
3-Hydroxyisovaleric acid	1.928	-0.041	0.059	0.497
Caprylic acid	1.516	-0.025	0.059	0.499
Glutamate, gamma-methyl ester	1.354	-0.043	0.057	0.505
Ribulose 5-phosphate	1.697	0.048	0.056	0.509
4-Hydroxycyclohexylcarboxylic acid	0.905	-0.034	0.056	0.511
Maleic acid	11.446	0.023	0.055	0.512
3-Octen-2-one	0.217	0.029	0.054	0.520
Aspartylglycosamine	3.113	0.021	0.053	0.521
2-C-Methylerythritol 4-phosphate	29.372	0.039	0.053	0.523
Fructose 2,6 diphosphate	24.502	0.033	0.051	0.529
2-Methylglutaric acid	0.973	0.033	0.051	0.530
Aspartate	0.917	-0.016	0.051	0.530
Beta-Alanine	1.327	-0.023	0.051	0.532
N-Acetyl ornithine	58.343	-0.047	0.049	0.540
Glycerol	0.801	0.007	0.048	0.543
Deoxyadenosine monophosphate	0.457	0.082	0.045	0.555
Isovalerylglycine	0.354	0.027	0.045	0.558
Lactoyl-isoleucine	1.784	-0.051	0.044	0.560
Glycerylphosphorylethanolamine	3.357	0.042	0.044	0.561
Malic acid	8.326	0.022	0.044	0.562
Hippuric acid	0.101	0.187	0.042	0.569
Sedoheptulose 7-phosphate	13.869	-0.061	0.042	0.570

Raffinose	0.167	-0.021	0.041	0.574
4-Methyl-2-ureido-pentanoic acid/Carbamoyl isoleucine	0.334	-0.048	0.039	0.585
3-Hydroxybutyric acid	2.599	0.022	0.037	0.595
Arabinonic acid	0.734	-0.017	0.037	0.596
Mesaconic acid	1.329	-0.024	0.036	0.601
4-Acetamidobutanoic acid	1.362	0.024	0.035	0.602
2-Isopropylmalic acid	9.723	0.028	0.035	0.606
Lactic acid	1.360	0.016	0.034	0.608
N-Acetyl-L-phenylalanine	1.150	-0.023	0.034	0.612
3-deoxy-2-keto-6-phosphogluconic acid	3.848	-0.039	0.034	0.613
Vanillin	0.168	0.015	0.031	0.625
3-Hydroxymethylglutarate	1.002	-0.008	0.031	0.627
4-Hydroxybutyric acid	2.712	0.015	0.030	0.631
5-Hydroxyhexanoic acid	1.910	-0.031	0.030	0.632
Syringic acid	0.424	-0.009	0.029	0.641
3-(2,5-Dioxoimidazolidin-4-yl)propanoic acid	0.179	0.009	0.028	0.643
L-Lactic acid	0.423	0.007	0.028	0.646
Methyl beta-D-glucopyranoside	1.259	-0.010	0.027	0.650
Naringenin	23.099	0.038	0.027	0.653
Nonate	0.242	0.014	0.025	0.661
Glycylproline	1.094	0.038	0.025	0.662
N-Acetylneuraminic acid (Sialic acid)	2.368	-0.027	0.025	0.662
2-Fucosyllactose	4.343	0.022	0.023	0.673
Glycolic acid	0.574	0.005	0.023	0.674
Kynurenic acid	0.699	-0.016	0.023	0.675
gamma-Glutamylphenylalanine	1.368	-0.024	0.023	0.677
Pyroglutamic acid	0.922	0.014	0.021	0.687
gamma-Glutamylmethionine	5.966	-0.019	0.020	0.693
8-Hydroxy-deoxyguanosine	0.237	-0.033	0.020	0.697
Caffeic acid	0.915	0.020	0.020	0.700
Ascorbate	0.775	0.004	0.019	0.703
Adenine	22.287	0.044	0.019	0.705
N-Acetyl-L-alanine	0.761	-0.013	0.018	0.709
Deoxyribose	0.384	0.012	0.018	0.714
Cytidine monophosphate N-acetylneuraminic acid	2.061	0.027	0.017	0.716
Parabanic Acid/Oxalylyurea	1.367	-0.006	0.017	0.722
N-Acetyl-aspartate	2.620	-0.013	0.015	0.732
gamma-CEHC	0.366	-0.020	0.013	0.753
Dihydroorotic acid	0.124	-0.010	0.013	0.756
N2-gamma-Glutamylglutamine	9.420	-0.014	0.012	0.764
Sorbitol	1.098	0.009	0.012	0.767

Hydroxypyruvic acid	3.488	0.006	0.011	0.777
Malonic acid	0.813	-0.004	0.010	0.781
Glutaric acid	6.987	-0.014	0.010	0.782
Phenylacetylglycine/Phenaceturic acid	0.120	-0.058	0.009	0.793
N-acetyl-glucosamine-1-phosphate	0.329	0.015	0.009	0.797
Hydroferulic acid	0.055	0.006	0.008	0.802
Galactaric acid (mucic acid)	2.179	0.011	0.008	0.807
Kojic acid	0.491	-0.003	0.007	0.817
Glucosamine	0.492	0.006	0.007	0.825
2-Furoic acid	0.344	-0.004	0.006	0.825
Malitol	0.255	-0.005	0.005	0.839
3-Hydroxytyrosol	0.808	0.010	0.005	0.841
Glutaconic acid	0.760	-0.003	0.005	0.847
Flavin Mononucleotide (unconfirmed)	0.528	-0.008	0.005	0.849
2-Phosphoglyceric acid	5.513	-0.026	0.005	0.849
2-Hydroxyhexanoic acid	0.359	-0.022	0.005	0.852
Hydrocinnamic acid	0.734	0.006	0.005	0.853
2-Hydroxyglutarate	2.508	0.004	0.003	0.875
Mannose	0.422	0.003	0.003	0.877
4-ethylphenylsulfate	0.098	-0.007	0.003	0.880
3,3 Dimethyl glutarate	4.670	-0.007	0.002	0.894
Citric acid	1.238	0.005	0.002	0.897
Ciliatine	1.490	0.003	0.002	0.903
Uridine	0.918	0.004	0.002	0.910
Mevalonic acid	0.385	0.002	0.002	0.915
Glycerol 3-phosphate	8.022	0.007	0.001	0.920
3'-AMP	0.276	0.007	0.001	0.934
4-Hydroxy-2-oxoglutarate	0.391	-0.001	0.000	0.953
Glutamine	0.314	0.008	0.000	0.959
Glucose 1-phosphate	4.749	0.002	0.000	0.973
Fructose 6-phosphate	0.967	-0.001	0.000	0.974
Adenosine diphosphate	1.058	0.001	0.000	0.979
1-Deoxy-D-xylulose 5-phosphate	1.457	0.006	0.000	0.981
2-Methoxyacetaminophen sulfate	2.296	0.003	0.000	0.983
gamma-Glutamylglutamic acid	0.236	0.001	0.000	0.983
Dihydroxyacetone	3.366	0.000	0.000	0.997
Adenosine monophosphate (AMP)	0.282	0.000	0.000	0.998

Table A5 Metabolites that positively or negatively correlated with tumour growth in psyllium plus inulin-treated mice.

Compound	Fold-change (relative to 0.2% cellulose)	Slope	R squared	P value
Deoxyribose	0.211	0.053	0.708	0.002
Pyruvic acid	0.243	0.052	0.656	0.005
Caffeic acid	0.232	0.106	0.640	0.006
Kynurenic acid	0.647	0.054	0.601	0.008
Mevalonic acid	0.318	0.033	0.589	0.010
Deoxyuridine	0.229	0.068	0.589	0.010
3-Methyl-2-oxovaleric acid	0.384	0.109	0.514	0.020
Glycerol	0.789	0.032	0.499	0.022
N-acetyl-glucosamine-1-phosphate	0.257	-0.192	0.495	0.023
Pantothenic acid	1.478	0.105	0.495	0.023
Hydroxypyruvic acid	1.583	0.055	0.481	0.026
Isoferulic acid	1.597	-0.062	0.473	0.028
2-Ketobutyric acid	0.315	0.072	0.472	0.028
Pentanal	1.012	0.111	0.456	0.032
3-(2,5-Dioxoimidazolidin-4-yl)propanoic acid	0.181	0.026	0.454	0.033
Fructose 6-phosphate	0.224	0.100	0.429	0.040
4-Acetamidobutanoic acid	0.113	0.082	0.424	0.041
Maleic acid	3.939	0.085	0.424	0.042
3-[3-(Sulfooxy)phenyl]propanoic acid	0.388	0.101	0.412	0.046
2-Furoic acid	0.318	-0.041	0.389	0.054
Glyceric acid	0.634	0.055	0.388	0.055
Taurine	3.192	0.021	0.383	0.056
Malic acid	3.005	0.145	0.383	0.057
Cysteine	1.399	0.063	0.382	0.057
2-Phosphoglyceric acid	0.473	-0.178	0.367	0.063
2-C-Methylerythritol 4-phosphate	0.706	-0.155	0.350	0.071
Hydrocinnamic acid	0.762	0.068	0.339	0.078
Butyric acid	0.803	0.061	0.336	0.079
Thiamine monophosphate	0.089	-0.180	0.328	0.084
Adenosine diphosphate	0.960	0.068	0.320	0.089
3-Hydroxysuberic acid	0.962	0.032	0.316	0.091
Quinic acid	0.051	-0.116	0.312	0.093
Chlorogenic acid	0.035	0.241	0.312	0.093
Orotic acid	0.110	0.041	0.310	0.095
NAD+	0.398	-0.181	0.283	0.114
Sedoheptulose 1-phosphate	0.559	-0.401	0.259	0.133
N-Acetylneuraminic acid (Sialic acid)	0.343	0.051	0.247	0.144
3'-AMP	0.487	-0.082	0.232	0.159
Galacturonic acid	0.999	0.037	0.230	0.161

Methylisocitric acid	0.230	0.028	0.230	0.161
6-phosphonoglucono-lactone	1.092	-0.186	0.228	0.163
Thymine	0.531	0.057	0.225	0.166
Dimethyl fumarate	0.352	0.014	0.213	0.179
Malonic acid	0.880	-0.028	0.203	0.192
N-Acetylglutamate	0.492	0.051	0.200	0.195
3-methoxyphenylacetic acid	0.629	-0.078	0.200	0.195
Acetylglycine	0.192	0.024	0.197	0.199
Sedoheptulose 7-phosphate	0.431	-0.180	0.196	0.201
3-Hydroxyisovaleric acid	0.659	0.052	0.191	0.206
Pectic acid	0.091	-0.057	0.188	0.211
Citric acid	1.630	-0.060	0.188	0.211
p-Hydroxyphenylacetic acid	0.299	0.050	0.183	0.218
Gluconolactone	0.668	-0.048	0.182	0.218
Caprylic acid	1.142	0.037	0.181	0.220
gamma-CEHC	0.226	0.047	0.174	0.230
3-Hydroxymethylglutarate	1.256	0.030	0.169	0.238
Homogentisic acid	0.144	0.040	0.165	0.245
Pimelic acid	0.151	0.032	0.164	0.245
3-Hydroxybutyric acid	0.044	0.036	0.164	0.246
N-Acetyl-D-glucosamine	1.048	0.027	0.164	0.246
Glycolic acid	0.536	0.007	0.163	0.247
Raffinose	0.200	-0.066	0.163	0.248
4-Hydroxyproline	0.539	-0.056	0.159	0.254
Cytidine monophosphate N-acetylneuraminic acid	1.100	0.121	0.152	0.266
N-Formyl-methionine	-	0.040	0.145	0.278
Adenine	17.222	0.154	0.145	0.278
Prostaglandin E2	0.056	-0.070	0.143	0.282
2-Hydroxyhexanoic acid	5.748	0.054	0.141	0.285
dAMP	0.283	0.080	0.140	0.287
Asparaginyl-Hydroxyproline	0.091	-0.185	0.140	0.287
Vanillylmandelic acid	0.377	0.019	0.136	0.295
Adonitol (ribitol)	1.844	-0.049	0.132	0.302
Cysteine-S-sulfate	1.064	-0.172	0.132	0.303
N-Propionylalanine	19.696	-0.085	0.128	0.311
Cysteic acid	1.727	0.037	0.125	0.316
Ciliatine	1.406	0.017	0.118	0.332
Acetoacetate	0.694	0.022	0.115	0.337
D-Aspartic acid	0.074	-0.074	0.110	0.350
4-Hydroxypyrrolidinone	0.398	0.029	0.109	0.351
2-Isopropylmalic acid	5.046	0.041	0.104	0.364
Pyroglutamic acid	0.855	0.026	0.103	0.366
Sorbitol-6-phosphate	0.596	-0.078	0.100	0.374

N-Formyl-DL-ethionine	0.413	0.023	0.096	0.385
Tyramine-O-sulfate	0.093	0.038	0.088	0.405
Vanillin	0.124	-0.017	0.088	0.405
5-Hydroxyhexanoic acid	1.111	0.040	0.086	0.411
Kojic acid	0.541	-0.020	0.074	0.446
N-Acetyl-aspartate	0.508	-0.051	0.073	0.449
N-Acetyl-L-alanine	0.262	0.043	0.071	0.457
8-Hydroxy-deoxyguanosine	0.712	-0.040	0.068	0.467
Ribose	1.137	-0.024	0.067	0.469
4-Hydroxy-2-oxoglutarate	0.176	-0.030	0.065	0.476
2-Hydroxy-4-phenylbutanoic acid	0.039	-0.021	0.065	0.478
3,3 Dimethyl glutarate	0.108	0.019	0.063	0.483
5-Hydroxymethyl-2'-deoxyuridine	0.802	0.022	0.060	0.496
3-Methyladipic acid	0.251	-0.157	0.056	0.512
Prolylglycine	4.538	-0.477	0.056	0.512
3-Nitrotyrosine	0.861	-0.346	0.055	0.513
Uridine	2.249	-0.271	0.054	0.518
Arabinonic acid	1.673	-0.045	0.051	0.531
Parabanic Acid/Oxalylyurea	0.826	-0.016	0.051	0.532
Methyl beta-D-glucopyranoside	0.922	-0.018	0.049	0.537
Ketoleucine	0.106	-0.011	0.049	0.538
3-Hydroxypicolinic acid	1.593	0.019	0.048	0.542
Oxoadipic acid	0.363	-0.013	0.047	0.548
Glutaric acid	1.471	0.025	0.047	0.548
Naringenin	2.988	-0.039	0.047	0.549
Glycylproline	81.643	-1.360	0.047	0.549
Succinic acid	5.944	-0.025	0.046	0.552
Glucosamine	0.455	0.018	0.046	0.552
3-Octen-2-one	0.204	-0.013	0.046	0.554
Ribothymidine	60.119	-0.843	0.045	0.555
gamma-Glutamylmethionine	3.710	0.029	0.045	0.555
Adenosine monophosphate (AMP)	0.400	-0.037	0.044	0.559
3,4-Dihydroxyhydrocinnamic acid	0.007	-0.059	0.043	0.564
Kynurenine	0.730	-0.064	0.043	0.567
Syringic acid	0.416	-0.027	0.042	0.569
Tyrosyl-Glutamine	213.949	-0.131	0.042	0.572
3-Dehydroquinate	1.025	-0.036	0.041	0.575
Phenylalanyl-Aspartate	0.601	0.024	0.036	0.598
N-Acetylmannosamine (ManNac)	0.937	0.024	0.036	0.599
Nonate	1.011	-0.009	0.036	0.600
EDTA	0.534	-0.018	0.036	0.600
Glucose	0.285	0.006	0.036	0.600
Galactaric acid (mucic acid)	2.201	0.026	0.034	0.611
Glutamine	1.619	-0.051	0.033	0.614

Deoxyadenosine monophosphate	0.136	0.031	0.033	0.618
Allantoin	120.103	-0.072	0.031	0.625
N-Alpha-acetyllysine	0.577	-0.149	0.031	0.626
Dihydroorotic acid	0.246	-0.022	0.031	0.628
1-Hydroxyibuprofen	0.153	0.021	0.030	0.630
Quinolinic acid	0.148	0.028	0.030	0.633
gamma-Glutamylglutamic acid	0.172	-0.061	0.030	0.634
Hydroferulic acid	0.041	-0.019	0.030	0.635
cis-Aconitic acid	0.695	-0.012	0.029	0.639
Mannose	0.423	-0.014	0.027	0.649
L-Homoserine	0.941	-0.012	0.026	0.658
gamma-Glutamylphenylalanine	2.276	0.033	0.025	0.663
Lactic acid	0.322	-0.007	0.025	0.666
Gluconate	2.935	-0.086	0.022	0.683
N-Acetyl ornithine	5.629	0.015	0.019	0.706
N-Acetyl proline	1.332	0.015	0.018	0.709
Malondialdehyde	0.666	0.010	0.017	0.716
Glycyl-Methionine	4.739	-0.028	0.017	0.722
N-Acetyl-L-phenylalanine	0.257	0.021	0.016	0.724
Hydroxyisoheptanoic acid	0.729	-0.014	0.016	0.726
Phenylacetylglycine/Phenaceturic acid	1.220	-0.054	0.015	0.736
Ascorbate	0.583	0.005	0.015	0.740
Proline betaine	0.109	-0.011	0.014	0.745
L-Lactic acid	3.472	0.005	0.013	0.750
Methionyl-Threonine	26.023	-0.048	0.013	0.751
Homovanillic acid	1.267	-0.012	0.013	0.751
2-Methylglutaric acid	0.240	-0.006	0.013	0.755
Glutamate, gamma-methyl ester	0.398	-0.012	0.013	0.758
Beta-Citryl-L-glutamic acid	0.906	-0.030	0.011	0.774
Phenyl acetate	22.904	-0.016	0.011	0.776
Flavin Mononucleotide (unconfirmed)	0.274	0.015	0.011	0.777
Glucose 1-phosphate	0.547	-0.027	0.010	0.778
Succinyl-Homoserine	0.599	0.011	0.010	0.779
Sebacic acid	0.417	0.007	0.010	0.784
Threitol	1.417	-0.008	0.010	0.788
Ribulose 5-phosphate	0.977	-0.032	0.009	0.789
Hippuric acid	2.640	-0.053	0.009	0.793
N-Acetyltaurine	2.773	0.013	0.009	0.793
2-Fucosyllactose	5.738	0.017	0.008	0.801
Isovalerylglycine	1.389	-0.031	0.008	0.811
4-Acetylbutyrate	0.583	0.051	0.007	0.822
Aspartate	0.985	0.005	0.006	0.835
3-deoxy-2-keto-6-phosphogluconic acid	0.853	0.019	0.005	0.842
4-Hydroxybutyric acid	0.470	0.005	0.004	0.856

Methylglutaric acid	0.683	0.005	0.004	0.866
2-Methoxyacetaminophen sulfate	1.811	-0.022	0.004	0.867
Lactoyl-isoleucine	0.439	-0.023	0.004	0.869
4,5-Dihydroorotic acid	0.013	-0.004	0.003	0.872
Sinapic acid	0.084	-0.004	0.003	0.874
Aspartylglycosamine	1.844	0.013	0.003	0.876
Cyclohexanecarboxylic acid	0.310	-0.008	0.003	0.884
3-Hydroxytyrosol	1.048	-0.006	0.003	0.887
4-Methyl-2-ureido-pentanoic acid	0.964	0.041	0.003	0.887
N-Acetylvaline	1.530	-0.010	0.003	0.889
2-Hydroxyglutarate	0.623	-0.002	0.002	0.901
Glycerylphosphorylethanolamine	1.558	-0.019	0.002	0.908
Dihydroxyacetone	1.611	-0.009	0.002	0.909
3,4-dihydroxyphenyl acetic acid	8.315	0.005	0.002	0.913
Hydantoin-5-propionic acid	0.801	-0.006	0.001	0.924
Citrulline	-	0.005	0.001	0.930
Mesaconic acid	0.717	0.002	0.001	0.933
Methyl phenylacetate	0.225	-0.003	0.001	0.936
2-Hydroxybutyric acid	1.879	-0.005	0.001	0.941
Glycerol 3-phosphate	3.490	-0.008	0.001	0.949
Sorbitol	2.029	-0.005	0.000	0.964
Fructose 2,6 diphosphate	16.936	0.003	0.000	0.969
Ophthalmic Acid	0.241	-0.003	0.000	0.973
Glutaconic acid	0.973	0.001	0.000	0.976
4-ethylphenylsulfate	0.007	0.001	0.000	0.976
N2-gamma-Glutamylglutamine	0.328	0.003	0.000	0.978
Adipate semialdehyde	0.158	0.001	0.000	0.986
Niacinamide	0.472	-0.001	0.000	0.987
4-Hydroxycyclohexylcarboxylic acid	0.546	-0.001	0.000	0.993
Tyramine	0.099	0.000	0.000	0.994
Hydroxyoctanoic acid	0.909	0.000	0.000	0.994
Beta-Alanine	1.024	0.000	0.000	0.994
Malitol	0.442	0.000	0.000	0.997

Table A6 Average and standard deviation of the relative abundance (%) for the top 30 taxa with the highest abundances for section 4.2.5.

Relative abundance of bacterial taxa (%)	0.2% Cellulose		RS		Inulin		Psyllium		Psyllium +RS		Psyllium +Inulin	
	Avg	STD	Avg	STD	Avg	STD	Avg	STD	Avg	STD	Avg	STD
p_Firmicutes|c_Bacilli|o_Lactobacillales|f_Lactobacillaceae|g_Lactobacillus|s_	13.1	5.2	16.2	6.6	26.1	11.7	3.1	3.8	4.1	5.9	9.7	4.8
p_Bacteroidetes|c_Bacteroidia|o_Bacteroidales|f_S24-7|g_|s_	7.4	1.2	11.7	4.2	11.3	2.4	7.0	1.8	7.5	1.4	8.1	2.1
p_Firmicutes|c_Clostridia|o_Clostridiales|f_|g_|s_	7.2	2.1	12.6	6.6	4.8	2.0	4.5	1.7	8.9	1.9	6.5	3.9
p_Actinobacteria|c_Actinobacteria|o_Bifidobacteriales|f_Bifidobacteriaceae|g_Bifidobacterium|s_animalis	0.0	0.0	2.4	5.7	12.3	13.5	0.8	0.7	0.5	0.7	30.4	3.6
p_Bacteroidetes|c_Bacteroidia|o_Bacteroidales|f_|g_|s_	12.5	1.8	11.5	2.1	2.5	1.2	4.0	0.6	5.8	0.5	0.1	0.2
p_Actinobacteria|c_Actinobacteria|o_Bifidobacteriales|f_Bifidobacteriaceae|g_Bifidobacterium|s_pseudolongum	12.4	3.3	8.6	6.9	7.2	6.5	0.0	0.0	0.3	0.6	0.0	0.0
p_Bacteroidetes|c_Bacteroidia|o_Bacteroidales|f_Bacteroidaceae|g_Bacteroides|s_acidifaciens	1.9	1.4	2.3	1.0	7.9	1.9	7.9	2.5	5.7	1.9	4.8	2.2
p_Bacteroidetes|c_Bacteroidia|o_Bacteroidales|f_Bacteroidaceae|g_Bacteroides|s_	2.0	0.9	1.3	1.1	1.9	1.3	2.0	2.2	1.5	0.9	0.9	0.6
p_Bacteroidetes|c_Bacteroidia|o_Bacteroidales|f_Rikenellaceae|g_|s_	8.3	2.7	5.7	1.7	3.5	0.9	4.5	1.3	3.3	1.1	2.0	0.5
p_Firmicutes|c_Clostridia|o_Clostridiales|_|_|_	4.0	1.7	4.1	2.4	2.0	1.4	7.6	1.5	4.1	1.3	2.1	1.4
p_Bacteroidetes|c_Bacteroidia|o_Bacteroidales|f_Bacteroidaceae|g_Bacteroides|_	0.1	0.0	0.1	0.0	0.4	0.2	11.4	0.7	10.4	3.5	7.0	2.1
p_Proteobacteria|c_Betaproteobacteria|o_Burkholderiales|f_Alcaligenaceae|g_Sutterella|s_	0.7	0.4	1.5	1.1	1.2	0.4	8.9	2.5	9.4	2.8	3.2	0.9
p_Firmicutes|c_Clostridia|o_Clostridiales|f_Lachnospiraceae|_|_	2.2	0.9	2.8	1.2	2.3	1.1	2.6	0.6	3.0	0.7	3.7	1.3
p_Firmicutes|c_Erysipelotrichi|o_Erysipelotrichales|f_Erysipelotrichaceae|g_Allobaculum|s_	4.5	2.0	3.0	1.7	1.1	1.2	3.4	1.8	3.1	1.7	1.3	0.9
p_Actinobacteria|c_Coriobacteriia|o_Coriobacteriales|f_Coriobacteriaceae|g_|s_	2.3	0.8	2.5	1.9	2.6	2.0	1.9	1.1	2.0	1.1	0.8	0.5
p_Bacteroidetes|c_Bacteroidia|o_Bacteroidales|f_Porphyromonadaceae|g_Parabacteroides|s_	1.0	1.5	0.4	0.2	0.4	0.4	4.2	1.8	3.5	1.1	1.9	2.5
p_Firmicutes|c_Clostridia|o_Clostridiales|f_Ruminococcaceae|g_Oscillospira|s_	2.3	0.9	2.4	1.1	0.9	0.4	1.4	0.5	1.3	0.6	1.0	0.4
p_Firmicutes|c_Clostridia|o_Clostridiales|f_Lachnospiraceae|g_[Ruminococcus]|s_gnavus	1.8	0.6	1.0	0.3	2.3	1.3	2.0	0.3	1.5	0.3	0.4	0.1
p_Firmicutes|c_Erysipelotrichi|o_Erysipelotrichales|f_Erysipelotrichaceae|g_Clostridium|s_cocleatum	0.4	0.3	0.5	0.6	0.2	0.1	3.8	1.3	3.1	0.7	0.6	0.4
p_Firmicutes|c_Clostridia|o_Clostridiales|f_Clostridiaceae|g_Clostridium|_	0.4	0.2	0.1	0.2	0.0	0.0	1.5	1.9	6.3	5.2	0.2	0.2
p_Firmicutes|c_Clostridia|o_Clostridiales|f_Lachnospiraceae|g_|s_	0.5	0.1	0.2	0.1	4.3	2.6	0.3	0.1	0.2	0.1	2.9	4.3
p_Firmicutes|c_Bacilli|o_Turicibacterales|f_Turicibacteraceae|g_Turicibacter|s_	0.0	0.0	0.0	0.0	0.0	0.0	4.1	5.6	3.3	2.8	0.2	0.4
p_Proteobacteria|c_Alphaproteobacteria|o_RF32|f_|g_|s_	0.1	0.1	0.1	0.1	0.5	0.5	1.3	0.7	1.6	1.1	3.6	2.5
p_Verrucomicrobia|c_Verrucomicrobiae|o_Verrucomicrobiales|f_Verrucomicrobiaceae|g_Akkermansia|s_muciniphila	1.3	0.8	1.1	0.5	1.2	0.4	1.0	0.6	0.9	0.4	1.2	0.4
p_Firmicutes|c_Bacilli|o_Lactobacillales|f_Streptococcaceae|g_Lactococcus|s_	1.6	0.5	0.5	0.2	0.2	0.1	1.5	0.5	1.2	0.4	0.6	0.4
p_Bacteroidetes|c_Bacteroidia|o_Bacteroidales|f_[Odoribacteraceae]|g_Odoribacter|s_	2.7	0.5	1.1	0.7	0.5	0.6	0.3	0.1	0.4	0.2	0.1	0.1
p_Firmicutes|c_Clostridia|o_Clostridiales|f_Ruminococcaceae|g_Ruminococcus|s_	0.8	0.4	0.9	0.4	0.3	0.1	1.0	0.4	1.2	0.6	0.5	0.3
p_Proteobacteria|c_Deltaproteobacteria|o_Desulfovibrionales|f_Desulfovibrionaceae|g_Bilophila|s_	1.2	0.5	0.8	0.3	0.3	0.2	0.7	0.4	0.6	0.4	1.0	0.3
p_Firmicutes|c_Clostridia|o_Clostridiales|f_Ruminococcaceae|_|_	2.1	1.5	0.4	0.5	0.0	0.0	0.4	0.4	0.8	0.4	0.6	0.3
p_Firmicutes|c_Clostridia|o_Clostridiales|f_Ruminococcaceae|g_|s_	0.6	0.9	0.8	0.7	0.9	0.4	0.4	0.3	0.4	0.3	0.7	0.6

Table A7 Average and standard deviation of the relative abundance (%) for the top 30 taxa with the highest abundances for section 4.3.3.

Relative abundance of bacterial taxa (%)	Normal chow		0.2% Cellulose		Psyllium		Psyllium +RS		Psyllium +Inulin	
	Avg	STD	Avg	STD	Avg	STD	Avg	STD	Avg	STD
p_Firmicutes|c_Bacilli|o_Lactobacillales|f_Lactobacillaceae|g_Lactobacillus|s_	16.9	3.8	15.8	8.0	1.1	0.9	0.9	0.6	9.2	3.8
p_Bacteroidetes|c_Bacteroidia|o_Bacteroidales|f_S24-7|g_|s_	32.3	3.0	11.3	2.9	23.2	1.9	18.1	4.0	16.6	2.2
p_Firmicutes|c_Clostridia|o_Clostridiales|f_|g_|s_	2.0	0.9	6.6	3.9	1.1	0.8	5.5	2.7	2.4	0.7
p_Actinobacteria|c_Actinobacteria|o_Bifidobacteriales|f_Bifidobacteriaceae|g_Bifidobacterium|s_animalis	0.2	0.2	0.0	0.0	0.0	0.0	1.1	0.6	34.1	5.8
p_Bacteroidetes|c_Bacteroidia|o_Bacteroidales|f_|g_|s_	3.8	1.3	3.9	1.2	0.5	0.3	5.4	1.6	0.5	0.4
p_Actinobacteria|c_Actinobacteria|o_Bifidobacteriales|f_Bifidobacteriaceae|g_Bifidobacterium|s_pseudolongum	0.0	0.0	0.0	0.0	0.0	0.0	0.0	0.0	0.0	0.0
p_Bacteroidetes|c_Bacteroidia|o_Bacteroidales|f_Bacteroidaceae|g_Bacteroides|s_acidifaciens	0.3	0.1	1.1	0.6	9.3	5.7	6.6	0.8	3.2	0.9
p_Bacteroidetes|c_Bacteroidia|o_Bacteroidales|f_Bacteroidaceae|g_Bacteroides|s_	2.1	0.4	1.3	0.8	1.2	1.7	2.0	0.4	1.8	1.3
p_Bacteroidetes|c_Bacteroidia|o_Bacteroidales|f_Rikenellaceae|g_|s_	5.5	0.9	8.9	3.0	1.8	0.7	2.2	0.7	1.2	0.6
p_Firmicutes|c_Clostridia|o_Clostridiales|_|_|_	4.1	1.8	11.4	2.4	2.9	1.1	6.0	1.1	0.5	0.2
p_Bacteroidetes|c_Bacteroidia|o_Bacteroidales|f_Bacteroidaceae|g_Bacteroides|_	2.7	1.3	0.1	0.0	11.5	1.7	8.6	2.2	9.3	2.8
p_Actinobacteria|c_Coriobacteriia|o_Coriobacteriales|f_Coriobacteriaceae|g_|s_	0.2	0.2	6.3	3.2	3.8	1.3	5.7	2.1	3.1	1.0
p_Firmicutes|c_Clostridia|o_Clostridiales|f_Lachnospiraceae|_|_	7.6	3.1	2.1	0.8	2.4	1.3	2.1	0.8	3.9	2.1
p_Firmicutes|c_Erysipelotrichi|o_Erysipelotrichales|f_Erysipelotrichaceae|g_Allobaculum|s_	0.1	0.0	1.4	0.4	2.8	1.0	4.7	1.5	0.1	0.0
p_Proteobacteria|c_Betaproteobacteria|o_Burkholderiales|f_Alcaligenaceae|g_Sutterella|s_	0.3	0.1	0.8	0.5	4.3	2.4	7.7	2.3	1.5	0.4
p_Bacteroidetes|c_Bacteroidia|o_Bacteroidales|f_Porphyromonadaceae|g_Parabacteroides|s_	0.1	0.1	3.9	1.4	3.4	1.0	2.6	1.2	1.4	0.7
p_Proteobacteria|c_Gammaproteobacteria|o_Enterobacteriales|f_Enterobacteriaceae|_|_	0.0	0.0	0.0	0.1	9.6	6.0	3.6	1.6	0.7	0.4
p_Firmicutes|c_Clostridia|o_Clostridiales|f_Ruminococcaceae|g_Oscillospira|s_	1.6	0.4	3.7	1.8	1.5	1.0	1.1	0.4	0.8	0.3
p_Firmicutes|c_Erysipelotrichi|o_Erysipelotrichales|f_Erysipelotrichaceae|g_Clostridium|s_cocleatum	0.0	0.0	0.9	0.5	3.6	1.8	3.0	1.0	0.7	0.3
p_Firmicutes|c_Bacilli|o_Lactobacillales|f_Lactobacillaceae|g_Lactobacillus|s_reuteri	3.9	0.5	2.6	1.3	0.0	0.0	0.0	0.0	0.0	0.0
p_Bacteroidetes|c_Bacteroidia|o_Bacteroidales|f_[Odoribacteraceae]|g_Odoribacter|s_	1.9	0.4	3.2	1.0	0.1	0.1	0.3	0.1	0.1	0.0
p_Firmicutes|c_Clostridia|o_Clostridiales|f_Lachnospiraceae|g_[Ruminococcus]|s_gnavus	1.2	0.6	2.0	0.8	0.8	0.3	0.9	0.3	0.2	0.1
p_Firmicutes|c_Clostridia|o_Clostridiales|f_Peptostreptococcaceae|_|_	0.0	0.0	0.0	0.0	2.8	1.0	3.2	1.0	0.0	0.0
p_Firmicutes|c_Clostridia|o_Clostridiales|f_Clostridiaceae|g_Clostridium|_	3.4	2.2	0.2	0.2	0.1	0.0	2.1	1.2	0.3	0.2
p_Firmicutes|c_Bacilli|o_Lactobacillales|f_Streptococcaceae|g_Lactococcus|s_	0.0	0.0	2.7	2.0	0.9	0.3	0.9	0.5	0.4	0.2
p_Proteobacteria|c_Deltaproteobacteria|o_Desulfovibrionales|f_Desulfovibrionaceae|g_Bilophila|s_	0.4	0.3	1.5	0.9	1.2	0.3	0.3	0.2	0.4	0.2
p_Firmicutes|c_Clostridia|o_Clostridiales|f_Lachnospiraceae|g_|s_	0.4	0.1	0.3	0.4	0.2	0.1	0.1	0.0	3.3	1.2
p_Firmicutes|c_Clostridia|o_Clostridiales|f_Ruminococcaceae|g_Ruminococcus|s_	0.7	0.2	0.9	0.5	1.6	0.6	0.6	0.3	0.5	0.2
p_Firmicutes|c_Clostridia|o_Clostridiales|f_Ruminococcaceae|g_|s_	0.3	0.1	2.0	1.3	0.0	0.0	0.1	0.2	0.2	0.3
p_Verrucomicrobia|c_Verrucomicrobiae|o_Verrucomicrobiales|f_Verrucomicrobiaceae|g_Akkermansia|s_muciniphila	0.0	0.0	0.1	0.2	0.3	0.1	0.2	0.1	0.2	0.1

Table A8 Average of the relative abundance (%) for the top 30 taxa with the highest abundances for section 4.4.7.

Relative abundance of bacterial taxa (%)	0.2% Cellulose		Psyllium		Psyllium+RS		Psyllium+Inulin	
	nonIR	IR	nonIR	IR	nonIR	IR	nonIR	IR
p_Firmicutes|c_Bacilli|o_Lactobacillales|f_Lactobacillaceae|g_Lactobacillus|s_	8.0	10.0	0.8	0.9	0.4	1.3	2.1	3.1
p_Bacteroidetes|c_Bacteroidia|o_Bacteroidales|f_S24-7|g_|s_	13.6	11.9	22.0	21.3	24.4	22.0	19.0	19.8
p_Firmicutes|c_Clostridia|o_Clostridiales|f_|g_|s_	5.3	5.2	2.1	1.6	3.6	2.0	6.6	4.6
p_Actinobacteria|c_Actinobacteria|o_Bifidobacteriales|f_Bifidobacteriaceae|g_Bifidobacterium|s_animalis	0.4	0.5	1.7	1.8	1.0	0.6	26.6	28.5
p_Bacteroidetes|c_Bacteroidia|o_Bacteroidales|f_|g_|s_	5.4	5.1	0.7	0.7	2.8	2.4	0.4	0.2
p_Actinobacteria|c_Actinobacteria|o_Bifidobacteriales|f_Bifidobacteriaceae|g_Bifidobacterium|s_pseudolongum	0.0	0.0	0.0	0.0	0.0	0.0	0.0	0.0
p_Bacteroidetes|c_Bacteroidia|o_Bacteroidales|f_Bacteroidaceae|g_Bacteroides|s_acidifaciens	1.8	1.9	6.3	5.9	5.2	4.6	5.5	6.0
p_Bacteroidetes|c_Bacteroidia|o_Bacteroidales|f_Bacteroidaceae|g_Bacteroides|_	0.1	0.1	12.0	10.8	8.8	10.7	8.3	7.8
p_Bacteroidetes|c_Bacteroidia|o_Bacteroidales|f_Rikenellaceae|g_|s_	10.3	8.6	2.9	2.5	3.7	3.3	1.7	1.4
p_Firmicutes|c_Clostridia|o_Clostridiales|_|_|_	6.1	6.0	3.5	3.4	3.3	3.7	1.4	1.6
p_Actinobacteria|c_Coriobacteriia|o_Coriobacteriales|f_Coriobacteriaceae|g_|s_	9.5	9.9	8.1	7.2	6.8	5.4	2.9	3.2
p_Proteobacteria|c_Betaproteobacteria|o_Burkholderiales|f_Alcaligenaceae|g_Sutterella|s_	1.4	1.0	6.4	7.8	7.1	6.5	2.7	3.4
p_Firmicutes|c_Erysipelotrichi|o_Erysipelotrichales|f_Erysipelotrichaceae|g_Allobaculum|s_	3.6	3.7	3.4	4.0	4.6	4.1	0.8	1.2
p_Proteobacteria|c_Gammaproteobacteria|o_Enterobacteriales|f_Enterobacteriaceae|_|_	0.0	0.0	6.4	7.9	3.8	5.1	0.2	0.5
p_Firmicutes|c_Clostridia|o_Clostridiales|f_Lachnospiraceae|_|_	2.8	3.3	2.0	2.1	2.5	1.8	4.5	2.9
p_Firmicutes|c_Clostridia|o_Clostridiales|f_Ruminococcaceae|g_Oscillospira|s_	5.4	5.4	1.5	1.4	1.6	1.6	1.5	1.0
p_Bacteroidetes|c_Bacteroidia|o_Bacteroidales|f_Bacteroidaceae|g_Bacteroides|s_	2.4	3.2	1.1	0.8	1.5	1.7	1.8	2.1
p_Firmicutes|c_Erysipelotrichi|o_Erysipelotrichales|f_Erysipelotrichaceae|g_Clostridium|s_cocleatum	0.8	0.4	3.2	2.1	3.4	3.7	0.8	0.5
p_Proteobacteria|c_Alphaproteobacteria|o_RF32|f_|g_|s_	0.2	0.2	0.5	1.7	2.0	0.8	4.4	3.5
p_Firmicutes|c_Bacilli|o_Lactobacillales|f_Streptococcaceae|g_Lactococcus|s_	3.3	2.7	1.3	1.3	0.6	1.0	0.4	0.4
p_Firmicutes|c_Clostridia|o_Clostridiales|f_Peptostreptococcaceae|_|_	0.0	0.0	2.1	2.7	1.8	3.0	0.0	0.1
p_Bacteroidetes|c_Bacteroidia|o_Bacteroidales|f_[Odoribacteraceae]|g_Odoribacter|s_	4.4	4.1	0.2	0.2	0.2	0.2	0.0	0.0
p_Firmicutes|c_Bacilli|o_Lactobacillales|f_Enterococcaceae|g_Enterococcus|s_	2.4	4.9	0.0	0.6	0.0	0.0	0.0	0.0
p_Firmicutes|c_Clostridia|o_Clostridiales|f_Lachnospiraceae|g_Blautia|s_producta	0.0	0.0	1.5	1.2	0.9	2.3	0.5	1.0
p_Firmicutes|c_Clostridia|o_Clostridiales|f_Ruminococcaceae|g_Ruminococcus|s_	1.0	0.8	0.9	1.2	1.2	1.1	0.6	0.4
p_Proteobacteria|c_Deltaproteobacteria|o_Desulfovibrionales|f_Desulfovibrionaceae|g_Bilophila|s_	2.0	1.4	0.7	0.5	0.8	0.6	0.7	0.4
p_Firmicutes|c_Clostridia|o_Clostridiales|f_Lachnospiraceae|g_[Ruminococcus]|s_gnavus	1.9	1.4	0.8	0.7	0.8	0.5	0.4	0.3
p_Bacteroidetes|c_Bacteroidia|o_Bacteroidales|f_Porphyromonadaceae|g_Parabacteroides|s_	0.4	0.5	1.3	1.3	0.7	1.3	0.4	0.3
p_Firmicutes|c_Clostridia|o_Clostridiales|f_Clostridiaceae|g_Clostridium|_	0.1	0.1	1.0	1.0	1.3	1.2	0.4	0.3
p_Verrucomicrobia|c_Verrucomicrobiae|o_Verrucomicrobiales|f_Verrucomicrobiaceae|g_Akkermansia|s_muciniphila	0.4	0.2	1.1	1.2	0.6	0.4	0.7	0.7

Table A9 Standard deviation of the relative abundance (%) for the top 30 taxa with the highest abundances for section 4.4.7.

Relative abundance of bacterial taxa (%)	0.2% Cellulose		Psyllium		Psyllium+RS		Psyllium+Inulin	
	nonIR	IR	nonIR	IR	nonIR	IR	nonIR	IR
p_Firmicutes|c_Bacilli|o_Lactobacillales|f_Lactobacillaceae|g_Lactobacillus|s_	3.09	5.92	0.60	0.42	0.20	0.77	2.42	2.26
p_Bacteroidetes|c_Bacteroidia|o_Bacteroidales|f_S24-7|g_|s_	1.39	2.62	2.66	3.77	1.77	3.97	1.32	2.55
p_Firmicutes|c_Clostridia|o_Clostridiales|f_|g_|s_	2.44	1.64	0.73	0.66	1.46	1.37	2.13	2.71
p_Actinobacteria|c_Actinobacteria|o_Bifidobacteriales|f_Bifidobacteriaceae|g_Bifidobacterium|s_animalis	0.48	0.52	0.82	1.08	0.31	0.45	2.84	3.39
p_Bacteroidetes|c_Bacteroidia|o_Bacteroidales|f_|g_|s_	0.97	1.36	0.29	0.46	1.41	1.11	0.22	0.13
p_Actinobacteria|c_Actinobacteria|o_Bifidobacteriales|f_Bifidobacteriaceae|g_Bifidobacterium|s_pseudolongum	0.00	0.00	0.00	0.00	0.03	0.01	0.00	0.00
p_Bacteroidetes|c_Bacteroidia|o_Bacteroidales|f_Bacteroidaceae|g_Bacteroides|s_acidifaciens	0.57	1.30	2.39	1.84	1.68	1.23	0.76	3.35
p_Bacteroidetes|c_Bacteroidia|o_Bacteroidales|f_Bacteroidaceae|g_Bacteroides|_	0.07	0.06	2.07	1.62	1.29	1.45	2.48	2.70
p_Bacteroidetes|c_Bacteroidia|o_Bacteroidales|f_Rikenellaceae|g_|s_	3.05	1.66	0.82	0.89	1.47	1.02	0.38	0.50
p_Firmicutes|c_Clostridia|o_Clostridiales|_|_|_	2.72	1.61	0.77	1.71	1.12	1.63	0.64	1.23
p_Actinobacteria|c_Coriobacteriia|o_Coriobacteriales|f_Coriobacteriaceae|g_|s_	1.65	3.50	1.63	1.94	1.57	1.48	0.79	1.24
p_Proteobacteria|c_Betaproteobacteria|o_Burkholderiales|f_Alcaligenaceae|g_Sutterella|s_	0.59	0.57	0.94	0.95	1.33	2.14	0.31	0.99
p_Firmicutes|c_Erysipelotrichi|o_Erysipelotrichales|f_Erysipelotrichaceae|g_Allobaculum|s_	1.06	1.28	0.73	0.86	1.61	1.93	0.18	0.83
p_Proteobacteria|c_Gammaproteobacteria|o_Enterobacteriales|f_Enterobacteriaceae|_|_	0.00	0.02	1.52	3.42	2.52	3.28	0.30	0.58
p_Firmicutes|c_Clostridia|o_Clostridiales|f_Lachnospiraceae|_|_	0.93	1.37	0.24	0.66	0.66	0.71	2.59	2.57
p_Firmicutes|c_Clostridia|o_Clostridiales|f_Ruminococcaceae|g_Oscillospira|s_	1.57	2.01	0.51	0.57	0.39	0.74	0.56	0.35
p_Bacteroidetes|c_Bacteroidia|o_Bacteroidales|f_Bacteroidaceae|g_Bacteroides|s_	1.23	2.01	0.64	0.95	0.19	1.11	0.93	0.62
p_Firmicutes|c_Erysipelotrichi|o_Erysipelotrichales|f_Erysipelotrichaceae|g_Clostridium|s_cocleatum	0.33	0.57	1.09	0.81	1.59	1.18	0.61	0.21
p_Proteobacteria|c_Alphaproteobacteria|o_RF32|f_|g_|s_	0.17	0.21	0.47	1.71	1.77	0.43	1.67	1.45
p_Firmicutes|c_Bacilli|o_Lactobacillales|f_Streptococcaceae|g_Lactococcus|s_	1.61	1.64	0.21	0.44	0.51	0.34	0.14	0.22
p_Firmicutes|c_Clostridia|o_Clostridiales|f_Peptostreptococcaceae|_|_	0.00	0.00	0.61	0.58	0.36	0.97	0.02	0.12
p_Bacteroidetes|c_Bacteroidia|o_Bacteroidales|f_[Odoribacteraceae]|g_Odoribacter|s_	0.46	1.20	0.15	0.18	0.08	0.04	0.02	0.01
p_Firmicutes|c_Bacilli|o_Lactobacillales|f_Enterococcaceae|g_Enterococcus|s_	3.67	4.75	0.06	0.68	0.03	0.04	0.00	0.01
p_Firmicutes|c_Clostridia|o_Clostridiales|f_Lachnospiraceae|g_Blautia|s_producta	0.00	0.00	0.19	0.35	0.17	0.81	0.25	1.21
p_Firmicutes|c_Clostridia|o_Clostridiales|f_Ruminococcaceae|g_Ruminococcus|s_	0.37	0.22	0.40	0.43	0.55	0.56	0.28	0.15
p_Proteobacteria|c_Deltaproteobacteria|o_Desulfovibrionales|f_Desulfovibrionaceae|g_Bilophila|s_	1.02	0.73	0.53	0.24	0.29	0.29	0.30	0.15
p_Firmicutes|c_Clostridia|o_Clostridiales|f_Lachnospiraceae|g_[Ruminococcus]|s_gnavus	0.82	0.48	0.31	0.28	0.22	0.22	0.18	0.13
p_Bacteroidetes|c_Bacteroidia|o_Bacteroidales|f_Porphyromonadaceae|g_Parabacteroides|s_	0.27	0.27	0.58	0.56	0.87	1.16	0.10	0.10
p_Firmicutes|c_Clostridia|o_Clostridiales|f_Clostridiaceae|g_Clostridium|_	0.15	0.15	0.44	0.73	0.59	0.90	0.38	0.29
p_Verrucomicrobia|c_Verrucomicrobiae|o_Verrucomicrobiales|f_Verrucomicrobiaceae|g_Akkermansia|s_muciniphila	0.33	0.18	0.32	0.65	0.19	0.20	0.19	0.28

Table A10 Average of the relative abundance (%) for the top 30 taxa with the highest abundances for section 5.1.4 (0.2% cellulose and psyllium).

Dietary group	0.2% Cellulose				Psyllium			
IR doses (Gy)	0	10	12	14	0	10	12	14
p_Firmicutes|c_Bacilli|o_Lactobacillales|f_Lactobacillaceae|g_Lactobacillus|s_	16.1	12.9	14.9	23.8	4.2	10.4	5.6	10.2
p_Bacteroidetes|c_Bacteroidia|o_Bacteroidales|f_S24-7|g_|s_	10.5	13.4	14.3	11.0	7.6	5.6	5.0	2.9
p_Firmicutes|c_Clostridia|o_Clostridiales|f_|g_|s_	7.1	7.3	8.2	3.7	1.7	0.6	1.0	0.8
p_Actinobacteria|c_Actinobacteria|o_Bifidobacteriales|f_Bifidobacteriaceae|g_Bifidobacterium|s_animalis	0.0	0.0	0.0	0.0	2.4	3.4	4.0	2.8
p_Bacteroidetes|c_Bacteroidia|o_Bacteroidales|f_|g_|s_	3.0	4.4	4.3	4.6	0.0	0.0	0.0	0.0
p_Bacteroidetes|c_Bacteroidia|o_Bacteroidales|f_Porphyromonadaceae|g_Parabacteroides|s_	0.3	0.2	0.2	1.1	0.9	7.7	4.0	9.2
p_Bacteroidetes|c_Bacteroidia|o_Bacteroidales|f_Bacteroidaceae|g_Bacteroides|s_acidifaciens	0.7	2.5	1.1	2.1	39.9	28.2	24.5	24.8
p_Bacteroidetes|c_Bacteroidia|o_Bacteroidales|f_Bacteroidaceae|g_Bacteroides|s_	1.9	3.3	0.8	0.9	1.2	0.7	1.2	0.9
p_Bacteroidetes|c_Bacteroidia|o_Bacteroidales|f_Bacteroidaceae|g_Bacteroides|_	0.1	0.1	0.1	0.1	5.3	5.6	7.8	5.4
p_Bacteroidetes|c_Bacteroidia|o_Bacteroidales|f_Rikenellaceae|g_|s_	5.4	6.8	6.4	5.9	0.0	0.0	0.0	0.0
p_Firmicutes|c_Clostridia|o_Clostridiales|_|_|_	7.3	10.4	7.4	8.0	5.1	5.0	4.9	6.0
p_Actinobacteria|c_Coriobacteriia|o_Coriobacteriales|f_Coriobacteriaceae|g_|s_	5.0	3.9	4.6	5.1	0.0	0.0	0.0	0.0
p_Proteobacteria|c_Betaproteobacteria|o_Burkholderiales|f_Alcaligenaceae|g_Sutterella|s_	0.5	1.0	0.6	1.6	6.3	6.7	7.9	6.4
p_Firmicutes|c_Erysipelotrichi|o_Erysipelotrichales|f_Erysipelotrichaceae|g_Allobaculum|s_	0.7	1.0	0.7	1.1	0.9	0.0	0.3	0.0
p_Proteobacteria|c_Gammaproteobacteria|o_Enterobacteriales|f_Enterobacteriaceae|_|_	0.0	0.0	0.1	1.1	1.7	4.1	4.7	6.3
p_Firmicutes|c_Clostridia|o_Clostridiales|f_Lachnospiraceae|_|_	2.4	3.0	2.5	2.2	6.5	3.3	2.6	2.1
p_Firmicutes|c_Erysipelotrichi|o_Erysipelotrichales|f_Erysipelotrichaceae|g_Clostridium|s_cocleatum	0.2	0.8	1.2	2.0	1.6	1.6	2.7	2.2
p_Proteobacteria|c_Alphaproteobacteria|o_RF32|f_|g_|s_	0.1	0.2	0.2	0.1	0.0	0.0	0.0	0.0
p_Firmicutes|c_Bacilli|o_Lactobacillales|f_Streptococcaceae|g_Lactococcus|s_	11.3	2.5	8.2	2.5	1.1	0.8	1.3	0.7
p_Firmicutes|c_Clostridia|o_Clostridiales|f_Peptostreptococcaceae|_|_	0.0	0.0	0.0	0.0	0.3	0.1	1.5	0.1
p_Bacteroidetes|c_Bacteroidia|o_Bacteroidales|f_[Odoribacteraceae]|g_Odoribacter|s_	2.1	4.0	3.4	2.7	0.0	0.0	0.0	0.0
p_Firmicutes|c_Bacilli|o_Lactobacillales|f_Enterococcaceae|g_Enterococcus|s_	4.6	2.3	2.9	2.2	3.2	7.2	10.5	7.6
p_Firmicutes|c_Clostridia|o_Clostridiales|f_Lachnospiraceae|g_Blautia|s_producta	0.0	0.0	0.0	0.0	0.0	0.0	0.0	0.0
p_Firmicutes|c_Clostridia|o_Clostridiales|f_Ruminococcaceae|g_Ruminococcus|s_	0.8	0.9	0.7	0.6	0.4	0.2	0.2	0.6
p_Proteobacteria|c_Deltaproteobacteria|o_Desulfovibrionales|f_Desulfovibrionaceae|g_Bilophila|s_	1.5	1.9	1.0	1.2	0.0	0.0	0.0	0.0
p_Firmicutes|c_Clostridia|o_Clostridiales|f_Lachnospiraceae|g_[Ruminococcus]|s_gnavus	1.7	2.0	1.2	1.0	1.5	1.4	1.2	1.1
p_Firmicutes|c_Clostridia|o_Clostridiales|f_Clostridiaceae|g_Clostridium|_	0.4	0.9	0.7	1.6	0.0	0.1	0.3	1.3
p_Verrucomicrobia|c_Verrucomicrobiae|o_Verrucomicrobiales|f_Verrucomicrobiaceae|g_Akkermansia|s_muciniphila	0.0	0.0	0.0	0.2	0.5	0.4	0.3	0.3
p_Firmicutes|c_Clostridia|o_Clostridiales|f_Ruminococcaceae|g_Oscillospira|s_	5.0	4.7	4.3	3.1	1.9	0.9	0.9	0.7
p_Firmicutes|c_Bacilli|o_Lactobacillales|f_Lactobacillaceae|g_Lactobacillus|s_reuteri	5.6	2.5	3.0	4.2	0.0	0.0	0.0	0.0

Table A11 Average of the relative abundance (%) for the top 30 taxa with the highest abundances for section 5.1.4 (psyllium plus RS and psyllium plus inulin).

Dietary group	Psyllium+RS				Psyllium+Inulin			
IR doses (Gy)	0	10	12	14	0	10	12	14
p_Firmicutes|c_Bacilli|o_Lactobacillales|f_Lactobacillaceae|g_Lactobacillus|s_	1.8	1.2	3.0	2.0	4.4	3.5	9.3	7.3
p_Bacteroidetes|c_Bacteroidia|o_Bacteroidales|f_S24-7|g_|s_	12.4	9.8	11.8	13.0	27.2	28.0	22.1	22.8
p_Firmicutes|c_Clostridia|o_Clostridiales|f_|g_|s_	1.7	2.3	2.6	2.1	0.9	0.8	1.9	0.4
p_Actinobacteria|c_Actinobacteria|o_Bifidobacteriales|f_Bifidobacteriaceae|g_Bifidobacterium|s_animalis	0.0	0.0	0.8	0.5	2.4	4.8	3.9	5.9
p_Bacteroidetes|c_Bacteroidia|o_Bacteroidales|f_|g_|s_	4.4	4.0	3.9	4.0	0.0	0.0	0.0	0.0
p_Bacteroidetes|c_Bacteroidia|o_Bacteroidales|f_Porphyromonadaceae|g_Parabacteroides|s_	3.3	5.1	3.5	6.2	0.7	1.0	2.6	1.2
p_Bacteroidetes|c_Bacteroidia|o_Bacteroidales|f_Bacteroidaceae|g_Bacteroides|s_acidifaciens	5.6	6.4	6.4	6.3	23.2	25.7	24.5	28.0
p_Bacteroidetes|c_Bacteroidia|o_Bacteroidales|f_Bacteroidaceae|g_Bacteroides|s_	4.0	2.0	2.7	2.0	2.3	1.8	4.2	1.5
p_Bacteroidetes|c_Bacteroidia|o_Bacteroidales|f_Bacteroidaceae|g_Bacteroides|_	11.9	12.5	11.4	12.6	3.6	2.9	2.7	3.9
p_Bacteroidetes|c_Bacteroidia|o_Bacteroidales|f_Rikenellaceae|g_|s_	1.9	1.8	2.1	3.2	0.0	0.0	0.0	0.0
p_Firmicutes|c_Clostridia|o_Clostridiales|_|_|_	6.8	7.6	6.1	6.2	3.8	1.5	2.8	3.0
p_Actinobacteria|c_Coriobacteriia|o_Coriobacteriales|f_Coriobacteriaceae|g_|s_	1.5	4.5	5.3	4.2	0.0	0.0	0.0	0.0
p_Proteobacteria|c_Betaproteobacteria|o_Burkholderiales|f_Alcaligenaceae|g_Sutterella|s_	4.6	6.8	7.3	6.3	6.4	5.3	5.1	5.4
p_Firmicutes|c_Erysipelotrichi|o_Erysipelotrichales|f_Erysipelotrichaceae|g_Allobaculum|s_	4.3	3.6	4.3	4.1	2.2	3.5	1.6	3.6
p_Proteobacteria|c_Gammaproteobacteria|o_Enterobacteriales|f_Enterobacteriaceae|_|_	8.6	6.0	5.6	4.9	0.1	0.9	0.2	1.1
p_Firmicutes|c_Clostridia|o_Clostridiales|f_Lachnospiraceae|_|_	1.6	0.9	1.2	2.4	14.5	9.0	7.0	2.2
p_Firmicutes|c_Erysipelotrichi|o_Erysipelotrichales|f_Erysipelotrichaceae|g_Clostridium|s_cocleatum	4.8	6.5	7.0	6.0	1.3	2.4	1.6	4.6
p_Proteobacteria|c_Alphaproteobacteria|o_RF32|f_|g_|s_	0.3	0.4	0.5	0.7	0.0	0.0	0.0	0.0
p_Firmicutes|c_Bacilli|o_Lactobacillales|f_Streptococcaceae|g_Lactococcus|s_	1.1	1.0	0.9	0.7	0.3	0.2	0.5	0.4
p_Firmicutes|c_Clostridia|o_Clostridiales|f_Peptostreptococcaceae|_|_	3.9	3.7	0.1	1.3	0.0	0.0	0.0	0.0
p_Bacteroidetes|c_Bacteroidia|o_Bacteroidales|f_[Odoribacteraceae]|g_Odoribacter|s_	0.1	0.2	0.4	0.3	0.0	0.0	0.0	0.0
p_Firmicutes|c_Bacilli|o_Lactobacillales|f_Enterococcaceae|g_Enterococcus|s_	0.3	0.3	0.7	0.1	0.2	0.0	1.7	0.8
p_Firmicutes|c_Clostridia|o_Clostridiales|f_Lachnospiraceae|g_Blautia|s_producta	1.3	0.0	0.0	0.0	0.0	0.0	0.0	0.2
p_Firmicutes|c_Clostridia|o_Clostridiales|f_Ruminococcaceae|g_Ruminococcus|s_	0.7	0.4	0.5	0.7	0.3	0.4	0.3	0.3
p_Proteobacteria|c_Deltaproteobacteria|o_Desulfovibrionales|f_Desulfovibrionaceae|g_Bilophila|s_	0.3	0.2	0.2	0.3	0.0	0.0	0.0	0.0
p_Firmicutes|c_Clostridia|o_Clostridiales|f_Lachnospiraceae|g_[Ruminococcus]|s_gnavus	0.6	0.6	1.0	0.8	0.5	0.3	0.3	0.4
p_Firmicutes|c_Clostridia|o_Clostridiales|f_Clostridiaceae|g_Clostridium|_	1.8	3.0	6.1	2.7	0.0	0.0	0.0	0.0
p_Verrucomicrobia|c_Verrucomicrobiae|o_Verrucomicrobiales|f_Verrucomicrobiaceae|g_Akkermansia|s_muciniphila	0.1	0.2	0.1	0.2	0.3	0.5	0.3	1.4
p_Firmicutes|c_Clostridia|o_Clostridiales|f_Ruminococcaceae|g_Oscillospira|s_	0.9	0.5	0.6	1.0	1.4	1.1	1.0	1.3
p_Firmicutes|c_Bacilli|o_Lactobacillales|f_Lactobacillaceae|g_Lactobacillus|s_reuteri	0.0	0.1	0.3	0.4	0.0	0.0	0.0	0.0

Table A12 Standard deviation of the relative abundance (%) for the top 30 taxa with the highest abundances for section 5.1.4 (0.2% cellulose and psyllium).

Dietary group	0.2% Cellulose				Psyllium			
IR doses (Gy)	0	10	12	14	0	10	12	14
p_Firmicutes|c_Bacilli|o_Lactobacillales|f_Lactobacillaceae|g_Lactobacillus|s_	5.1	5.4	11.3	7.7	1.4	5.1	4.5	10.4
p_Bacteroidetes|c_Bacteroidia|o_Bacteroidales|f_S24-7|g_|s_	2.4	2.3	6.9	1.7	1.1	0.9	1.4	0.5
p_Firmicutes|c_Clostridia|o_Clostridiales|f_|g_|s_	3.8	3.6	4.2	0.7	0.4	0.2	0.6	0.4
p_Actinobacteria|c_Actinobacteria|o_Bifidobacteriales|f_Bifidobacteriaceae|g_Bifidobacterium|s_animalis	0.0	0.0	0.0	0.0	0.5	1.1	1.9	1.1
p_Bacteroidetes|c_Bacteroidia|o_Bacteroidales|f_|g_|s_	0.9	1.9	1.9	1.5	0.0	0.0	0.0	0.0
p_Bacteroidetes|c_Bacteroidia|o_Bacteroidales|f_Porphyromonadaceae|g_Parabacteroides|s_	0.0	0.2	0.1	0.7	0.6	1.4	2.9	2.9
p_Bacteroidetes|c_Bacteroidia|o_Bacteroidales|f_Bacteroidaceae|g_Bacteroides|s_acidifaciens	0.2	1.8	0.8	1.1	7.0	10.7	9.3	11.8
p_Bacteroidetes|c_Bacteroidia|o_Bacteroidales|f_Bacteroidaceae|g_Bacteroides|s_	0.6	2.5	0.6	0.6	0.3	0.2	0.2	0.2
p_Bacteroidetes|c_Bacteroidia|o_Bacteroidales|f_Bacteroidaceae|g_Bacteroides|_	0.0	0.0	0.1	0.1	1.9	1.3	2.9	1.5
p_Bacteroidetes|c_Bacteroidia|o_Bacteroidales|f_Rikenellaceae|g_|s_	0.6	2.4	3.7	3.2	0.0	0.0	0.0	0.0
p_Firmicutes|c_Clostridia|o_Clostridiales|_|_|_	0.3	2.4	1.9	1.8	0.3	1.1	0.6	2.7
p_Actinobacteria|c_Coriobacteriia|o_Coriobacteriales|f_Coriobacteriaceae|g_|s_	2.1	2.4	2.9	1.8	0.0	0.0	0.0	0.0
p_Proteobacteria|c_Betaproteobacteria|o_Burkholderiales|f_Alcaligenaceae|g_Sutterella|s_	0.2	0.6	0.4	0.6	1.1	1.9	3.4	2.6
p_Firmicutes|c_Erysipelotrichi|o_Erysipelotrichales|f_Erysipelotrichaceae|g_Allobaculum|s_	0.4	0.6	0.5	0.4	0.1	0.0	0.3	0.1
p_Proteobacteria|c_Gammaproteobacteria|o_Enterobacteriales|f_Enterobacteriaceae|_|_	0.0	0.0	0.1	1.6	0.8	4.0	4.5	2.0
p_Firmicutes|c_Clostridia|o_Clostridiales|f_Lachnospiraceae|_|_	1.3	1.1	0.8	0.9	1.1	1.7	1.8	1.0
p_Firmicutes|c_Erysipelotrichi|o_Erysipelotrichales|f_Erysipelotrichaceae|g_Clostridium|s_cocleatum	0.3	1.2	1.6	1.5	0.4	0.4	1.9	0.6
p_Proteobacteria|c_Alphaproteobacteria|o_RF32|f_|g_|s_	0.0	0.1	0.2	0.1	0.0	0.0	0.0	0.0
p_Firmicutes|c_Bacilli|o_Lactobacillales|f_Streptococcaceae|g_Lactococcus|s_	5.7	1.4	5.7	0.8	0.5	0.3	0.6	0.3
p_Firmicutes|c_Clostridia|o_Clostridiales|f_Peptostreptococcaceae|_|_	0.0	0.0	0.0	0.0	0.2	0.1	2.2	0.3
p_Bacteroidetes|c_Bacteroidia|o_Bacteroidales|f_[Odoribacteraceae]|g_Odoribacter|s_	0.4	1.7	1.6	0.8	0.0	0.0	0.0	0.0
p_Firmicutes|c_Bacilli|o_Lactobacillales|f_Enterococcaceae|g_Enterococcus|s_	2.6	1.2	2.7	1.6	0.2	4.9	4.2	3.1
p_Firmicutes|c_Clostridia|o_Clostridiales|f_Lachnospiraceae|g_Blautia|s_producta	0.0	0.0	0.0	0.0	0.0	0.0	0.0	0.0
p_Firmicutes|c_Clostridia|o_Clostridiales|f_Ruminococcaceae|g_Ruminococcus|s_	0.3	0.3	0.3	0.1	0.1	0.1	0.1	0.3
p_Proteobacteria|c_Deltaproteobacteria|o_Desulfovibrionales|f_Desulfovibrionaceae|g_Bilophila|s_	1.1	0.8	0.6	0.5	0.0	0.0	0.0	0.0
p_Firmicutes|c_Clostridia|o_Clostridiales|f_Lachnospiraceae|g_[Ruminococcus]|s_gnavus	0.5	0.7	0.2	0.4	0.3	0.2	0.8	0.3
p_Firmicutes|c_Clostridia|o_Clostridiales|f_Clostridiaceae|g_Clostridium|_	0.2	0.4	0.4	1.0	0.0	0.0	0.5	0.8
p_Verrucomicrobia|c_Verrucomicrobiae|o_Verrucomicrobiales|f_Verrucomicrobiaceae|g_Akkermansia|s_muciniphila	0.0	0.0	0.0	0.2	0.1	0.2	0.2	0.1
p_Firmicutes|c_Clostridia|o_Clostridiales|f_Ruminococcaceae|g_Oscillospira|s_	1.3	2.2	1.4	1.0	0.4	0.5	0.5	0.4
p_Firmicutes|c_Bacilli|o_Lactobacillales|f_Lactobacillaceae|g_Lactobacillus|s_reuteri	1.4	0.9	2.0	1.0	0.0	0.0	0.0	0.0

Table A13 Standard deviation of the relative abundance (%) for the top 30 taxa with the highest abundances for section 5.1.4 (psyllium plus RS and psyllium plus inulin).

Dietary group	Psyllium+RS				Psyllium+Inulin			
IR doses (Gy)	0	10	12	14	0	10	12	14
p_Firmicutes|c_Bacilli|o_Lactobacillales|f_Lactobacillaceae|g_Lactobacillus|s_	0.8	0.7	2.1	1.1	3.1	1.0	5.7	3.2
p_Bacteroidetes|c_Bacteroidia|o_Bacteroidales|f_S24-7|g_|s_	2.8	1.6	4.0	2.8	1.9	2.2	4.5	3.6
p_Firmicutes|c_Clostridia|o_Clostridiales|f_|g_|s_	1.4	1.3	1.7	0.9	0.3	0.4	1.9	0.2
p_Actinobacteria|c_Actinobacteria|o_Bifidobacteriales|f_Bifidobacteriaceae|g_Bifidobacterium|s_animalis	0.0	0.0	0.5	0.3	1.4	1.3	1.4	3.0
p_Bacteroidetes|c_Bacteroidia|o_Bacteroidales|f_|g_|s_	3.7	0.8	1.7	0.9	0.0	0.0	0.0	0.0
p_Bacteroidetes|c_Bacteroidia|o_Bacteroidales|f_Porphyromonadaceae|g_Parabacteroides|s_	1.3	0.7	1.7	1.2	0.0	0.2	3.6	0.9
p_Bacteroidetes|c_Bacteroidia|o_Bacteroidales|f_Bacteroidaceae|g_Bacteroides|s_acidifaciens	0.6	0.8	2.1	1.3	3.8	2.3	2.4	3.7
p_Bacteroidetes|c_Bacteroidia|o_Bacteroidales|f_Bacteroidaceae|g_Bacteroides|s_	3.2	0.3	1.3	0.4	1.0	0.5	4.0	0.6
p_Bacteroidetes|c_Bacteroidia|o_Bacteroidales|f_Bacteroidaceae|g_Bacteroides|_	1.4	1.9	1.8	2.3	0.7	0.6	0.7	1.2
p_Bacteroidetes|c_Bacteroidia|o_Bacteroidales|f_Rikenellaceae|g_|s_	2.1	0.4	1.1	0.8	0.0	0.0	0.0	0.0
p_Firmicutes|c_Clostridia|o_Clostridiales|_|_|_	0.9	1.5	1.5	1.1	0.7	0.8	0.5	1.9
p_Actinobacteria|c_Coriobacteriia|o_Coriobacteriales|f_Coriobacteriaceae|g_|s_	0.5	1.2	1.8	1.2	0.0	0.0	0.0	0.0
p_Proteobacteria|c_Betaproteobacteria|o_Burkholderiales|f_Alcaligenaceae|g_Sutterella|s_	1.9	1.0	1.8	2.2	1.9	0.7	2.3	2.2
p_Firmicutes|c_Erysipelotrichi|o_Erysipelotrichales|f_Erysipelotrichaceae|g_Allobaculum|s_	1.7	0.8	1.2	1.7	0.7	0.2	1.7	2.0
p_Proteobacteria|c_Gammaproteobacteria|o_Enterobacteriales|f_Enterobacteriaceae|_|_	5.3	2.1	4.2	4.8	0.1	0.4	0.5	1.0
p_Firmicutes|c_Clostridia|o_Clostridiales|f_Lachnospiraceae|_|_	0.5	0.3	0.6	0.4	3.4	2.7	3.0	1.4
p_Firmicutes|c_Erysipelotrichi|o_Erysipelotrichales|f_Erysipelotrichaceae|g_Clostridium|s_cocleatum	1.5	1.8	2.2	1.9	0.6	0.9	0.4	2.0
p_Proteobacteria|c_Alphaproteobacteria|o_RF32|f_|g_|s_	0.2	0.4	0.4	0.5	0.0	0.0	0.0	0.0
p_Firmicutes|c_Bacilli|o_Lactobacillales|f_Streptococcaceae|g_Lactococcus|s_	0.2	0.4	0.4	0.2	0.1	0.1	0.2	0.1
p_Firmicutes|c_Clostridia|o_Clostridiales|f_Peptostreptococcaceae|_|_	0.6	0.6	0.1	1.0	0.0	0.0	0.0	0.0
p_Bacteroidetes|c_Bacteroidia|o_Bacteroidales|f_[Odoribacteraceae]|g_Odoribacter|s_	0.1	0.0	0.3	0.1	0.0	0.0	0.0	0.0
p_Firmicutes|c_Bacilli|o_Lactobacillales|f_Enterococcaceae|g_Enterococcus|s_	0.3	0.3	1.1	0.1	0.0	0.1	1.9	0.6
p_Firmicutes|c_Clostridia|o_Clostridiales|f_Lachnospiraceae|g_Blautia|s_producta	0.6	0.0	0.0	0.0	0.0	0.0	0.0	0.4
p_Firmicutes|c_Clostridia|o_Clostridiales|f_Ruminococcaceae|g_Ruminococcus|s_	0.3	0.1	0.4	0.3	0.0	0.1	0.1	0.2
p_Proteobacteria|c_Deltaproteobacteria|o_Desulfovibrionales|f_Desulfovibrionaceae|g_Bilophila|s_	0.3	0.1	0.2	0.2	0.0	0.0	0.0	0.0
p_Firmicutes|c_Clostridia|o_Clostridiales|f_Lachnospiraceae|g_[Ruminococcus]|s_gnavus	0.4	0.1	0.4	0.3	0.1	0.1	0.2	0.3
p_Firmicutes|c_Clostridia|o_Clostridiales|f_Clostridiaceae|g_Clostridium|_	0.4	0.9	2.4	0.8	0.0	0.0	0.0	0.0
p_Verrucomicrobia|c_Verrucomicrobiae|o_Verrucomicrobiales|f_Verrucomicrobiaceae|g_Akkermansia|s_muciniphila	0.0	0.1	0.1	0.1	0.1	0.1	0.1	2.6
p_Firmicutes|c_Clostridia|o_Clostridiales|f_Ruminococcaceae|g_Oscillospira|s_	0.4	0.2	0.4	0.3	0.3	0.4	0.1	0.9
p_Firmicutes|c_Bacilli|o_Lactobacillales|f_Lactobacillaceae|g_Lactobacillus|s_reuteri	0.0	0.1	0.3	0.3	0.0	0.0	0.0	0.0

Glossary

Abundance	A measure of bacterial numbers and mass per unit volume.
Alignment	The comparison between sequences (nucleic acids or amino acids); the result will be some common letters within their sequence structures.
Alpha diversity	A measure of similarity within communities.
Alpha rarefraction	Primarily used to determine if the richness of the samples has been fully observed or sequenced.
Beta diversity	A measure of similarity between communities.
Bray-Curtis dissimilarity	Fraction of overabundant counts.
Chimera	A first source of error originates from chimera formation within the PCR amplification step, thereby creating a chimeric sequence which consists of two or more segments from distinct species.
Cladogram	An evolutionary tree that plots evolutionary relationships among organisms and branch points show different relationships in time.
CFU	A unit used to estimate the number of viable bacteria or fungal cells in a sample. Viable is defined as the ability to multiply via binary fission under the controlled conditions.
Clustering	Classification, or putting samples into (perhaps hierarchical) classes, is often useful when one wishes to assign names to, or to map, ecological communities.
Deblur	Deblur uses sequence error profiles to associate erroneous sequence reads with the true biological

	sequence from which they are derived, resulting in high quality sequence variant data.
Depth	The number of unique reads that include a given nucleotide in the reconstructed sequence.
Diversity	A measure of the number of species in a community, and a measure of the abundance of each species.
DS-FDR	A method of understanding the rate of type I errors in null hypothesis testing when performing multiple comparisons. It greatly improves the power to detect differential taxa by exploiting the discreteness of the data.
Effect size	A quantitative measure of the magnitude of a phenomenon.
Evenness	A description of the distribution of abundance across the species in a community.
Faith's phylogenetic diversity	An alpha diversity metric that uses a phylogenetic tree to compute sample diversity.
Greengenes	A 16S rRNA gene database which addresses the limitations of public repositories by providing chimera screening, standard alignment, and taxonomic classification using multiple published taxonomies.
KEGG	A database resource for understanding high-level functions and utilities of biological systems, such as the cell, the organism and the ecosystem, from molecular-level information, especially large-scale molecular datasets generated by genome sequencing and other high-throughput experimental technologies.
LEfSe	A method for determining the features (organisms, clades, operational taxonomic units, genes, or functions)

	most likely to explain differences between classes by coupling standard tests for statistical significance with additional tests encoding biological consistency and effect relevance.
Library	A collection of DNA fragments with known adapter sequences at one or both ends that is derived from a single clinical or environmental sample.
Metagenomics	A molecular tool used to analyse DNA acquired from environmental samples, in order to study the community of micro-organisms present, without the necessity of obtaining pure cultures.
Microbiota	A collective term for all of the genetic material within a microbiota and this can also be referred to as the metagenome of the microbiota.
Microbiota	A collective term for the micro-organisms that live in or on the human body.
MiSeq	A DNA-to-data sequencing platform, integrating cluster generation, amplification, sequencing, and data analysis into a single instrument.
OTU	A cluster of similar sequence variants of the 16S rDNA marker gene sequence. Each of these clusters is intended to represent a taxonomic unit of a bacteria species or genus depending on the sequence similarity threshold.
PCoA	A method of representing the distances between samples in a low-dimensional, Euclidean space. In particular, it maximizes the linear correlation between the distances in the distance matrix, and the distances in a space of low dimension (typically, 2 or 3 axes are selected).

Phylogenetics	A study of the evolutionary history and relationships among individuals or groups of organisms (e.g. species, or populations). These relationships are discovered through phylogenetic inference methods that evaluate observed heritable traits, such as DNA sequences or morphology under a model of evolution of these traits. The result of these analyses is a phylogeny (also known as a phylogenetic tree).
Phylogeny	The history of descent of a group of taxa such as species from their common ancestors, including the order of branching and sometimes the absolute times of divergence; also applied to the genealogy of genes derived from a common ancestral gene.
PICRUSt	A bioinformatics software package designed to predict metagenome functional content from marker gene (e.g., 16S rRNA) surveys and full genomes.
Pielou's evenness	An alpha diversity metric that measures relative evenness of species richness.
Plugin	A method providing microbiota (i.e. domain-specific) analysis functionality that is accessible to users through a variety of interfaces built around the QIIME 2 framework.
Q-score	A quality control metric for DNA sequencing that is logarithmically related to the base calling error probabilities and serves as a measurement of read accuracy.
Rarefaction	A resampling approach to develop a curve to identify and allow comparisons among samples using the minimum sample size of all the collections.

Reads	Inferred sequences of base pairs corresponding to part of or all of a single DNA fragment.
Relative abundance	The percent composition of an organism of a particular kind relative to the total number of organisms in the area.
Richness	The number of species in a community.
Sequence alignment	Regions of local similarity of DNA, RNA or amino acid sequences.
Shannon's index	An alpha diversity metric that accounts for both abundance and evenness of the taxa present.
Taxon	A group of one or more populations of an organism or organisms seen by taxonomists to form a unit.
Taxonomy	The science of naming, defining (circumscribing) and classifying groups of biological organisms on the basis of shared characteristics. Organisms are grouped together into taxa (singular: taxon) and these groups are given a taxonomic rank; groups of a given rank can be aggregated to form a super-group of higher rank, thus creating a taxonomic hierarchy. The principal ranks in modern use are domain, kingdom, phylum (division is sometimes used in botany in place of phylum), class, order, family, genus, and species.
Volcano plot	A type of scatter-plot that is used to quickly identify changes in large data sets composed of replicate data.